



**HAL**  
open science

# Recomposition de l'interactome du ribosome au cours des infections virales

Thibault Sohier

► **To cite this version:**

Thibault Sohier. Recomposition de l'interactome du ribosome au cours des infections virales. Biochemistry [q-bio.BM]. Université de Lyon, 2021. English. NNT : 2021LYSEN068 . tel-03934712

**HAL Id: tel-03934712**

**<https://theses.hal.science/tel-03934712>**

Submitted on 11 Jan 2023

**HAL** is a multi-disciplinary open access archive for the deposit and dissemination of scientific research documents, whether they are published or not. The documents may come from teaching and research institutions in France or abroad, or from public or private research centers.

L'archive ouverte pluridisciplinaire **HAL**, est destinée au dépôt et à la diffusion de documents scientifiques de niveau recherche, publiés ou non, émanant des établissements d'enseignement et de recherche français ou étrangers, des laboratoires publics ou privés.



Numéro National de Thèse : 2021LYSEN068

**THESE DE DOCTORAT DE L'UNIVERSITE DE LYON**  
opérée par  
**l'Ecole Normale Supérieure de Lyon**

**Ecole Doctorale N° 340**  
**Biologie Moléculaire, Intégrative et Cellulaire**

**Spécialité de doctorat : Virologie**  
**Discipline** : Sciences de la vie et de la santé

Soutenue publiquement le 30/11/2021, par :  
**Thibault SOHIER**

---

**Ribosome interactome recomposition  
by viral infections**

Recomposition de l'interactome du ribosome  
au cours des infections virales

---

Devant le jury composé de :

PFEFFER, Sébastien, Directeur de Recherche, IBMC, Strasbourg  
MARTINEZ SALAS, Encarnacion, Professeure, CBMSO, Madrid  
JALINOT, Pierre, Directeur de Recherche, ENS de Lyon, Lyon  
DIEZ ANTON, Juana Maria Professeure, UPF, Barcelone  
RICCI, Emiliano, Chargé de Recherche, ENS de Lyon, Lyon

Rapporteur  
Rapporteuse  
Examinateur  
Examinatrice  
Directeur de thèse

# Foreword

When I arrived at the lab I had the intuition that endogenous tagging of ribosomal proteins could serve to investigate multiple aspect of translation regulation. We decided to implement this strategy and sought out to characterize the ribosome interactome. Four months into this work, a study published in Cell by Simsek and colleagues published the ribosome interactome, pretty much using the same method that we were planning to implement. Thus, we shifted our focus and decided to look at the changes in ribosome interactome following viral infection, an ancient topic falling into the realm of “specialized ribosome” that has gained significant traction in the recent years. This proved to be much more difficult than expected and forced us to optimize our ribosome purification method to the limit of what we believe can be achieved. Using the alphavirus model SINV, we were able to show that viral infection significantly recomposes the ribosome interactome, with potential implications in viral life cycle.

In Chapter I, I will detail the control of translation during alphavirus infection, essentially focusing on SINV, to highlight the extent to which cellular translation is altered during viral infection and present the very unusual mechanism by which the SINV subgenomic RNA is translated.

In Chapter II, I will discuss more specifically how the idea of “specialized ribosomes” applies to viral infection, and show that ribosome specialization is a common mechanism by which viral mRNAs are preferentially translated.

The bulk of my PhD results is presented in Part I, where the strategy for investigation of the ribosome interaction changes is developed and performed during SINV infection. An offshoot of this main project is presented in Part II, where I tried to investigate the molecular determinants controlling interaction of the SINV nsP2 protein with the ribosome.

The experience acquired during my PhD was additionally put to the task in several collaborations, two of which have lead to publications that are presented in Annex 1 and 2 of this manuscript.

# Résumé de la thèse

Les virus sont des parasites obligatoires qui dépendent intégralement de la machinerie cellulaire pour produire leurs propres protéines. Les ribosomes, les machines supramoléculaires qui traduisent les ARN messagers en protéines, sont donc au cœur des interactions hôtes pathogènes. Historiquement, les ribosomes ont été perçus comme une machine monolithique. Cependant, des données récentes suggèrent que les ribosomes ne constituent pas une population homogène. En effet, ils peuvent différer par les modifications post-traductionnelles des protéines ribosomales, les modifications post-transcriptionnelles des ARNs ribosomiques ou la diversité des protéines qui s'y associent. Au cours de ma thèse, j'ai développé une approche de purification par affinité des ribosomes afin d'identifier l'ensemble des protéines associées à ces derniers. Cette stratégie, qui s'appuie sur l'étiquetage de certaines protéines ribosomales par un épitope synthétique grâce au système CRISPR/Cas9, a permis d'identifier de manière extrêmement robuste un grand nombre de protéines associées au ribosome. Une fois optimisée, j'ai appliqué cette méthode à l'étude des changements de composition du ribosome au cours d'une infection virale. En utilisant l'alphavirus Sindbis comme modèle, j'ai pu montrer que l'infection modifie drastiquement la composition des ribosomes. Ces données mettent en évidence les manifestations moléculaires de l'inhibition de la traduction induite par le virus, cumulé à une altération de la maturation des sous-unités du ribosome. Enfin, certaines protéines dont l'association au ribosome est dynamique au cours de l'infection semblent avoir un rôle direct dans la traduction des ARNs viraux.



# Abstract

Viruses are obligatory parasites that depend entirely on the host-cell machinery to produce their own proteins. Ribosomes, the supramolecular machines that translate messenger RNAs into proteins are consequently at the core of host-pathogen interactions. Historically, ribosomes have been largely considered as monolithic machines, with poor intrinsic regulatory activity. However, recent data suggests that ribosomes do not constitute an homogenous population. In fact, they can differ by the post-translational modifications of ribosomal proteins, post-transcriptional modifications of ribosomal RNAs or by the diversity of proteins that associate with them. During my PhD, I developed a new method of affinity purification of ribosomes in order to identify the pool of proteins that associate to them. This strategy, which involves the endogenous tagging of ribosomal proteins using the CRISPR/Cas9 system, allows for the purification of ribosomes with unprecedented purity, and the robust determination of the ribosome interactome. Once optimized, I applied this method to the study of the changes in ribosome partners during viral infection. Using the alphavirus SIndbis as a model, I was able to show that viral infection drastically remodels the ribosome interactome. This data highlights the molecular manifestations of host translational shut-down, as well as perturbations to ribosome maturation. Finally, certain proteins whose association with the ribosome is dynamic along the course of infection appear to participate directly in the translation of the viral messenger RNAs.

## Table of contents

Chapter I: The control of translation during Alphavirus infection.....	6
1. SINV life cycle.....	9
Structural proteins.....	10
C.....	10
E1, E2 and E3.....	11
6K/TF.....	12
Non-structural proteins.....	12
nsP1.....	13
nsP2.....	14
nsP3.....	15
nsP4.....	15
2. Introduction to canonical translation initiation.....	15
3. Host-cell shut-off in alphaviruses infection.....	17
Phosphorylation of eIF2 $\alpha$ following alphavirus infection.....	17
Destabilization of stress granules by nsP3.....	18
4. Unconventional mode of translation initiation of the sgRNA.....	20
Translation of the sgRNA is mediated by a non-canonical cap-dependent process.....	20
The DSH/DLP structure downstream of sgRNA confers eIF2 $\alpha$ independency.....	25
sgRNA translation initiation involves an eIF4A-independent scanning process.....	28
Conclusion and Perspectives.....	30
Chapter II: Ribosome specialization during viral infections.....	33
Introduction.....	33
Definitions and Scope.....	34
1. Substoichiometric ribosomal proteins and specific functions of ribosomal proteins in viral translation.....	35
2. Ribosomal proteins post-translational modifications.....	39
3. Viral proteins interacting with the ribosome.....	40
4. The role of ribosome-associated proteins.....	45
5. rRNA modifications in viral infection.....	46
Conclusion: the rise of ribo-centric methods.....	49

Part I: Recomposition of the ribosome interactome by SINV infection.....	51
Introduction.....	51
Results.....	53
Development of affinity purification of endogenously tagged ribosomes.....	53
Optimization of the formaldehyde crosslinking step.....	58
Alteration of host-cell translation during SINV infection.....	60
SINV infection recomposes the ribosome interactome.....	61
Contribution of total and cytoplasmic proteome to changes in ribosome interactome.....	64
Absence of correlation between changes ribosome interactome and mRNA interactome.....	65
Discussion.....	65
Biochemical and genetic screens to decipher viral biology.....	65
Development of differential ribosome interactomics.....	69
Pervasive remodeling of the ribosome interaction following SINV infection.....	71
Requirements of canonical translation factors in the translation of SINV sgRNA.....	72
Alteration of ribosome biogenesis.....	74
Perspectives.....	76
Material & Methods.....	78
Part II: Investigating alphavirus nsP2-RPS6/eS6 interaction using quantitative yeast two-hybrid..	85
Introduction.....	85
Results.....	87
Discussion.....	88
Materials & Methods.....	89
Annex 1.....	126
Genome editing in primary cells and in vivo using viral-derived Nanoblades loaded with Cas9-sgRNA ribonucleoproteins.....	126
Annex 2.....	128
System-wide Profiling of RNA-Binding Protein Uncovers Key Regulators of Virus Infection.	128

# Chapter I: The control of translation during Alphavirus infection

Alphaviruses are a genus of viruses from the *Togaviridae* family. They form a complex group of small (~70 nm) enveloped RNA viruses of positive polarity. Their classification includes 31 known species (Lefkowitz et al., 2018) of which twelve can infect humans (Forrester et al., 2012). They are divided into three groups based on their geographic distribution and phylogenetic relationships : 1. Old World alphaviruses, found in Europe, Africa, Asia and Oceania; 2. New World alphaviruses, found in the Americas, and 3.« Aquatic Viruses ». Aquatic viruses include the Salmon Pancreatic Disease Virus (SPDV) and the Southern Elephant Seal Virus (SESV), and infect salmon and trouts, and elephant seals respectively (Forrester et al., 2012). Excluding aquatic viruses, all known alphaviruses are transmitted by mosquitoes, mostly of the *Aedes* and *Culex* genres. The “Old World” and “New World” alphaviruses classification are based on geographic distribution and do not represent monophyletic groups (Forrester et al., 2012) . This classification is thus supplanted by the phylogenetically relevant antigenic complex classification (Table 1).

Virus	Abbreviation	Antigenic Complex	Known reservoir	Mosquito vector	Human disease
Salmon pancreatic disease	SPDV		Salmon	<i>Lepidothirus</i>	
Southern elephant seal	SESV		Seal	<i>macrolini</i>	
Barmah Forest	BFV	BF		Culex and Aedes spp	Yes
Middelburg	MIDV	MID		Aedes spp.	Yes
Ndumu	NDUV	NDU		Aedes spp.	Yes
Sagiyama	SAGV	SF		Culex and Aedes spp	
Getah	GETV	SF	Cattle and horses	Culex and Aedes spp	
Ross River	RRV	SF	Rodents	Culex and Aedes spp	Yes
Bebaru	BEBV	SF		Culex spp	
Semliki Forest	SFV	SF			Yes
Mayaro	MAYV	SF		<i>Haemogous spp.</i>	Yes
				Psophora and Aedes spp.	
Una	UNAV	SF		Aedes aegypti and	
Chikungunya	CHIKV	SF	Humans, nonhuman primates	Aedes albopictus	Yes
O'nyong nyong	ONNV	SF	Humans	Anopheles spp.	Yes
Venezuelan equine encephalitis	VEEV	VEE	Rodents, horses, humans	Aedes, Culex and Psophora spp.	Yes
Everglades	EVEV	VEE	Birds	Culex spp.	
Tonate	TONV	VEE			
Mucambo	MUCV	VEE		Culex spp.	
Pixuna	PIXV	VEE			
Cabassou	CABV	VEE		Culex portesi	
Rio Negro	RNV	VEE		Culex spp.	
Eastern equine encephalitis	EEEV	EEV	Birds, rodents	Culex and Aedes spp.	Yes
Aura	AURAV	WEE		Culex spp.	
Buggy Creek	BCRV	WEE (recombinant)	Cliff sparrow	Oeciacus vicarius	
Fort Morgan	FMV	WEE (recombinant)	Birds	Oeciacus vicarius	
Highlands J	HJV	WEE (recombinant)	Birds	Culex melanura	
Sindbis	SINV	WEE	Birds	Culex and Aedes spp.	Yes
Trocaria	TROV	WEE		Culex serratus	
Western equine encephalitis	WEEV	WEE (recombinant)	Birds, rodents	Aedes and Culex spp.	Yes
Whataroa	WHAV	WEE	Birds	Culiseta and Culex spp.	

**Table 1: List of known Alphavirus species, with antigenic complex and known host and vectors, adapted from (Forrester et al., 2012)**

The twelve alphaviruses that infect humans (Table 1) cause acute febrile illness, as well as rashes, encephalitis and arthritis(Forrester et al., 2012). These viruses also infect terrestrial vertebrates including, mammals, birds that constitute their main reservoir. Among these twelve viruses, only Chikungunya virus (CHIKV) is transmitted from human-to-human by the anthrophilic *Aedes africanus*, *Aedes albopictus* and *Aedes aegypti* mosquitoes, independently of a wild animal reservoir(Forrester et al., 2012).

CHIKV, the etiopathological agent of chikungunya fever, is the most prominent human-infecting alphavirus, and a serious threat to public health (Weaver and Forrester, 2015). The first formerly described outbreak of Chikungunya fever happened in East Africa, along the coastal plateau of Mawia, Makonde and Rondi, in present day Tanzania (Lumsden, 1955) in 1952, although older outbreaks of the disease in the 18<sup>th</sup> and 19<sup>th</sup> century may have been mis-attributed to dengue fever (Halstead, 2015). Soon after, CHIKV was detected in Asia, and caused an outbreak in 1958 in Bangkok, Thailand (Hammon et al., 1960), then continuously causing outbreaks during the end of the 20<sup>th</sup> century (Weaver and Forrester, 2015). In 2004, a new strain of CHIKV appeared with an increased ability to be transmitted by the *Aedes albopictus* mosquito, which resulted in massive outbreaks in Kenya (Chretien et al., 2007; Kariuki Njenga et al.) and French Island of La Réunion (Vazeille et al., 2007). Since then, the distribution of *Aedes albopictus* has severely widened (Knudsen, 1995), especially in Europe where it was absent until the 1990s, due to the increased suitability of Europe's climate to *Aedes albopictus*, a consequence of climate change (Oliveira et al., 2021). As a result, small outbreaks due to local transmission have been reported in northern Italy (Rezza et al., 2007) and southern France (Grandadam et al.). European climate's suitability to *Aedes albopictus* is expected to extend further, which substantially increases concerns over incoming outbreaks of CHIKV as well as dengue virus (Oliveira et al., 2021).

Semliki Forest Virus (SFV) and Sinbis Virus (SINV) (Table 1), do not pose serious global threat to human health. Infection to SINV and SFV infection generally leads to milder but similar symptoms – illness, malaise, arthritis and encephalitis - compared to CHIKV (Braack et al., 2018) although SFV infection can, rarely, be fatal (Willems et al., 1979). Both are endemic in Africa (Braack et al., 2018), and have caused outbreaks (Mathiot et al., 1990), but SINV is also found in northern Europe (Lundström et al., 2019). SINV and SFV have both been extensively used to study translation and transcription regulation, as well as to understand host-pathogen interactions (Carrasco et al., 2018), and are the most studied model viruses for Alphavirus infection.

In the current chapter, I will detail the alphavirus replication cycle, essentially focusing on the most studied SINV, SFV and CHIKV, with a strong emphasis on SINV. I will present the SINV genome, its architecture and the roles of viral proteins. Finally, I will talk about host-pathogen interactions during alphavirus infection, with a focus on translation regulation. Otherwise specified, the mechanisms described here relate to alphaviruses infection in mammalian cells.

# 1. SINV life cycle

SINV virions are enveloped 70 nm particles (in diameter) coated with the E1 and E2 viral-encoded glycoproteins. SINV entry into the cell is driven by interaction of the envelope proteins E1 and E2 with cellular receptors expressed at the host cell membrane. In mammals, SINV entry involves DC-SIGN and L-SIGN C-type lectins(Klimstra et al., 2003; Wang et al., 1992), as well as Natural Resistance-Associated Macrophage Protein 2 (NRAMP2) metal ion transporter (Figure 1)(Rose et al., 2011), while in insects, only the NRAMP2 insect homolog NRAMP is expressed and serves as a point of entry(Rose et al., 2011). NRAMP2-deficient mouse embryonic fibroblasts (MEFs) but not wild type MEFs are refractory to SINV infection which suggests that NRAMP2 acts as the main receptor in mammals as well (Rose et al., 2011). DC-SIGN and L-SIGN C-type lectins only appear to contribute as co-receptors, in the form of attachment receptors(Klimstra et al., 2003). Other attachment receptors for SINV in mammals include laminin receptor RPSA(DiGiacomo and Meruelo, 2016; Wang et al., 1992) and phosphatidylserine receptor TIM-1(Jemielity et al., 2013; Moller-Tank et al., 2013). Interestingly, receptor and co-receptor are not fully conserved between alphaviruses and can vary significantly (reviewed in (De Caluwé et al., 2021)). As such, MARX8 is a receptor for members of the SFV complex of which CHIKV and SFV belong, but not for the more distantly related SINV and VEEV(Basore et al., 2019, 2019; Zhang et al., 2018b). Following receptor recognition, viral particles deliver their cargo through two possible mechanisms. Virions can enter through clathrin mediated endocytosis(Leung et al., 2011b), or by directly fusing with the plasma membrane(Vancini et al., 2013), then deliver a 11.7 kb capped and polyadenylated single-stranded RNA genome coated with the nucleocapsid protein C(Strauss and Strauss, 1994) into the cytoplasm(Figure 1)(Leung et al., 2011b). Nucleocapsid disassembly occurs through a peculiar mechanism that involves the 60S subunit of the ribosome. Strikingly, 60S are necessary and sufficient for nucleocapsid disassembly, yet it is not inhibited by the translation inhibitor puromycin, thus indicating that this process is independent of translation(Singh and Helenius, 1992). Uncapsidation involves capture of C by the ribosome 60S and relies on 18s rRNA interaction with a C subdomain(Wengler, 2009).

Following genomic RNA (gRNA) delivery, the first ORF (ORF1) of the gRNA is translated to produce the non-structural proteins, in the form of polyproteins nsP123 and nsP1234 in a ~9:1 ratio (Figure 1). This ratio is controlled by read-through of a stop codon downstream of nsP3 and further elongation into the nsP4 coding sequence. nsP1, -2, -3, and -4 assemble into invaginations of

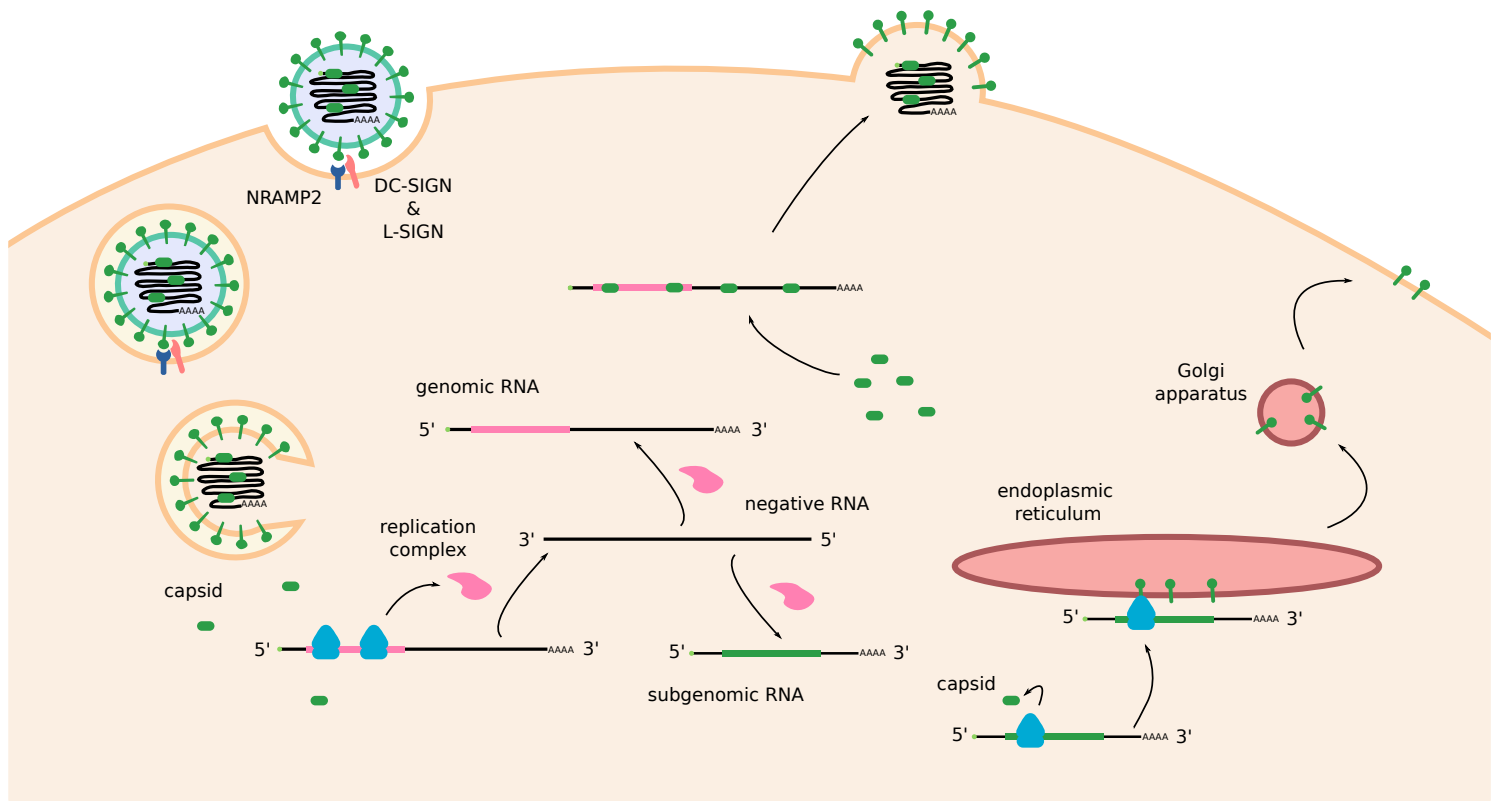


### Figure 1: Overview of the SINV replication cycle

SINV viral particle attachment is mediated by the receptor NRAMP2 and co-receptors DC-SIGN and L-SIGN. Following, clathrin-mediated endocytosis, acidification of the endosome leads to fusion of the endosome and viral membranes and delivery of the viral positive genomic RNA. Nucleocapsid disassembly allows translation of the non-structural proteins from the gRNA. Complexes made of the non-structural proteins replicate the gRNA into the complementary negative intermediate, which is then used to transcribe the gRNA and the sgRNA. Following translation of the capsid coding sequence, C is autocatalytically cleaved of the nascent peptide, exposing a signal recognition peptide in it. The SRP serves as a signal for endoplasmic reticulum addressing of the remainder of the ORF and the polyprotein precursor of the enveloped is translocated co-translationally. Envelope proteins are matured in the Golgi apparatus and exposed to the cellular membranes. Envelope proteins recruit C-covered gRNA to make new particles.



endosome-derived vacuoles called spherules(Pietilä et al., 2017), and synthesize the negative strand genomic RNA(Figure 1, 2). This negative strand RNA is then used as a template for the transcription of genomic and subgenomic positive viral mRNAs, using specific sites on the negative sense RNA as transcription start sites (Figure 1, 2). The positive subgenomic RNA bearing the second ORF (ORF2) is transcribed and translated as early as 4 hours post-infection and encodes the polyprotein C/E3/E2/6K/E1. In about 10% of cases, a -1 programmed ribosomal frameshifting signal drives a -1 frameshifting event inside 6K and produces the transframe protein (TF), in the form of the C/E3/E2/TF polyprotein (Figure 2).

Following C exposure outside of the ribosome exit channel, C is autocatalytically cleaved off by a protease moiety in the C-terminal of C(Hahn et al., 1985, 1989; Melancon and Garoff, 1987) and the remaining of the protein is co-translationally translocated in the ER membrane (Figure 1) (Carrasco et al., 2018). E1, E2 and E3 transit and are matured through the trans-Golgi network before exposition at the plasma membrane(Figure 1). There, C acts as a bridge between the viral genomic RNA and the glycoprotein E2 to form new viral particles that bud at the membrane.

## Structural proteins

### C

The nucleocapsid protein C is 264 amino acid in length and is encoded in ORF2 of the sgRNA in the form of the C/E3/E2/6K/E1 polyprotein(Mendes and Kuhn, 2018) (Figure 2). C is automatically self-cleaved off during translation of the polyprotein by the C-terminal chymotrypsin-like serine protease domain of C(Aliperti and Schlesinger, 1978; Choi et al., 1991; Hahn et al., 1985). This subsequently reveals a signal peptide and allows co-translational insertion of the remainder of the polyprotein into the double lipid layer of the ER(Kalkkinen et al., 1980; Mayne et al., 1984). C interacts with the gRNA and assembles into a core particle of 20 nm in diameter(Choi et al., 1991) composed of 240 copies of C(Fuller, 1987). Core particles uptake into budding virions is mediated by direct interaction between the nucleocapsid C and the envelope glycoprotein E2(Lee et al., 1996; Tang et al., 2011). Despite its obvious role in particles assembly (extensively reviewed in (Mendes and Kuhn, 2018)), activities of C in the cell that contribute to host-cell shut-off have been reported. New World alphaviruses EEEV and VEEV C, but not Old World alphaviruses SFV or SINV C, form a tetrameric structure with CRM1 and Importin  $\alpha/\beta$  and physically blocks the nuclear pore complex(Atasheva et al., 2010) which is associated with host-cell transcriptional shut-

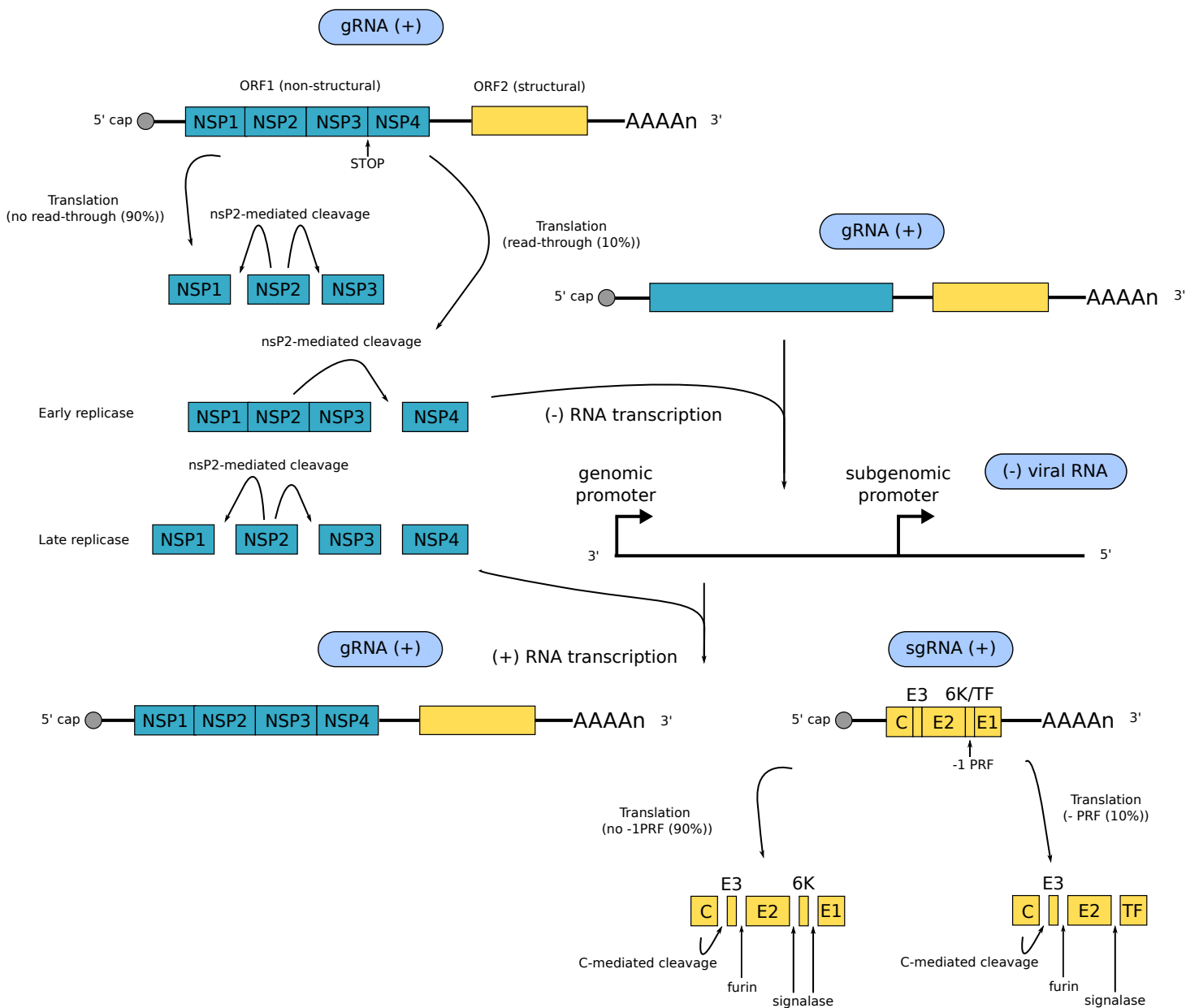


## Figure 2: SINV genome replication, translation and processing of non-structural and structural polyproteins

The genomic RNA (gRNA) has one open-reading frame (ORF1) encoding the non-structural proteins nsP1, 2, 3 & 4 in the form of a polyprotein. Translation read-through of a stop codon at the end of the nsP3 coding sequence allows translation of nsP4 in at a 10% occurrence. nsP2 mediates cleavage of nsP4 from the nsP123 polyprotein. nsP123 and nsP4 assemble to form a replication complex capable of synthesizing the negative strand RNA intermediate. Further cleavage of the nsP123 polyprotein renders it capable of transcribing the gRNA and subgenomic RNA (sgRNA) using the negative RNA as a template. The sgRNA possesses the second ORF (ORF2) encoding for C, E3, E2, 6K and E1. A -1 programmed ribosomal frameshifting signal within 6K is used to produce the TK protein at a 10% occurrence. C is autocatalytically cleaved-off the remainder of ORF2 co-translationally. This exposes an endoplasmic reticulum addressing peptide within E3 for co-translational translocation of the envelope proteins. The polyprotein is further processed by endogenous furin and signalase.

off(Garmashova et al., 2007a, 2007b). Recently, an additional role of C in inhibiting IRAK1-dependent TLR signalling was described(Landers et al., 2021). The direct interaction between C with TLR and IL-1R signal transduction pathways component IRAK1 was shown using Nanoluc BiMolecular Complementation(Landers et al., 2021). This in turns impairs IRAK1-dependent TLR signaling, as both expression of C and Sindbis infection were shown to limit cell response to TLR4 and TLR7 agonists. This suggests a role of alphaviruses C in evading innate immunity detection.

## E1, E2 and E3

Structural proteins E1, E2 and E3 are expressed from the C/E3/E2/6K/E1 polyprotein (Figure 2). After C autocatalytic and co-translational cleavage, a signal peptide present in the E3 N-terminal region addresses translation to the ER and results in co-translational translocation of the E3/E2/6K/E1 polyprotein. This precursor is cleaved at two locations by endogenous signalases in the lumen of the ER, producing the p62 precursor made of E3 and E2, 6K and E1(Strauss and Strauss, 1994). E1 and p62 form an heterodimeric complex that constitutes an intermediate form of the viral envelope. p62 is later cleaved at the Golgi apparatus through a pH dependent process catalysed by furin(Lobigs and Garoff, 1990; Zhang et al., 2003). Deletion of E3 abrogates E1-E2 complex formation and mutations in the E3-E2 cleavage site prevents fusion of the viral particule with the cell membrane(Lobigs et al., 1990; Sjöberg et al., 2011). Although E3 is cleaved from E2 during transit through the trans-Golgi, it remains closely associated with E2 and protects an “acid-sensitive region” of E2(Voss et al., 2010). E3 thus has a double role in virion maturation: it first stabilizes E2 in a conformation that allows the p62-E1 complex to form, then prevents premature low pH conformation changes of the spike complex during transit through the trans-Golgi network, so that only low pH-mediated endocytosis of the virion provokes the final conformational changes needed for viral entry. E1, E2 and E3 are subject to multiple post-translational modifications. (Sefton, 1977; Sjöberg et al., 2011). E1 is glycosilated at positions 139 and 245, E2 is glycosilated at positions 196 and 318 while E3 is monoglycosilated at position 13(Garoff et al., 1990; Jose et al., 2009). When produced in insect cells, all sites are glycosilated by high-mannose while in mammalian cells, glycosilation can be both high-mannose and complex sugars, depending on accessibility of the glycosilation site(Hsieh and Robbins, 1984; Hsieh et al., 1983; Lancaster et al., 2016). The role of these glycosilations on viral infectivity remains unclear: mutations of the E2 glycosilation sites increases viral titer and virulence *in vivo* while mutations of E1 glycosilation sites impair viral replication(Knight et al., 2009). E2 is also palmytoylated at positions 396, 416 and 417, which is postulated to contribute to the reorientation of the C-terminal region of E2 after 6K/TF cleavage from a trans-membrane situation to a membrane-anchored cytoplasmic configuration and to

contribute to proper E2 folding(Ivanova and Schlesinger, 1993). This C-terminal domain is involved in direct interaction with the C protein and promotes particle assembly(Wilkinson et al., 2005).

## 6K/TF

The 6K and TF proteins are respectively generated from signalase cleavage of the polyproteins C/E3/E2/6K/E1 and C/E3/E2/TF (Figure 2). TF is produced by -1 programmed ribosomal frameshifting within 6K coding sequence which occurs at a conserved UUUUUUA slippery sequence followed by a stem-loop structure at an estimated 10% rate(Firth et al., 2008). As a consequence, 6K and TF share a significant N-terminal amino acid sequence with varying length in the Alphaviruses genus. 6K and TF are both translocated in the ER membrane during translation of their precursor polyproteins. TF, but not 6K, is palmytoylated on a cluster of cystein residues that is located at the end of the shared sequence(Ramsey et al.). This is thought, similarly to E2, to anchor this TF region to the cytoplasmic side of the ER membrane and to contribute to virion incorporation of TF(Ramsey et al.). The role of 6K and TF remain for the most part enigmatic. 6K is a viroporin, a type of virus-induced ion channel, and leads to membrane permabilization(Sanz and Carrasco, 2001). How this contributes to viral fitness is for the most part unclear and has been discussed elsewhere(Ramsey and Mukhopadhyay, 2017).

## Non-structural proteins

Non-structural proteins of alphaviruses are expressed early in infection by translation of ORF1 of the genomic RNA. This produces two different polyproteins nsP123 and nsP1234 which differ by the presence of nsP4(Strauss et al., 1983). In 90-95% of cases, translation of ORF1 stops at the end of nsP3, producing nsP123 (Figure 2). In the remaining cases, the UGA stop codon that signals the end of elongation is bypassed and can be suppressed by several aminoacyl-tRNAs(Li and Rice, 1993). This leads to read-through of the stop-codon and translation of nsP4, making a nsP1234 polyprotein precursor. nsP1234 processing starts by autocatalytic cleavage of nsP4 from the remainder of the protein thanks to nsP2 protease activity (Figure 2). nsP123 is subsequently cleaved by the same activity, releasing nsP1, nsP2, and nsP3 into the cell. Early in infection, most of nsP123 remains as a non-processed polyprotein to catalyse, together with nsP4, the synthesis of negative strand viral RNA from the positive strand RNA template. Later, after nsP123 autoproteolysis, a nsP1, nsP2, nsP3 and nsP4 complex exclusively catalyses positive transcription(Lemm et al., 1994; Shirako and Strauss, 1994). These nsP-containing replication complexes are called spherules(Pietilä

et al., 2017). The vast majority of alphavirus non-structural proteins exist in their cleaved form at later time post infection, are located outside of spherules and have other functions that are detailed below. Interested readers are encouraged to read these recent reviews for a more thorough discussion of their roles in Alphavirus replication (Abu Bakar and Ng, 2018; Pietilä et al., 2017; Rupp et al., 2015).

## nsP1

Alphaviruses gRNA and sgRNA are protected by a type-0 m<sup>7</sup>G(5')ppp(5')ApUp- cap from the cell RNA degradation machinery (Hefti et al., 1976; Pettersson et al., 1980). This cap structure is also involved in cap-dependent initiation of translation of viral mRNAs. nsP1 is ~541 amino acid in length and is the mRNA capping enzyme that caps these mRNAs, in conjunction with nsP2 (Ahola and Kääriäinen, 1995; Cross, 1983; Laakkonen et al., 1994). Capping starts with the removal of the 5' terminal phosphate group of the viral RNA by the triphosphatase activity of nsP2, leaving a biphosphate 5' terminal adenosine (Vasiljeva et al., 2000). Then, nsP1 catalyses GTP addition to the 5' end of the mRNA through its guanylyltransferase function, which results in a 5'-5' triphosphate linkage. Finally, nsP1 methylates the 5' terminal guanosine to form the type-0 capped mRNAs. This whole process occurs within spherules composed of nsP1, 2, 3 and 4, where viral RNAs are replicated (Pietilä et al., 2017, 2018). Spherules are anchored to endosome-derived vacuoles by multiple cysteine S-palmitoylations on nsP1 (Ahola et al., 2000; Laakkonen et al., 1996; Peränen et al., 1995; Spuul et al., 2007; Zhang et al., 2019) whose deposition is catalyzed by palmitoyl acyltransferases ZDHHC2 and ZDHHC9 (Zhang et al., 2019) in the case of CHIKV at least. Intriguingly, and contrary to nsP2 and nsP3, nsP1 only displays localization at the endosomal membrane (Salonen et al., 2003). Given that nsP 1, 2 and 3 are produced in equimolar ratio and that nsP2 and nsP3 essentially display nuclear and cytoplasmic foci localization respectively (Salonen et al., 2003) this would leave the majority of membrane-associated nsP1 devoid of nsP2 and nsP3, and raise the question of its role in this context. A possible answer to this question came from a recent structure of CHIKV nsP1 capping pores (Jones et al., 2021). CHIKV nsP1 was shown to assemble as a dodecameric pore complex anchored to the membrane. If spherules require 12 copies of nsP1, this explains how the majority of nsP2 and 3 can be localized elsewhere. Also, the requirement of 12 nsP1 copies to form a capping core at the membrane somewhat aligns with the approximate 10% readthrough efficiency that produces the RNA-dependent RNA polymerase nsP4. This suggests that spherules are made of 12:1:1:1 nsP1/nsP2/nsP3/nsP4 complexes, leaving approximately 90% of nsP2 and nsP3 free for other tasks while virtually all nsP4 produced is localized in spherules. The

role of nsP1 in viral RNA capping makes it essential to alphaviruses life cycle, and accordingly, inhibition of its guanylation activity leads to a marked decrease in CHIKV replication(Delang et al., 2016).

## nsP2

nsP2 is a ~807 (SINV) amino acid long protein with three major enzymatic activities: helicase, protease and phosphatase. The protease domain is involved in autocatalytic processing of the nsP123 and nsP1234 polypeptides(Vasiljeva et al., 2003)(Figure 2). It is a papain-like protease domain that lies in the C-terminal region of nsP2(Ding and Schlesinger, 1989; Hardy and Strauss, 1989; Strauss et al., 1992; Takkinen et al., 1991). nsP2-mediated cleavage occurs in a sequential fashion, with cleavage of nsP4 from the remainder of the polyprotein(de Groot et al., 1990) if applicable, then nsP3(Hardy and Strauss, 1989), and finally between nsP1 and nsP2(Hardy and Strauss, 1989). This mechanism coordinates the release of the non-structural proteins: early in infection, non-structural proteins mostly exist in nsP123+nsP4 spherules and participate in negative strand synthesis(Lemm and Rice, 1993a, 1993b). Then, nsP12+nsP3+nsP4 spherules transcribe the positive viral mRNAs and lose their ability to synthesize the negative RNA. Only at later time of infection can free nsP2 and nsP3 be found in other compartments. The helicase domain is thought to participate in RNA replication where it unwinds secondary structures and allows the nsP4 RNA-dependent RNA polymerase (RdRp) to progress along the RNA(Das et al., 2014; Gomez de Cedrón et al., 1999). Mutations in the NTPase domain(Rikkonen et al., 1994), that provides energy for RNA unwinding, abolish helicase activity and indicate that this function is critical for viral replication(Gomez de Cedrón et al., 1999; Rikkonen, 1996). As mentioned before, nsP2 displays a triphosphatase activity involved in viral RNAs capping in cooperation with nsP1(Vasiljeva et al., 2000). The C-terminal region of nsP2 also harbors a nuclear localization sequence and consequently approximately half of nsP2 locates in the nucleus later in infection(Peränen et al., 1990; Rikkonen, 1996; Rikkonen et al., 1992). nsP2 of all SINV, SFV and CHIKV localizes in the nucleus and promotes the degradation of RPB1, a component of the RNA polymerase II complex, by an ubiquitin-dependent pathway(Akhrymuk et al., 2012). Although diverse mutations in nsP2 affect this activity, the precise mechanism by which this happens has not been resolved(Akhrymuk et al., 2012). Additionally, nsP2 of SFV, VEE and SINV have been reported to either cosediment and/or copurify with ribosomes (Atasheva et al., 2007; Montgomery et al., 2006; Ranki et al., 1979). In particular, RPS6/eS6-Flag immunoprecipitation copurifies VEE nsP2(Montgomery et al., 2006). Co-expression of nsP2 of VEE, SINV and SFV and RPS6 from human in a cell-free translation

system shows copurification of the two proteins as well, meaning that this interaction exists independently of RPS6 integration into ribosomes, and suggesting that RPS6 is the direct site of interaction for nsP2. Finally, VEE nsP2 is able to interact with *Aedes albopictus* RPS6, and as such, RPS6-nsP2 interaction appears to be conserved with different Alphaviruses in different hosts (Montgomery et al., 2006). More recently, yeast two-hybrid screening of CHIKV nsP2 interactions gave a positive signal for RPS6 and RPL4/uL4 interaction, suggesting again that RPS6 is nsP2 interaction site on the ribosome (Bourai et al., 2012). Interestingly, RPS6 becomes highly phosphorylated during mTOR activation, the effect of which leads to translation repression (Meyuhas, 2015a). As such, RPS6 phosphorylation has been postulated to participate translation inhibition, but this remains largely unclear (Meyuhas, 2015a). Whether mTOR is activated during *Alphavirus* infection remains somewhat unclear. Conflicting results report that SFV does induce RPS6 phosphorylation (Thaa et al., 2015) while other reports that it does not (Montgomery et al., 2006), with CHIKV only moderately activating mTOR (Thaa et al., 2015). As for SINV, SINV infection does not induce RPS6 phosphorylation in mammalian cells (Mohankumar et al., 2011) yet does so in arthropod cells (Patel and Hardy, 2012). This is extremely intriguing, as the vast majority of viral infection give rise to RPS6 phosphorylation, essentially through modulation of the mTOR pathway (Li, 2019). The role of this interaction between nsP2 and the ribosome has not been resolved. Current hypotheses view this interaction as a possible way for nsP2 to program the ribosome for the translation of the viral mRNAs, or to participate in host translational shut-down (Montgomery et al., 2006). A possible role for this interaction in sgRNA translation is proposed further down.

### nsP3

The ~549-556 (SINV) amino acid long nsP3 is an essential component of spherules (Gorchakov et al., 2008; Hahn et al., 1989) and is required for negative sense and subgenomic RNA synthesis (LaStarza et al., 1994; Wang et al., 1994), but the vast majority of free nsP3 displays a cytoplasmic localization in the form of granules (Gorchakov et al., 2008; Jayabalan et al., 2021; Salonen et al., 2003). This has been linked to a role of nsP3 in inhibiting stress granules formation during late Alphavirus infection (Götte et al., 2018; Jayabalan et al., 2021), at least for SINV, SFV and CHIKV (Kim et al., 2016). This role of nsP3 is detailed further down below.

## nsP4

nsP4 is the RNA-dependent RNA polymerase of Alphaviruses and is ~610 amino acid in length. It participates in synthesis of both negative and positive sense viral RNAs in context of nsP1-2-3 containing spherules(Figure 1, 2)(Pietilä et al., 2017). No other functions in Alphaviruses life cycle have been reported.

## 2. Introduction to canonical translation initiation

Eukaryotic translation is a complex process that involves an mRNA, the 40S small subunit of the ribosome, the 60S large subunit of the ribosome, as well as several translation factors and the involvement of transfer RNAs (tRNAs) that deliver the successive amino acids needed for protein synthesis. Translation is divided into four successive steps. It starts with the initiation phase, where the 40S is recruited to the 5' extremity of the mRNA and scans the mRNA in the 3' direction until it finds an AUG triplet that signals the start of the translation elongation phase and the 60S is recruited. During elongation tRNAs cognate to consecutive triplets deliver the corresponding amino acid to be incorporated in the growing polypeptide chain. UAG, UGA and UAA triplets signal the end of the elongation phase. The polypeptide chain is released and the two ribosomal subunit dissociate from one another and from the mRNA in a process called termination. The 40S then enters the recycling step which prepares the 40S subunit for the subsequent round of translation.

Translation regulation is generally considered to be controlled essentially at the initiation phase, a consideration that remains valid overall when addressing viral-host interactions. A few rare cases of translation elongation control have been described, and are discussed in Chapter II. Alphavirus infection is no different and significant alteration to the way translation initiation happens in the cell are present during infection. To better detail how this step differs from that of healthy cells, the canonical pathway of eukaryotic translation is detailed below and Figure 3.

Cellular mRNAs harbor a 5' "cap" consisting of an 3'-5' oriented methylguanosine ligated to the 5' end of the mRNA by a triphosphate linker, denoted m<sup>7</sup>GpppN. This cap protects mRNAs from the degradation of 5'-3' endonucleases and serves as a mark of translatable RNAs. mRNAs are additionally extended in their 3' direction in the form of a polyA sequence of varying length, it too being a mark of mRNAs identity. Cytoplasmic mRNAs associate with the eIF4F complex made of eIF4E, eIF4A and eIF4G by direct binding of eIF4E to the cap while the polyA tail is covered by



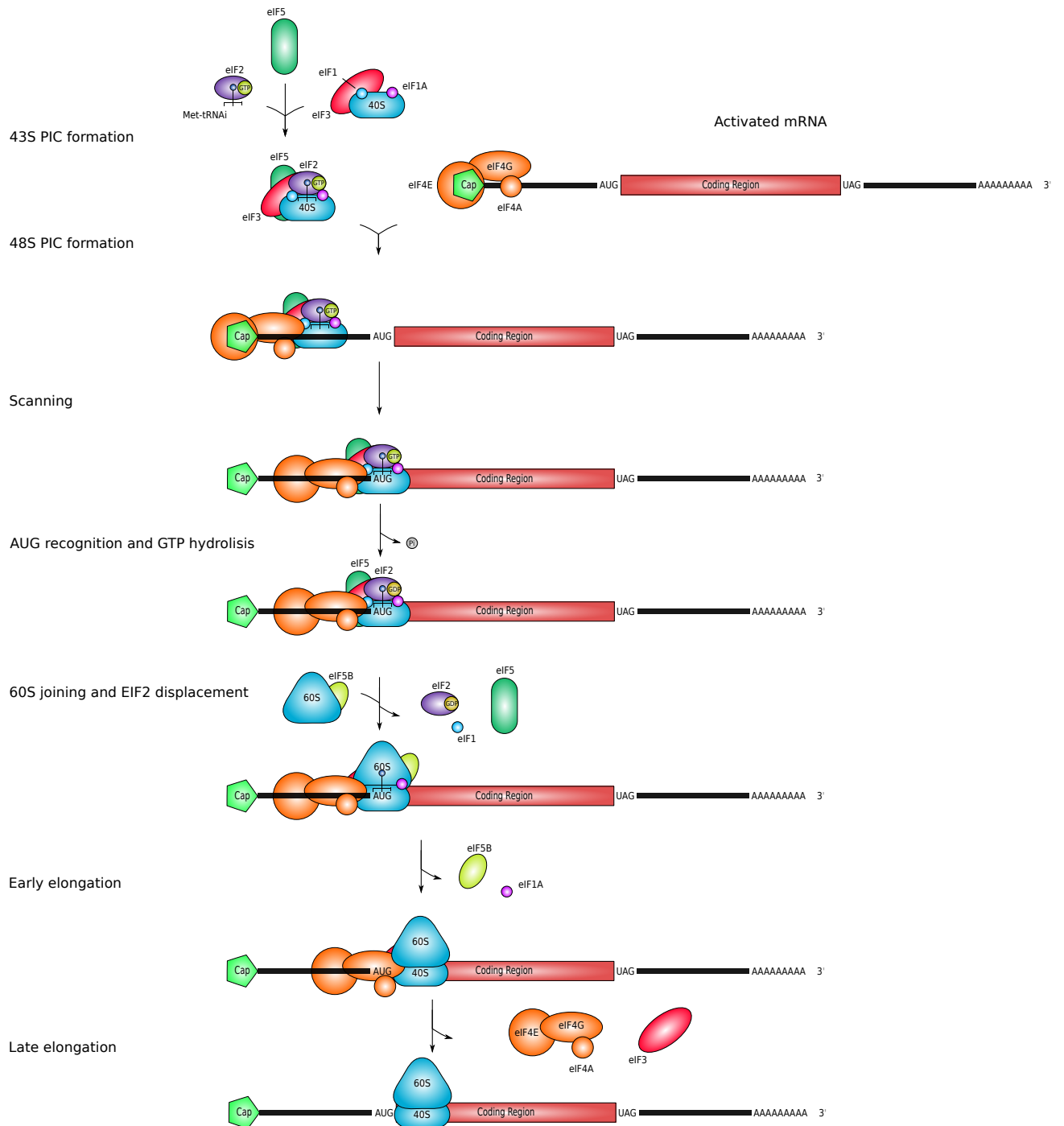


**Figure 3: The mechanism of canonical translation initiation.**

Translation initiation is a complex mechanism involving the 40S small ribosomal subunit, the 60S large ribosomal subunit and multiple additional proteins called initiation factors.

PABP(Jackson et al., 2010). Post-recycling 40S subunits are associated with translation initiation factors eIF1, eIF1A and the 13-protein eIF3 complex. This complex further associates with eIF5 and the ternary complex made of the GTP bound eIF2 trimer and the Met-tRNA<sub>i</sub> initiator tRNA to form the 43S pre-initiation complex (43S PIC), a process stimulated by eIF1A. The 43S PIC is then recruited to eIF4F-bound mRNAs at the 5' extremity of the mRNA by direct interaction of the scaffolding eIF4G with the 40S, eIF3, and PABP to form the 48S PIC. The current model of 43S PIC recruitment is a “slotting” mechanism where the 43S PIC associates with eIF4F at its 3' (Brito Querido et al., 2020). The 48S then progresses in the 3' direction in a process called scanning, whose directionality is provided by ATP hydrolysis by the RNA helicase eIF4A. Indeed, the 40S is able to slide in both direction, but eIF4A acts as a ratchet to prevent movement in the 5' direction(Brito Querido et al., 2020). It is unclear if eIF4E remains attached to the cap or not, but given that eIF4E stimulates eIF4A activity(Feoktistova et al., 2013), it most likely remains bound to the rest of the eIF4F complex(Bohlen et al., 2020). During scanning RNA secondary structures located at the 3' of the 48S are likely unwound by other helicases such as DHX29(des Georges et al., 2015) or even an additional eIF4A. The 48S scans the 5'UTR of the mRNA until an AUG triplet with eIF1 preventing mis-recognition of non-AUG triplet. AUG recognition is additionally controlled by the neighboring nucleotides with an optimum context of GCC(A/G)CCAUGG(Kozak, 1987). This preference is postulated to be provided by direct contact between the eIF2 $\alpha$  subunit of eIF2 and/or interaction of the surrounding sequence with AA<sup>1818-1819</sup> of helix 44 of the 18S rRNA(Pisarev et al., 2006). Recognition of the AUG triplet is accomplished by base-pairing of the AUG bases by the complementary tRNA anti-codon loop. This process induces hydrolysis of the eIF2 $\alpha$ -bound GTP and is catalysed by eIF5. Following GTP hydrolysis by eIF2, eIF1 and eIF5 are released and eIF5B mediates 60S joining(Pestova et al., 2000). EIF5B and eIF1A are then released while eIF4F and eIF3 remain associated with the elongating ribosome and are progressively lost during the first rounds of translation(Bohlen et al., 2020).

### 3. Host-cell shut-off in alphaviruses infection

Alphavirus infection provokes a profound host-cell gene expression arrest(Strauss and Strauss, 1994), partially, but not entirely explained by nsP2-induced degradation of the RNA polymerase II subunit RPB1 mentioned earlier(Akhrymuk et al., 2012). This effect on transcription inhibition is indeed preceded by an earlier translational arrest that stems from the phosphorylation of the eIF2 $\alpha$

subunit of the translation factor eIF2, and is responsible for the bulk of host-cell gene expression arrest early in infection.

## Phosphorylation of eIF2 $\alpha$ following alphavirus infection

eIF2 $\alpha$  becomes phosphorylated during infection with alphaviruses, which is a common feature of host-cell shut-off for many viruses. eIF2 $\alpha$  phosphorylation can originate from the activation of four different pathways involving PKR, PERK, GCN2 or HRI. eIF2 $\alpha$  phosphorylation stabilizes interaction of eIF2 $\alpha$  with the GTP recycling factor eIF2B, which renders eIF2 $\alpha$  unable to exchange GDP with GTP. Given that initiation codon recognition necessitates GTP hydrolysis, this prevents recognition of the initiation codon and the recruitment of the 60S large ribosome subunit, resulting in stalled initiating 48S ribosomes that trigger the formation of stress granules (McCormick and Khapersky, 2017). PKR (EIF2AK2) recognizes dsRNA, an intermediate of positive RNA viruses replication, as a signal of viral infection (McCormick and Khapersky, 2017). Following dsRNA recognition, PKR phosphorylates itself and eIF2 $\alpha$  leading to an inactive form of eIF2 $\alpha$  in translation. PERK (EIF2AK3) responds to ER stress, which is the accumulation of unfolded proteins in the lumen of the ER. Phosphorylation of eIF2 $\alpha$  by PERK reduces the global level of translation, thus alleviating the burden of intense ER translation onto the folding enzymes that reside in the ER. Finally, HRI (EIF2AK1) responds to oxidative stress, while GCN2 is triggered by an excess of uncharged tRNAs, a consequence of amino acid starvation.

Cells expressing a non-phosphorylatable mutant eIF2 $\alpha$  (S51A) are resistant to the alphavirus-induced shut-off (McInerney et al., 2005), indicating that eIF2 $\alpha$  phosphorylation is essential for the shut-off to occur. PKR activation has been the major pathway that contributes to translational shutdown consecutive to alphaviruses infection. Indeed, PKR becomes phosphorylated following SINV infection in MEFs (Gorchakov et al., 2004; Ventoso et al., 2006). Contrary to eIF2 $\alpha$  mutant cells though, PKR deficient MEFs still see the decrease in host-cell protein expression, despite a massively reduced levels of phosphorylated eIF2 $\alpha$  compared to WT cells (Gorchakov et al., 2004; Ventoso et al., 2006). This is likely explained by the additional participation of GCN2. The primary function of GCN2 is the recognition of uncharged tRNAs, but surprisingly, GCN2 is also activated by SINV RNA *in vitro* (Berlanga et al., 2006). While PKR is activated by both the SINV RNA and polyI:C, GCN2 activation was shown to be specific for SINV RNA, and a specific region inside nsP1 coding sequence, was found to be the GCN2 activating RNA (GAR). GCN2 deficient cells present a decreased basal level of phosphorylated eIF2 $\alpha$  and sustain the translation of SINV structural proteins as early as 4 hpi, compared to 8 hpi in WT cells (Berlanga et al., 2006). In

infected GCN2 mutant cells though, the level of phosphorylated eIF2 $\alpha$  and the strength of the translational shut-off ends up higher than in WT cells(Berlanga et al., 2006). This suggests that in GCN2 deficient cells, the reduced levels of eIF2 $\alpha$  phosphorylation early in infection increases the translation of the eIF2 $\alpha$  sensitive gRNA and promotes viral replication earlier than in WT cells, which consequently leads to earlier and higher activation of PKR activation.

In summary, both GCN2 and PKR mediated eIF2 $\alpha$  phosphorylation appear critical in alphaviruses infection host-cell shut-down. Early in infection, GCN2 recognizes the gRNA through a sequence inside nsP1 coding region and induces the phosphorylation of eIF2 $\alpha$ . This may slow down – or even abrogates at low MOI – viral replication(Boersma et al., 2019). If the infection is successful and productive replication is in place, PKR recognizes the replication dsRNA intermediate and further increases the level of eIF2 $\alpha$  phosphorylation, which triggers stress granule assembly. As such, depending on the cell type and its ability to robustly display certain types of innate immune response, and on the amount of viruses delivered, alphaviruses can skip certain checkpoints of infection. This is echoed by a recent report indicating that successful replication upon infection of a cell with a single viral particle does not constitute the norm in positive RNA viruses infection in cultured cells(Boersma et al., 2020). As many as 20% of cells infected by coxsackievirus B3 are able to arrest viral replication at a stage where the amount of dsRNA is too low to induce PKR activation and as such translation shut-down in the very first step of infection was shown to be critical to restrict replication (Boersma et al., 2020).

## Destabilization of stress granules by nsP3

Stress granules are aggregates composed of many RNA-binding proteins (RBPs) and 48S pre-initiation complex in complex with mRNA, as well as many translation initiation factors, such as eIF3b, and prevent mRNAs from degradation(McCormick and Khapersky, 2017). They form (among other) in response to stress-induced inhibition of translation and are thus very frequent during viral infection, especially for viruses that induce translational shut-down(McCormick and Khapersky, 2017). Stress granules are an important part of host-cell response to infection as they sequester 40S small ribosomal subunits and translation initiation factors that viruses need for their own translation. In consequence, many viruses have evolved mechanisms to impair stress granules formation(Reineke and Lloyd, 2013). Alphaviruses are no exception(McInerney et al., 2005), and do so by a mechanism essentially involving nsP3(Fros et al., 2012; Jayabalan et al., 2021; Panas et al., 2012). SINV and SFV nsP3 interacts with the RasGAP SH3 domain G3BP1 and

G3BP2(Gorchakov et al., 2008; Panas et al., 2012), two essential components of stress granules(Kedersha et al., 2016; Matsuki et al., 2013; Tourrière et al., 2003). nsP3 features three main domains: a N-terminal macrodomain with phosphatase activity and nucleic acid binding ability, an alphavirus unique domain (AUD), and a C-terminal hypervariable domain (HVD). nsP3 interaction with G3BP1 and G3BP2 is mediated on the nsP3 side by the C-terminal HVD(Panas et al., 2014), by the use of a FGDF repeat peptide motif(Panas et al., 2015), which associates with N-terminal NTF2 domain of G3BP1 and -2 (Cristea et al., 2006). This leads to the formation of nsP3 condensates that sequester both G3BP1 and G3BP2 in the cytoplasm(Jayabalan et al., 2021). However, the HVD motif alone cannot suppress stress granules formation alone and rather cooperates with the macrodomain, which was found to possess an ADP-ribosylhydrolase activity(Jayabalan et al., 2021). ADP-ribosylation is the post-translational addition of one or several ADP-ribose into proteins. They are very abundant in stress granules sequestered proteins, and contribute to stress granules formation and maintenance(Duan et al., 2019; Leung et al., 2011a). As such, the macrodomain is thought to induce destabilization of stress granules while the HVD domain sequesters its essential components G3BP1 and G3BP2(Jayabalan et al., 2021). The nsP3 granules involve other RNA binding proteins that are canonical component of stress granules. TIA1 and HuR/ELAVL1 are mostly found in the nucleus, and participate in stress granules assembly(McCormick and Khapersky, 2017), but are relocalized in the cytoplasm during alphavirus infection(Dickson et al., 2012; Sanz et al., 2015; Sokoloski et al., 2010) and are integrated in nsP3 granules(Jayabalan et al., 2021).

In summary, alphavirus infection triggers eIF2 $\alpha$  phosphorylation and stress granules formation early in infection. Later, when levels of free nsP3 are high enough, nsP3 destabilizes stress granules by hydrolysis of ADP-ribosylation, and retains most RBPs, but not 43S PIC and translation initiation factors, in nsP3 granules, alleviating the pressure in ribosome availability and sustaining viral protein synthesis.

#### 4. Unconventional mode of translation initiation of the sgRNA

Alphaviruses gRNA and sgRNA are translated in fundamentally different ways. Although transcription of the gRNA is sustained at late stages of the replication cycle, its translation decreases after the early phase of infection, concomitantly with the translation shutoff of host-cell mRNAs(Strauss and Strauss, 1994). In contrast, translation of the sgRNA is unaffected by the

global translational shutoff, indicating that its mechanism of translation is strikingly different than that of the gRNA. To better understand this phenomenon, Van Steeg and colleagues investigated in 1981 the translational activity of gRNA, sgRNA and cellular mRNAs in an *in vitro* reconstituted translation system, and programmed it with lysates from infected and uninfected cells. Similarly to what had been observed in infected cells, they found that although translation of the gRNA and cellular mRNAs was decreased when lysates from infected cells were used, translation of the sgRNA was unaffected(van Steeg et al., 1981a, 1981b). This showed that something in the identity of the sgRNA confers resistance to the host-cell shut-off that the gRNA is devoid of. Since then, the spotlights have been focused on the sgRNA, and although many aspects of sgRNA translation have been lightened up, most of it remains in the shadows.

## Translation of the sgRNA is mediated by a non-canonical cap-dependent process

Both the gRNA and sgRNA are protected at their 5' termini by a type-0 cap structure where only the cap is methylated and not the following nucleotides(Dubin et al., 1979). This is in contrast with host-cell mRNAs which are often protected by type-1 or type-2 cap structures where the first and second nucleotide after the cap are also methylated(Pelletier et al., 2021). However, because both the gRNA and sgRNA share the type-0 cap, this difference versus host-cell mRNAs is not enough to explain the specific mechanism by which the sgRNA is translated.

Decapping of the sgRNA decreases its ability to be translated in *in vitro* translation systems, similarly to both gRNA and host-cell mRNAs(van Steeg et al., 1981a). This is not due to increased sensitivity to RNases present in the system because the EMCV mRNAs, whose translation is dependent on an IRES sequence, is not affected by this procedure(Martinez-Salas et al., 2018; van Steeg et al., 1981a). This suggests that translation of the sgRNA occurs through a cap dependent process. Uncapped replicons harboring the Luciferase reporter gene in fusion with the viral protein C are not able to drive Luciferase expression when transfected in cells(Sanz et al., 2010). This is in contrast with replicons where the sgRNA leader has been replaced with PV, EMCV, and HCV IRESs that do drive translation of the downstream reporter, indicating that the sgRNA does not contain an IRES and requires cap recognition by the translation machinery. Yet, somehow, the cap-dependent translation process of the sgRNA does not appear to be dependent on eIF4E. The PI3K/Akt/mTOR signaling pathways controls many aspects of translation regulation and in

particular the phosphorylation state of the eIF4E binding protein 4E-BP (Mohankumar et al., 2011). In its unphosphorylated state, 4E-BP stably binds eIF4E and inhibits eIF4E-dependent cap-driven translation. SINV infection inhibits the PI3K/Akt/mTOR pathway and reduces the level of phosphorylated 4E-BP. Further inhibition of the PI3K/Akt/mTOR pathway by Torin which leads to almost complete disappearance of phosphorylated 4E-BP does not affect SINV replication (Mohankumar et al., 2011). Altogether, these results suggest that translation of the sgRNA is a cap-dependent, yet eIF4E independent translation pathway.

The unusual requirements for initiation factors has prompted comparison with other mRNAs with non-canonical initiation pathways. As such, the proto-oncogene c-Jun mRNA shares some similarities with the sgRNA, and a partial overlap between these mechanisms has been invoked (Carrasco et al., 2018). The c-Jun protein accumulates in glioblastoma despite no increase in mRNA expression compared to non malignant cells, and this accumulation is not due to an increased stability of the protein (Blau et al., 2012). This points to an increase in translation of the c-Jun mRNA in malignant cells. Similarly to the sgRNA, inhibition of the PI3K/Akt/mTOR pathway by rapamycin and LY294002 does not affect c-Jun translation. This indicates a cap-independent, or at least eIF4E independent mechanism. When placed in a bicistronic vector upstream the second ORF, the c-Jun 5'-UTR drives the translation of the downstream ORF, and hence acts as an IRES. Later, it was found that c-Jun can also be translated by a cap-dependent mechanism, albeit an eIF4E-independent one, through specific recognition of the cap by the eIF3 component eIF3d (Lee et al., 2015, 2016). eIF3 4-thiouridine PAR-CLIP precipitates a subset of mRNAs with eIF3a, eIF3b, eIF3d and eIF3g being involved in direct contacts with the mRNAs, as revealed P<sup>32</sup> labelling of RNAs. This subset of mRNAs contains, among others, BTG1 and c-Jun mRNAs. Importantly, PAR-CLIP data highlighted the specific region bound by eIF3, and reporters with deletion in these regions where constructed for c-Jun and BTG1, and either transfected in cells or translated *in vitro*. Surprisingly, deletion of the eIF3 binding domain decreased c-Jun translation but drastically increased BTG1 translation *in vivo*. Results obtained *in vitro* were identical, and competition of cap-dependent translation by free m<sup>7</sup>G cap abrogated translation of c-Jun and BTG1, pointing to a cap-dependent mechanism. SHAPE analysis and RNA structure prediction indicated that eIF3 binding sites were conserved, yet highly dissimilar, stem-loops for both mRNAs. Although both loops were shown to be indispensable for the eIF3-mediated translation control, recombinant eIF3 was only able to bind the c-Jun stem-loop, not the BTG1 stem-loop. Fractionation of RRL programmed with c-Jun mRNAs show that the 48S complex translating this mRNA is depleted in all eIF4F factors when compared to ACTB 48S fraction (Lee et al., 2016). This is

intriguing because c-Jun translation is cap-dependent(Lee et al., 2015) and in fact, the cap-dependency is provided by an unusual mechanism in which eIF3d directly recognizes the cap(Lee et al., 2016). Indeed, eIF3d possesses a cap-binding domain and is able to bind the c-Jun cap directly, an interaction that is sensitive to m<sup>7</sup>G cap competition. Glucose-deprivation stimulates eIF3-mediated translation of the c-Jun mRNA through a decrease in eIF3d phosphorylation levels(Lamper et al., 2020) and eIF3d was found phosphorylated on two positions, Ser258 and Ser259. The role of eIF3d phosphorylation was investigated using mutant cell lines whose eIF3d was substituted for mutants eIF3d. eIF3d binding ability of c-Jun mRNA was decreased for the phosphomimetic mutant (S258D/S259D) while the phosphoinhibitory mutant (S258N/S259N) bound c-Jun mRNA more. Examination of c-Jun mRNA distribution in polysome gradients in mutant cells further validated that eIF3d phosphorylation inhibits c-Jun translation. The source of the decreased phosphorylation of eIF3d was identified as the CK2 kinase, whose activity is decreased in glucose-deprivation conditions. Finally, eIF3d was found to recognize the cap of many transcripts, among which the Raptor mRNA, who harbors a stem-loop with similar structures as c-Jun (U-rich loop, C-rich bulge), which are both similar to HCV IRES domain IIIb(Walker et al., 2020) and are thought to confer eIF3 binding by similarity(Lamper et al., 2020; Lukavsky, 2009). Similarly to c-Jun, disruption of this stem-loop in the HCV IRES abrogates eIF3d cap binding. These studies paint a complicated picture of eIF3 specialized translation. eIF3 PAR-CLIP and eIF3d cap-binding targets only show partial overlap and not all target mRNAs have the stem-loop structure that is critical in Raptor and c-Jun for eIF3-mediated translation. Even more puzzling is the fact that some eIF3 bound transcripts, like BTG1, are actually translationally repressed by eIF3 binding(Lee et al., 2015). Finally, while the eIF3-mediated translation pathways of c-Jun is clearly cap-dependent, c-Jun 5'UTR can function as an IRES in bicistronic reporters. It has been reported that any sequence longer than 50 nucleotide might, by chance, display IRES activity(Yang and Wang, 2019a), but the strong levels of c-Jun IRES-mediated translation in bicistronic reporters compared to the EMCV IRES strongly suggests a proper IRES translation(Blau et al., 2012).

It is unclear whether eIF3d could be the sgRNA cap-binding protein. So far, all mRNAs whose translation has been definitely shown to be mediated by the eIF3d pathway also display a conserved stem-loop that strongly resembles that of HCV domain IIIb, a structure that alphavirus sgRNA does not have. Some mRNA targets of the eIF3d binding domain do not have that structure though, so it might be that for some mRNAs, interaction of the cap via eIF3d is sufficient to promote the eIF3d translation pathway. In that regard, it would be interesting to substitute eIF3d for its phosphomimetic mutant in infected cells and investigate how sgRNA translation is altered.



What are other candidates for the sgRNA cap-binding protein (CBP) then? Of all the alternative CBPs known in humans, most are reported to have a negative regulatory role in translation (Pelletier et al., 2021). LARP1 is a cap-binding protein that is able to interact with 5' TOP containing mRNAs. The 5'TOP motif consist of a cytosine as the first nucleotide immediately downstream the cap, followed by a track of 4-14 pyrimidines (Levy et al., 1991). This motif is common mRNAs coding for ribosomal protein and translation factors (Levy et al., 1991). The affinity of LARP1 for 5'TOP containing mRNAs is conferred by an elongated cap-binding region that specifically recognizes the first cytosine and the downstream pyrimidines (Lahr et al., 2017). Although a role of LARP1 has been suggested in stimulating the translation of 5'TOP mRNAs (Tcherkezian et al., 2014), the current model rather points to LARP1 inhibiting the translation of 5'TOP mRNAs, by competition with eIF4E binding (Lahr et al., 2017). LARP1 represses translation of 5'TOP mRNA following mTOR inhibition (Fonseca et al., 2015). The sgRNA does not have a 5'TOP sequence, which makes it unlikely to be bound by LARP1, although not all LARP1 target have the canonical 5'TOP sequence, with approximately 30% starting with an A (Philippe et al., 2020). This together with the fact that so far the role of LARP1 in translation appears mostly inhibitory, make it highly unlikely that LARP1 is the sgRNA binding protein. Similarly, the cap-binding protein eIF4E2/4EHP blocks translation initiation (Chapat et al., 2017) and is involved in stalled/collided ribosome recycling (Hickey et al., 2020; Juskiewicz et al., 2020a).

eIF4E3 is an other CBP, but its role remains mostly uncharacterized. eIF4E3 is able to interact with eIF4G, and can stimulate eIF4G/eIF4A mediated translation (Pelletier et al., 2021). However, eIF4E3 affinity for the the cap is 10-40 lower than that of eIF4E which casts doubt on how it may regulate translation (Osborne et al., 2013). Also, eIF4E3 is not ubiquitous and its level of expression is only significant in heart, lung and skeletal muscle (Joshi et al., 2004). Given that sgRNA translation appears eIF4G and eIF4A independent, no current data can support a role of eIF4E3 in sgRNA translation, especially in light of its limited expression and limited cap affinity.

Examination of the changes in UV-crosslinked RBP to mRNAs in infected cells does not bring new information (Garcia-Moreno et al., 2019). This work, in which I was involved, aimed at measuring the changes in RNA binding proteins of mRNAs (RBPome) consecutive to SINV infection. Given that at 18hpi, approximately 50% of cellular mRNAs were of viral origin, one might expect that if a different CBP is used for translation of the SINV sgRNA, its abundance in the RBPome would be altered, and so would be that of eIF4E. Unfortunately, UV-crosslinking failed to stabilize the

interaction of eIF4E with mRNAs and it was not detected by the mass-spectrometry analysis. LARP1 was nevertheless recovered, but its abundance was not affected upon infection. The fact that eIF4E was not detected can probably be explained by its mode of recognition of the cap structure. RNA Binding Motifs are efficiently crosslinked to RNA following UV exposure, but this relies on the specific mode of recognition of the bases, which is different from the mode of interaction of proteins to the cap(Lee et al., 2015). Formaldehyde crosslinking, which is less specific and crosslinks both RNA:RNA and protein:RNA interaction might help examine this question.

An important distinction between the *in vitro* experiments performed by van Steeg and colleagues and today's RRL-based *in vitro* translation systems might bring valuable information to the table(van Steeg et al., 1981a, 1981b). Van Steeg and colleagues investigated the translational activity of gRNA, sgRNA and cellular mRNAs in an *in vitro* reconstituted translation system, called the "pH5 system", programmed with lysates from infected and uninfected cells. They found that although translation of the gRNA and cellular mRNAs was decreased when lysates from infected cells were used, translation of the sgRNA was unaffected. This contrasts with contemporary experiments that show that when transfected in uninfected and infected cells, translation of the sgRNA remains poor(Sanz et al., 2007). This is surprising, because the sgRNA produced in infected cells is actually readily translated and it was proposed that translation is coupled to transcription, possibly because translation happens in a specific subcellular location in the presence of a particular set of initiation factors(Sanz et al., 2007, 2015). However, another explanation, involving RNA modification, is possible. Indeed, the viral sgRNAs used by van Steeg et al. were purified directly from infected cells and were not *in vitro* transcribed. This may matter because the sgRNA cap was found to be partly modified. Examination of the cap composition of the sgRNA shows that, unlike the gRNA, the sgRNA can be protected by three different cap variants: m<sup>7</sup>G (50% of all sgRNAs), m<sub>2</sub><sup>2,7</sup>G (31%) and m<sub>3</sub><sup>2,2,7</sup>G (18%) (Dubin et al., 1977; Hsuchen and Dubin, 1976). m<sub>2</sub><sup>2,7</sup>G cap does not appear to be naturally detectable in mammalian cells, however m<sub>3</sub><sup>2,2,7</sup>G cap is a common feature of snRNAs, snoRNAs and certain mRNAs coding for selenoproteins (Wurth et al., 2014). m<sub>3</sub><sup>2,2,7</sup>G is deposited by the trimethylguanosine synthase TGS1 and is postulated to confer eIF4E independence to selenoproteins mRNAs(Wurth et al., 2014). This makes cap hypermethylation a seducing candidate to explain the inconsistencies raised before. m<sub>2</sub><sup>2,7</sup>G cap was reported to bind a CBP (its identity remains unclear though) 1.5 times better than m<sup>7</sup>G cap, while m<sub>3</sub><sup>2,2,7</sup>G binding was reduced compared to m<sup>7</sup>G(Strauss and Strauss, 1994). If these variants are involved in translation of the sgRNA, it could contribute to the resistance of the sgRNA to cap analog competition(van Steeg et al., 1981b). However, experiments *in vitro* and in infected cells show that m<sup>7</sup>G translation is favored

even in infected cells given that m<sup>7</sup>G-protected sgRNA distributes preferably into polysomes than the other two variants(Darzynkiewicz et al., 1988; van Duijn et al., 1986). Translation efficiency of the cap variants in infected cells was investigated at an unknown MOI at 7 hpi which gives some room for interpretation. The time at which translation switches from conventional initiation to the particular mechanisms of the sgRNAs greatly depends on MOI and time after infection, so there is a possibility that this switch was not significant to sustain hypermethylated cap translation.

## The DSH/DLP structure downstream of sgRNA confers eIF2 $\alpha$ independency

Alphavirus infection leads to a sharp increase in eIF2 $\alpha$  phosphorylation, which represses host-cell and gRNA translation. Yet translation of the sgRNA is maintained and even increases in infected cells, which means that it is resistant to eIF2 $\alpha$  phosphorylation(Frolov and Schlesinger, 1994). This activity was mapped to a sequence located downstream of the AUG start codon, in the coding sequence of C, an unusual location for RNA structures with regulatory activity in translation(Frolov and Schlesinger, 1994, 1996). This region is predicted to adopt a stem-loop structure called downstream loop (DLP) or downstream stable hairpin (DSH), called DSH herein. Deletion of the DSH does not affect the translation of the sgRNA in PKR deficient infected MEF cells, but does affect translation of the sgRNA in wild-type cells(McInerney et al., 2005; Ventoso et al., 2006). Not only does the DSH confer eIF2 $\alpha$  phosphorylation independency, it also directs translation initiation at a specific position. Indeed, when the AUG is replaced by other codons such as CUG or GUG translation initiation still takes place, albeit at lower levels(Sanz et al., 2009b, 2019). The fact that eIF2 $\alpha$  phosphorylation does not affect sgRNA translation leads to the hypothesis that other factors might substitute for it. Indeed eIF2A, not to be confused with eIF2 $\alpha$ , is a single-component initiation factor that resembles prokaryotic eIF2 and can substitute for eIF2 in situations where eIF2 $\alpha$  mediated translation is impaired, such as when it is phosphorylated(Komar and Merrick, 2020). However, knock-out of eIF2A in HAP1 cells does not affect viral replication, which eliminates this possibility(Sanz et al., 2017a). Another enigmatic translation factor, eIF2D, may also be able to substitute for eIF2(Dmitriev et al., 2010; Skabkin et al., 2010), and is important for regulation of translation of the ATP4 gene(Vasudevan et al., 2020) though its main role is related to ribosome recycling. However, downregulation of eIF2D and eIF2D expression with siRNAs in HAP1 cells fails to affect sgRNA translation, relegating eIF2D with eIF2A on the list of initiating factors that do not substitute eIF2 for sgRNA translation(Sanz et al., 2017a).

It has been proposed that HCV and sgRNA might employ similar mechanisms for translation, at least with regards to eIF2 dependency (Carrasco et al., 2018). sgRNA and HCV IRES translation share striking functional similarities that extend into the structure of their 5'UTR. As such, HCV IRES domain II is similar to SINV sgRNA DSH, and has been proposed to confer to the HCV IRES its eIF2 $\alpha$  phosphorylation independency as well (Pestova et al., 2008). These structures share approximately the same length, and the same exposed sequence in the loop. Similarly to the sgRNA, it was proposed that HCV translation might involve eIF2A (Dmitriev et al., 2010) and eIF2D (Dmitriev et al., 2010) but recent reports show otherwise (González-Almela et al., 2018; Jaafar et al., 2016). Although the SINV DSH and the domain II of HCV IRES are similar in shape, their different location raises questions. sgRNA DSH is found downstream the start codon, an unusual location for RNA regulatory motifs, while HCV's domain II is found upstream of domain III which is involved in eIF3 recognition and 40S binding (Hashem et al., 2013). The HCV domain II loops back onto the 40S subunit and reaches across the intersubunit space (Quade et al., 2015a). This is conferred by the bent conformation that is allowed by the intra-stem bulges (Locker et al., 2007). Positioning of domain II within the intersubunit domain near the E-site is incompatible with the presence of eIF2, which might explain how eIF2 release is stimulated by domain II independently of GTP hydrolysis? (Hussain et al., 2014; Quade et al., 2015a). If the DSH were to function in the same manner, it would have to loop back as well and it is currently unclear if it can reach that far. A potential bulge in the DSH might help in that regard, but without structures of the 40S in complex with the sgRNA, this remains speculative. In fact, predicted structures of DSH from other alphaviruses show that although the location of the DSH is conserved, their size and apical sequence can change drastically, and many such as SFV, definitely cannot reach that far (Toribio et al., 2016a). It thus appears that the structure and its position, more than anything, is responsible for the effect discussed here.

Marilyn Kozak reported more than 40 years ago that a simple stable hairpin placed downstream of a AUG start codon can force initiation, even in a poor Kozak context (Kozak, 1990). She found that optimal positioning of this hairpin corresponds to 14 nucleotides downstream the AUG, which does not align with the 28-30 nucleotides that separate the AUG and the DSH for most alphaviruses. To accommodate this issue, it has been proposed a two ribosome model: in this model, a translating 80S ribosome is blocked by the DSH and is collided by the scanning 40S (Frolov and Schlesinger, 1996). This prevents the 40S from scanning beyond the AUG, thus forcing initiation. Changing the distance between the AUG and the DSH shows that eIF2 $\alpha$  phosphorylation independency is

abrogated below 28 nucleotides and starts falling down for when longer than 43 nucleotides (Toribio et al., 2016a). The two ribosome model somewhat implies that the distance between the AUG and the DSH must be carefully controlled to accommodate for the scanning 40S and the downstream 80S, but the permissiveness observed for the AUG-DSH distance tells otherwise. It is also unclear whether the 28 distance can accommodate for a scanning 40S and a translating 80S. Ribosome profiling data shows that 80S footprints are 28-30 nucleotides in length, which does not leave enough room for the 40S to be in place to recognize the AUG (Ingolia et al., 2014a). Some alphaviruses DSH do have internal bulges that might allow a process where the DSH is partially unwound before blocking the 80S, but not all do, nor are these bulges in a conserved location inside the DSH (Toribio et al., 2016a).

Other mechanisms have been proposed for the function of the DSH and they again suggest that the function of the DSH is entirely different from that of HCV domain II. Rather than folding back into the E-site, data based on RNA-RNA crosslinking assays points to the DSH being trapped in the ES6S region of the 40S subunits that is exposed on its solvent side (Toribio et al., 2016a). In this model, the DSH remains stuck on the side of the ribosome, stalls the ribosome, and forcibly ends scanning. Because the ribosome is locked in place, recognition of the AUG start codon is no longer dependent on eIF2, and a Met-tRNA<sup>i</sup> enters the P-site to initiate translation. Substantiating this model are the fact that changes in the distance between the AUG and the DSH affect sgRNA translation in infected cells (Toribio et al., 2016a). Translation of cellular genes in context of eIF2 $\alpha$  phosphorylation is a rare, yet described mechanism. GCN4 and ATF4 are master transcriptional activators whose expression is tightly controlled by the level of eIF2 $\alpha$  phosphorylation by the presence of upstream ORFs (uORFs). When eIF2 $\alpha$  is not phosphorylated, translation of the GCN4 and ATF4 leads to recognition of these uORFs AUGs and inhibit the recognition of the downstream AUG of the main ORF (Vattem and Wek, 2004). In cases where most eIF2 $\alpha$  is phosphorylated, eIF2-GDP cannot catalyze the recognition of the uORFs AUGs and 40S scan through their coding sequence, a process called leaky scanning. This process is postulated to give additional time for the 40S to exchange incompetent eIF2-GDP-Met-tRNA<sup>i</sup> ternary complex for rare initiation competent eIF2-GTP-Met-tRNA<sup>i</sup> ternary complex that may have avoided eIF2 $\alpha$  phosphorylation, and effectively allows for translation of the main ORF. Inspired by this mechanism, we propose a model in which the DSH locks the 40S onto the AUG of the ORF, thereby preventing leaky scanning of the AUG. This locking mechanism probably gives additional time for the 40S to acquire a competent ternary complex and proceed with translation elongation (Figure 4). Strikingly, transfection of a SINV replicon where a second AUG is placed upstream the canonical AUG in

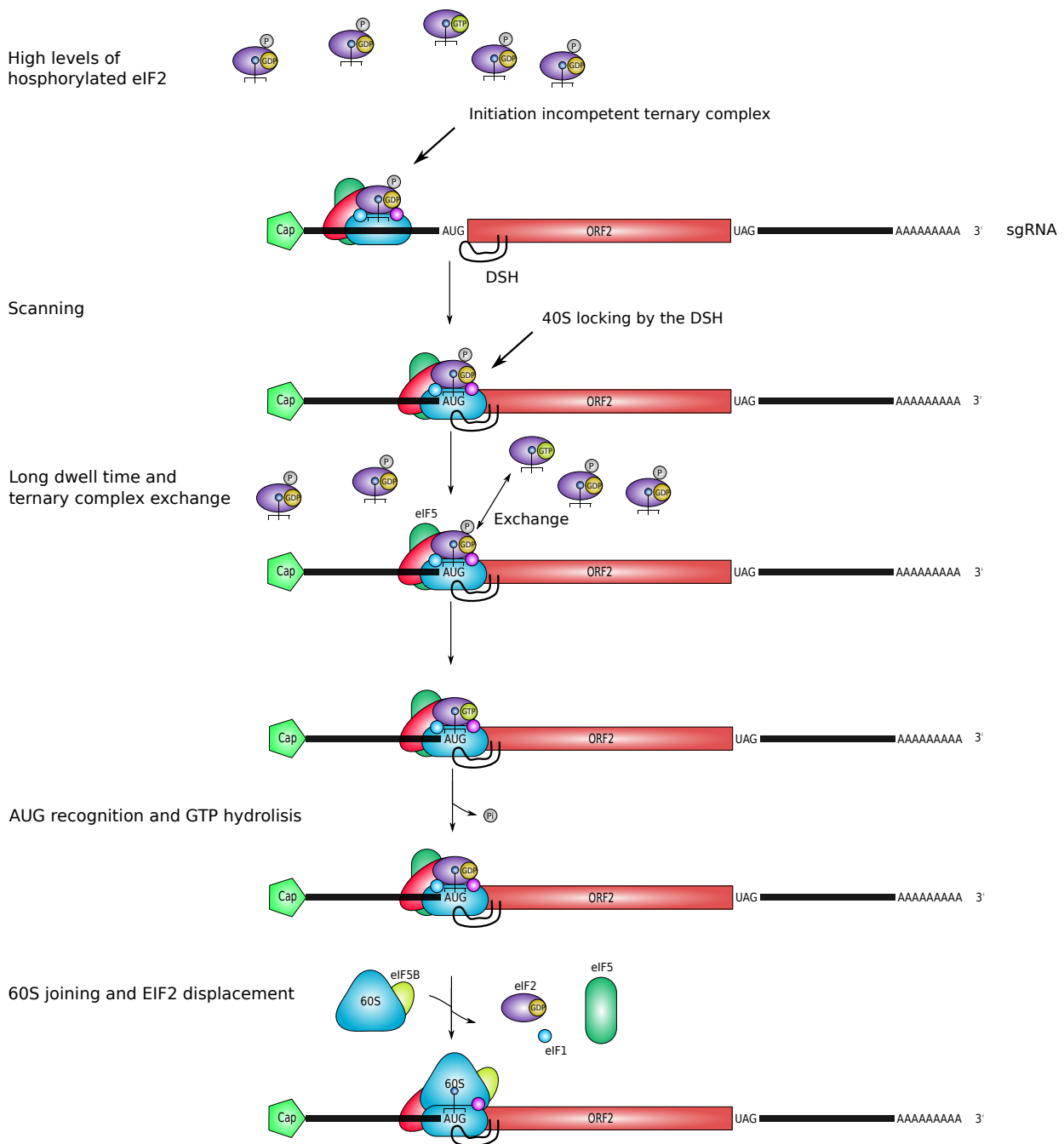


### Figure 4: A proposed mechanism for sgRNA resistance to eIF2 $\alpha$ phosphorylation

At the start of initiation, an initiation incompetent ternary complex with phosphorylated eIF2 $\alpha$  and eIF2 $\alpha$ -GDP is recruited by the 40S. Scanning progresses until the DSH locks the 40S onto the sgRNA AUG. This imposed long dwell time allows ternary complex exchange with low abundance initiation competent ternary complex. Finally, the AUG codon is recognized and GTP is hydrolysed, allowing for recruitment of the 60S subunit.

PKR deficient cells, which do not induce eIF2 $\alpha$  phosphorylation in response to replicon replication, leads to the preferred initiation of the upstream AUG(Garcia-Moreno et al., 2015). In WT cells however, where eIF2 $\alpha$  becomes phosphorylated, only the canonical AUG serves for initiation. These results thus fit with a mechanism in which eIF2 $\alpha$  phosphorylation provokes leaky scanning of the 40S, but because the DSH blocks the 40S onto the canonical AUG, it is given time to acquire an initiation competent ternary complex.

## sgRNA translation initiation involves an eIF4A-independent scanning process

Placement of stable hairpins upstream the sgRNA AUG strongly inhibits translation and suggests that sgRNA translation is a scanning-dependent process(Garcia-Moreno et al., 2015; Toribio et al., 2016b). Stable hairpins with different lengths and placed immediately upstream the AUG codon impact sgRNA translation depending on the predicted stability of the hairpin. This indicates that this effect is not due to disruption of upstream RNA structures but rather that stable hairpins must be unwound for the 40S to correctly recognize the AUG codon(Toribio et al., 2016b). Placement of hairpins further upstream the AUG codon lead to the same effect showing again that this is not due to alterations of the 5'UTR structure, and that scanning of the entire 5'UTR is required for sgRNA translation. This is surprising because expression of poliovirus protease 2A, which cleaves eIF4G, does not affect translation of the sgRNA(Castelló et al., 2006). eIF4G is the scaffolding factor of the eIF4F complex and interacts with eIF4E, eIF4A, eIF3 and PABP, which makes it a critical factor for cap-dependent and some IRES-dependent translation. Because of this very important role in structuring the translation initiation machinery, eIF4G requirement is intimately linked with the scanning process. As such, HCV-like viral IRESs that do not involve a scanning step are independent of eIF4G(González-Almela et al., 2018; Martínez-Salas et al., 2018). Not only sgRNA translation is independent of eIF4G, it is also insensitive to eIF4A activity inhibition. Inhibition of eIF4A, the eIF4F helicase responsible for unwinding the 5'UTR during scanning, by Pateamin A and hyppuristanol do not affect translation of the sgRNA in cells transfected with SINV replicons(Garcia-Moreno et al., 2013, 2015; González-Almela et al., 2015).

The fact that stable hairpins placed in the sgRNA 5'UTR inhibit sgRNA translation and that stability of the hairpin has a direct role on translation initiation efficiency strongly suggests that a helicase is involved in the scanning process. *In vitro* experiments show that DHX29, a DEAH-box

helicase with a known role in translation initiation(Parsyan et al., 2009; Pisareva and Pisarev, 2016), stimulates the formation of the 48S complex on the sgRNA(Skabkin et al., 2010), but whether it replaces eIF4A in the scanning process in infected cells remains unclear(Garcia-Moreno et al., 2015).

The structure of the human 48S PIC was recently released and may help understand the mechanisms at place here(Brito Querido et al., 2020). Although the participation of the different initiation factors in the process of translation initiation is rather well understood, how they are placed on the ribosome 40S has remained enigmatic. Two models have emerged to explain how EIF4A provides the directionality of processing during the scanning step of translation initiation. In the “threading” model, the EIF4F sits at the leading edge of the 40S subunit, near the mRNA channel, and threads the mRNA into the channel(Kumar et al., 2016). In the “slotting” model, EIF4F is placed at the opposite, at the trailing edge of the 40S subunit. The mRNA “slots” in the 40S and that the mRNA is “pulled” through the 40S during scanning. The mechanism by which this would happen is that the 40S slides randomly onto the mRNA, by ATP hydrolysis by EIF4A acts as a ratchet and provides directionality of the process. The “slotting” mechanism implies that a “blind spot” exists, which is that AUG start codon that are very near the cap cannot be recognized by the translation machinery because of the minimal length between the cap and the start codon that is imposed by the structure of the complex. The recent structure of the 48S pics provide clear evidence that the “slotting” mechanism exists and authors detected a blind spot of approximately 40 nucleotide in length from the cap(Brito Querido et al., 2020). It is important to note though that some human mRNAs have an exceptionally short 5'-UTR and that their mechanism of translation initiation may be different(Brito Querido et al., 2020; Kumar et al., 2016). SINV sgRNA is 49 nucleotide in length and possesses in small hairpin that may effectively render this length even smaller. The EIF4A independence of the sgNA translation initiation can be discussed in the light of both models. In the “slotting” model, the 40S P-site would already be very close (~10 nucleotide ahead) from the AUG right at the start of the initiation process. Given that 40S sliding is the primary source of movement during the scanning process, it is possible that for small 5'UTR, the activity of EIF4A is not needed because the AUG start codon is already close enough for the 40S to randomly encounter it, without the need of a ratchet that provides the directionality. For small 5'UTRs, the “threading” model would be preferred and an helicase sitting at the entrance of the mRNA channel would be involved, with EIF4A but also DHX29 having been shown to take this role(Brito Querido et al., 2020; des Georges et al., 2015).



A possibility, unexplored to this date, is that the helicase could be nsP2. nsP2 has been reported to interact with both the ribosome and the poly-A binding protein PABPC1 (Bourai et al., 2012) and is crosslinked by UV treatment to the pool of mRNAs infected by SINV (Garcia-Moreno et al., 2019). This, however, may be partly due to the participation of nsP2 in viral transcription. Additionally, nsP2 has been shown to interact with RPS6/eS6, a ribosomal protein that sits not so far off the mRNA entry channel (Khatter et al., 2015; Montgomery et al., 2006). Substitution of the translation initiation machinery by viral proteins is not unheard of. Hantavirus N protein binds the cap of hantavirus mRNAs and substitutes for the entire eIF4F complex for their translation (Mir and Panganiban, 2008) (see Chapter II). Unfortunately, the participation of nsP2 in translation is difficult to test. sgRNA modes of translation strongly differ between *in vitro*, uninfected cells and infected cells (Carrasco et al., 2018; Sanz et al., 2009b) and it makes the most sense to examine it in infected/replicon-transfected cells, but because nsP2 is involved in many aspects of alphaviruses life cycle and its helicase activity is critical for viral replication, experiments based on nsP2 mutants are bound to be inconclusive.

## Conclusion and Perspectives

Although extremely studied, translation of the alphaviruses sgRNA largely remains a mystery. It uses a cap-dependent process, yet does not rely on eIF4E binding. It uses a scanning mechanism, yet is insensitive to eIF4A inhibition. Finally, it is insensitive to eIF2 $\alpha$  phosphorylation but the precise mechanism by which this happens is unclear. A major source of confusion is that sgRNA translation does not behave in the same way *in vitro* and *in vivo*, and in uninfected cells versus infected cells. A common theme of all the studies that attempted to decipher these mechanisms is that they aimed at identifying which factors are not *necessary* for the translation of the sgRNA, rather than identifying the factors involved in translation of the sgRNA. In other terms, I think it is time to ask what sgRNA translation *is*, not what it *isn't*, with the help of mass-spectrometry analysis. By programming RRL with the c-Jun mRNA and purifying initiating 48S subunits, Lee and colleagues were able to show that all components of eIF4F are absent of the 48S complexes scanning this mRNA (Lee et al., 2016). This indicates that a similar strategy is likely to succeed in identifying the initiation factors involved in sgRNA translation. In the case of alphaviruses, it appears critical to look at initiation factors present in 48S from infected cells, because *in vitro* systems are unable to recapitulate the mechanisms involved in alphavirus translation.

Purification of initiating 48S from living cells is extremely difficult and requires multiple steps of purification (Archer et al., 2016). Archer et al. devised a purification method called translation complex profiling followed by sequencing (TCP-seq) to look at initiation sites on yeast mRNAs. This requires *in cell* formaldehyde crosslinking, because scanning 48S are not as tightly bound to mRNAs than elongating 80S ribosomes are. Initiating 48S were purified by purification of polysomes by pelleting polysomes through ultra-centrifugation, digestion with RNase, re-fractionation of digested polysomes and extraction of the 40S fraction. This way, free 40S are excluded from the first purification, and only 40S ribosomal subunit that were present on polysomes – hence initiating 48S – were purified. Initiating 48S represent an extremely low fraction of the material present in polysomes therefore this method requires a high amount of starting material. Conveniently, although initiation factors interaction to ribosome is rather weak and they are lost during standard purification, formaldehyde crosslinking stabilizes these interactions, making them observable by a putative TCP-MS method (Bohlen et al., 2020), (personal data, see Results). If this method were to be applied to perform mass-spectrometry quantification of initiating 48S, it would probably require even more material, because mass-spectrometry analysis does not involve an amplification step like TCP-seq does for the amplification of sequencing libraries by PCR.

In infected cells, the fact that host-cell mRNA translation is impaired at late infection times suggest that this strategy is applicable. Because almost only the sgRNA is translated at this stage, no purification based on mRNA identity is required. However, translation of the sgRNA, although efficient, only involves a low proportion of the translation machinery, which is highlighted by the low levels of polysomes in infected cells (see Results). This casts doubt on the feasibility of a TCP-MS method in infected cells, because it would likely require immense amount of starting material. I do believe though, that it would be the best strategy to get a comprehensive look at the initiation factors involved in the translation of the sgRNA in physiological conditions.

# Chapter II: Ribosome specialization during viral infections

## Introduction

Viruses rely on the host-cell ribosomes, and they must find ways to exploit and divert the ribosome from the cells mRNA in order to optimize their replication. One of such mechanisms, the use of specialized ribosomes, is the subject of this review. “Specialized ribosomes” is a term to denote the fact that not all ribosomes are the same, as they can differ based on chemical heterogeneity, and this heterogeneity is postulated to change the behavior of the ribosome.

The idea that viruses could leverage ribosomes with different composition can be traced back to the early seventies, when an Influenza A Virus (IAV) non-structural protein (NS), uncharacterized at the time, was found to co-sediment with polysomes in sucrose gradients (Compans, 1973). Dissociation of ribosomes by EDTA was shown to also prevent sedimentation of the protein in heavy fractions, leading to the hypothesis that the NS protein interacts with the translation machinery, if not the ribosome itself. Hence, authors noted that “*an obvious possible function for such a polypeptide is in directing the ribosome to recognize viral messenger RNA in preference to cellular RNA.*” Similarly, vaccinia virus infection was found to induce phosphorylation of several ribosomal proteins (RPs) (Kaerlein and Horak, 1976a), and authors recognized it was “*tempting to speculate that the phosphorylation of ribosomal proteins is related to the switch off in protein synthesis in virus-infected cells or to the specific selection of viral or cellular mRNAs for translation*“. These papers, and other along them, introduced the idea that alteration of the ribosome itself could participate in translational control during infection, by promoting viral synthesis, or by inhibiting the host response.

Fast forward today, and most in depth reviews of the landscape of translation regulation in virus-infected cells report very few cases of actual alterations to the ribosome composition (Jan et al., 2016; Stern-Ginossar et al., 2019; Walsh and Mohr, 2011; Walsh et al., 2013). Rather, research has been concentrated on translation initiation, a critical step of translation that is responsible for the overall protein output. Yet, the realm of translation control is not restricted to translation initiation, as viruses often rely on non-canonical elongation and termination pathways to produced numerous proteins from a genome constrained in size by the encapsidation process (Firth and Brierley, 2012).

And even alternative initiation pathways can involve the use dedicated types of ribosomes(Pooggin and Ryabova, 2018).

The field of “specialized ribosomes” reemerged in the last 10 years, and was initiated by studies focusing on developmental biology. But it has now gained enough traction that it’s starting to significantly intersect with other fields, such as cancer(Erales et al., 2017), homeostasis and stress response(Ghulam et al., 2020; Song et al., 2019a), and, of course, virology(Jha et al., 2017; Wang et al., 2019). This regain of interest has been accompanied by the improvement of tools at the disposal of biochemists and molecular biologists to tackle these questions in a more high-throughput and unbiased way. In particular, we expect recent advancements in mass spectrometry techniques such as SRM-based quantification of RPs (Shi et al., 2017), native ribosomal particles mass spectrometry(Waterbeemd et al., 2018), top-down identification and quantification of ribosomal post-translational modifications(Waterbeemd et al., 2018), and label-free quantification of ribosome interactants(Simsek et al., 2017), to contribute to the understanding of the role played by specialized ribosomes during infection. Similarly, rRNA variants quantification by RNA-seq(Song et al., 2019a) and focus on rRNA post-translational modifications by RiboMeth-seq(Birkedal et al., 2015; Krogh et al., 2016; Marchand et al., 2016) or nanopore sequencing(Begik et al., 2021), can be used to question rRNA heterogeneity.

## Definitions and Scope

The concept of specialized ribosomes is rooted in the observation that ribosomes are much more diverse in composition than the textbook view suggests. Sources of heterogeneity come from several aspects of ribosome biochemistry, such as RPs paralogs usage, RPs stoichiometry, RPs, modifications heterogeneity, rRNA variants usage, rRNA modifications heterogeneity, and ribosome-associated proteins (RAPs)(Guo, 2018). The latter is probably the most difficult set to define, as previously discussed (Ferretti and Karbstein, 2019), since proteins can interact indirectly with the ribosome, or only for a short period of time such as during the initiation of translation, and can be recruited by cis-acting RNA motifs during the course of elongation. As such, defining whether each case fits the concept of specialized ribosomes is perilous and requires careful examination of the data.

Another fundamental aspect of the specialized ribosomes hypothesis is that they might add another layer of translation regulation. Typically altered functions can be, preference for subpool of mRNAs (Jha et al., 2017; Shi et al., 2017; Simsek et al., 2017), better abilities in certain non-canonical translation pathways (Firth and Brierley, 2012) such as ribosome shunting (Pooggin and Ryabova, 2018), or programmed ribosomal frameshifting (Wang et al., 2019). Such details on the specific roles of specialized ribosomes during infection is often lacking in the literature, as old studies remained mostly descriptive owing to the lack of proper tools to address these questions. However, we choose to include most of them, as we feel it is now time to revisit these old questions with the new techniques at our disposal.

There are two possibilities for viruses and host cells to exploit specialized ribosomes: pre-existing subpools of ribosomes can be leveraged during infection, or the infection itself can lead to the appearance of new kinds of specialized ribosomes, in what could be called “virus-induced ribosome specialization”. Distinction between the two is not always easy, but both strategies are equally interesting. In particular, the utilization of pre-existing types of ribosomes raises the question of the roles of these ribosomes in healthy cells, and as such, studying these cases can shed new light on fundamental pathways of translation (Wang et al., 2019). When appropriate, whether each case falls into what category will be discussed.

Finally, the aim of this chapter is to highlight the benefits of ribosome-centric methods when deciphering translation regulation in infected-cells. By focusing on the biochemical characterization to the ribosome itself, new layers of regulation can be identified. In particular, high-throughput and unbiased methods mentioned earlier are particularly helpful to identify subpools of ribosomes, and we expect them to get traction in the years to come. Thus, we will detail such methodological advancements and describe how they may be used to better understand the role that the ribosome takes place in host-pathogen interactions.

## 1. Substoichiometric ribosomal proteins and specific functions of ribosomal proteins in viral translation

Recent reports show that translating ribosomes in polysome fractions are heterogeneous in their RPs compositions, as some RPs can be absent from these ribosomes. Quantification of this heterogeneity

requires dedicated mass spectrometry experiments, such as Selected Reaction Monitoring (SRM) (Shi et al., 2017) or native mass spectrometry of ribosomal particles (Waterbeemd et al., 2018), as label-free experiments do not allow the precise quantification of such small variations. In mouse embryonic stem cells (mESCs), RPL10a/uL1, RPL38/eL38, RPS7/eS7, RPS25/eS25 are found to be present in only 40-60% of all ribosomes in average, while a minor depletion of 10% is reported for RPL11/uL5 and RPL40/eL40 (Shi et al., 2017). Interestingly, RPS25/eS25 and RPL10a/uL1 ribosomes were shown to translate specific subpools of mRNAs, which suggests a functional role for this type of RP heterogeneity. Substoichiometric presence of RPS25/eS25 was later confirmed by native mass-spectrometry of ribosomal particles purified from HEK293 cells and additional incomplete incorporation of RPS10/eS10 was discovered (Waterbeemd et al., 2018). More work will be required to properly define the extent to which these populations of ribosomes exist, and how they differentially participate in translation in different cell types and organisms.

Whether such heterogeneous populations of ribosomes participate differently in translation during infection remains mostly unclear. Attempts at identifying specific roles of ribosomal proteins in viral mRNAs translation by genetic approaches such as siRNA screens have been reported but the potentially radical changes in cell homeostasis and ribosome availability complicate the analysis, similarly to what is discussed in the ribosomopathies field (Mills and Green, 2017). Ribosomopathies are caused by heterozygous mutations in ribosomal proteins and manifest in pathologies that generally affect only certain cell lineages. For instance, twelve different RPs mutations can cause similar erythropoiesis and skeletal development defects called Diamond Blackfan Anemia. A long-standing question is whether this is due to impaired translation of mRNA pools that require the participation of specific ribosomal proteins for their translation, or to a difference in sensitivity of certain mRNAs to reduced functional ribosome concentrations. The fact that mutations in different RPs manifest in similar phenotypes is a strong argument for the latter. Accordingly, differences in intrinsic initiation rates have been proposed to explain the variable sensitivity of mRNAs to reduced pool of functional ribosomes, and to be the cause of ribosomopathies (Mills and Green, 2017). As such, a lot of attention must be dedicated to providing the necessary controls to support the role of specific ribosomal proteins in viral translation.

Additionally, the specific requirement of certain RPs for the translation of viral mRNAs does not necessarily suggest a specialized ribosome pathway of translation. In fact, the specialized ribosome hypothesis is deeply anchored in the idea of biochemical heterogeneity within the ribosome population. In the absence of ribosome heterogeneity, the requirements for specific RPs to translate

subclasses of mRNAs rather tend to suggest the diversity of pathways that can be used by the ribosome to translate mRNAs. Ironically, the exogenous depletion of ribosomal proteins and its manifestations rather show that, in the first place, the ribosome is an unspecialized machine, equipped for the translation of many different mRNAs.

As mentioned before, the precise measurement of RPs stoichiometry requires dedicated mass spectrometry experiments (Shi et al., 2017; Waterbeemd et al., 2018) that have so far been absent from studies in the field of host-pathogen interactions. Whether viruses are able to subvert specific populations of RP-lacking/containing ribosomes, or even change the population in that regard is, for the most part, unclear.

As such, a siRNA-based screen of ribosomal proteins participation in VSV replication was conducted with the help of a GFP-expressing virus (Lee et al., 2013). Eight siRNAs against RPS were found to significantly affect VSV replication in the absence of noticeable cellular defects. Further experiments concentrated on RPL40/eL40 depletion and showed a reduction in VSV mRNA translation, with the same effect being noted on other viruses from the same family. However, the specificity of this effect remains unclear, as only B-actin mRNA translation was measured as a control. In fact, since depletion of seven other RPs produces the same defect in replication, it seems that a more profound effect is at place, reminiscent of the reduced pool of functional ribosome hypothesis.

RPLP1 and RPLP2 are two ribosomal proteins that form, together with RPLP0, a protuberance of the 60S ribosomal subunit called the ribosome stalk. The ribosome stalk is a pentameric structure, with two copies of the RPLP1/RPLP2 dimer and one copy of RPLP0 (Liljas and Sanyal, 2018). This structure has been referred to as the GTPase Activation Center owing to its participation in the activation of several GTPases involved in translation (Liljas and Sanyal, 2018). The ribosome stalk forms in the cytoplasm, from a free cytoplasmic pool of RPLP0, RPLP1 and RPLP2. Interestingly, exchange between the cytoplasmic pool of RPLP1 and RPLP2 and their ribosome-bound counterparts has been described (Ballesta and Remacha, 1996; Remacha et al., 1995). RPLP0, P1 and P2 depletion affects cell growth, but not cell viability and polysome gradients profiles are only moderately affected by P1 and P2 depletion, with an increased amount of free 60S subunit but a modest reduction in polysome abundance (Martinez-Azorin et al., 2008). This is further complicated by cell-line dependency of P1 and P2 depletion on translation throughput: metabolic labeling experiments show that translation is impaired by P1 and P2 depletion in Huh-7, but not in A549

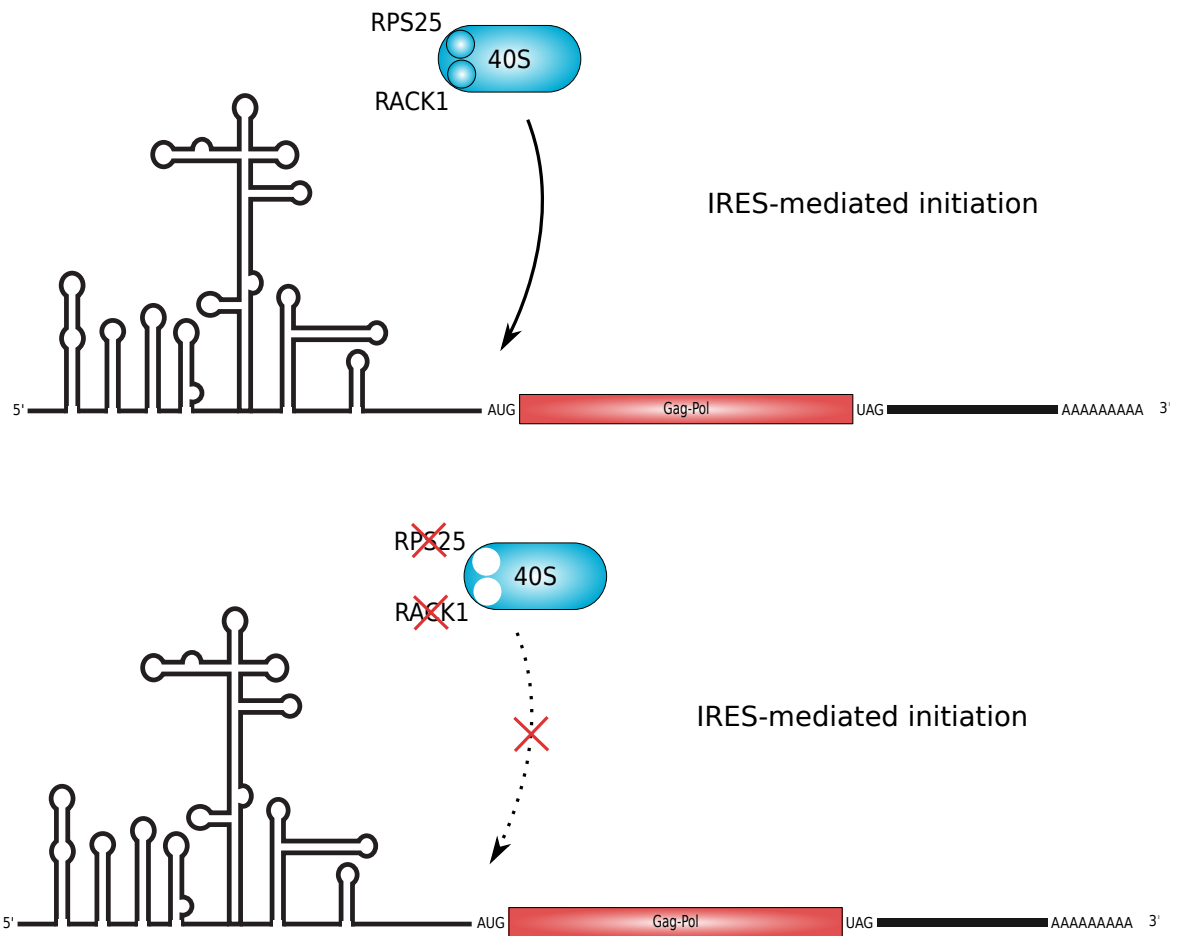
cells(Campos et al., 2017). CRISPR-based screen and siRNA screen identified P1 and P2 as host factors necessary for *Flaviviruses* DENV-2 and YFV respectively(Sessions et al., 2009; Sommer et al., 2012). Further experiments confirmed this dependency, extending it to ZIKV, in A549 and Huh-7 cells(Campos et al., 2017). It is unclear whether this is due to the aforementioned effect of P1 and P2 depletion on translation throughput or to the specific requirements of these factors for Flavivirus translation. Since P1 and P2 depletion does not affect translational throughput but readily affects *Flavivirus* translation in A549 cells, it is tempting to postulate that this effect is specific. However, because P1 and P2 exist largely as a ribosome-free cytoplasmic pool, the effect reported here could be a translation-independent role of P1 and P2 in *Flavivirus* replication. An important question remains whether this constitutes a case of viral-induced specialization as the property of P0, P1 and P2 to go on-and-off the ribosome opens the possibility for Flaviviruses to control this exchange rate, and to favor the ribosome-bound or free cytoplasmic pool of these proteins.

RACK1 is dispensable for cell viability and proliferation, although RACK1 mutant flies are not viable(Majzoub et al., 2014). Yet, it is required for CrPV 5' IRES (Gross et al., 2017), DCV 5' IRES, HCV, PV, EMCV IRES -mediated translation, but not CrPV IGR-IRES, and cap-dependent FHV and VSV translation(LaFontaine et al., 2020; Majzoub et al., 2014)(Figure 5A) The structure of the HCV IRES bound to the 40S subunit does not reveal an obvious role of RACK1, as RACK1 does not make direct contact with the IRES(Quade et al., 2015b). What's more, RACK1 has not been reported to be a substoechiometric RP in translating ribosomes(Shi et al., 2017; Waterbeemd et al., 2018). This tends to suggest a role in the recruitment of additional factors to assist the translation of the IRES(Majzoub et al., 2014), rather than a true direct participation of RACK1 in IRES translation. Interestingly though, RACK1 depletion also reduces VACV replication, but further investigation revealed that the regulatory role of RACK1 in VACV translation lies in a viral-induced phosphorylation state(Jha et al., 2017). As such, it is unclear if RACK1 actually controls IRES-mediated translation, or if it instead acts as a platform for the assembly of initiation factor complexes. Finally, over-expression of RACK1 stimulates CrPV replication. RACK1 requirement for viral replication extends to Dengue virus (Hafirassou et al., 2017), which also seem to rely on IRES-mediated translation(Song et al., 2019b).

The most compelling evidence of a viral mRNA specialized translation pathways comes from the critical role of RPS25/eS25 in IRES-mediated translation. RPS25 is one of the few substoichiometric ribosomal protein in translating ribosomes in healthy cells(Shi et al., 2017; Waterbeemd et al., 2018), which suggests a possibility for specialized translation. Structural



A



B

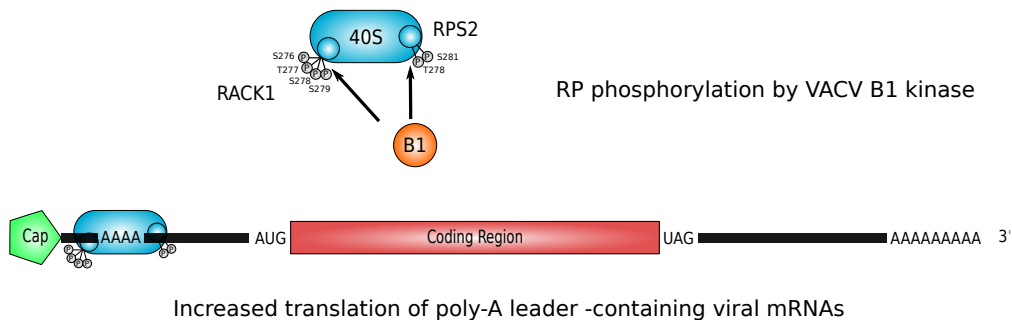


**Figure 5: Alterations to the ribosome composition affect viral translation**

**A.** Depletion of ribosomal proteins RPS25 and RACK1 inhibits translation mediated by many types of IRESes, while not affecting cap-dependent translation. The example of the EMCV IRES is shown here.

**B.** Phosphorylation of RACK1 and RPS2 by the VACV B1 kinase promotes translation initiation of polyA-leader containing viral mRNAs.

evidences notably point towards a role for RPS25 in translation of Intergenic Region Internal Ribosome Entry Site (IGR-IRES) of viruses from the *Dicistroviridae* family, among which PSIV and CrPV are the most studied, a process that does not require any translation initiation factors nor the initiator tRNA. Both CrPV and PSIV IGR-IRESs directly interact with RPS25, as revealed by 4-thiouridine-labeled PSIV IGR-IRES crosslinking(Nishiyama et al., 2007), and structural studies(Fernández et al., 2014; Muhs et al., 2011, 2015; Schüler et al., 2006). Accordingly, RPS25 knock-out reduces CrPV IGR-IRES-mediated translation in yeast while mildly affecting global translation, readthrough, ribosome biogenesis, and programmed ribosomal frameshifting(Landry et al., 2009; Yamada et al., 2019)(Figure 5A). This is explained by impaired binding of RPS25-depleted ribosomes to CrPV and PSIV IGR-IRESs(Landry et al., 2009; Muhs et al., 2011). Interestingly, RPS25 depletion also affects HCV IRES-mediated translation(Landry et al., 2009) and structure of the HCV IRES bound to the human ribosomes highlights a similar role in RPS25 in IRES binding(Quade et al., 2015b). Although the general mode of interaction is different from *Dicistroviridae* IGR-IRESs, the contacts between RPS25 and both types of IRESs are surprisingly similar. A role for RPS25 in HIV and HTLV IRESs translation has been suggested(Carvajal et al., 2016; Olivares et al., 2014), although structural information is lacking. Finally, *Flaviviridae* replication is diminished with RPS25 knock-out (Hafirassou et al., 2017; Marceau et al., 2016), which may be related to IRES-mediated translation as well(Song et al., 2019b). The requirement for RPS25 in IRES-mediated translation has been proposed to be more general, as several cellular IRES-containing mRNAs are also sensitive to RPS25 depletion(Hertz et al., 2013; Shi et al., 2016). Additional requirement for RPS25 in other non-canonical translation pathways such as RAN translation(Yamada et al., 2019) and ribosome shunting(Hertz et al., 2013) have been shown, but mechanistic details are still lacking. Overall, the very special place of RPS25 in unconventional translation initiation pathways and its substoichiometric incorporation into translating ribosomes make this the archetypal case of ribosomes specialized for viral translation. An outstanding question remains as to whether the incorporation of RPS25 into ribosomes changes during infection, and whether viruses or the infected cell manipulate the amount of RPS25 containing ribosomes.

## 2. Ribosomal proteins post-translational modifications

The first discovery of a post-translational modification (PTM) status change of ribosomal proteins in response to virus infection was made in 1976(Kaerlein and Horak, 1976a), two years after the discovery of RPS6/eS6 phosphorylation in rat liver samples(Gressner and Wool, 1974).

Phosphorylation of ribosomal proteins in response to the archetypical *Poxviridae* Vaccinia Virus (VACV) infection was investigated using 2D gel electrophoresis of purified ribosomes from VACV-infected cells in culture medium containing P32. An increase in RPS6/eS6 phosphorylation was identified (later attributed to other factors than VACV infection (Buendia et al., 1987)), as well as new phosphorylation of RPS2/uS5 and an other ribosomal protein than could be not be attributed. This protein was later identified as RPS13/uS15 (Buendia et al., 1987). The parallel use of four complementary 2D systems able to resolve acidic proteins allowed to identify RPSA/uS2 phosphorylation as well (Buendia et al., 1987). The viral kinase B1 was later identified as the kinase implicated in RPS2/uS5 and RPSA/uS2 phosphorylation but not RPS13/uS15, and B1 was especially able to phosphorylate purified ribosomes *in vitro* (Banham et al., 1993; Beaud et al., 1989, 1994). The picture of VACV-induced ribosomal phosphorylation was further expanded more than 40 years later by the Walsh lab with the phosphorylation of the ribosomal protein RACK1 in translating ribosomes (Jha et al., 2017). RACK1 only made it to the list of ribosomal proteins in 1999 through the use of mass spectrometry (Link et al., 1999). It had remained excluded because of its high molecular weight and low pI (6,04 for its *S. cerevisiae* homolog Asc1) compared to most other ribosomal proteins (Link et al., 1999), making it impossible to resolve by standard 2D gels of pH10 first dimension (Kaerlein and Horak, 1978). Interestingly, although it could not be resolved by standard 2D gel methods, two of the four alternative 2D gel systems used in (Buendia et al., 1987) were theoretically able to resolve it and as such, one spot position that fits with RACK1 size and isoelectric point, can retrospectively be attributed to phosphorylated RACK1 on their radiography. Four phosphorylation sites in an extended loop of RACK1 were identified in the form of a STSS cluster (Jha et al., 2017). B1 viral kinase, but not F10 kinase, is necessary for the phosphorylation of RACK1, and for increased translation of polyA leader-containing (stretches of As in the 5'UTR) mRNAs such as VACV mRNAs (Figure 5B). Interestingly, translation poly-A leader containing mRNAs has been shown to be both eIF3 and eIF4F independent, although the precise mechanism by which this happens remains unknown (Shirokikh and Spirin, 2008). It thus appears as though phosphorylation of RACK1 facilitates this very unusual mechanism of translation initiation. The study of the Walsh lab is the first ever example of a functional link between phosphorylation of ribosomal proteins and translation control of viral mRNAs in infected cells. The same group later rediscovered and characterized the previously reported RPS2/uS5 phosphorylation by mass-spectrometry analysis (DiGiuseppe et al., 2020). They confirmed that the B1 viral kinase is directly involved in the phosphorylation of RPS2 and identified residues T278 and S281 as the primary targets (DiGiuseppe et al., 2020). Similarly to RACK1, phosphorylation of RPS2 on these two residues appears to favor translation of polyA leader-containing mRNAs (Figure 5B). Finally, they

described VACV induced phosphorylation of RPS28/eS28 by mass-spectrometry analysis, but were not able to identify the precise residue involved, nor to show an effect on viral replication. All together, VACV infection has been shown to induce phosphorylation of five different RPs, with direct evidence that the viral kinase B1 is involved in phosphorylation of RACK1 and RPS2. Phosphorylation of these two proteins at multiple positions improves translation of poly-A leader containing VACV mRNAs, possibly by facilitating an unusual eIF4F and eIF3 independent mechanism of translation initiation (Jha et al., 2017).

Phosphorylation of RPS6/eS6 is a hallmark of the infection by many viruses. RPS6/eS6 phosphorylation is a consequence of the activation of the mTOR pathway, an important pathway in host-pathogen interactions. Although mTOR activation ends in translation arrest, the role taken by RPS6/eS6 phosphorylation lies unclear, despite decades of research (Meyuhas, 2015a). Consequently, and despite the ubiquitous presence of this modification in the field of virology, we decide to leave the discussion regarding its roles to others (Meyuhas, 2015a; Miller et al., 2021).

### 3. Viral proteins interacting with the ribosome

The simplest way viruses can alter the translation machinery functions is by producing viral proteins that bind directly to the ribosome itself. There have been many - *many* - reports in the literature of viral proteins that were found to be associated with ribosomes, dating back to the 70s (Compans, 1973), but a significant proportion lack proper characterization of the interaction, and functional relevance. Naturally, we cannot review all occurrences of said interactions. We focus on well-defined mechanisms and choose a subset that highlights the diversity of functions exerted by ribosome-interacting viral proteins. The present examples show effects ranging from host translational shut-down, to preference for translation of viral mRNAs as well as assistance for non-canonical translation pathways such as ribosome frameshifting.

In the 1970s, several reports indicated that VACV infection induces host-cell translation shut-off and that this effect is maintained even in the absence of viral replication and/or translation of viral mRNAs (Bablanian et al., 1978; Esteban and Metz, 1973; Moss, 1968; Moss and Filler, 1970; Person and Beaud, 1978, 1980; Rosemond-Hornbeak and Moss, 1975; Shatkin, 1963). In 1980, Person and Beaud showed that host-cell translation shut-off is at least partly explained by inhibition of the ternary complex formation (Person et al., 1980). Coincidentally, Ben-Hamina and Beaud found

that solubilized virion components inhibit translation in rabbit reticulocyte lysates (RRL) and Ehrlich ascites tumor cell-free systems (Ben-Hamida and Beaud, 1978). Sagot and Beaud later found that F17 (then called VP11b), a VACV core protein present in virions, cosediments with ribosomes both *in vivo* and *in vitro* (Sagot and Beaud, 1979) and postulated it may be related to the host-cell shut-off. Indeed, solubilized and purified F17 was later shown to be able to inhibit translation (Ben-Hamida et al., 1983; Person-Fernandez and Beaud, 1986), by preventing the formation of the 40S-Met-tRNA<sup>i</sup> complex *in vitro*. Surprisingly, and although other indirect roles in F17 regulating translation via the mTOR pathways have been described (Meade et al., 2018, 2019), F17 interaction with the 40S ribosome subunit has not been revisited to this date. Yet, the results shown by the Beaud lab suggest a direct and physical blockage of the 40S/Met-tRNA<sup>i</sup> interaction, possibly by directly interacting with the 40S (Figure 6A). Structural information are nevertheless required to shed light on how this blockage is achieved.

An other viral actor of VACV-induced translation inhibition is Protein 169. 169 is an early-expressed cytoplasmic viral protein found to be partly associated with polysomes (Strnadova et al., 2015) and is able to inhibit cap-dependent translation, as well as IRES-driven translation from FMDV and CrPV reporters. Notably, CrPV IGR-IRES does not require any eIFs for initiation to take place and as such, 169 appears as a general inhibitor of translation. The mechanistic details of this regulation are still lacking though, and in particular, whether this relies on direct interaction of 169 with ribosomal proteins is unknown.

*Coronaviridae* are a family of single-stranded positive RNA viruses that include Severe Acute Respiratory Syndrome Coronavirus 1 and 2 (SARS-CoV and SARS-CoV2), as well as Middle-East Respiratory Syndrome Coronavirus (MERS-CoV) and Porcine Epidemic Diarrhea Virus (PEDV). SARS-CoV and SARS-CoV2 NSP1 share 84,4% identity (Gordon et al., 2020) and strongly induce host translational shut-off (Banerjee et al., 2020; Kamitani et al., 2009; Lokugamage et al., 2012; Schubert et al., 2020; Tanaka et al., 2012; Thoms et al., 2020). NSP1 of SARS-CoV1 and 2, but not of the closely related PEDV or MERS-CoV (Lokugamage et al., 2015; Shen et al., 2018), interact with the ribosome 40S subunit, as well as 80S translationally-inactive monosomes devoid of mRNA (Kamitani et al., 2009; Schubert et al., 2020; Thoms et al., 2020). NSP1 C-terminus region resides in the mRNA entry channel, which physically prevents 40S association with mRNAs and thus translation. Strikingly, viral mRNAs, and chimeric reporters bearing the 5' viral leader are resistant to NSP1 induced translational shut-down (Banerjee et al., 2020; Schubert et al., 2020; Tanaka et al., 2012). A stem-loop structure, coined SL1, in the 5'UTR of viral mRNAs is necessary

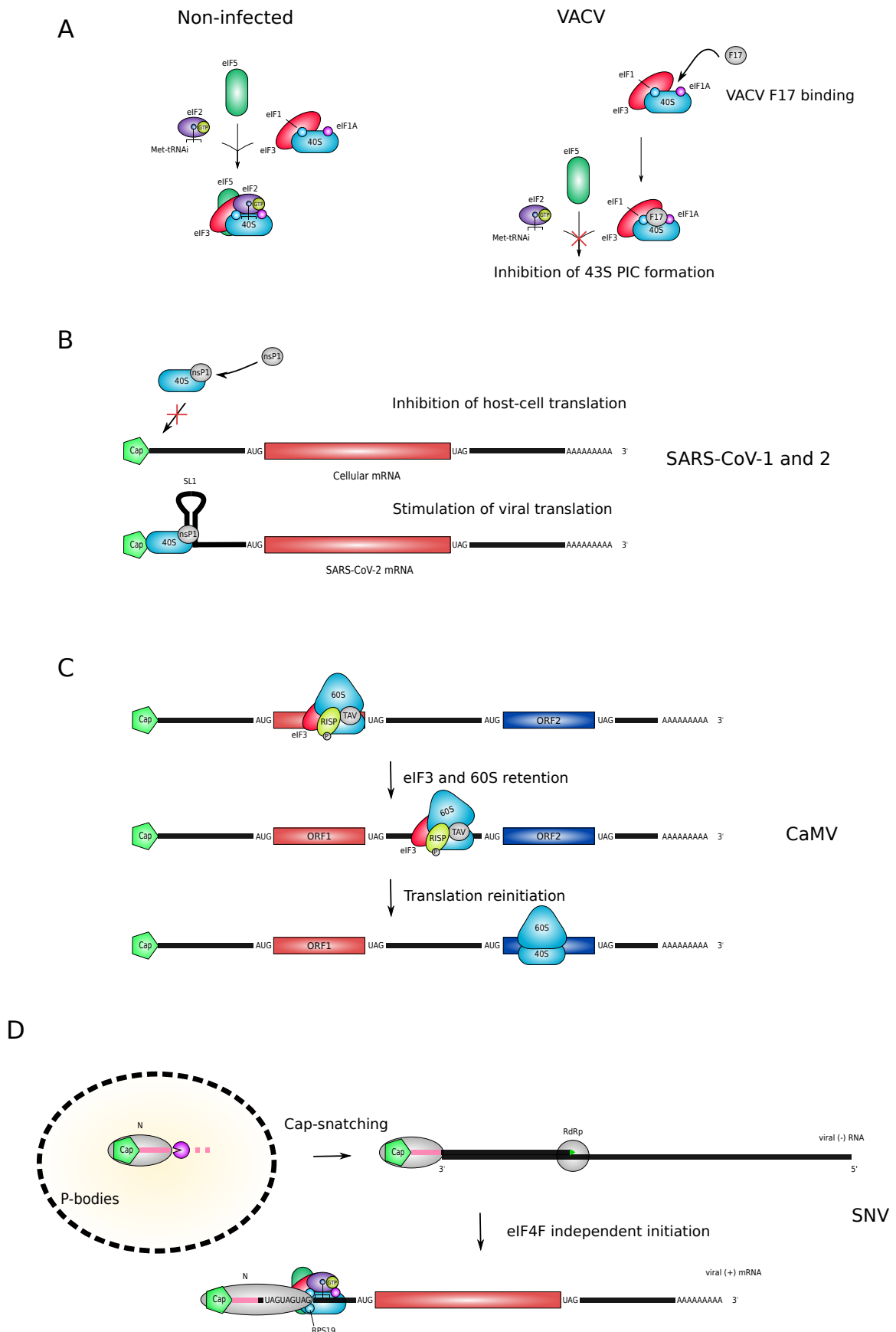


## Figure 6: Ribosome specilization by viral proteins

**A.** VACV F17 viral protein binds free 40S and prevents 43S formation.

**B.** SARS-CoVs nsP1 viral protein prevents nsP1 recruitment to host-cell mRNAs while promoting association to viral mRNAs by physically interacting with the SL1 stem-loop.

**C.** CaMV TAV recruits host protein RISP in its phosphorylated form to prevent eIF3 and 60S dissociation, hence promoting translation reinitiation of the viral mRNA.

**D.** SNV N protects host-cell mRNAs 5' extremity from P-bodies mRNA degradation for use in cap-snatching then substitutes for the entier eIF4F complex.

for viral mRNAs resistance to shut-down(Banerjee et al., 2020; Tanaka et al., 2012). How exactly this structure protects viral mRNAs from NSP1-mediated shut-down remains to be elucidated though (Figure 6B). Additionally, NSP1 also induces host mRNAs cleavage in a 40S-dependent manner. NSP1 does not have intrinsic endonuclease activity, but is able to induce host mRNA degradation *in cellulo*, as well as in cell-free translation systems(Gaglia Marta Maria et al., 2012; Huang et al., 2011). Viral mRNAs – and reporters bearing the viral 5'-UTR - are resistant to degradation as well. This suggests that NSP1-mediated mRNA degradation involves the ribosome, and more precisely, the 40S subunit. NSP1-mediated host-translational shut-off and mRNAs degradation are clearly distinct mechanisms though, as a NSP1 mutants defective for RNA cleavage still induce host translational shut-off while promoting viral mRNAs resistance to shut-off(Lokugamage et al., 2012). It is however surprising that both mechanisms involve interaction with the 40S subunit, and that viral mRNAs resist to both only through their 5'-UTR region. Additionally, interaction of the nucleocapsid N of several Coronaviruses with the ribosome, including SARS-CoV2, has been suggested(Chen et al., 2021; Emmott et al., 2013; Gordon et al., 2020), with no clear functional characterization to this date. However, Mouse Hepatitis Virus (MHV) N is reported to act as a non-sense mediated decay (NMD) inhibitor, protecting viral mRNAs from the host degradation machinery(Wada et al., 2018). Whether this is related to the potential interaction with the ribosome detailed earlier is unknown.

The Cauliflower mosaic virus (CaMV) transactivator viroplasm (TAV) protein strongly stimulates termination-reinitiation during the translation of the CaMV 35S pre-genomic polycistronic RNA(Bonneville et al., 1989; Fütterer and Hohn, 1991; Scholthof et al., 1992). TAV interacts with RPL24/eL24 and RPL18/eL18 as well as eIF3G(Park et al., 2001). TAV also recruits host-cell RISP, a protein that is not associated with polysomes in uninfected cells, on elongating ribosomes (Thiébeauld et al., 2009). TAV can also interact with TOR, which leads to TOR-dependent phosphorylation of RISP(Schepetilnikov et al., 2011). Thus, phosphorylated RISP acts as a scaffold for the ribosome/TAV/eIF3G interaction, which maintains the association of the eIF3 complex and the 60S ribosomal subunit during the course of elongation and after termination, and promotes reinitiation of downstream ORFs (Figure 5C).

*Hantaviridae* are a family of segmented negative antisense RNA viruses, of which Sin Nombre Virus (SNV) is the most studied. SNV expression relies on cap-snatching for the transcription of viral mRNAs. During this process, host cell mRNAs are cleaved 10-14 nucleotides downstream of the cap, and used by the viral RNA dependent RNA polymerase (RdRp) as primers to transcribe

viral mRNAs. During SNV infection, host-cell mRNAs are directed to P bodies for degradation (Mir et al., 2008). There, SNV N protein binds to capped mRNAs and protects 180 nucleotides downstream the cap from the RNA degradation machinery, hereby preserving the capped RNA fragment, before being further trimmed down to 10 nucleotides and used in viral mRNAs transcription (Garcin et al., 1995; Jin and Elliott, 1993; Mir and Panganiban, 2004; Mir et al., 2008). N then remains associated with the capped viral mRNAs through a specific AUGAUGAUG triplet present in the 5'-UTR of viral mRNAs (Mir and Panganiban, 2010). Interestingly, N is able to interact with the 40S subunit via RPS19/eS19, which is located near the mRNA exit channel (Cheng et al., 2011; Ganaie et al., 2014; Haque and Mir, 2010). As such, N directs the 40S ribosome subunit for translation of viral mRNAs and substitutes for the whole EIF4F complex. Indeed, N binds the cap, the ribosome and abrogates the need for EIF4A. Functionally, N reprograms the 40S ribosome subunit for the preferred translation of cap-snatched viral mRNAs (Figure 5D).

Enteroviruses, family *Picornaviridae*, produce a single uncapped positive RNA species, covalently linked at its 5' terminus by the viral protein Vpg. Translation is driven by an IRES in the 5'UTR of the mRNA (Martínez-Salas et al., 2015). Enteroviruses infection is accompanied by host cell translation shut-off, a mechanism mostly driven by the cleavage of translation factors EIF4G and PABP by the viral protease 2A (Bonderoff et al., 2008; Etchison and Fout, 1985; Etchison et al., 1982; Lloyd et al., 1987). Enterovirus A71 serotype RdRp associates with polysomes when overexpressed, and is able to interact with RPS6/eS6 in GST-pulldown experiments (Lee et al., 2020). A71 RdRp is able to stimulate A71-IRES-driven translation over cap-dependent translation *in cellulo* when overexpressed, although both pathways are stimulated in *in vitro* translation experiments (Lee et al., 2020). How exactly RdRp stimulates translation remains mostly unclear, and molecular characterization of this mechanisms is highly needed. In the context of infection, A71 RdRp could be another layer of regulation that favors IRES translation of viral mRNAs against cap-mediated translation of cellular mRNAs, by bridging the 60S ribosomal subunit to the IRES. This type of mechanism is regrouped under the term IRES transactivating factors (ITAFs), of which a plethora have been described for Enteroviruses, but all from host-cell origin (Martínez-Salas et al., 2015).

*Arteriviridae* are a family of positive RNA viruses who infect vertebrates, with a genome of ~15 kb long that serves as a template for antisense negative RNA intermediate. This (-)RNA is used for the transcription of the genomic RNA (gRNA) as well as several subgenomic RNAs. The gRNA



features two ORFs, ORF1a and ORF1ab, the second being produced as the fusion of domains ORF1a and ORF1b following -1 programmed ribosomal frameshifting (-1 PRF) at the end of ORF1a. This PRF is stimulated by a pseudoknot structure 5 nucleotides downstream of a slippery sequence where frame-shifting happens. A second PRF signal was discovered using Porcine Reproductive and Respiratory Syndrome Virus (PRRSV), a member of the *Arteriviridae* (Li et al., 2014). It lies within ORF1a, and can trigger both -1 and -2 PRF, and either produce a truncated form of nsp2 (-1) called nsp2N, or an extended transframe form of nsp2 (-2) called nsp2TM. Surprisingly, this PRF signal is not associated with any downstream RNA structure. Rather, -1 and -2 PRF are both stimulated by the viral nsp1B. Poly(rC) Binding Protein 1 and 2, two proteins that interact with nsp1B (Beura et al., 2011; Wang et al., 2012), were later found to participate in PRF transactivation as well (Naphthine et al., 2016), and both nsp1B and PCBP to interact directly with the gRNA, presumably at a C-rich motif downstream of the slippery sequence (Patel et al., 2020). This mechanism is conserved in other *Arteriviridae*, with the exception of Equine Arteritis Virus (EAV) and Wobbly Possum Disease Virus (WPDV) (Li et al., 2019a). Interestingly, nsp1B was found to interact with ribosomal proteins RPS14/uS11 and RPS5/eS25 (Beura et al., 2011). Whether this interaction participates in PRF remains unknown.

An other occurrence of PRF transactivation was described with Encephalomyocarditis Virus (EMCV), a member of the *Picornaviridae* family (Naphthine et al., 2017). EMCV encodes a transframe protein coined 2B\*, which results from -1 PRF within the 2B coding sequence (Loughran et al., 2011). Production of 2B\* is regulated by the viral protein 2A, which binds an RNA stem-loop 13-14 nucleotide downstream of a slippery sequence. Because the level of 2A protein increases dramatically at late-time infection, this drives production of 2B\* towards the end of the replicative cycle. These results extend to other *Picornaviridae*, such as Theiler's murine encephalomyelitis virus (TMCV) (Naphthine et al., 2019).

## 4. The role of ribosome-associated proteins

As shown earlier with the case of PCBP2 regulation of PRRSV PRF (Naphthine et al., 2016), host-cell proteins that interact with the ribosome can regulate viral translation as well. In fact, a wide number of ribosome associated proteins (RAPs) are defined as IRES Trans-Activating Factors (ITAFs) (see (Imami et al., 2018; Simsek et al., 2017) for lists of RAPs and (King et al., 2010; Lee et al., 2017; Martínez-Salas et al., 2013, 2015; Stern-Ginossar et al., 2019) for ITAFs and their

roles) and participate in IRES-mediated translation of many viruses. Since this subject has been largely reviewed, we chose not to address it and direct interested readers to previously mentioned reviews. Similarly, we exclude the mechanisms of host-translational shutoff, that, for the most part, do not fit into the category of “specialized ribosomes”. For reviews, see (Cao et al., 2017; Carrasco et al., 2018; Dhungel et al., 2020; Fros and Pijlman, 2016; Hoang et al., 2018; Poblete-Durán et al., 2016; Stern-Ginossar et al., 2019).

DExD and DExH -box RNA helicases are two large families of enzymes with the ability to melt double-stranded RNA structures. The helicases are implicated in all the major pathways of gene expression (Bourgeois et al., 2016), and translation is no exception (Shen and Pelletier, 2020). DDX3X, a member of the DExD family, is an essential factor for the replication of many viruses, with roles including, but not limited to, IRES transactivation (Hernández-Díaz et al., 2021; Soto-Rifo and Ohlmann, 2013). In human cells, DDX3X directly interacts with the ribosome 40S small subunit 18S rRNA, as well as a subpopulation of mRNAs with highly structured 5'UTRs (Calviello et al., 2021). Consequently, siRNA depletion of DDX3X provokes reduced translation of these target mRNAs (Calviello et al., 2021; Soto-Rifo et al., 2012). A similar role has been found for the translation of Retroviridae HIV-1 (Soto-Rifo et al., 2012, 2013). DDX3X is necessary for unwinding of the trans-activation responsive element (TAR), the very first stem-loop of HIV-1 mRNA 5'UTR, and allows scanning of the small ribosome subunit (Figure 7A). In canonical translation, eIF4A is the helicase that unwinds RNA structures during scanning, yet since TAR is a stem-loop that comprises the cap of HIV-1 mRNAs, scanning of the mRNA cannot even begin. As such, if the mRNA is extended in the 5' direction by a non-structured sequence, scanning can start and DDX3X dependency is abrogated (Soto-Rifo et al., 2012). Finally, DDX3X inhibitors are showing promising effects in HIV-1 treatment (Rao et al., 2021).

SHFL (also called Shiftless, C19orf66, IRAV and RyDEN) is an Interferon Induced Gene (ISG) whose role has only been recently described. SHFL is induced during HIV-1 infection and is able to inhibit -1 PRF recoding within the Gag-Pol ORF, which leads to premature termination of translation (Wang et al., 2019) (Figure 7B). SHFL also affects PRF of many viruses, namely RSV, HTLV, MMTV, HIV-2, SIV, SINV, as well as cellular genes PEG10 and CCR5. SHFL was shown to co-sediment with polysomes and to display weak interaction towards RPS31/eS31 and RPL11/uL5 in GST-pulldown experiments (Wang et al., 2019). Live-cell imaging revealed that only a subset of a reporter mRNA produce robust frameshifting (Lyon et al., 2019). This suggests a role of mRNA modifications or local concentration of cellular proteins in regulating frame-shifting. The role of

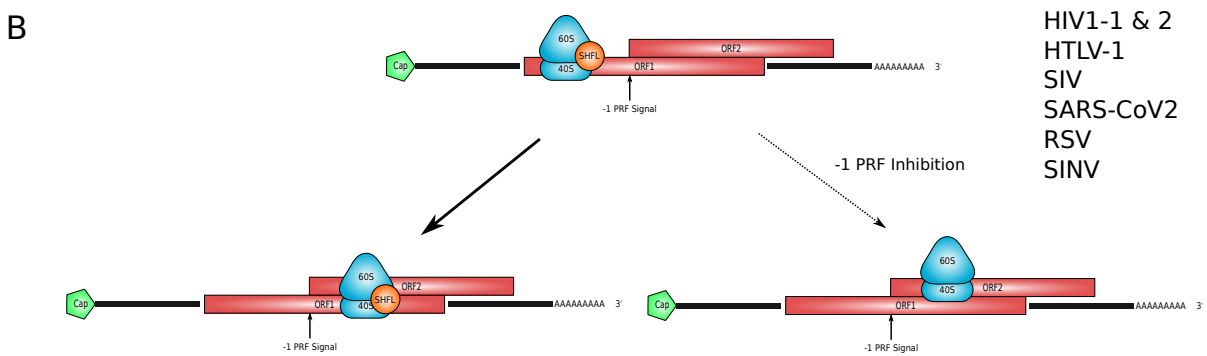
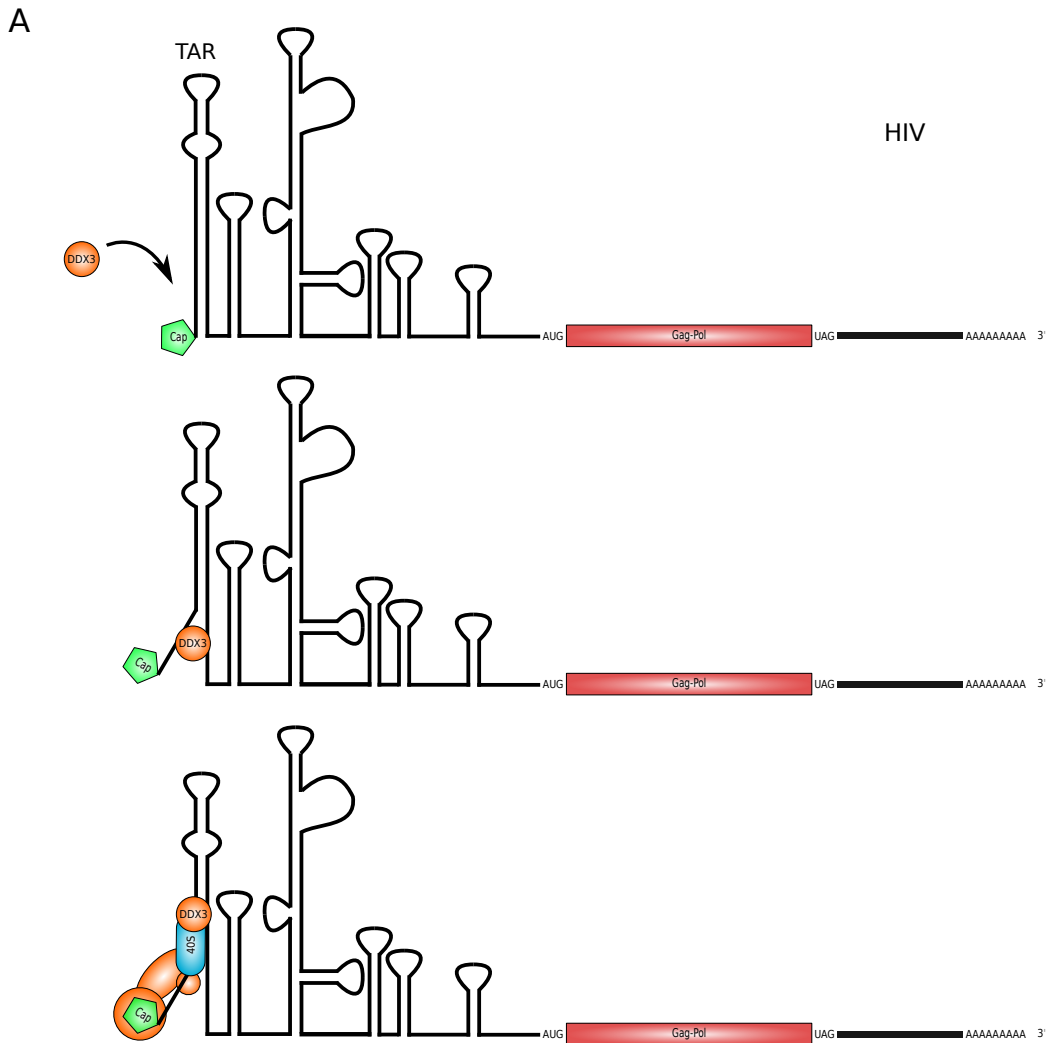


**Figure 7: Translation control of viral mRNAs by cellular proteins**

**A.** DDX3 unwinds the 5' extremity of HIV TAR to allow 40S joining

**B.** SHFL inhibits -1 PRF of several viral mRNAs

SHFL in regulating frameshifting fits with this observation, as only mRNAs devoid of SHFL would be able to reliably induce frameshifting(Lyon et al., 2019; Wang et al., 2019). Recently, SHFL was shown to be associated with SARS-CoV2 gRNA(Lee et al., 2021a; Schmidt et al., 2021a), and to inhibit PRF, which is necessary for the production of ORF1b encoding the viral RdRp. Numerous other roles of SHFL have been described in inhibiting viral replication, in particular of viruses that do not feature PRF, such as Dengue virus (DENV)(Balinsky et al.; Kinast et al., 2020; Rodriguez et al.; Suzuki et al., 2016; Wu et al., 2020). So its place in restricting infection is probably not limited to PRF dampening.

## 5. rRNA modifications in viral infection

rRNA are highly modified core constituents of the ribosome(Natchiar et al., 2017; Sharma and Lafontaine, 2015) and represent two third of the ribosome mass, the remaining third corresponding to RPs. 95% of reported modifications of rRNAs are 2'-O ribose methylation(2'-O-Me), a mark deposited on the sugar backbone of RNAs, and pseudouridylation ( $\Psi$ ), a conversion of uridines into pseudouridines. The remaining 5% of modifications are base modifications, such as base methylation.

2'-O-Me and  $\Psi$  deposition are guided by small nucleolar RNAs (snoRNAs) by base pairing with the target site. Two types of snoRNAs, C/D box snoRNAs and H/ACA snoRNAs, are distinguished based on their conserved sequence motifs. C/D box snoRNAs guide 2'-O-Me, and interact both with the rRNA site and a four-member complex composed of SNU13, NOP56, NOP58 and FBL, with FBL being the methyltransferase. H/ACA snoRNAs, on the other hand, guide the four-member complex made up of NOP10, NHP2, GAR1 and DKC1, with DKC1 catalyzing pseudouridylation(Bachellerie et al., 2002; Lafontaine, 2015).

Heterogeneity in levels of 2'-O-Me have been found HeLa cells(Erales et al., 2017; Krogh et al., 2016). Several positions in 18S and 28S rRNA where found to be uncompleted methylated, in contrast with the vast majority of positions (16 out of 105)(Erales et al., 2017). FBL knockdown in HeLa cells further reduced methylation levels at all lowly methylated sites as well as other previously fully methylated sites. FBL was then shown to specifically reduce IRES-mediated translation over cap-dependent translation *in cellulo*, using reporters harboring cellular and viral IRES sequences. Namely, IGF1R and FGF1 but not VEGFA cellular IRES-mediated translation was

inhibited, as well as ECMV IRES- and CrPV IGR-IRES-mediated translation. Reconstituted RRL using ribosomes from FBL-depleted cells showed reduced levels of CrPV IGR-IRES translation compared to capped Globin and GAPDH reporters, that only showed modest non-significant decrease. These results are partly challenged by the Mazumder lab (Basu et al., 2011; Chaudhuri et al., 2007). Their studies were prompted by the discovery that RPL13a/uL13 becomes phosphorylated and is released from the ribosome following IFN- $\gamma$  treatment, to interact with GAPDH, the Glutamyl-Prolyl-tRNA-synthetase EPRS1 and HNRNPQ/SYNCRIP/NSAP1 (Mazumder et al., 2003, 2014; Sampath et al., 2004). Once formed, this complex, called the Gamma-Interferon Activated Inhibitor of Translation (GAIT) complex, inhibits the translation of mRNAs harboring a responsive element, called the GAIT element. The Mazumder lab investigated whether RPL13a/uL13-devoid ribosomes were affected in their ability to mediate different canonical and non-canonical translation pathways, by silencing RPL13a (Basu et al., 2011; Chaudhuri et al., 2007). RPL13a depletion was shown not to affect cap-dependent translation, translation fidelity or -1 PRF of SARS-CoV and HIV-1. However, rRNA methylation was shown to be drastically diminished, which coincided with a stark decrease in IRES-mediated translation. Namely, IRES-driven translation of cellular genes STAT2, p53 and p27 was inhibited, but that of the HCV and CrPV IGR-IRESs was not. Inhibition of rRNA methylation by the methylation inhibitor cycloleucine, or by FBL knockdown produced the same effects, suggesting that this effect was directly related to rRNA methylation (Figure 8). Although the Mazumder and Diaz lab both report an effect of rRNA methylation on IRES-mediated translation, the discrepancy regarding CrPV IGR-IRES dependency calls for additional examination. FBL is necessary for the replication of Hendra virus (HeV) and Nipah virus (NiV) and Respiratory Syncytial Virus (RSV), three of the *Paramyxoviridae* family, but not that of the unrelated Influenza A Virus (IAV) (Deffrasnes et al., 2016). These viruses do not rely on IRES-mediated translation though, and rather use conventional capped and polyA-tail mediated translation (Noton and Fearn, 2015). It is thus unclear whether the FBL role in regulating *Paramyxoviridae* replication is mediated by 2'-O-Me levels or to other functions attributed to FBL (Iyer-Bierhoff et al., 2018; Tessarz et al., 2014). Additionally, reports have indicated that some viral proteins interact with FBL, which could suggest that viruses themselves modify rRNA methylation (Cristea et al., 2010; Yoo et al., 2003).

Strikingly, the role of  $\Psi$  in translation appears to be in part similar to 2'-O-Me. Mutations in the pseudouridylase DKC1 impair IRES-driven translation of cellular XIAP and p27, as well as BCL2L1/Bcl-xL, whose translation doesn't involve an IRES, and CrPV IGR-IRES-driven translation, with cap-dependent translation being unaffected (Yoon et al., 2006) (Figure 8).

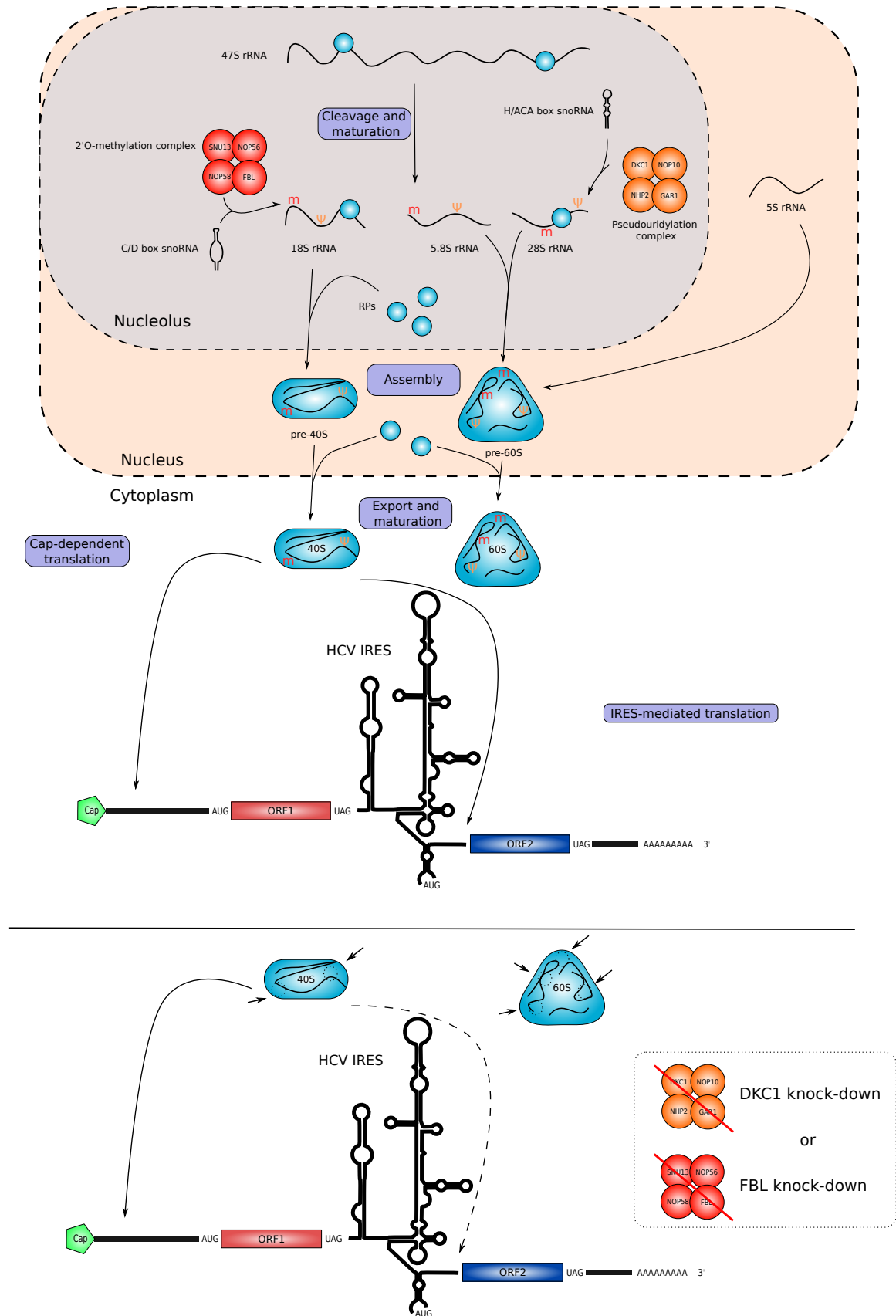


**Figure 8: Reduced levels of rRNA 2'O-methylation (m) and pseudouridylation (Ψ) lead to inhibition of IRES-mediated translation**

2'O-methylation and pseudouridylation complexes modify ribosomal RNAs at several positions. Knock-down of FBL and DKC1, the catalytical subunits of these complexes reduces the level of HCV IRES-mediated translation in a bicistronic reporter.

Impairment of CrPV IGR IRES translation are explained by a reduction in affinity of the 40S subunit towards the IRES.(Jack et al., 2011). However, the D95A inactivating mutations in DKC1 yeast homolog also reduces translation fidelity, and strongly enhances -1 and +1 PRF of L-A yeast virus and Ty1 retrotransposable element respectively(Jack et al., 2011). This carries over to human cells, where -1 PRF of HIV-1 and cellular genes CCR5 and IL7R is increased following DKC1 siRNA treatment. Finally, recent reports indicate that H/ACA snoRNA depletion causes increased levels of read-through(McMahon et al., 2019), a mechanism used several viruses.

Altogether, these studies suggest that many of the alternative translation pathways used by viruses can be controlled by rRNA modification levels, which raises the question whether the host cell or viruses manipulate rRNA modifications during infection. RNA viruses infection strongly affects nucleolar organization where snoRNAs are produced(Hiscox, 2007; Salvetti and Greco, 2014), and such CHIKV infection affects the abundance of several C/D and some H/ACA snoRNAs(Saxena et al., 2013). Although no direct link between viral infection, rRNA modification alterations, and translation control of viral mRNAs have surfaced to date, it is tempting to hypothesize that rRNA modification alterations can influence the replication of viruses. In particular, since cellular IRESs typically serve in stress response (Yang and Wang, 2019b), decreased translation of cellular IRESs caused by reduced levels of rRNA modification could be a way for viruses to impair the host response to infection, most importantly for viruses that do not rely on IRES-mediated translation.

Lastly, Ribosome Inactivation Proteins (RIPs) probably constitute the most drastic case of rRNA modifications related to infection. RIPs are a class of N-glycosidase expressed by plants that primarily depurinate rRNAs. RIPs, of which ricin is the most known, are largely implicated in the resistance of plants to pathogens, especially of bacteria, fungi and insects, and causing translation arrests in the pathogen cells by depurinating rRNA of the attacker(Zhu et al., 2018). However, roles of RIPs have been shown for many viral infection as well. Given that viruses rely on the host ribosomes, this would suggest that plant RIPs can contribute to translation arrest in the infected cells to prevent viral spread(Parikh and Tumer, 2004). However, RIPs that restrict viral infection have not been found to be able to depurinate rRNA of the infected cells(Song et al., 2000; Tumer et al., 1997), suggesting that the effect rather lie in viral RNA modification(Domashevskiy et al., 2012; Picard et al., 2005; Vandenbussche et al., 2004). The role of RIPs in pathogen resistance has been well-reviewed recently, and we direct interested readers to (Zhu et al., 2018).

## Conclusion: the rise of ribo-centric methods

As shown in this review, viral subversion of heterogenous populations of ribosomes can be found throughout the field of virology. As of now, all major pathways of ribosome specialization, with the exception of ribosomal proteins paralogue usage, have been shown to be important for viral mRNAs translation, with examples dating back to 1970s. This field has mostly progressed under the radar until now, with low count citation numbers on papers that yet laid the foundations of this domain. Many of the old studies remained purely descriptive, but some rare mechanisms have been thoroughly studied and now represent archetypical cases of viral subversion of specialized ribosomes(Landry et al., 2009; Nishiyama et al., 2007), or even viral-induced ribosome specialization(Jha et al., 2017). This specialization is functionally linked with translation and especially with non-canonical translation pathways, of which viruses are extremely fond of(Firth and Brierley, 2012).

In recent times, many technological advancements have been made towards the high-throughput, unbiased, highly-detailed characterization of ribosome heterogeneity, but they have yet to be used in the context of infection. We list here the biggest questions of the field, and mention methods on how to answer them.

Does viral infection influence the level of incorporation of RPs into translating ribosomes ? SRM-based quantification of RPs, an extremely precise mass-sprecrtomety based quantification method, should answer this question(Shi et al., 2017).

What is the extent of post-translational modifications that are deposited onto ribosomes during infection, and how do these modification link to viral translation ? Phosphoproteome(Avey et al., 2015; Greenwood et al., 2016; Mohl et al., 2017; Oberstein et al., 2015; Söderholm et al., 2016; Yángüez et al., 2018), ubiquitome(Zhang et al., 2018a), changes have been looked at using modification- enrichment during viral infection, yet none actually focused ribosomal proteins. Additionally, top-down proteomics provides strong benefits compared to this strategy, as it is not restricted to one modification and is more quantitative(Chen et al., 2018; Waterbeemd et al., 2018).

To what extent is the ribosome interactome recomposed during infection? This should be answered using mass-spectrometry quantification of ribosome interactants from purified ribosomes(Simsek et al., 2017). Identifying all the viral proteins that interact with the ribosome is also possible here.



Are viruses able to modify the post-translational modification status of rRNA ? RiboMeth-seq(Marchand et al., 2016) and Nanopore sequencing(Begik et al., 2021) are precious tools here.

What are the functional relevance of ribosome heterogeneity in the context of infection? Affinity-purification based of ribosomes bearing particular interactants is of great help here. Additionally, reconstituted cell-free translation systems can help isolate the role of the ribosome from the general context of infection(Penzo et al., 2016).

The methods mentioned here have all been developed in the last ten years, which means it is now time to revisit these questions. After all, and as mentioned before, virology had a major role in the discovery of ribosome heterogeneity, and new technological advancements now call for further investigation of ribosome heterogeneity and of how it may contribute to host-pathogen interactions.

# Part I: Recomposition of the ribosome interactome by SINV infection

## Introduction

As shown before, viral infections induce profound alterations to the translation machinery. Some viruses rely on specific translation initiation pathways that are partly independent of canonical initiation factors for the translation of their own mRNAs and they may directly impact the ribosome biochemistry and exploit subset of specialized ribosomes, either for translation initiation or alternative elongation pathways such as frame-shifting. Thus, we sought out to characterize the extent to which the ribosomes are remodeled during infection. We developed a method to precisely measure the changes in ribosome associated proteins (RAPs) consecutive to infection by specific affinity-purification of endogenously tagged ribosomes and quantitative measure of RAPs abundance. By using 40S tagged ribosomes, we are able to question the changes in initiation factors requirements as well as that other RAPs that may impact other aspects of RNA biology. We used the alphavirus Sindbis (SINV) as a model to question ribosome interactome recomposition during infection. Many aspects of SINV biology makes it a great candidate for this approach. Firstly, SINV infection leads to a massive translational shut-off during infection, and at late time points only the viral sub-genomic mRNA is substantially translated. As such, changes in RAPs abundance are expected to show profound changes in ribosome activity. Secondly, initiation factors requirements of the SINV sgRNA are drastically different from that of host-cell mRNAs, in that its translation is eIF4E, eIF4G, eIF4A independent and is insensitive to the phosphorylation of eIF2 $\alpha$  that infection leads to.

SINV was recently used as a model to decipher the changes in interaction of RNA binding proteins to the pool of mRNAs in infected cells. The RBPome and RAPs partly overlap and this provides an unprecedented opportunity to look at two related aspects of RNA biology in concert. Our results uncover pervasive changes in RAPs abundance consecutive to SINV infection. We show that ribosome biogenesis is altered by SINV infection and leads to 40S pre-ribosome retention in the nucleus and accumulation of unprocessed 60S pre-ribosome in the cytoplasm. We also show that many of the RAPs changes consecutive to infection correlate with subcellular localization changes.

Finally, our data provides critical information that may help better decipher the mode of SINV sgRNA translation.

The traditional methods for ribosome purification rely on ultra-centrifugation-based separation of cellular components. Assembled ribosomes have a 80S sedimentation coefficient which is higher than most cytoplasmic components. When several ribosomes translate the same mRNA and constitute what are called polysomes, this sedimentation coefficient is further increased because the complex is heavier and denser than isolated 80S monosomes. Polysomes fractionation is thus the method of choice for separating elongating ribosomes from the non-translated mRNAs and free ribosomal subunits. It has been extensively used in ribosome profiling experiments which involves RNase treatment of a cytoplasmic lysate which separates ribosomes from one-another followed by sucrose-gradient and ultra-centrifugation-based isolation of the resulting 80S peak (Ingolia et al., 2014b). In this situation, nucleotides that reside in the ribosomes are protected by the ribosome for RNase degradation and 28-32 nucleotide long fragments of mRNAs can be recovered to assess the position of translating ribosomes. Although this strategy has been applied for characterization of ribosomal interactants by mass-spectrometry analysis (Reschke et al., 2013), it suffers one major limitation. Several other cellular components are found in heavy complexes with sedimentation coefficient of 80S and more. Cellular membranes in particular can migrate in the same fractions than ribosomes in sucrose-gradient and as such, proteins like clathrin distribute throughout the gradients (Simsek et al., 2017). Although this kind of method can be applied to investigate the changes in RAPs during infection (Aviner et al., 2021), many of the proteins whose abundance changes in the gradient are not *bona fide* ribosome interactants and the analysis is limited to those for which the association with the ribosome has been properly defined. This strategy is especially improper to detect viral proteins that may interact with the ribosome. Others have separated polysomes gradients into very small fractions that are smaller than the average size of peaks into polysomes (Imami et al., 2018). This allows to measure the fluctuations in ribosomal proteins abundance that are due to the separation of polysomes of different size (disomes, trisomes, etc). Accordingly, proteins that interact with polysomes fluctuate in abundance along the gradients, following that of ribosomal proteins. This strategy, although very elegant, suffers major drawbacks. First, it is extremely costly because it requires the analysis of 36 samples per gradient to achieve the required resolution. Second, polysomes peaks need to be well resolved, and as consequence, the amount of material that is loaded on the gradient is limited, which in turn limits the detection of protein of low abundance. Finally, because this method requires intact polysomes, RNA binding

proteins that interact with only the mRNA and not the ribosome are recovered as well and cannot be discriminated from *bona fide* ribosome interactants.

## Results

### Development of affinity purification of endogenously tagged ribosomes

We sought out to use an affinity purification-based method for the isolation of ribosomes, similar to what has since been published (Simsek et al., 2017). We chose to use epitope-tagged ribosomes over antibodies directed against ribosomal proteins for several reasons. First, few commercial antibodies are compatible with immunoprecipitation assays and screening for the ones that do allow for immunoprecipitation is costly and time-consuming. Second, even fewer commercial antibodies are likely to allow for competitive elution of the affinity purified complex, a critical aspect of purification for subsequent mass-spectrometry analysis (see below), because the affinity may be too strong. This is further complicated by the fact that the epitope recognized is generally not disclosed and that custom peptide synthesis is very expensive. Third, characterization of a complex interactome requires a comparison with a control condition. Although non-specific immunoglobulins can be used as a control, they fail to account for the unspecificity that is conferred by the paratope. Finally, we wanted this method to be universal and applicable to animal cells other than humans and especially mice. Cross-reactivity of antibodies is generally limited and this means that changing of model species requires to validate new antibodies to perform the purification. In contrast, because the structure of the ribosome is extremely conserved among eukaryotes, tagged ribosomal proteins are likely to support the purification of ribosomes similarly in many species.

To ensure that the tagged ribosomal proteins is entirely integrated into translating ribosomes, we performed endogenous tagging of the ribosomal proteins genes using the CRISPR/Cas9 method. Other methods such as transient expression from plasmids or expression by an inducible promoter such as the Flip-In T-Rex system overexpress the gene of interest on top of the endogenous expression levels and as a consequence, a significant proportion of the tagged protein is likely to remain unassociated with the ribosome.

At the time we started this project, only a limited number of ribosomal proteins had been showed to support tagging of ribosomal proteins and subsequent isolation of ribosomes in mammals. eL22/RPL22 has endogenously been tagged in C-terminus by the HA epitope peptide in mice and

allows for purification of translating ribosomes(Sanz et al., 2009a). However, no specific sgRNA could be designed targeting this gene. In fact, many ribosomal proteins genes are present in the genome in the form of pseudogenes, sometimes in dozens of copies, which is also the case for RPL22. As a consequence, they cannot be specifically targeted by the Cas9 system and all possible sgRNAs that could be used for endogenous tagging also target the pseudogenes. This can result genome rearrangement(Cullot et al., 2019), which we sought to avoid. uL1/RPL10A had also been tagged in mice using a N-terminal fusion to GFP(Doyle et al., 2008; Heiman et al., 2008). We reasoned that if RPL10A tolerated GFP, it would tolerate smaller tags that would be compatible with our approach. However, shortly after we had constructed a cell line with endogenously tagged RPL10A, it was shown the RPL10A is not present in all ribosomes in the cell and that RPL10A-containing ribosomes translate a specific subset of mRNAs(Shi et al., 2017). As we wanted our method to precipitate all kinds of ribosomes, we decided to choose other proteins. Shortly after, Simsek and colleagues showed that ribosomes could be immunoprecipitated using endogenously Flag-tagged eS17/RPS17 and eL36/RPL36 in mouse embryonic stem cells. However, and similarly to RPL22, these genes also exist in the form of pseudogenes in the human genome and cannot be specifically targeted by the CRISPR/Cas9 method. Thus, we decided to lookout for other ribosomal proteins for our strategy.

We investigated the potential for ribosomal proteins to serve as an anchor for epitope-based purification of ribosomes using the structure of the human ribosome. We selected proteins based on accessibility on one of the termini on the surface of the ribosome. Then, we only retained those for which specific sgRNA could be designed, using Genome Browser integrated sgRNA design tool. eS12/RPS12, uS10/RPS20, uS7/RPS5, uL5/RPL11 and eL8/RPL7A were selected following these rules (Figure 9).

To perform CRISPR/Cas9-directed endogenous tagging, sgRNAs targeting a 10-nucleotide window centered around the start or stop codon were chosen according to what extremity is accessible on the surface of the ribosome. We used 200-long nucleotide single-stranded oligonucleotides as a matrix for homologous-directed recombination. Homologous directed recombination can be achieved using plasmid-sized recombination matrices with >800 nucleotide homology arms, however it is extremely inefficient and requires construction of the matrix prior to transfection. In contrast, single-stranded oligonucleotides can be used for endogenous homologous-directed recombination with very high efficiency, but are limited in size of the desired modification, and can

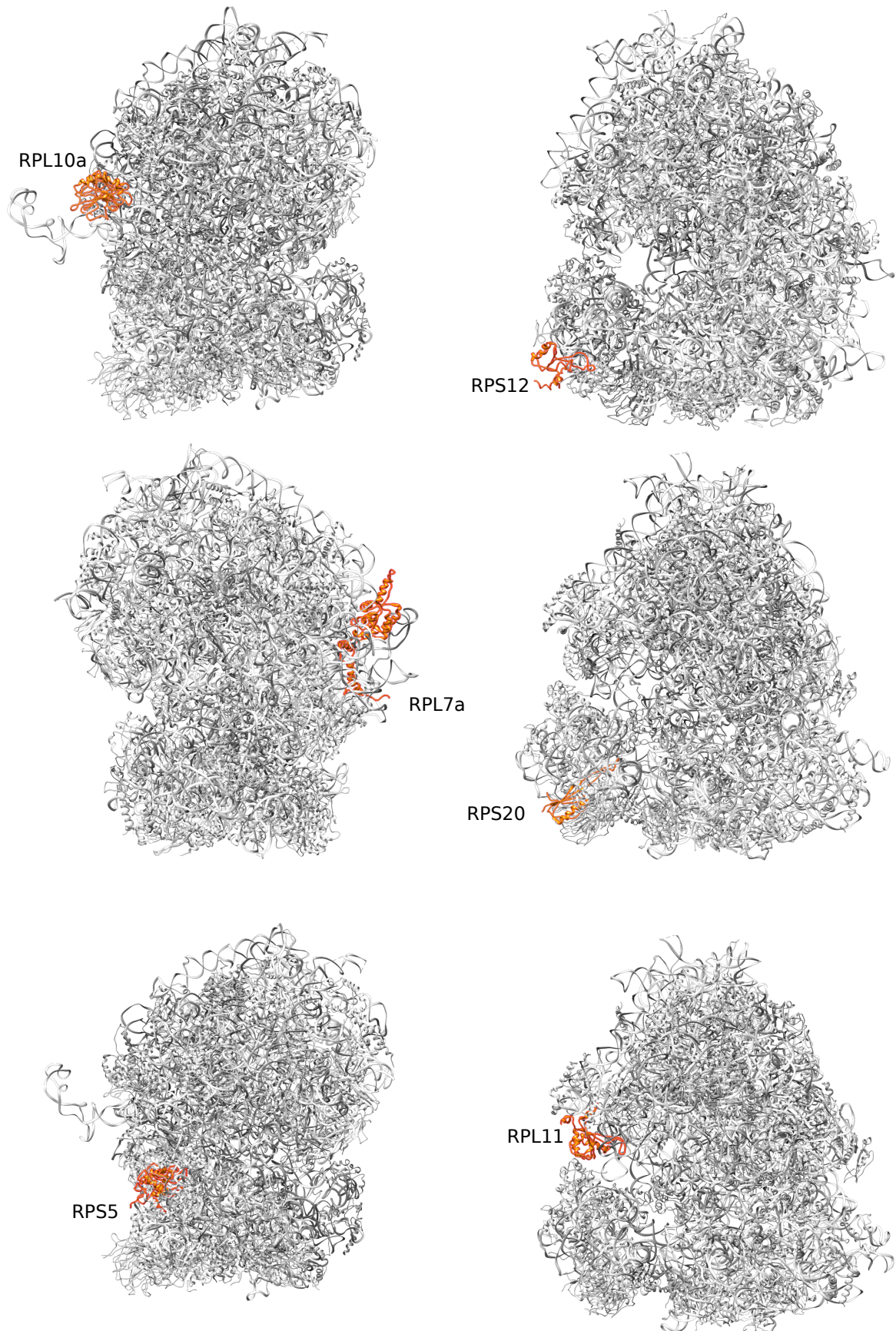


**Figure 9: Localization of ribosomal proteins candidates for endogenous tagging on the surface of the ribosome**  
The structure of the ribosome (PDB: 4UG0, (Khatter et al., 2015)) was loaded into Chimera and selected proteins were highlighted.

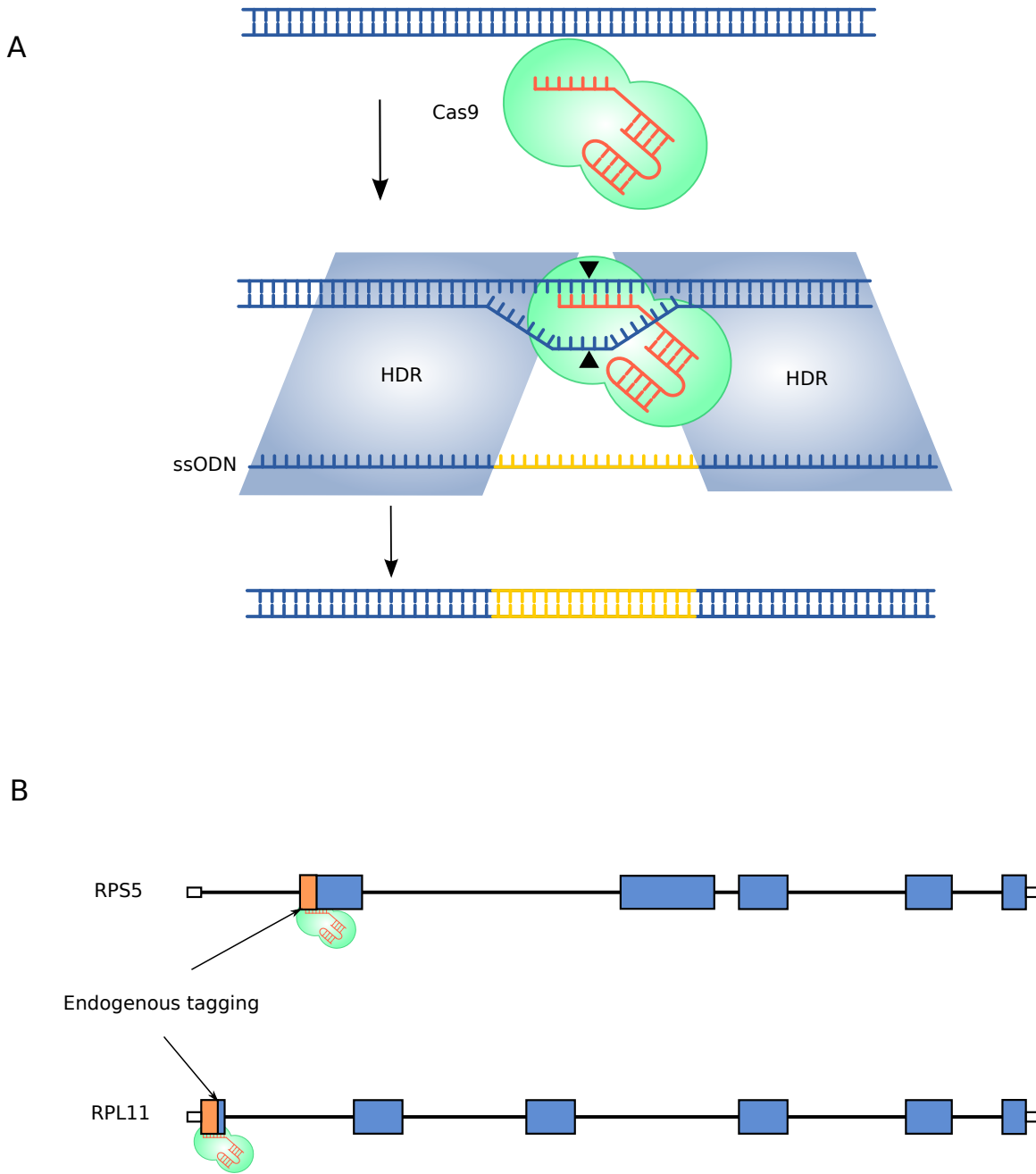


**Figure 10: CRISPR-mediated endogenous tagging of ribosomal proteins**  
**A.** Schematic representation of ssODN-mediated CRISPR-induced endogenous tagging.  
**B.** Schematic representation of the strategy used to endogenously tag RPS5 and RPL11 at their N-termini.

be ordered directly in the form of oligonucleotides(Richardson et al., 2016; Yoshimi et al., 2016). We chose this approach as it aligns perfectly with our epitope-based purification (Figure 10A).

We chose the short 8-amino acid long Flag-peptide (DYKDDDDK) as an anchor for affinity-based purification. Unlike several other commonly used epitope tags, Flag-based affinity purified protein complexes can be eluted off the affinity resin using competition with excess free Flag peptide(Kimple et al., 2013). This drastically improves purity over other strategies based on complete or partial denaturation of the antibodies. Because of its reduced size, it is also considered less likely to alter protein function compared to other bigger tags(Kimple et al., 2013).

Of the 5 ribosomal proteins mentioned earlier, we ended up selecting RPL11/uL5 and RPS5/uS7 for our method (Figure 10B). Shortly, RPS20/uS10 Flag-tagged cells did not tolerate the integration of the Flag-tag sequence at the N-terminus of the protein and although integration of the sequence was very efficient, the presence of the recombined allele decreased rapidly overtime. This suggests that presence of the tag affected the functionality of the protein or interfered with the binding of a crucial ribosomal interacting protein. RPS12/eS12 Flag-tagged cells tolerated the Flag-sequence well, but we observed a strong immunoprecipitation bias towards free 40S (not shown), possibly because the protein extremity was not accessible in elongating ribosomes or because the Flag-sequence is masked by an interacting protein. Finally, although tolerated by the cells, Flag-RPL7A/eL8 immunoprecipitation was much less efficient than RPL11/uL5 and RPS5/uS7, probably because of limited accessibility to the antibody.

HEK293T cells expressing the tagged versions of RPS5/uS7 and RPL11/uL5 were produced and clones were derived to ensure a homogenous cell population. Flag-immunoprecipitation followed by Western Blot analysis revealed successful immunoprecipitation of both Flag-tagged proteins and co-immunoprecipitation of RPS3a and RPL30, indicating that 80S ribosomes could be immunoprecipitated (Figure 11).

We then proceeded to verify the specificity of our immunoprecipitation approach. To correctly describe the ribosome interactome, the eluate from the beads needs to be compared with a mock IP where no tag is expressed. This is notoriously difficult to achieve for ribosomes as they are among the most abundant complex in the cell. In fact, ribosomes are so abundant that ribosomal proteins, translation factors and heat-shock proteins are very common contaminants of immunoprecipitations(Mellacheruvu et al., 2013). This means that when comparing ribosome immunoprecipitation to a control, it is difficult to achieve a high enrichment factor for ribosomal



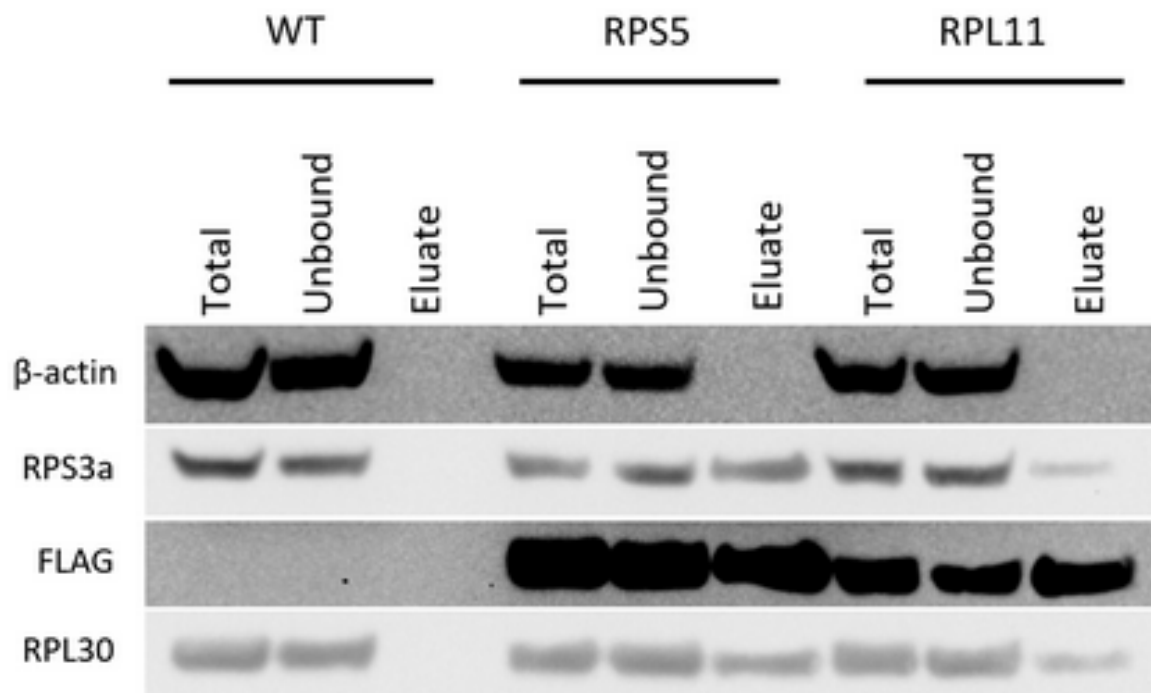


**Figure 11: Purification of ribosomes using endogenously tagged Flag-RPS5 and Flag-RPL11 cells**

WT, Flag-RPS55, Flag-RPL11 were submitted to Flag immunoprecipitation. The cytoplasmic fraction (Total), cytoplasmic fraction after immunoprecipitation (unbound), and bead eluate (Eluate) were collected, methanol-chloroform precipitated and analyzed by Western Blot.

proteins and RAPs. The data released by Simsek and colleagues highlights this difficulty (Simsek et al., 2017). The median enrichment for ribosomal proteins over control immunoprecipitation was only about 5 in log<sub>2</sub> or 32 in linear scale in their RPS17/eS17 immunoprecipitation. This puts a hard limit to the enrichment that can be observed for RAPs between control and ribosome purifications. RAPs abundance is tied to ribosome abundance and as such, the enrichment of RAPs cannot, in theory, exceed that of RPs.

Our desire to investigate the changes in RAPs following infection puts harder pressure on the ability of the method to answer this question. Changes in RAPs following infection are likely to go both ways: some proteins may become more associated with the ribosome while others will be less associated with the ribosome as a result of infection. There is a fundamental limit to the fold change that can be observed in the “less” direction. If proteins are only enriched by a factor of 2 over a control IP, the fold change in ribosome association following infection cannot be stronger than -2, because then, contribution of the noise due to aspecific binding to the beads becomes the major contribution to peptide abundance. Furthermore, we wanted to be able to compare fold changes in the minus direction between different proteins. At late time during SINV infection, host-cell translation is almost entirely abolished and only the sgRNA is significantly translated. Thus, we expected that initiation factors would generally be less associated with the ribosome, but because the sgRNA needs for initiation factors differs drastically from cellular mRNAs, the fold change in ribosome association would likely be different depending on whether the factor is required or not. This requires that initiation factors levels are significantly above background levels for the difference to appear and be measurable.

We set a very high bar for the quality that our method should reach. We wanted to reach the best enrichment factor for ribosomal proteins that we could, which would provide a longer dynamic range for changes to be observed. Contaminants levels should be kept to a minimum and we wanted reliable identification of initiation factors. Our strategy was optimized over the course of three years, with multiple rounds of optimization and analysis by mass-spectrometry.

We performed a previously published protocol for Flag-based immunoprecipitation (Ricci et al., 2014; Sharma et al., 2016) on WT and Flag-RPS5 HEK293T (Figure 12, Step 1). Shortly, cells were lysed and nuclei were eliminated by centrifugation. Immunoprecipitation was performed using anti-FLAG M2 Agarose Affinity Beads. Finally, ribosomes were eluted by Flag peptide competition and analyzed samples were analyzed by mass-spectrometry. We found that although ribosomes were readily enriched, the immunoprecipitation was highly aspecific, as is highlighted by the large

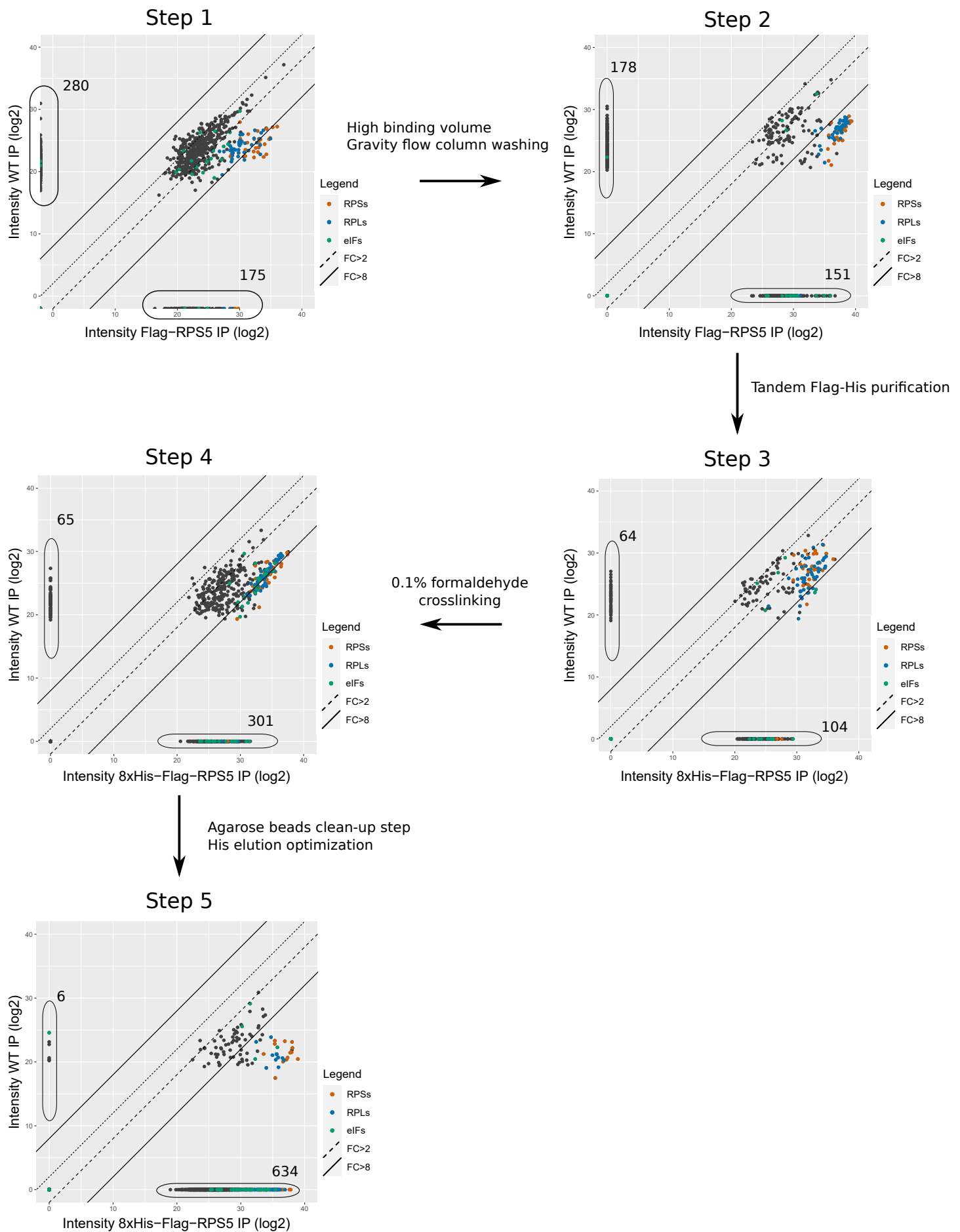


**Figure 12: Development and optimization of ribosome affinity purification**  
 Eluates from WT and RPS5-tagged cells were prepared and analyzed by LC/MS-MS. Signal intensity for each detected protein was computed and plotted for both WT and RPS5-tagged cells. The method was optimized iteratively for a total of five steps, and arrows indicate the successive steps and the successive modifications of the protocol.

number of proteins that were detected only in the WT samples (280), and the poor enrichment of ribosome associated proteins. This was especially the case for translation initiation factors that failed to be enriched. The anti-FLAG M2 Agarose Affinity Beads used in this protocol are thought to contribute largely to this phenomenon, which has been previously reported (Mellacheruvu et al., 2013; Simsek et al., 2017), possibly because agarose beads are irregular in shape and trap large complexes that are difficult to wash out and eventually eluate during the elution step.

To prevent this, we drastically modified the method. First, we reasoned that performing the anti-Flag affinity purification in a large volume would reduce the likelihood of contaminants to attach to the beads, and performed the binding step in a 25X larger volume. Second, in Step 1, agarose beads were washed multiple times by centrifugation of the beads-lysate/washing buffer mixture, but because agarose beads are large, they trap a significant amount of liquid at the bottom of the tube after centrifugation. This means that, for the most part, the washing steps only effectively dilute this dead volume, and abundant proteins such as ribosomes are difficult to eliminate. Rather than performing additional rounds of washing, we poured the beads-lysate mixture onto gravity-flow chromatography column and washed with a large amount of washing buffer. This way, no dead-volume is present and beads can be washed thoroughly and more quickly. These changes to the method drastically improved the enrichment for ribosomal proteins in the Flag-RPS5 IP versus WT IP (Figure 12, Step 2). Although it did help reducing the amount of contaminants, a large number of proteins were still present in the control IP, which did not satisfy us.

As a result, we implemented a tandem affinity purification strategy, and choose the 8xHis tag as a second handle for a subsequent purification. His-tag variants are not a common choice for purification of endogenous proteins in mammalian cells because His residues are more frequent in mammalian proteins than bacterial proteins (Kimple et al., 2013). This can lead to significant contamination of His-based affinity purification by His-rich endogenous proteins. However, in the case of a tandem affinity purification, the first purification provides an already decent purity, and His-rich proteins are expected to be significantly less abundant than in a complete lysate. Compared to other commonly used tags, the His-tag has a significant advantage in that it can be eluted competitively by imidazole, which helps further reduce contamination. Finally, His-tag affinity matrices can be found in the form Dynabeads. The type of contaminants is different depending on the type of matrix used for affinity purification (Dunham et al., 2012) and consequently, using two different types of matrices – agarose and Dynabeads – further improves background reduction.

We generated 8xHis-Flag-RPS5 and 8xHis-Flag-RPL11 HEK293T cells and performed tandem Flag-His affinity purification of ribosomes from WT and 8xHis-Flag-RPS5 cells (Figure 12, Step 3). The number of proteins identified only in the WT sample was strongly reduced compared to single affinity purification, in line with the expected improved specificity, but the number of partners identified in the 8xHis-Flag-RPS5 sample was also reduced. We reasoned that this was due to interactant loss during the now longer affinity purification. We also noted a reduction in enrichment of ribosomal proteins compared to Step 2, an issue that we later identified as incomplete elution of His-tagged ribosomes from the beads and was solved in Step 5.

To prevent the loss of interactants during the tandem Flag-His affinity purification, we included a crosslinking procedure using formaldehyde whole-cell crosslinking at a concentration of 0.1% (w/v) (Ricci et al., 2014)(discussed down below) (Figure 12, Step 4). This led to the recovery of many more interactants than Step 3, which shows the potential of chemical-crosslinking in stabilizing pre-existing interactions.

Finally, we incorporated a cleaning step between the Flag peptide elution step and the His-tag binding step. We indeed noted that agarose beads were difficult to completely eliminate from eluates by centrifugation only, which led to variable amounts of anti-FLAG antibody being detected in eluates (not shown). Thus, we used small centrifuge filter columns to remove the excess agarose beads. Additionally, the His-tag elution step was improved to allow complete elution of His-tagged ribosomes. These final adjustments drastically improved both the efficiency and specificity of the purification strategy (Figure 12, Step 5). Ribosomal proteins were now so enriched in the 8xHis-Flag-RPS5 sample versus WT sample that a significant number of them was only identified in the 8xHis-Flag-RPS5 sample. Additionally, more than 600 proteins were now significantly enriched in the ribosome purification.

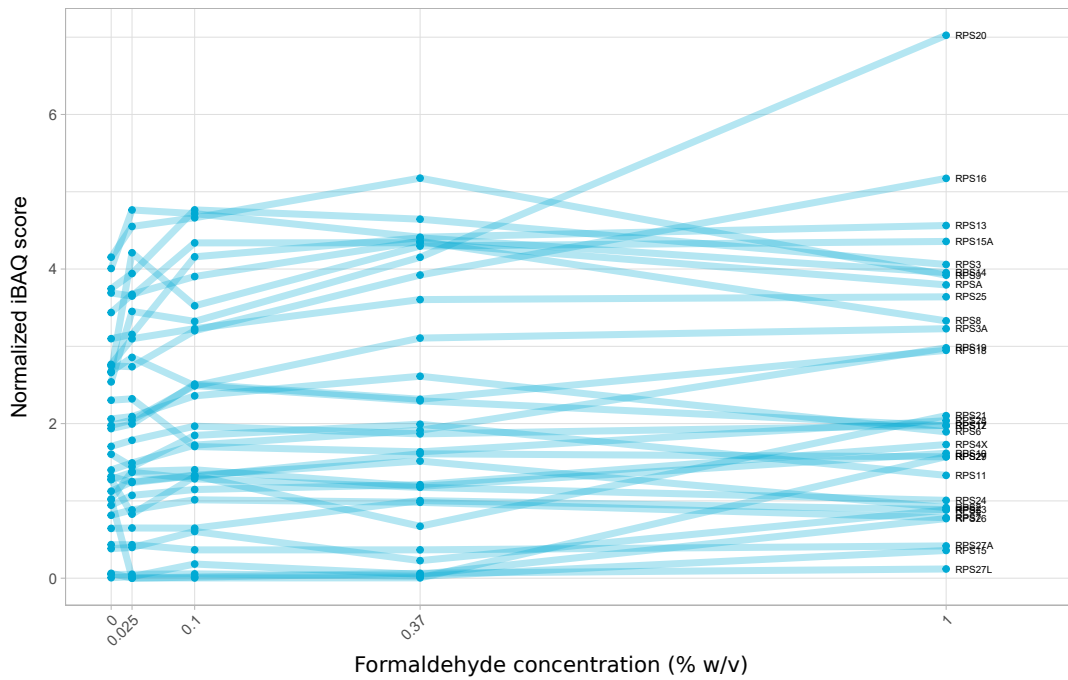
## Optimization of the formaldehyde crosslinking step

During the optimization of the method, it appeared clear that the recovery of some ribosome interactants was low, in particular for many initiation factors, and similarly to previously reported native ribosome interactome (Simsek et al., 2017). This indicated that these interactions were not strong enough to survive the entire duration of the purification despite our effort to keep temperature low, experiment time short, and moderate salt level, all of which influence complex dissociation. We thus included a short and low temperature 10 min/4°C formaldehyde crosslinking

procedure prior to cell lysis. Formaldehyde crosslinking generates covalent bonds between protein in close contacts, mainly by crosslinking lysines and arginines(Tayri-Wilk et al., 2020). Although many other kinds of crosslinking agents have been developed, formaldehyde remains a crosslinker of choice with many advantages(Sutherland et al., 2008). The main advantages of formaldehyde for stabilizing protein:protein interactions lie in three major characteristics. Its ability to diffuse freely through cell membranes allows the crosslinking procedure to be performed prior to cell lysis, and stabilizes *in cell* interactions. Formaldehyde is also a “zero length crosslinker” meaning that it can only crosslink amino acids that are in close proximity (about 5Å)(Tayri-Wilk et al., 2020). This characteristic provides more specificity towards direct interactions compared to crosslinkers of higher length. Finally, formaldehyde crosslinking is very fast and efficient, and can be stopped by glycine which reacts rapidly with free formaldehyde.

A common critique of crosslinking experiments is the risk of over-crosslinking. With high concentrations of crosslinking agent and given enough time, crosslinking agents might crosslink proteins that do not truly interact, but only come in contact by simple diffusion within the cell. As a result, crosslinking increases the risk of false-positive in interactome experiments(Sutherland et al., 2008). Others’ and our own preliminary data indicate that ribosomes co-purify with cytoskeleton components such as actin and tubulin(Simsek et al., 2017) and given the highly connected cytoskeleton network within cells, overcrosslinking is likely to notably result in recovery of many cytoskeleton associated proteins, that do not directly contact the ribosome. It is important to note though that because ribosomes and cytoskeleton filament are extremely stable, this chain-link behavior is likely to happen in some extent even in the absence of a crosslinking agent. To minimize the risk of overcrosslinking, we evaluated the effect of different formaldehyde concentrations on ribosomes interactant recovery. Cells were submitted to concentrations of formaldehyde commonly used in the literature: 0, 0.025(Bohlen et al., 2020), 0.1(Patton et al., 2020; Ricci et al., 2014), 0.37, 1(Valášek et al., 2007) (%w/v). The number of detected proteins is likely to increase with the concentration of formaldehyde, both by stabilization of relevant interactions, or by overcrosslinking. Thus, rather than evaluating the number of proteins detected, we focused on the behavior of initiation factors such as components of the eIF3 complex that have been shown to respond to formaldehyde crosslinking(Bohlen et al., 2020; Valášek et al., 2007). iBAQ scores were calculated for each detected protein and normalized to the median RP iBAQ to account for variations in ribosome recovery. Individual RPs iBAQ score were not significantly affected by formaldehyde which was expected given the very high stability of the ribosome (Figure 13A). In contrast, the recovery of eIF3 complex components was strongly enhanced by formaldehyde

A



B

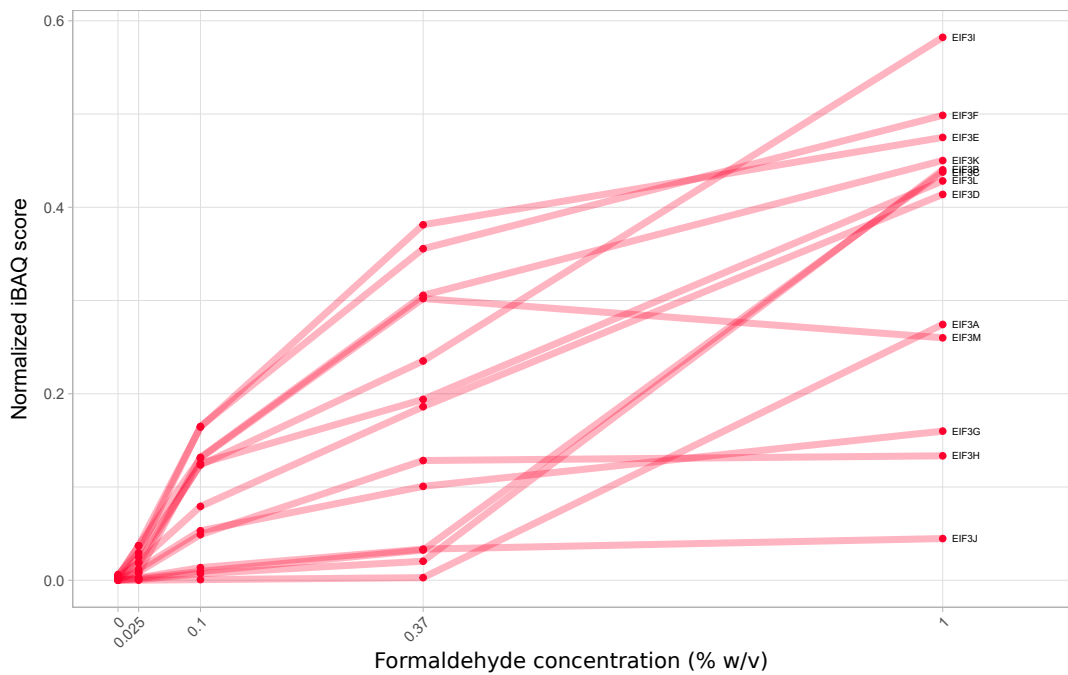


**Figure 13: Formaldehyde crosslinking stabilizes the interaction on eIF3 components**

8xHis-Flag-RPS5 were crosslinked at different formaldehyde concentration and submitted to tandem affinity purification of ribosomes and eluates were analyzed by LC/MS-MS. iBAQ scores were calculated and normalized by median RP abundance to correct for variations in recovery.

**A.** Normalized iBAQ scores for ribosomal proteins of the small subunit as a function of formaldehyde concentration (% w/v)

**B.** Normalized iBAQ scores for eIF3 subunits as a function of formaldehyde concentration (% w/v).

crosslinking and most followed the typical saturation curve that can be expected for ribosome interactants, with a linear regime between 0 and 0.1% (Figure 13B). We reasoned that 0.1% formaldehyde was ideal for our experiments as it provides four times better recovery than 0.025% but is still within the linear regime of the curve, a domain where overcrosslinking is kept to its minimum.

## Alteration of host-cell translation during SINV infection

SINV infection induces a profound translational arrest during infection. In order to identify the most relevant time points to investigate the changes in ribosome interactome following SINV infection, we used O-propargyl-puromycin (OPP) labeling of cells infected at different time points. OPP is a cell membrane permeable puromycin analog that incorporates into the growing polypeptide chain during translation elongation and causes premature chain termination during translation. Because OPP possesses an alkyne moiety, a fluorescent picolyl azide can be added by Click chemistry, thus labeling the peptide. As a result, only peptides being synthesized are ultimately labeled and the level of fluorescence in the cell reveals the overall intensity of translation. We infected the cells with a modified SINV virus expressing mCherry in a deduplicated promoter (Figure 14A), allowing co-visualization of viral replication progression and translation intensity by flow-cytometry analysis. Our results confirm the effect of SINV on translation inhibition and show that this effect is essentially triggered between 10 and 12 hours post-infection (hpi), coinciding with a sharp increase in late viral gene expression reflected by mCherry signal intensity (Figure 14B).

To better visualize how SINV infection affects translation, we performed polysome gradient analysis of cells infected at different time points (Figure 14C). Similarly to the OPP results, we observed a stark decrease in polysome abundance in the 8 to 12 hpi window, concomitant with an increase in the amounts of 80S monosomes.

We chose the 4, 8 and 18 hpi time points for the subsequent ribosome interactome analysis. These time-points represent key stages of viral infection progression. The 4 hpi time point represents a stage of SINV infection where no host-cell translation shut-off is detected, the latter effect starting at 8 hpi and being complete at 18 hpi.



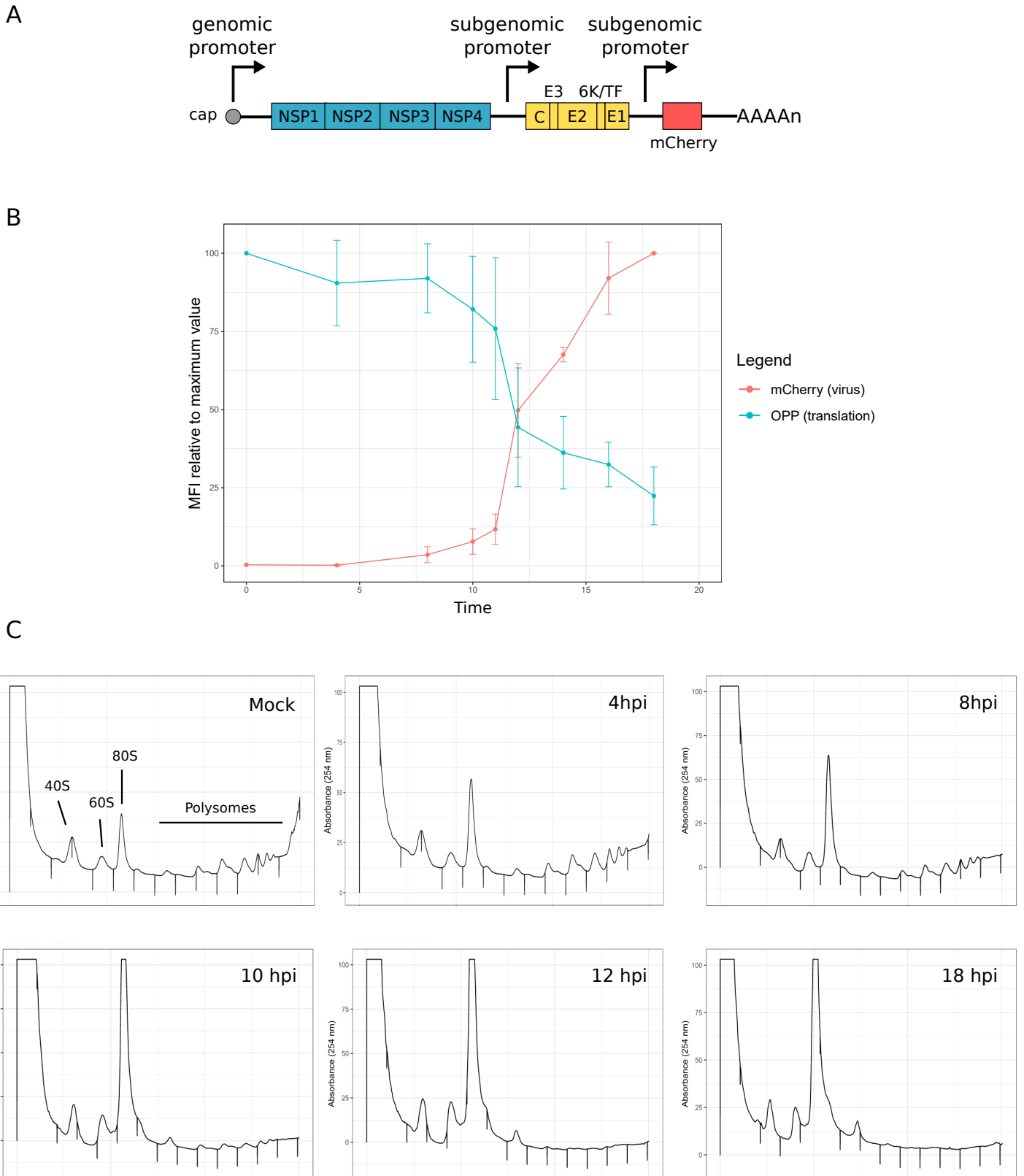


**Figure 14: SINV infection induces host-cell translational shut-down**

**A.** Schematic representation of the modified SINV virus expressing mCherry from a deduplicated sgRNA promoter.

**B.** OPP and mCherry flow-cytometry quantification of SINV-mCherry infected cells at different time points. (n=4).

**C.** Polysome gradients analysis of SINV-mCherry infected cells at different time points.

## SINV infection recomposes the ribosome interactome

We next investigated how the ribosome interactome is recomposed during SINV infection using our optimized tandem affinity purification of formaldehyde crosslinked ribosomes. Viral proteins are only expressed in infected cells and in consequence, evaluating whether they are part of the ribosome interactome requires comparison a ribosome IP from 8xHis-Flag-RPS5 cells with a mock IP performed from WT cells, both being infected. So, 8xHis-Flag-RPS5 and WT cells were used and infected in order to define the ribosome interactome at each time point. 8xHis-Flag-RPS5 and WT cells were mock infected or infected by the SINV-mCherry virus at for 4, 8 and 18 hours, crosslinked with formaldehyde, polysomes were separated by Nuclease S7 treatment and ribosomes were purified using the tandem affinity purification methods. Five replicates of this experiment were made and analyzed by LC/MS-MS. Protein intensity values were calculated and, in case a protein was not detected in a replicate, missing values were replaced by pseudo-values corresponding to noise signal intensity, thus allowing calculation of enrichment (Sysoev et al., 2016). The ribosome interactome was defined at each time-point using paired WT and 8xHis-Flag-RPS5 samples with a cut-off of adjusted  $p$ -value  $< 0.01$ , and the combined set of ribosome interactants were used to calculate changes between time points.

We found limited changes of the ribosome interactome at 4 hpi compared to mock infection (adjusted  $p$ -value  $< 0.1$ ) with only 9 proteins being differentially associated out of a combined mock/4hpi set of 906 RAPs (Figure 15A). 4 of these proteins were only detected in one condition, indicating that they either reflect an “on-off” situation or mis-attribution to the ribosome interactome in one of the two conditions. Limited changes were also found at 8 hpi, with 14 differentially associated RAPs of which 7 were only found in one condition (Figure 15B). In contrast, we detected a significant remodeling of the ribosome interactome at 18 hpi with 144 differentially associated RAPs out of 954, of which 128 were part of both mock and 18hpi ribosome interactome (Figure 15C). This indicates that most of the changes here result from actual changes in RAPs abundance and not mis-attribution to the ribosome interactome. The complete set of differentially RAPs at 18hpi is presented in Figure 16 at three different zoom levels for improved clarity.

We identified several families of process related factors that differentially associate with the ribosome at 18hpi. All subunits of the eIF3 complex were largely depleted (Figure 17), which is in line with the shut-down of translation observed during SINV infection. We found that subunits EIF2S1(eIF2 $\alpha$ ), EIF2S2(eIF2 $\beta$ ) and EIF2S3(eIF2 $\gamma$ ) of the translation factor eIF2 were all depleted

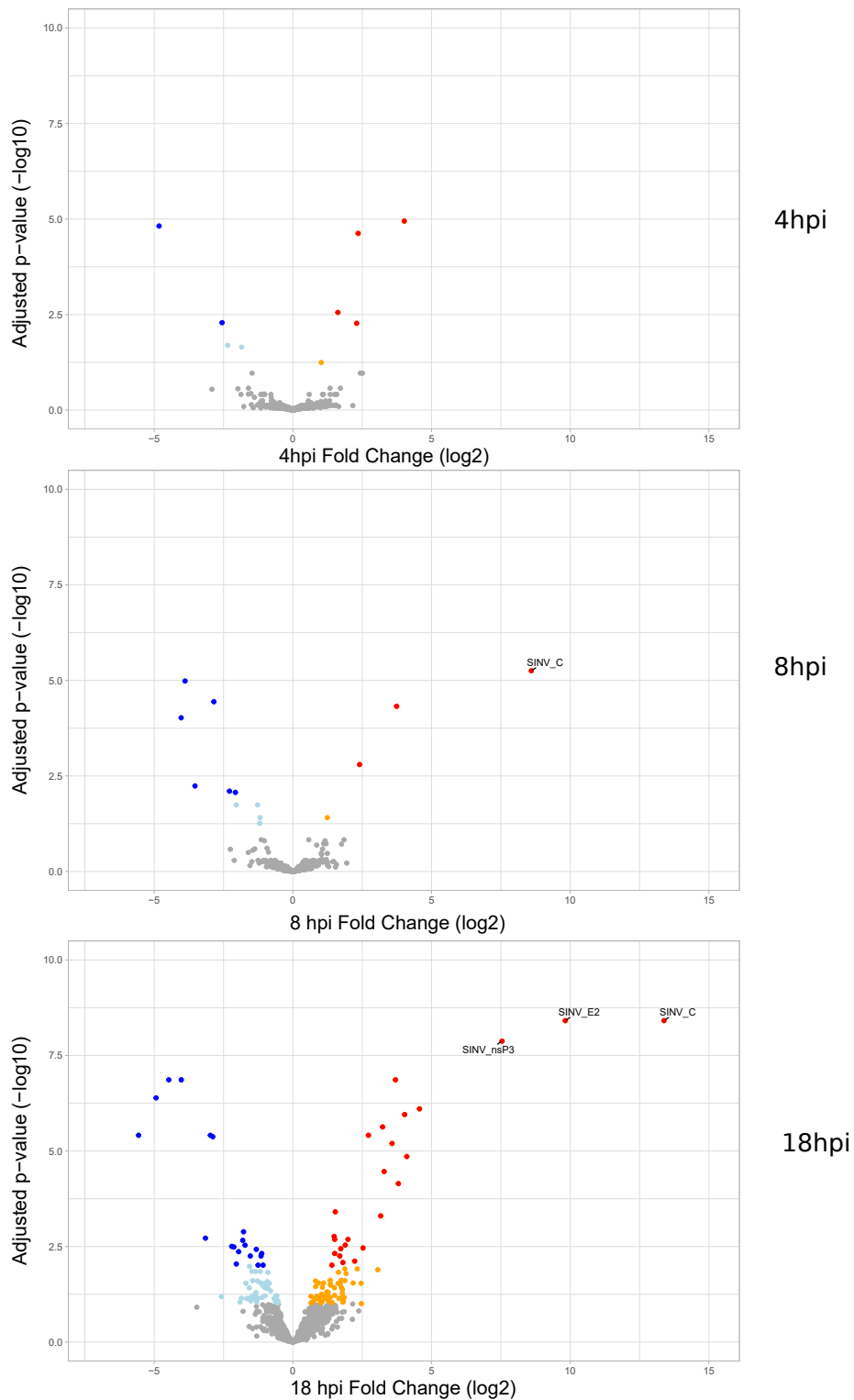


**Figure 15: Changes in ribosome interactome by SINV at 4, 8 and 18 hpi**

8xHis-Flag-RPS5 and WT cells were formaldehyde crosslinked, cytoplasmic extracts were prepared, digested by Nuclease S7 and submitted to tandem Flag-His purification. Samples were analyzed by LC/MS-MS and protein intensity calculated. Paired WT and 8xHis-Flag-RPS5 were used to define the ribosome interactome at each time-point, and ribosome interactomes were compared between mock and 4 hpi (A), mock and 8 hpi (B), and mock and 18 hpi (C). Volcano plots showing fold change (log2) and adjusted p-values (-log10). Significance is indicated by colors. red: FC > 0, adj p-val < 0.01; orange: FC > 0, adj p-val < 0.1, dark blue: FC < 0, adj p-val < 0.01 and light blue: FC < 0, adj p-val < 0.1



to a similar level (Figure 17), suggesting a decrease in assembled 43S PIC. eIF4F subunits were also generally depleted (Figure 17), however, the fold-change of eIF4E was noticeably stronger than that of other factors. This suggests that eIF4E association with the remaining factors of the eIF4F complex is inhibited by SINV infection. Three to four DEAD-box helicases - DDX27, DDX50, DDX18, DDX21 (adjusted p-value of  $\sim 0.108$ ) - were significantly enriched out of a total 15 ribosome associated DEAD-boxes (Figure 17). Most strikingly, the complete set of an early cytoplasmic set of pre-40S maturation factors (Ameismeier et al., 2018) were all significantly depleted (Figure 17) which can be interpreted by the idea that SINV infection impairs nuclear pre-40S maturation or export, resulting in a decreased cytoplasmic presence of the early cytoplasmic intermediate. Surprisingly, LRRC47 and RIOK1, two factors involved in a later stage of pre-40S maturation (Ameismeier et al., 2020), were not depleted (Figure 17). We hypothesize that pre-40S maturation defects are a late effect of SINV infection, and that effects at later stages of pre-40S maturation may only be present at even later times of infection. SEPT2, SEPT9, SEPT11 and SEPT7, four members of the septin group that form rings and filaments and hence are part of the cytoskeleton (Weirich et al., 2008), were significantly enriched following infection (Figure 17). Septins assemble into hetero-hexamers or hetero-octamers, incorporating two copies of one member from four separate septin families. Strikingly, the set of four septins detected here is a compatible form of hetero-octamer, with each septin representing a distinct member of the four septin families (Weirich et al., 2008). It thus appears that a specific form of the septin complex associates more strongly with the ribosome during SINV infection, which may be related to localized translation of the lately expressed viral sgRNA. Finally, we found that STT3A, a member of the OST-A complex involved in co-translational glycosylation was enriched after infection, with other members being enriched to a lesser degree (Figure 17). The viral proteins E1, E2 and E3 are all glycoprotein, and given that the sgRNA represents most of translation at 18hpi, this shows that our method is able to unveil the specific requirement of RAPs during translation of the sgRNA.

To extend on this finding, we repeated this experiment, this time first pre-purifying polysomes by polysome fractionation before performing the tandem purification of ribosomes. 8xHis-Flag-RPS5 purification from cytoplasmic lysates effectively purifies not only assembled ribosomes, but also pre-40S, 43S and 48S. We thus sought out to more precisely investigate proteins that may participate in sgRNA translation at the elongation step by performing ribosome tandem affinity purification from polysomes rather than cytoplasmic ribosomes. Because polysomes are largely depleted at 18hpi, we found difficult to purify a sufficient amount for the LC/MS-MS analysis. Also, and because we did not observe significant changes at 4 and 8 hpi, we focused on an

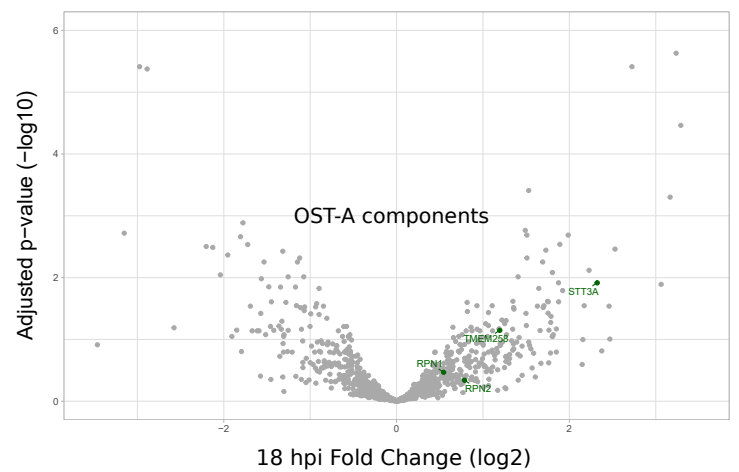
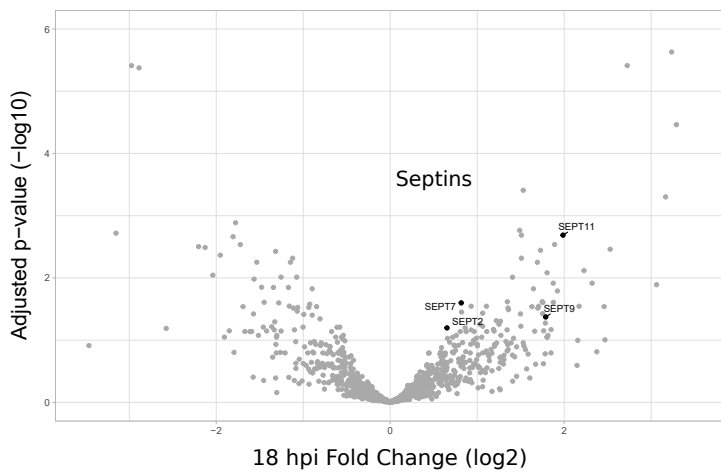
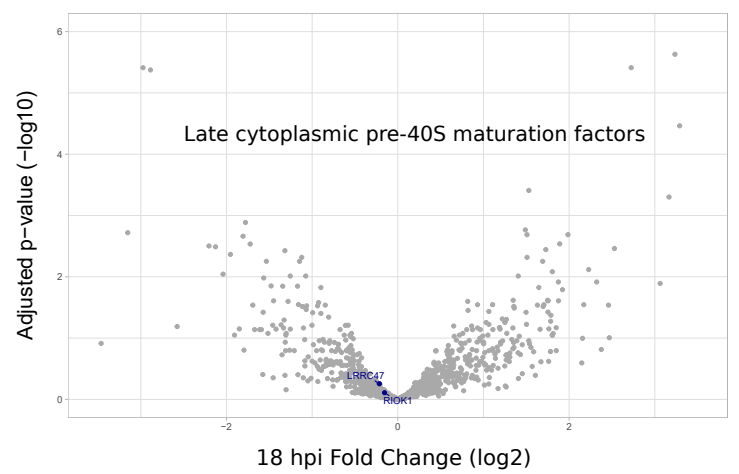
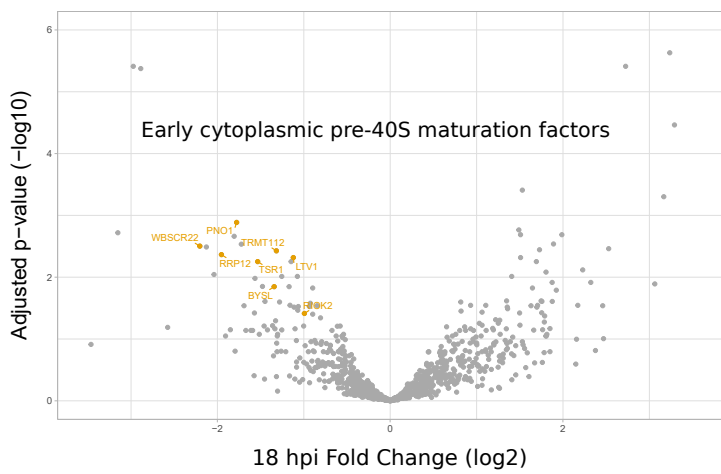
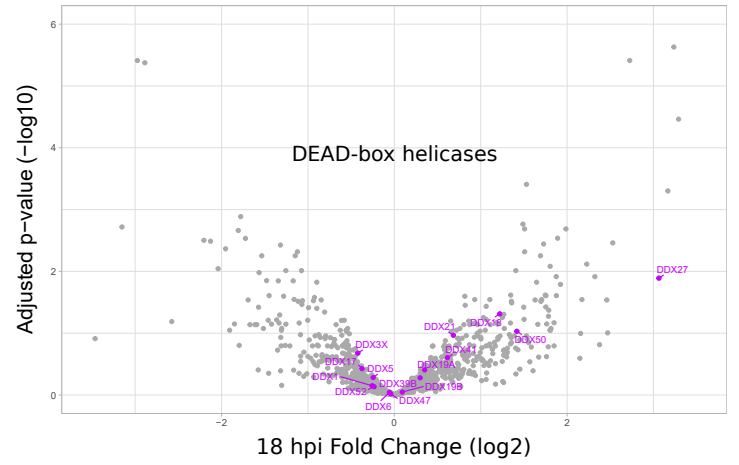
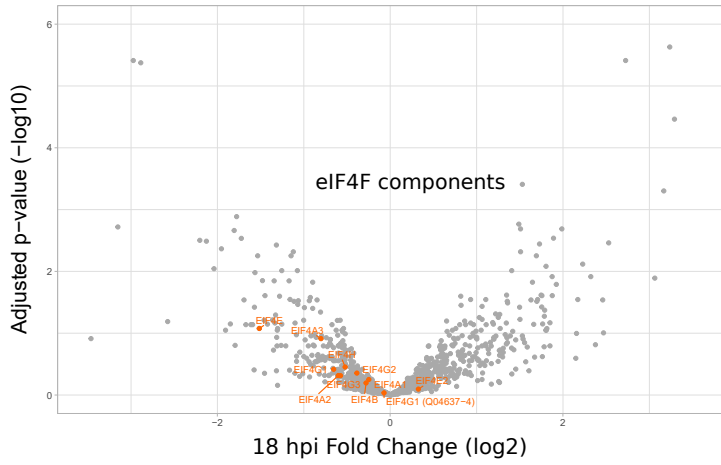
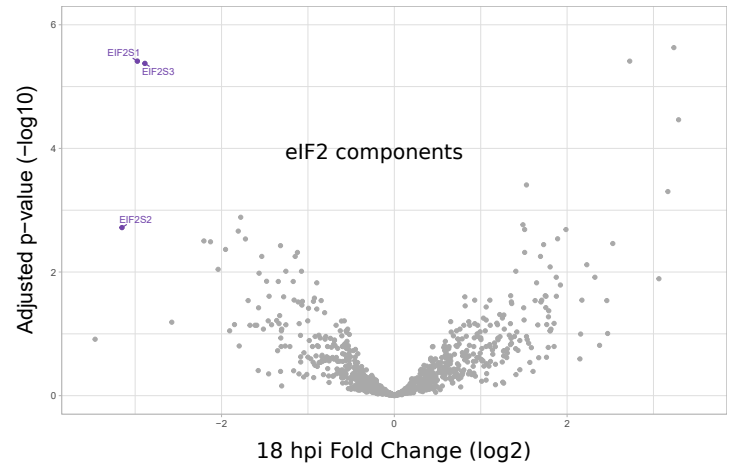
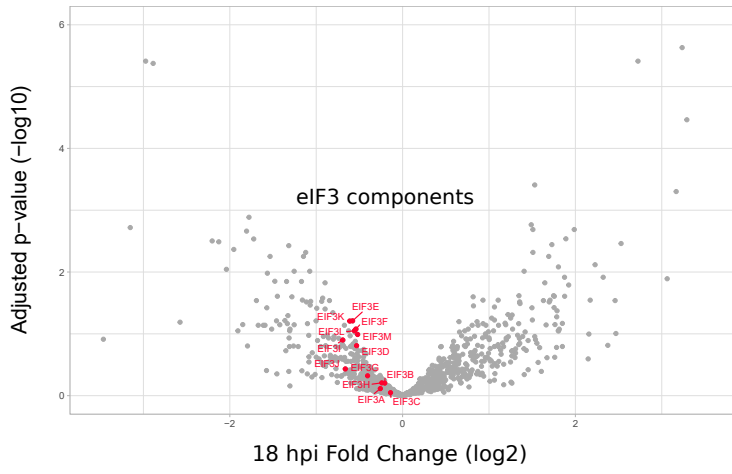


**Figure 17: Changes in ribosome interactome by SINV at 18 hpi, highlights on specific proteins family and pathway-related factors**

intermediate time point, at 12 hpi, after which most of the translational shut-down has already happened (Figure 14), but where the amount of polysome is still adequate. 8xHis-Flag-RPS5 and WT cells were mock infected or infected for 12 hours and formaldehyde crosslinked. Lysates were submitted to polysome gradients fractionation and fractions corresponding to disomes and upwards were pooled and subjected Nuclease S7 digestion and to tandem ribosome purification. Three replicates were generated and submitted to LC/MS-MS quantification (Figure 18A). Similarly to the first experiment, the ribosome interactome was defined separately for each time point using the paired 8xHis-Flag-RPS5 and WT time point conditions, and the combined set of mock and 12hpi ribosome interactants was used for differential analysis of the ribosome interactome (Figure 18B). Changes in the polysome interactome at 12hpi partially matched the those of the ribosome interactome at 18hpi, with similar changes in OST-A complex (Figure 18C) and DEAD-box helicases abundance (Figure 18D). Interestingly, we found that two members of the ASC-1 complex were differentially associated to polysomes at 12hpi (Figure 18D), a result that was not found in the previous experiment. The ASC-1 complex is involved in resolution of collided ribosomes and this results may suggest an increased rate of ribosome collisions in SINV infected cells (Juszkiewicz et al., 2020b). Given that host-cell translation is generally repressed, we hypothesize that this might concern translation of the sgRNA.

We picked several up and down-associated RAPs and validated their changes in ribosome interactome along the course of infection by Western Blot analysis. Given there was no significant changes in RAPs abundance at 8hpi, we substituted the 8hpi time point by a 12hpi time point, which corresponds to a point where most of the translational shut-down has already happened. Because the additional purity provided by the His-tag was likely not required for Western Blot validation, WT, 8xHis-Flag-RPS5 and 8xHis-Flag-RPL11 cells were used for a single round of Flag purification. We were able to both validate the specific association of all tested factors with the ribosome and their changes in ribosome association following infection (Figure 19). DDX18, DDX21 and DDX27 were all shown to associate more abundantly with ribosomes along the course of infection by both RPS5 and RPL11 IPs. We noted their amount was higher in the RPL11 IP than in the RPS5 IP, a result in line with their previously reported association to both free 60S and polysomes, but not free 40S (Imami et al., 2018). HNRNPM, a protein that was detected as differentially associated in our RPS5-based ribosome LC/MS-MS analysis was virtually absent for the RPS5 eluates here, but its abundance in the RPL11 IP did changed accordingly to the LC/MS-MS results. This suggests that HNRNPM associates primarily with free 60S. We found that ASCC3, a member of the ASC-1 complex was only more associated with ribosomes at 12hpi, which explains

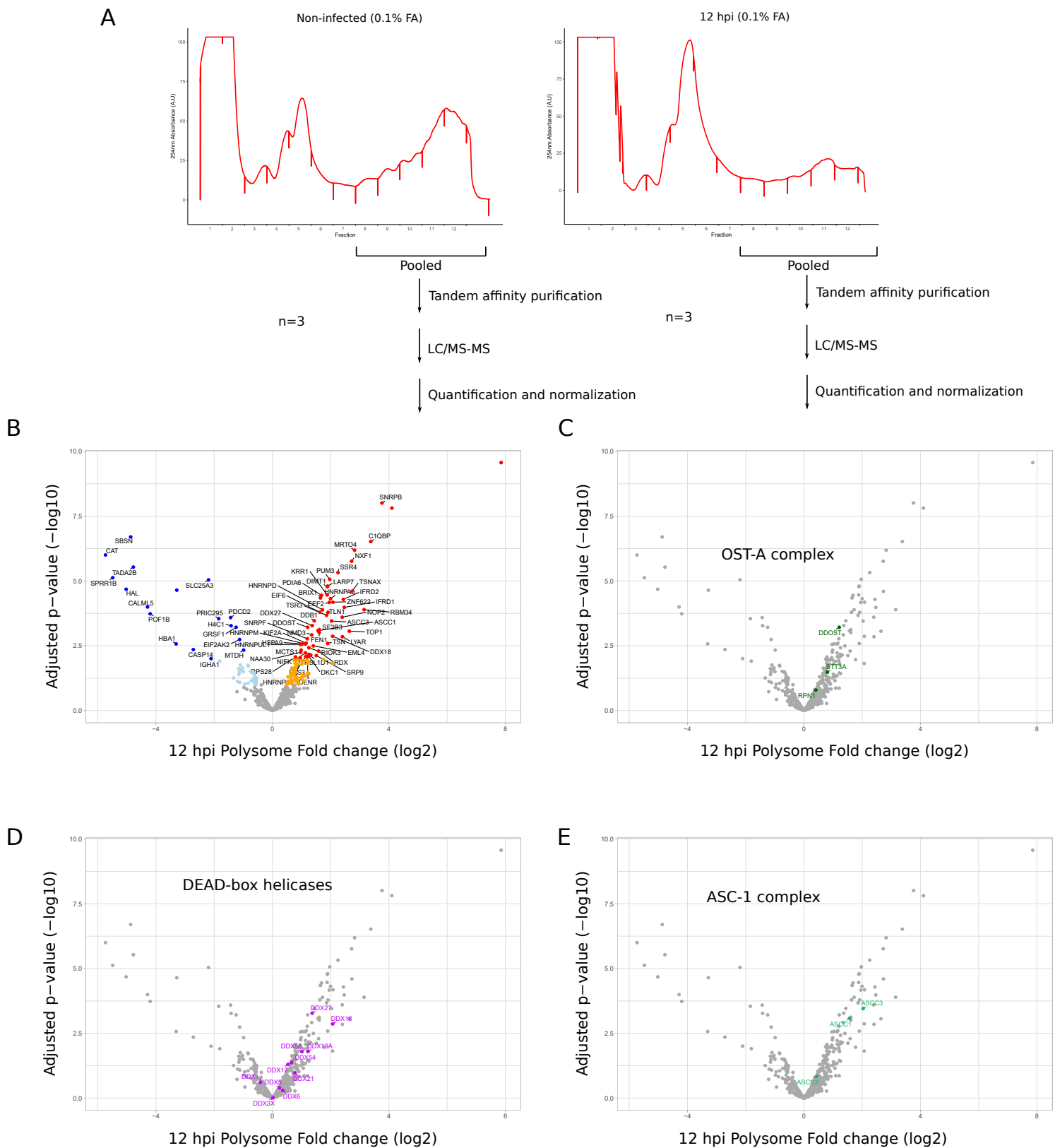


**Figure 18: Changes in polysomes associated proteins at 12 hours post-infection**

**A.** 8xHis-Flag-RPS5 and WT cells were crosslinked at different formaldehyde concentration, fractionated by polysome fractionations and fractions correspondign to disomes and upwards were pooled, ribosomes were purified by tandem affinity purification and eluates were analyzed by LC/MS-MS (n=3). The polysome interactome was defined for both time-point, and the combined set of polysome associated proteins were used to calculate changes in polysome association.

**B.** Volcano plot showing the  $\log_2$  fold change and the significance (adjusted p-value) of each protein between 12 hpi and uninfected condition using data from three biological replicates. Points with adjusted p-value  $< 0.01$  are labeled. Additional plots highlighting detected OST-A complex (**C**), DEAD-box helicases (**D**), and the ASC-1 complex (**E**) are shown.



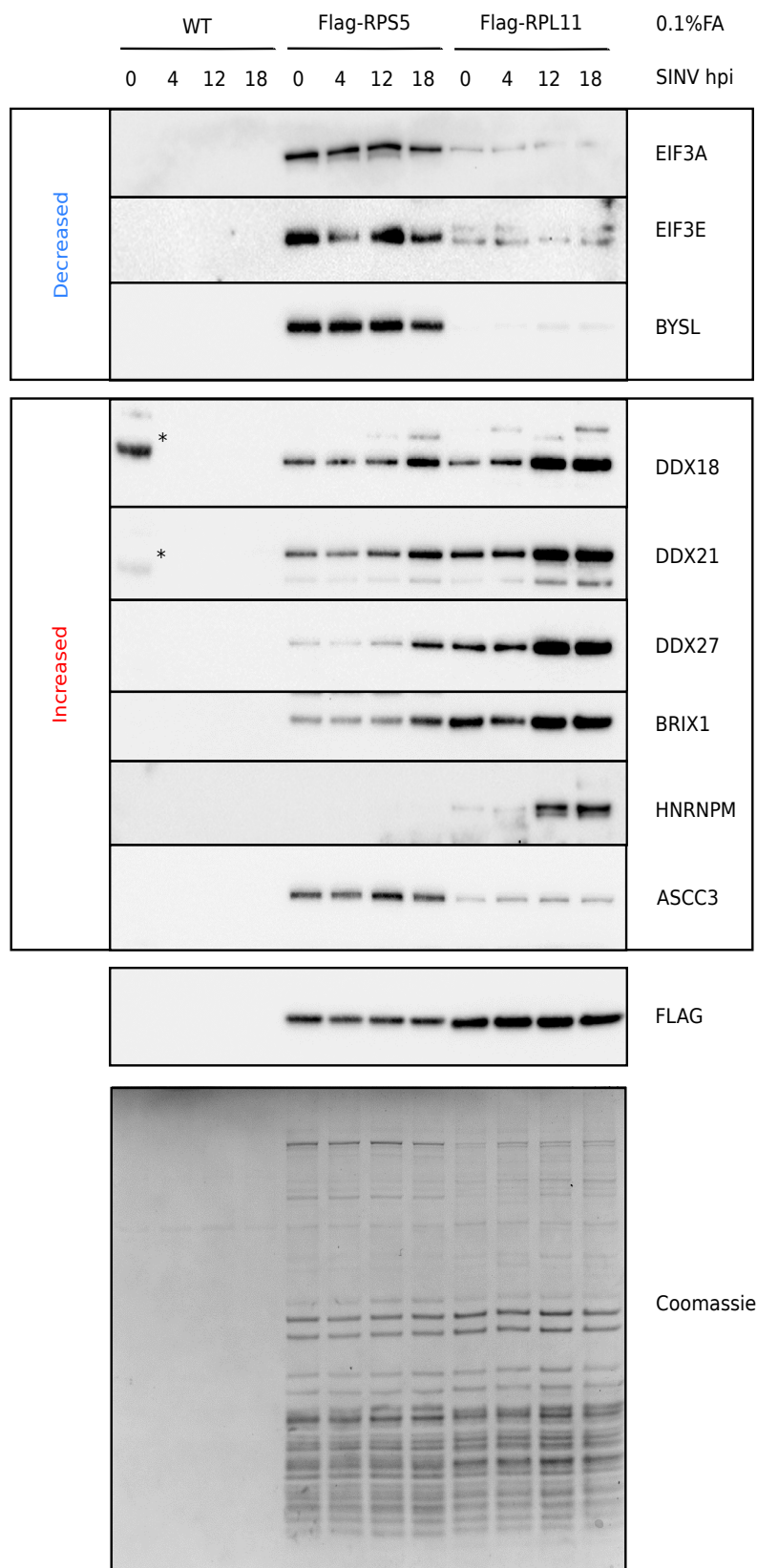


**Figure 19: Western Blot validation of the changes observed by LC/MS-MS** WT, 8xHis-Flag-RPS5 and 8xHis-Flag-RPL11 cells were infected for 0, 4, 12 and 18 hours, crosslinked by 0.1% formaldehyde (FA) (w/v) and submitted to a single Flag affinity purification. Eluates were analyzed by Western Blot. Stars (\*) denote aspecific recognition of the protein ladder co-deposited in the WT 0h eluate. Coomassie staining of the post-transfer SDS-PAGE.

why it was missed by our first 18hpi ribosome analysis and only identified it in the 12hpi polysome analysis. The decreased in eIF3a and eIF3e was modest at 18hpi but in line with the Fold Changes observed by mass spectrometry. Finally, BYSL was shown to be less associated with the 40S subunit at 18hpi only, indicating that perturbations to 40S maturation/export only manifest late in infection.

We next investigated how these factors distribute within polysome gradients (Figure 20). As before, to ensure a minimal amount of polysomes, cells were infected for 12 hours only. Because polysome gradients fractions from mock and 12hpi cells were blotted different membranes, absolute level of proteins between the two membranes cannot be compared, and only distribution of the RAPs is analyzed. Overall, distributions of the tested RAPs were not modified by infection at 12hpi. ASCC3, however, was visibly enriched in fractions corresponding to disomes and trisomes, a surprising result considering that ribosome collision is expected to be more strongly affect highly loaded mRNAs. Surprisingly, ASCC1 and 2, the two other members of the ASC-1 complex distributed similarly in both non-infected and infected conditions, with no visible enrichment in the disomes and trisomes fractions. Additionally, we find a different distribution of helicases DDX18 and DDX27. Both were only found in 60S containing fractions but while DDX18 distribution in polysomes gradients followed that of ribosomes, DDX27 presence fell throughout the gradient, a behavior that has already been described(Imami et al., 2018). The decreased DDX27/ribosome ratio within the gradient fits with a model where DDX27 only associates with ribosomes during early elongation.

## Contribution of total and cytoplasmic proteome to changes in ribosome interactome

The differential presence of RAPs after infection could only be a consequence of their altered abundance in the cell as a result of infection. To investigate this idea, we used our collaborators data set of LC/MS-MS analysis of the total proteome following infection at 18hpi(Garcia-Moreno et al., 2019). Comparison of the changes in ribosome interactome and protein abundance showed no clear correlation (Figure 21A), indicating that the changes in RAPs are not driven by whole-cell protein abundance variation.

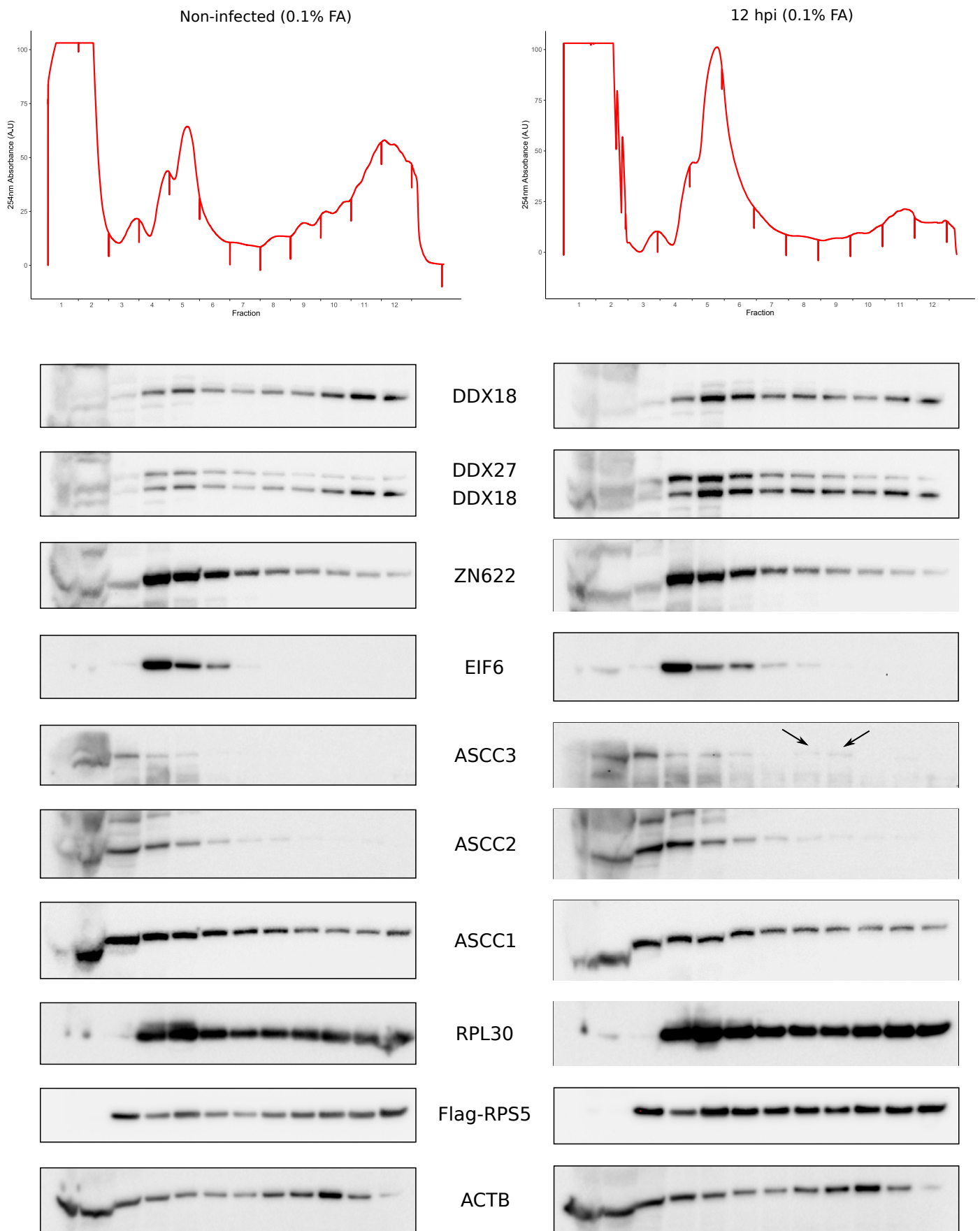
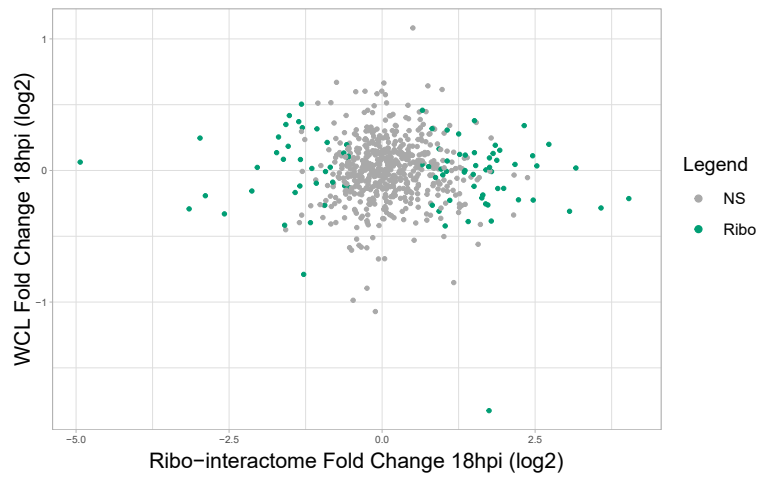
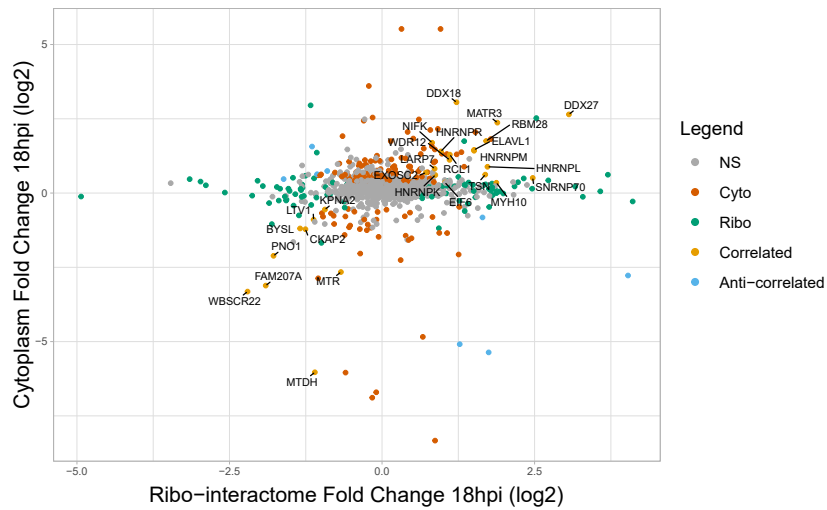


**Figure 20: Distributions of RAPs within polysome gradients in non-infected and 12 hours infected cells**  
 8xHis-Flag-RPS5 were crosslinked at 0.01% formaldehyde (w/v) and submitted to polysome gradients analysis. Fractions were recovered and analysed by Western Blot. Arrows indicate ASCC3 presence in disome and trisome fractions.

A



B



C

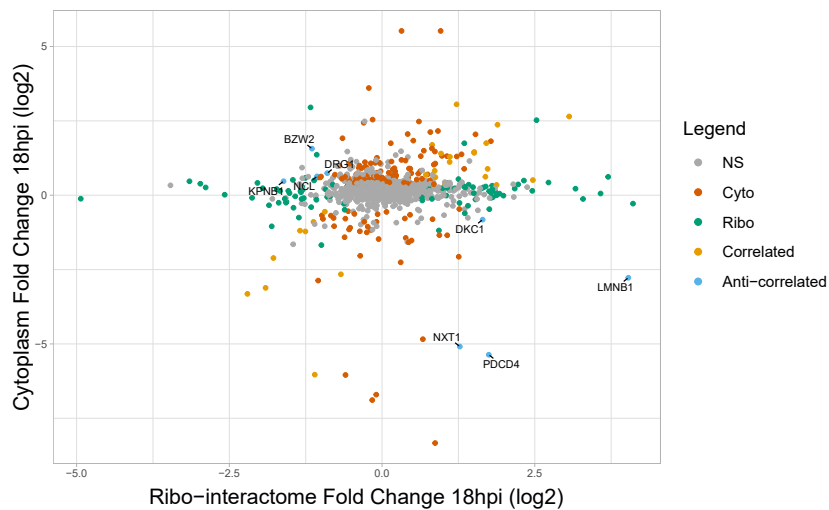


**Figure 21: Correlation between changes in total and cytoplasmic changes with ribo-interactome changes at 18hpi**

**A.** Fold Change in total proteome (WCL: whole cell lysate) vs ribo-interactome at 18hpi. Differentially associated ribo-interactants are labeled in green. No statistical differences in total protein abundance were found.

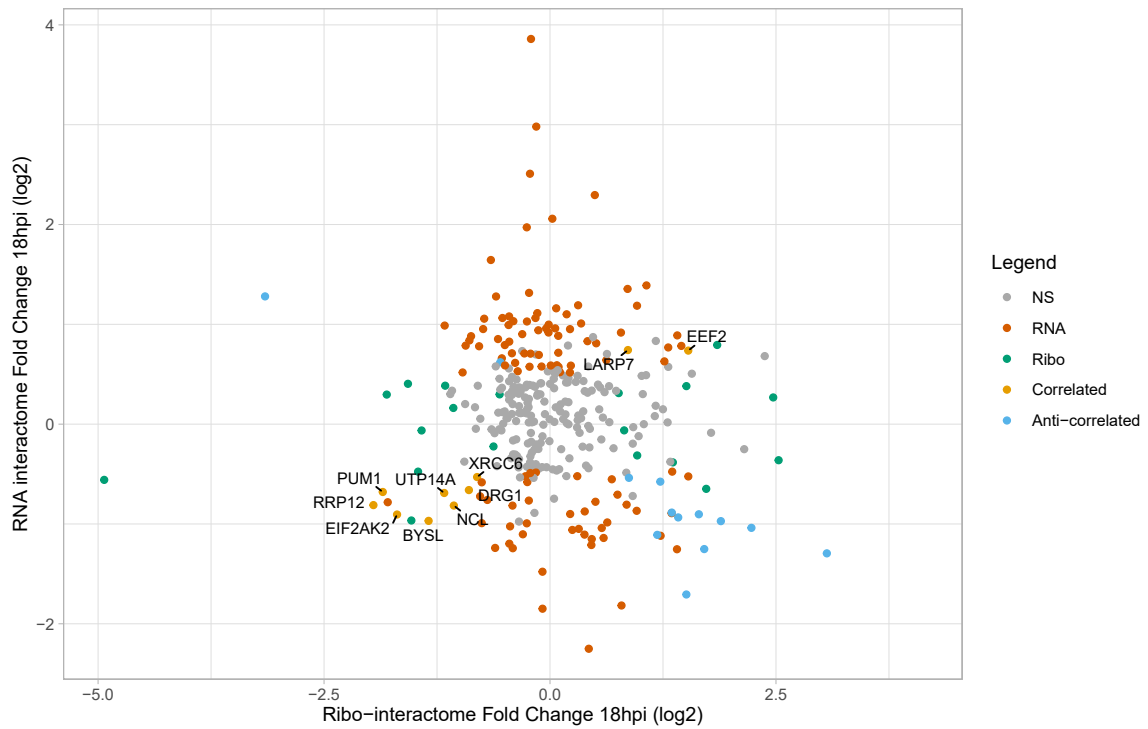
**B and C.** Fold Change in cytoplasmic abundance vs ribo-interactome at 18hpi. Significant changes (adj. p-value 0.1) are highlighted in color (Cyto: Cytoplasmic change only, Ribo: ribosome change only, Correlated: cytoplasmic and ribosome in the same direction, Anti-correlated: cytoplasmic and ribosome in opposite direction). **B.** Highlight on correlated changes. **C.** Highlight on anti-correlated changes

We noticed that several up-associated RAPs – and in particular DDX18, DDX21, DDX27 - were primarily annotated as nucleolar localized (Protein Atlas database), which prompted us to investigate whether the changes for these proteins were related to a potential delocalization of these proteins. We used our collaborators data set (unpublished) of cytoplasmic abundance changes at 18hpi and compared it to the changes in ribosome interactome. We found limited correlation between the changes in cytoplasmic abundance and ribosome association, with only 27 that varied significantly in both data set (adj. P-value<0.1) (Figure 21B and C). Of note, DDX18, DDX21 and DDX27 were in fact significantly enriched in the cytoplasm at 18 hpi, along with several HNRNPs (Figure 21B). This however poses the question whether export of these proteins from the nucleus facilitates their increase association with ribosomes, or if instead the latter limits their uptake into the nucleus. Similarly, ELAVL1, a factor known to be redistributed by SINV infection (Dickson et al., 2012) was both more abundant in the cytoplasm and in the ribosome interactome. Interestingly, LTV1, BYSL, PNO1 and WBSCR22 four of the previously mentioned early cytoplasmic pre-40S maturation factors had significantly reduced cytoplasmic presence, validating our finding that late SINV infection prevents the export of this early cytoplasmic intermediate (Figure 22C). It thus appears that, in some part but not all, cytoplasmic abundance changes correlate with ribosome interactome changes.

## Absence of correlation between changes ribosome interactome and mRNA interactome

Many of the ribosome interacting proteins are also RNA binding proteins. As a result, if a protein interacts with both mRNAs and ribosomes, the changes in mRNA interactome and ribosome are expected to go in the same direction following infection. We used our collaborators dataset on mRNA interactome recomposition following infection and compared it with our own dataset at 18hpi using proteins detected in both dataset. Strikingly, we observed very little correlation between both dataset, with only 10 proteins moving in the same direction (adj. P-value<0.1) (Figure 22A). Moreover, 13 proteins moved in opposite direction, with especially 11 proteins that were found to interact simultaneously more with the ribosome but less with mRNAs at 18hpi (Figure 22B). Among them, we found, again, three DEAD-box helicases DDX18, DDX27 and DDX50. This suggests that a switch operates from preferential mRNA binding to ribosome association following infection. Finally, many of the changes in the RBPome do not translate in an increased association

A



B

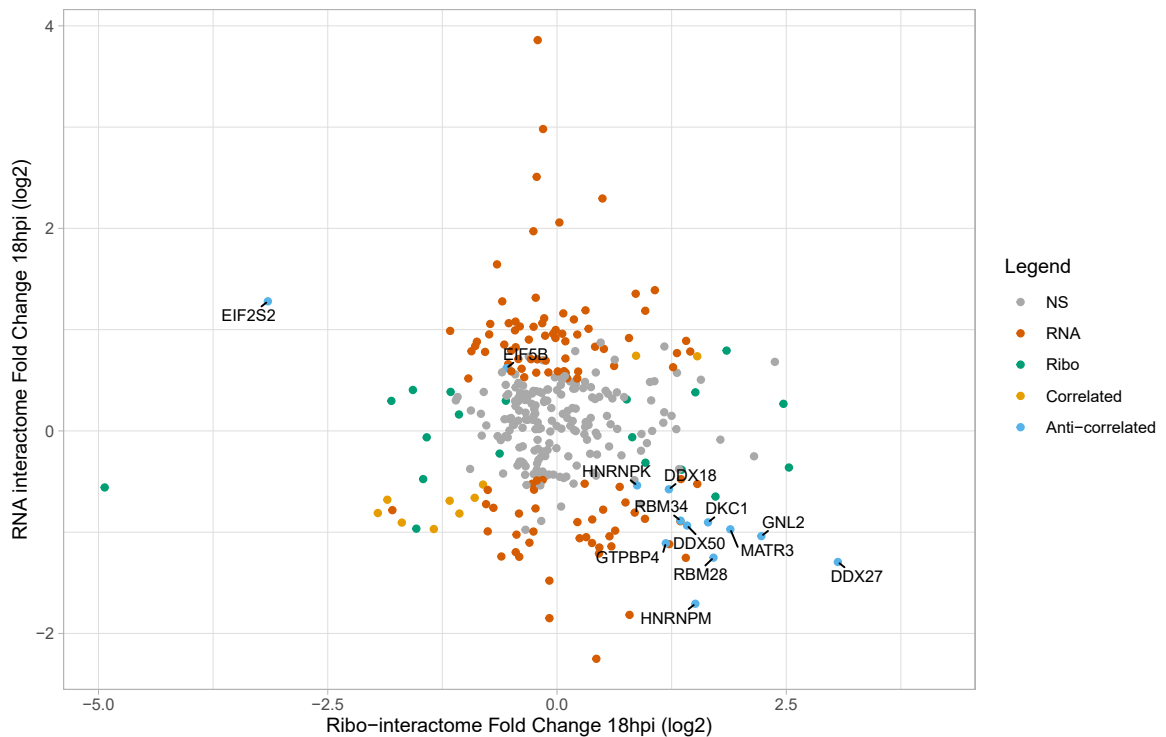


## Figure 22: Correlation between changes in mRNA interactome and Ribo interactome

mRNA interactome changes (Garcia-Moreno, et al. 2019) were compared with changes in ribo interactome (our study). Differentially associated proteins (adj. p-value<0.1) were colored depending on their changes in each dataset (RNA: mRNA change only, Ribo: ribosome change only, Correlated: mRNA and ribosome in the same direction, Anti-correlated: mRNA and ribosome in opposite direction). Highlights of correlated (**A**) and anti-correlated (**B**) proteins are shown.

with the ribosome, and so the RNA binding properties and ribosome association properties of these proteins appear to function largely independently.

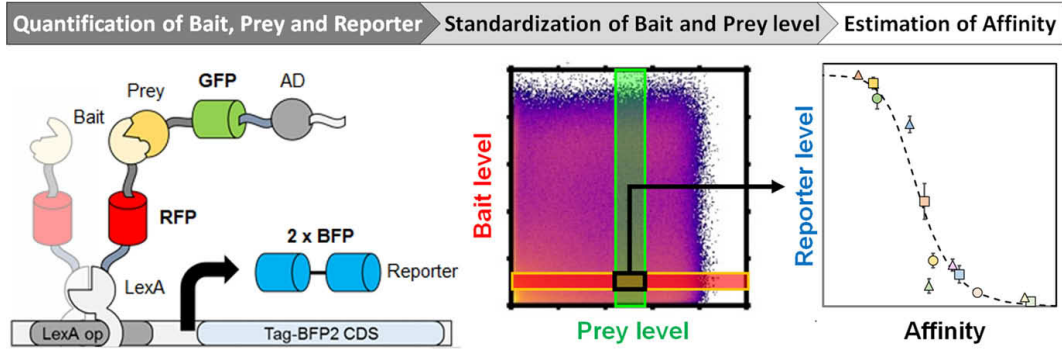
## Discussion

### Biochemical and genetic screens to decipher viral biology

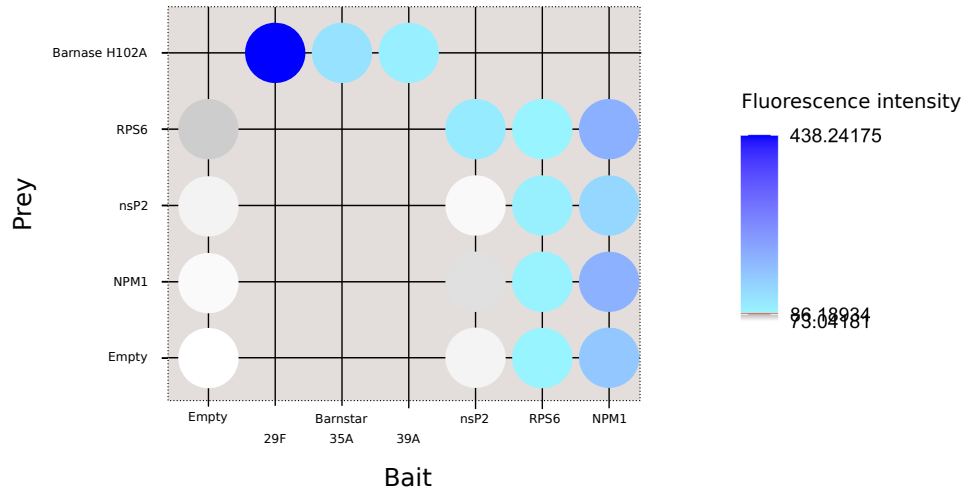
In contrast to other pathogens such as bacteria, fungi and non-obligate parasites, virus replication is intimately linked with how viral proteins and genetic material interact with host-cell components. Because their genome length is constrained by the size of the viral particles they produce, the amount of different proteins they can encode for is extremely restricted (Chaudhari et al., 2021). They have thus evolved and continuously adapt to rely on host-cell proteins to participate in the expression of their genetic material, translation of their proteins, virion assembly and ultimately release of said virions. As such, understanding how cellular components are exploited by viruses is at the core of modern virology. With around 20,000 estimated genes within the human genome, and numerous non-coding RNAs, the vast majority of which have multiple roles, identifying host-cell components that participate in viral biology is not an easy task.

In the 20<sup>th</sup> century, biochemical characterization of the processes that govern viral replication and host-pathogen interactions was performed through time-consuming hypothesis-driven strategies. In the 1970s, when Western Blot did not exist, chemical characterization generally involved radioactive labeling of viral or cellular components, followed by tedious analytical methods with limited resolution such as separation by ultra-centrifugation and 2D-gel electrophoresis. Using P<sup>32</sup> labelling and 2D-gel electrophoresis, Kaerlein and Horak discovered in 1976 that several ribosomal proteins become phosphorylated during VACV infection. Follow up studies further showed that the viral kinase B1 was responsible for the deposition of this mark on RPS2/uS5 and RPSA/uS2 (Banham et al., 1993; Beaud et al., 1989, 1994; Kaerlein and Horak, 1976b). Others used P<sup>32</sup> labeled Sendai viruses to investigate binding of phosphorylated virion components to host cell ribosomes (Bukrinskaya et al., 1969) or took advantage of translation shut-off during poliovirus replication to label only viral proteins and investigate their binding to host ribosomes (Wright and Cooper, 1974). These were among the first studies to investigate how viral infection alters cellular component's biochemistry and it is no surprise that these studies investigated the interaction between viruses and the translation machinery, because the ribosome could be easily separated and resolved in ultra-centrifugation experiments thanks to its high stability and size.

A



B



C

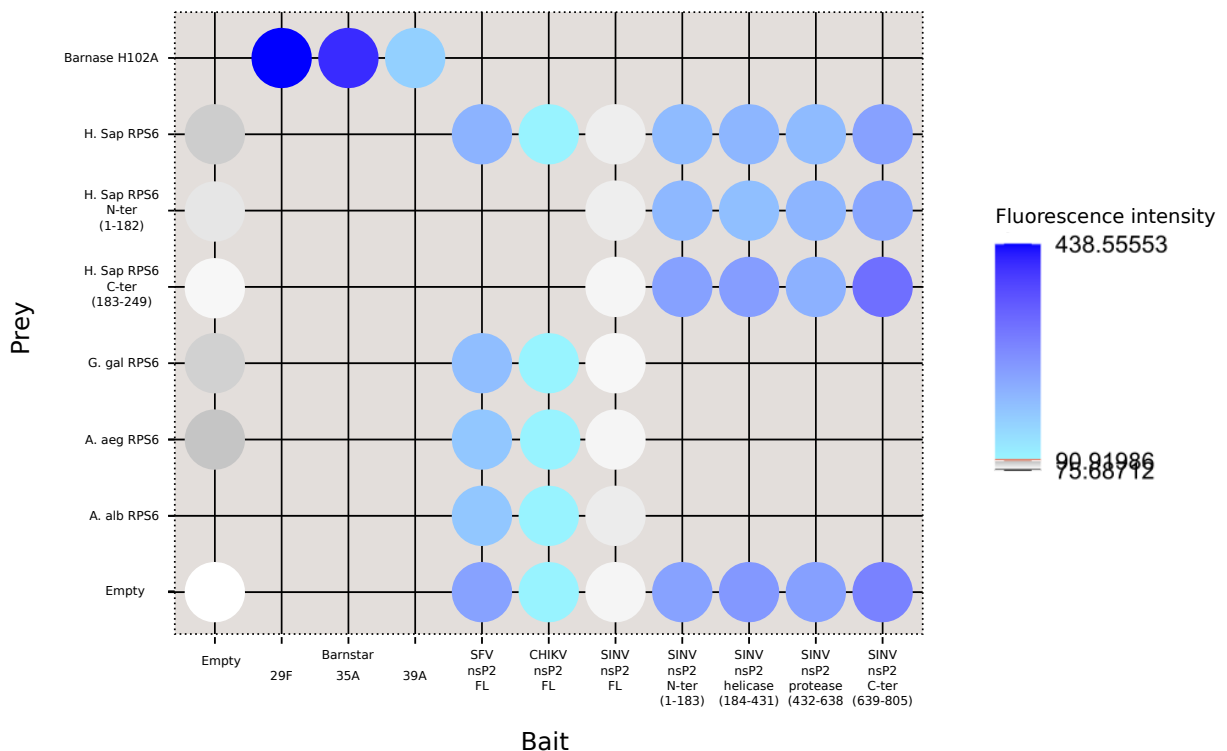


## Figure 25: Investigation of the RPS6-nsP2 interaction by quantitative two-hybrid

**A.** Interaction between Bait and Prey proteins is investigated by co-measurement of Bait expression (mCherry), Prey expression (TagGFP), and Reporter expression (TagBFP). A gating procedure is applied to standardize measurements to similar Prey and Bait expression between conditions. Relative affinity strength can be determined by comparison with interactants with known affinity. (Cluet et al., 2020)

**B and C.** BFP fluorescence intensity values are displayed on a grid mimicking standard two-hybrid yeast colony results. Colors indicate the relevance of the measured signal. white-grey: 10% of Empty-Empty fluorescence value, negative; blue: positive



Modern virology really took a turn with the discovery and implementation of RNA silencing. It suddenly became possible to perform siRNA or shRNA-mediated knock-down of host-cellular mRNAs, hence reducing the expression of the corresponding encoded proteins, and investigate how this affects viral replication, generally through the use of viral derived luciferase reporters, or by immunofluorescence labelling of viral proteins(Hirsch, 2010). Although siRNAs and shRNAs allowed to study the role of specific proteins in viral replication, the unbiased quest for new antiviral or proviral factors was made possible through the advent of large siRNA libraries that can target almost every protein encoding gene of the host cell(Hirsch, 2010). As such, RNAi screens have been used successfully to identify host-factors involved in the replication of HCV(Ng et al., 2007; Tai et al., 2009), HIV(Brass et al., 2008; König et al., 2008), CHIKV(Karlas et al., 2016), SINV(Ooi et al., 2013; Panda et al., 2013), IAV(Karlas et al., 2010; König et al., 2010), DENV(Sessions et al., 2009), WNV(Krishnan et al., 2008) or VACV(Sivan et al., 2013). Interestingly, a significant overlap was found between many of these studies regarding proviral proteins, suggesting a conserved activity of central protein networks in regulating viral replication(Hirsch, 2010; Karlas et al., 2016). Despite their ability to screen host-cell protein involved in viral replication in a genome-wide manner, siRNA-based screens suffer from major limitations. siRNA libraries are made up of thousands of 3-to-4-siRNA pools, each targeting one gene(Hirsch, 2010), that are transfected individually into cell wells. This results in a massive number of conditions to treat and analyze, a process that imposes automation. Because siRNAs are subject to offtargets – unspecific targeting of mRNAs species – 3-to-4 siRNA pools can lead to false positive, and hits need to be manually examined using single, validated siRNAs. This makes this whole process tedious and time consuming.

More recently, RNAi-based screen have been replaced with CRISPR-based strategies. In this setup, cells are transduced with lentiviral vectors encoding the Cas9 protein and specific single-guide RNAs (sgRNAs) programmed to induce double-strand breaks at the coding region of cellular genes leading to their inactivation. Then, cells are infected with viruses, resistant cells are recovered and the sequence of the sgRNAs integrated in their genome are amplified and sequenced. Abundance of each sgRNA sequence in resistant cells is compared to its abundance in non-infected cells: sgRNAs that are depleted in resistant cells correspond to genes with antiviral activity, while enriched sgRNAs correspond to proviral genes. CRISPR-based screening strategies have been extensively used in the recent years to identify host cell viral factors in SINV(Petitjean et al., 2020), CHIKV(Meertens et al., 2019), Zika virus(Li et al., 2019b), HIV(Bonaventure et al., 2021;

Krasnopolsky et al., 2020), IAV(Li et al., 2020), HAV(Kulsuptrakul et al., 2021), and SARS-CoV-2(Baggen et al., 2021; Daniloski et al., 2021; Rebendenne et al., 2021; Schneider et al., 2021; Wang et al., 2021; Wei et al., 2021; Zhu et al., 2021). However, because cell viability is the primary read-out of these strategies, they may only reveal host-factors with a very strong effect on viral replication. Also, cell viability is highly impacted by the cell type used in the experiment, and hits for SARS-CoV-2 CRISPR screens have shown poor reproducibility between cell lines(Rebendenne et al., 2021). Finally, the strategies are unable to identify cellular proteins involved in viral fitness whose KO is lethal.

Genetic screen strategies such as RNAi and CRISPR-based screens further suffer from additional limitations. The type of read-out that can be used to evaluate the role of host-cell proteins in viral replication is highly constrained by the genome-wide nature of these strategies. As such, a single parameter such as cell viability or viral protein expression from replicating viruses or reporter constructs are generally used as a read-out and hits are extremely dependent on the chosen readout. Additionally, it has appeared clearer and clearer in the last 20 years that protein moonlighting – the ability for one protein to exert multiple functions – is the norm, rather than the exception(Singh and Bhalla, 2020). As a result, deciphering the precise role of host proteins in viral biology is challenging, as it may lead researchers into multiple directions at once, often outside of their field of expertise.

The other common type of experiments that aim at identifying host-cell proteins that participate in viral replication are biochemistry-based strategies. In this field, mass-spectrometry has become the tool of choice to identify cellular proteins that bind viral components, such as viral proteins and viral RNAs. A significant number of these studies use Affinity Purification (AP) of tagged viral proteins followed by protein identification and quantification of associated-proteins (AP-MS). Although tagged viral proteins are often expressed from plasmids in healthy or infected cells(Gordon et al., 2020; Jäger et al., 2012; Mayer et al., 2007; Taylor and Knipe, 2004), viral genome engineering has allowed AP-MS studies to be performed in infected cells with the viral genome directly encoding the tagged protein(Frolova et al., 2006; Gorchakov et al., 2008; Hafirassou et al., 2017; Moorman et al., 2008; Wang et al., 2017a). Recently, several studies have focused on the characterization of the viral RNAs interactomes. This is especially important in the case of RNA viruses, because a large number of cellular proteins participate in viral RNA replication, modifications, stability and translation(Li and Nagy, 2011). Multiple strategies that specifically target and purify viral RNAs for identification of its RBPome have been used to study

HIV(Knoener et al., 2017), SARS-CoV-2(Kamel et al., 2021; Lee et al., 2021b; Schmidt et al., 2021b), and SINV(Kamel et al., 2021). A different approach was undertaken by our collaborators at the Castello lab. Rather than focusing on viral mRNAs, their strategy involves poly(dT)-based purification of whole cell mRNAs and associated RNA binding proteins at different time points upon infection. They have applied this strategy to SINV and SARS-CoV-2 infected cells(Garcia-Moreno et al., 2019; Kamel et al., 2021) to show that the cell RBPome is recomposed during viral infection, with most of the observed differences originating by the important part taken by viral mRNAs within the cell transcriptome. As a consequence, their data significantly overlaps the viral mRNAs interactome(Garcia-Moreno et al., 2019; Kamel et al., 2021).

Inspired by their approach, we have developed a differential affinity purification method to investigate how the ribosome interactome is recomposed during viral infection. This method is, to our knowledge, one of the first attempt at differential protein complex interactomics. Wang and colleagues have examined the changes in human proteasome interactome after H<sub>2</sub>O<sub>2</sub> treatment using partially formaldehyde crosslinked tandem-affinity purified proteasomes(Wang et al., 2017b). Using this strategy, they were able to identify that ECM29, a weakly associated proteasome interactant, is recruited to the proteasome during oxydative stress. More recently, Aviner and colleagues have used an ultra-centrifugation-based strategy to examine the changes in polysome interactome consecutive to ZIKV, PV and DENV(Aviner et al., 2021). They identified several proteins whose association with polysomes changed during viral infection and showed that several peptidyl-prolil isomerases participate in co-translational folding of viral proteins. However, because their strategy does not involve an affinity-purification method and that several non-polysome associated proteins co-migrate with polysomes in sucrose-gradients, their method requires pre-existing knwoledge of the ribosome interactome, or careful examination of the differentially associated proteins.

Differential affinity purifications methods are extremely attractive to decipher how viruses alter important cellular complexes during infection. Interactome changes are likely to highlight specific requirements for viral biology or cellular response that are directly linked to the complex being studied. In contrast with genetic screens, this provides a strong starting point for a detailed characterization of the mechanisms involved. By focusing on a single complex, new roles of cellular proteins can also be uncovered within this specific context. The ribosome represents a seducing complex to be looked at during viral infection. It lies at the center of host-pathogen interactions, with significant alterations of the ribosome properties being present during infection of

most viruses. Given the sheer size of the ribosome interactome (~510(Simsek et al., 2017) – ~850 (us)), this leaves ample room for control via changes in ribosome partners abundance.

## Development of differential ribosome interactomics

To question the changes in ribosome interactome during viral infection, we have endogenously tagged the small subunit ribosomal protein RPS5 and the large subunit ribosomal protein RPL11 using the CRISPR/Cas9 method, adding these two to the list of ribosomal proteins that tolerate endogenous tagging(Simsek et al., 2017). Our dual 8xHis-Flag tag, coupled to a tandem affinity purification procedure, provides high specificity and unprecedented signal/noise ratio that allows a wide-dynamic range to monitor changes in ribosome association. RPS5-based ribosome purification encompasses multiple aspects of small ribosomal subunit biology and purifies free 40S, ternary complexes, 43S PIC, 48S initiating ribosomes, 80S translating ribosomes, 80S inactive monosomes, as well as pre-40S maturing small subunits, all of which contribute to the ribosome interactome described here. By comparing these results with RPL11-based purification, we are able to more closely define factors that associate specifically with 80S translating ribosomes and 80S monosomes and to extend our analysis to pre-60S maturation.

A major hurdle in comparing interactomes between different cellular conditions is the possibility that complexes or individual proteins may dissociate and re-associate during the experiment, consequently erasing pre-existing differences in protein complexes composition. This is in contrast with RNA-centric methods that all involve a UV or formaldehyde crosslinking procedure that covalently binds proteins to RNAs. When followed by denaturing washes this leads to dissociation non-crosslinked proteins, and reduces post-lysis dynamics, although uncrosslinked protein may remain associated(Trendel et al., 2018). To address the issue of post-lysis dynamics, we have minimized processing time to the best of our capability, adapted Nuclease S7 treatment to low temperatures, and performed cell lysis and ribosome capture in a large volume, all of which are expected to reduce post-lysis re-association. Additionally, we included a mild, carefully optimized formaldehyde crosslinking step that aims at stabilizing weak and transient interactions that are not recovered by native affinity purification. We selected a formaldehyde concentration of 0.1% that does not lead to overcrosslinking while maximizing the recovery of transient partners. Although we have not entirely excluded the possibility that post-lysis re-association may arise during our experiment, it can clearly be excluded proteins that are readily enriched by the crosslinking

procedure, among which eIF3 subunits. A method to definitely resolved this question is presented in the Perspectives section

## Pervasive remodeling of the ribosome interaction following SINV infection

We show that SINV infection induces a profound recomposition of the ribosome interactome with both loss and enrichment of specific RAPs at late time during infection (12hpi and 18hpi). The observed changes are, in part, due to relocalization of RAPs: we observe a nuclear retention of a group of pre-40S early cytoplasmic maturation factors as well as cytoplasmic accumulation of specific primarily nucleus localized factors, notably DDX18, DDX21 and DDX27 at 18hpi. An important question remains as whether this accumulation is triggered by their increased association with the ribosome, hence preventing their uptake into the nucleus, or by active export of these factors into the cytoplasm. Cytoplasmic accumulation of nuclear and nucleolar factors are common in viral infection (Salveti and Greco, 2014), and has been reported in the case of SINV, with ELAVL1/HuR accumulating in the cytoplasm (Barnhart et al., 2013). ELAVL1 cytoplasmic retention appears to be primarily mediated by the specific binding of ELAVL1 with the 3' UTR of the viral mRNAs (Barnhart et al., 2013). An other mechanism for cytoplasmic retention of nuclear protein has been described. nsP2, which localizes primarily in the nucleus aside from its participation into replication complexes in spherules, promotes CRM1-mediated nuclear export of the signal transducer and activator of transcription 1 (STAT1) involved in interferon response (Göertz et al., 2018). By doing so, nsP2 effectively inhibits the interferon response. nsP2 C-terminal methyltransferase-like domain was shown to be necessary and sufficient for this activity, however the precise molecular mechanism is unknown. Specifically inhibiting nucleus export and import would likely help identify whether the increased association of DDX18, DDX21 and DDX27 to the ribosome is a consequence, or a cause, of their cytoplasmic redistribution.

We find a stronger interaction of the ASC-1 complex subunit ASCC3 helicase at 12hpi, suggesting an increase in ribosome collision at that time-point. Strikingly, ASCC3 interaction with polysomes is only detectable in disomes and trisomes fractions. This is surprising because ribosome collisions is expected affect highly loaded mRNAs. One possible explanation is that ribosome collisions

affects newly synthesized mRNAs in the first rounds of translation. Translation of the sgRNA starts by the synthesis of the C protein, which is autocatalytically cleaved before exposition of E3 and co-translational insertion of the remainder of the polyprotein into the ER membrane. It is possible that ribosomes mark a pause after exposition of the signal peptide to allow for timely recognition of the signal peptide by the SRP at the surface of the ER (Collart and Weiss, 2020). If recognition by the SRP or addressing to the ER takes too much time, the following ribosome would collide with the leading one and trigger activation of the RQC pathway. The coding sequence of C is 792 nucleotide long, so it is in theory able to accommodate for much more translating ribosomes at a time than only 2 or 3. Of course, ribosomal density on mRNAs is highly controlled by the initiation rate, but mRNAs that are shorter than ~600 nucleotides are more likely to be translated by only one ribosome in yeast (Heyer and Moore, 2016). So if the initiation rate of the sgRNA is comparable to that of cellular mRNAs, presence of only 2 to 3 ribosomes in the C coding sequence is possible. We thus postulate that the ASC-1 complex rescues collided ribosomes that translate the sgRNA in its first round of translation. When the sgRNA is already addressed to the ER by other ribosomes translating the sgRNA ORF beyond the C coding sequence, the E3 signal peptide protruding from incoming ribosomes is more rapidly recognized by the SRP and ribosomes translating C do not collide anymore. Why, however, we do not see an enrichment of ASC3 at 18hpi is unclear. It could simply be that the stronger translational shut-down at 18hpi leads to an overall reduction of ASC3 requirement for host-cell mRNA which compensates for its requirement for sgRNA translation. Alternatively, sgRNA translation intensity appears to decrease at 18hpi and forward (Garcia-Moreno et al., 2019), which is possibly explained by resource exhaustion or by the strong alterations to the cell metabolism.

Surprisingly, we find little overlap between the changes in total mRNA interactome and ribosome interactome, despite the fact that several RAPs also are RNA binding proteins. Our ribosome purification method involves a Nuclease S7 treatment optimized to split polysomes into monosomes during the purification step. This is accomplished to identify RNA binding proteins that associate directly with the ribosome and not with the translated mRNA, although the two are not mutually exclusive. In consequence, although the RNA interactome and the ribosome interactome significantly overlap, changes affecting one interactome are not found in the other. This suggests that the RNA binding and ribosome binding properties behave independently and that their primary mode of function can switch depending on the situation. Another factor contributing to this result is also probably due to the mRNAs being sampled. In their mRNA interactome purification strategy, our collaborators performed whole-cell purification of mRNAs. At 18hpi, the vast majority of

mRNAs, and especially host mRNAs, is not being translated due to the translational shut-down in place. As a result, the mRNA purification strategy employed is sampling mostly untranslated mRNA. In contrast, purifying ribosomes means that only mRNAs that are being translated, and in particular viral mRNAs, are recovered by our strategy. In consequence, the surprising lack of overlap between the two strategies results may be partly explained by the different populations of mRNAs being recovered. Our strategy may indeed better reflect the sgRNA interactome, because it is likely to contribute greatly to the results presented here.

## Requirements of canonical translation factors in the translation of SINV sgRNA

At 18h post-infection, cellular translation shut-off is complete and mostly viral proteins expressed from the viral sub-genomic RNA are reliably translated (Garcia-Moreno et al., 2019). As a result, changes in canonical translation factors in RPS5 affinity purifications likely reflect the intensity of translation and the requirements of the sgRNA for initiation factors. We observe a global decrease in the association of canonical initiation factors following infection, affecting eIF2, eIF3 and eIF4F complexes that likely mirror the decreased rate of translation initiation. We notably observe a strong fold change for eIF2 factors (-3 (log<sub>2</sub>)) which indicates a decrease in eIF2-containing 43S PICs. This is probably due to the effect of eIF2 $\alpha$ /EIF2S1 phosphorylation which prevents formation of the 43S PIC. Thus, this is in line with the reported low sensitivity of sgRNA translation to eIF2 $\alpha$  phosphorylation.

An important discovery of our study is that eIF4E protein abundance in RPS5 eluates is substantially lower than that of other eIF4F components. This is in line with the current understanding of sgRNA translation, where eIF4E is not necessary for sgRNA translation initiation (Castelló et al., 2006; Sanz et al., 2017b) and excluded from viral factories where sgRNA translation takes place (Sanz et al., 2009c), despite the fact that sgRNA translation is perceived as a cap-dependent process (Carrasco et al., 2018). A possible explanation could be that SINV infection induces dephosphorylation of 4E-BP, hence promoting its association to eIF4E and competing for binding of eIF4E to the rest of the eIF4F complex. In fact, SINV has been shown to inhibit activation of the mTOR pathway that controls the phosphorylation level of 4E-BP, and should accordingly lead to higher levels of dephosphorylated 4EBP, although authors did not test that

particular modification(Mohankumar et al., 2011). We are in the process of investigating that finding further.

Unfortunately, our data does not provide new information on the identity of the potential cap-binding protein that could substitute for eIF4E. We observe a minor, non-significant, enrichment for eIF4E2 (Figure 16), a homolog of eIF4E with a cap-binding activity. eIF4E2 is generally seen as an inhibitor of translation(Chapat et al., 2017), with a role in stalled/collided ribosome recycling(Hickey et al., 2020; Juskiewicz et al., 2020a) although a role in translation activation has been suggested in response to interferon stimulation(Okumura et al., 2007). Rather than indicating that eIF4E2 substitutes for eIF4E for sgRNA translation, we believe that the small increase seen in eIF4E2 association can be linked with an increase in ribosome collisions during infection (see below). We also observe a strong enrichment for LARP1 a non-canonical cap-binding proteins that controls the initiation of 5'TOP containing mRNAs. LARP1 was recently identified as a SINV C interacting protein using a proximity biotinylation assay, which is coherent with the fact that both C and LARP1 are ribosome associated proteins in our experiments(Landers et al., 2021). Interestingly though, LARP1 association with mRNAs is not increased following SINV infection(Garcia-Moreno et al., 2019), which suggests that LARP1 increased association with the ribosome is not mediated by an increased binding to mRNAs. LARP1 association with mRNAs comes from multiple activities: its cap-binding activity(Lahr et al., 2017; Philippe et al., 2020), the extended cap-binding domain that provides 5'TOP recognition(Lahr et al., 2017; Philippe et al., 2020), direct interaction with the polyA-tail(Mattijssen et al., 2021) and interaction with PABP(Mattijssen et al., 2021). eIF4E is not recovered by conventional UV-crosslinking procedures(Garcia-Moreno et al., 2019) which indicates that cap-binding domains are not efficiently crosslinked to the cap by UV irradiation. If LARP1 behaves similarly, the discrepancy between our data and our collaborators' suggests that LARP1 interaction with PABP is increased following infection, or that a mode of cap recognition that does not involve the 5'TOP selective domain is at place. However, a recent report suggests that LARP1 is generally an antiviral protein, a behavior incompatible with a role in translation initiation of the sgRNA(Contu et al., 2021). LARP1 was identified as a SFV nsP3 interacting protein, and a siRNA screen investigating viral replication on the basis of a nsP3-GFP fusion suggested an antiviral role of LARP1(Contu et al., 2021). It is important to note though that given GFP expression level reflected gRNA and not sgRNA translation, it may be that LARP1 exerts both proviral and antiviral role at different steps of the viral life cycle. Other reports point to LARP1 being an antiviral factor for SARS-CoV-2 infection suggest that LARP1 is a broadly



antiviral protein(Lee et al., 2021b; Schmidt et al., 2021b). More work is required to properly defined how this activity is achieved.

## Alteration of ribosome biogenesis

Our data suggests that ribosome biogenesis is globally altered during infection. Numerous nucleolar proteins involved in 60S maturation (DDX18, DDX21, DDX27, RSL1D1, BRIX1, ZNF622, WDR12) accumulate in the cytoplasm late during infection and are recovered by our ribosome purification. This came as a surprise, as unprocessed 60Ss should not be able to interact with the 40S, and be recovered by RPS5-based purification. However, we find that both RPS5 and RPL11-based purification are able to recover DDX18, DDX21, DDX27 and BRIX1 in similar amounts, although slightly lower in RPS5 AP. This is in contrast with BYSL and HNRNPM whose interaction is strictly restricted to free 40S and 60S respectively. DDX18, DDX21 and ZNF622 distributed throughout polysome gradients indicating that their interaction with the ribosome is not limited to unprocessed 60S. Certain 60S maturation factors could thus participate in translation regulation. In particular, DDX21 has been shown to participate in repression of IRES-mediated translation of FMDV mRNA(Abdullah et al., 2021). However, given that DDX21 appears to primarily interact with the 60S subunit of the ribosome (see below), how it can affect translation initiation is unclear. Perhaps FMDV IRES-mediated translation involves a particular mode of 60S recruitment that is inhibited by DDX21.

When analyzing the distribution of these helicases in polysome gradients, our results show that DDX18 associates with polysomes throughout the gradient, with abundance mirroring that of ribosomal proteins and suggest that DDX18 associates with elongating ribosomes. In contrast, DDX27 interaction with ribosomes is not observed throughout the gradient and its abundance per ribosome drops with increasing polysome size, a behavior in line with a potential role in translation initiation or early elongation. Unfortunately, we were unable to test DDX21 association in polysome due to time constraints. Mass-spectrometric analysis of ribosome associated protein distribution in polysome gradients reveals similar findings(Imami et al., 2018). DDX18, DDX21 and DDX27 were found to be associated with polysomes, with DDX18 abundance following that of ribosomal proteins, and abundance of DDX21 and DDX27 relative to ribosomal proteins dropping along the gradients. All three helicases were found in the 60S fraction but not the 40S fraction which confirms that they interact with the ribosome through the 60S subunit(Imami et al., 2018). The participation of these helicases in 60S maturation raises the question of whether this changes in

ribosome association might indicate a defect of 60S maturation and export of un-matured 60S to which DDX18, DDX21 and DDX27 remain attached. Although we do observe that most of the changes in DDX18, DDX21 and DDX27 are attributable to free 60S and monosomes rather than elongating ribosomes, this could also be explained by the general decrease of polysome abundance. Co-localization experiments of these helicases with viral factories would help decipher whether they participate in sgRNA translation.

Mirroring the accumulation of 60S maturation factors is the retention of pre-40S particles into the nucleus. All components of a pre-40S cytoplasmic intermediate(Ameismeier et al., 2018) were found to be depleted in ribosomes eluates at 18hpi, a behavior that aligns with the changes in cytoplasmic abundance of these factors. 40S maturation is a multi-step process that starts in the nucleolus and ends in the cytoplasm. The 40S ribosome biogenesis factors that are depleted during infection all belong to closely related late nuclear and early cytoplasmic steps. Crucially, RIOK1 and LRRC47, two factors involved in a downstream step that we do capture through affinity purification, are not reliably depleted(Ameismeier et al., 2020). This suggests, along with the detection of BYSL on RPS5 eluates, that pre-40S nuclear retention is a late event of infection. In contrast, accumulation of the 60S maturation factors mentioned before is detected much earlier, as soon as 4 hours post infection. Interestingly, 60S maturation defects have been shown to reduce 40S export(Wild et al., 2010). This would mean that 60S maturation is the primarily target of ribosome biogenesis alterations by SINV.

## Perspectives

This project was massively affected by the current pandemic both in terms of lost bench time, interruption of ongoing experiments, and long delays of mass-spectrometric analysis due to closing of the mass-spectrometric platforms for months. Although we were ready to perform the purification of ribosomes from SINV infected cells in March 2020, we only received our results in February 2021. As a consequence, a significant number of questions regarding the role of differentially associated ribosome interacting proteins remain.

An unresolved question remains as to whether post-lysis reassociation participates to the changes observed here. Few proteins are expected to be able to reform complexes given that cytoplasmic lysates are largely diluted during the purification step. As to whether this re-association may lead to

false-positive hits in our differential analysis, we expect this to be even more unlikely. However, it is a concerning possibility for proteins that accumulate in the cytoplasm during infection such as DDX18, DDX21 and DDX27, and are thus also more abundant in cytoplasmic lysates. To definitely answer this question and identify proteins that are susceptible to post-lysis reassociation, we have devised a strategy based on SILAC labelling of tagged and non-tagged ribosomes, with pre or post-affinity purification mixing. Cells expressing tagged ribosomes were labeled with heavy arginine and lysine while WT cells were labeled with light amino acids. When samples are mixed pre-AP, “light” proteins may be given the chance to re-associate with “heavy” ribosomes, and be eluted along them. In a control experiment, samples were mixed post-AP to correctly define the part of aspecific binding to beads in “light” proteins recovery. Unfortunately, we were unable to present these results here, as a tube broke during shipment and the sample was lost. We are in the process of repeating this experiment to clearly test whether post-lysis reassociation contributes significantly to the results presented here. While performing this experiment we realized that a similar strategy had been used successfully used to assess the part that post-lysis reassociation takes in human proteasome interactome data(Wang and Huang, 2008). A portion of the proteasome interactants (16/67) was shown to completely or partially re-associate during affinity purification, with a high dependency on purification duration. Importantly though, their purification strategy did not include the optimization described earlier, in particular a crosslinking procedure or high-volume binding step. Similarly, this strategy has been applied to RNA:protein interactions to investigate the proportion of non-UV crosslinked RNA binding proteins that remain bound to RNAs despite a stringent purification process by phenol extraction(Trendel et al., 2018).

To better understand if changes in ribosome association correlate with a requirement of these factors for viral translation, we plan on using CIRPSR/Cas9 induce knock-out of genes coding for these factors, and evaluate how infection is altered in these cells. So far, we have generated multiple sgRNA targeting several factors and but are only beginning testing viral replication in KO cell lines. Interestingly though, all tested factors shown to be enriched in the RBPome of mRNAs during SINV infection have a proviral activity on viral replication(Garcia-Moreno et al., 2019). Whether this may apply similarly to the ribosome interactome remains unclear.

To better understand how ribosome interacting proteins may regulate translation, we are developing an approach to localize ribosomes decorated with ribosome associated factors on mRNAs. Our strategy involves RNase-mediated generation of ribosome footprints, followed by sequential purification of ribosomes and ribosomes interacting proteins to isolate only the subset of ribosomes

that harbor particular interactant, and subsequent high-throughout sequencing, an approach similar to RIPiT-seq(Ricci et al., 2014). Rather than relying on commercial antibodies for the second step of the purification, we plan on using a tag-mediated affinity purification to provide a universal method that does not require buying individual antibodies for each purification. Similarly to our ribosomal protein tagging approach, we have set out to endogenously tag proteins of interests. This represents the most physiological strategy to express tagged proteins in cell lines. This time however, rather than relying on ssODN-mediated HDR to incorporate the tag sequence, we use the CRISPaint strategy(Schmid-Burgk et al., 2016), which allows C-terminal tagging of proteins and subsequent puromycin selection of correctly tagged proteins. Although this strategy leads to integration of a longer exogenous sequence than conventional HDR, a puromycin selection in the CRISPaint cassette drastically facilitates the generation of multiple tagged cell lines at a time. So far, we have tagged multiple proteins with the c-myc tag that we planned on using for our dual purification strategy. However, we discovered that affinity of commercial antibodies for the c-myc tag is rather weak and does not allow immunodetection and immunoprecipitation of most endogenously tagged proteins, with only tagged ribosomal proteins being reliably detected, possibly due to their high expression levels compared to other proteins. We are in the process of evaluating alternative tags with better affinity for their cognate antibody. Our current work involves evaluation of 3xc-myc, 3xV5(Hanke et al.), and Twin-Strep(Schmidt et al., 2013) tags for efficient immunodetection and immunoprecipitation. We expect that the avidity provided by the multiplicity of the epitope in these tags will help better detect and purify proteins with low expression levels.

Finally, we plan on using our ribosome AP-MS strategy to investigate ribosome interactome recomposition during infection of other viruses. We have already generated samples for HSV-1 infection and are awaiting for the mass-spectrometry results. We expect to get these results before my defense and to be able to share them then. Similarly to SINV, HSV-1 infection induces a profound arrest in host-cell translation, yet the mechanisms used by the virus to resist to translation shut-off are largely different to that of SINV(Smith et al., 2008). Contrary to SINV, HSV-1 is a DNA virus, not RNA, but still, PKR is activated by HSV-1 infection. This is presumably due to dsRNA substructure formed during transcription of overlapping genes on opposite DNA strands. Two viral proteins however, ICP34.5 and US11, counteract PKR activation and decrease its intensity(Cassady et al., 1998). Crucially, US11 is able to interact directly with the ribosome(Roller and Roizman, 1992), but whether this relates to the role mentioned earlier is currently unknown(Smith et al., 2008). An other viral protein ICP27, stimulates the translation of specific viral mRNAs(Smith et al., 2008), but how this is achieved, again, is unknown. HSV-1 encodes more

than 70 proteins and more viral proteins may be able to directly affect the properties of the ribosome. So far, only our own work and that of Aviner and colleagues have questioned the ribosome interactome recombination during viral infection(Aviner et al., 2021), however both our studies were focused on RNA viruses. We believe that it would be of great interest to extend this strategy to DNA viruses such as HSV-1 with potentially different strategies for control of the ribosome.

## Material & Methods

### *Genome editing*

Genome editing of HEK293T cells were achieved by using CRISPR/Cas9 nuclease-mediated recombination. sgRNA guide sequences were cloned into the BbsI-digested PX459 expression plasmid bearing both sgRNA scaffold backbone (BB) and Cas9 nuclease. pSpCas9(BB)-2A-Puro (PX459) V2.0 was a gift from Feng Zhang (Addgene plasmid # 62988 ; <http://n2t.net/addgene:62988> ; RRID:Addgene\_62988) (Ran et al., 2013) . sgRNA guide sequences and ssODN repair templates used are detailed in Table 2 .  $1 \times 10^6$  HEK293T were plated onto a single 6-well plate, 18 hr prior to transfection of the relevant sgRNAs cloned into the PX459 plasmid and the ssODN template. 1  $\mu$ g of sgRNA plasmid and 10 pmols of ssODN were transfected using 3  $\mu$ L of JetPRIME (Polyplus, catalog no. 114-75). 24 hr after transfections, cells were trypsinized and plated into 10 cm plates and let for 3-4 days to approach confluency. Then cells were seeded at an approximate 1000 cells per 10 cm plate and colonies were grown for two weeks. HEK293T clones were picked under a EVOS FL microscope (ThermoFischer, catalog no. 12-563-460) and seeded in 96 well plates. Plates we grown for a week and duplicated. One of the two plates was used for subsequent PCR amplification of the modified region using the appropriate PCR oligos detailed in Table 2 and GoTaq G2 DNA polymerase (catalog no. M7841 ). PCR products displaying at least one band at the expected size were subcloned using TOPO TA Cloning Kit for Subcloning (ThermoFiescher catalog no. 451641) and sequenced. Expression of the tag was verified by Western Blot using mouse anti-Flag antibody (Sigma, catalog no. F3165).

RPS5 sgRNA	GCCTGTCCCAGGATGACCGAG
RPS5 8xHis-Flag ssODN	TGGGAATGAGTGCGCCTTTGCTCCATGCTAGCTGAGCTCTGACGTTTTTTTCCT GTCATCACCCGTGCCAGGATGCACCATCACCATCACCATCACCATGACTACA

	AAGACGATGACGACAAGACCGAGTGGGAGACAGCAGCACCAGCGGTGGCAG AGACCCCAGACATCAAGCTCTTTGGGAAGTGGAGCACCGATG
RPS5_PCR_F	GAGTTGGGAATGAGTGCGCC
RPS5_PCR_R	AATCACCAAGTTCCTCACCT
RPL11 sgRNA	CATCATGGCGGTGAGTAGCT
RPL11 8xHis-Flag ssODN	TGGGAAAAGAGCCCGCCTCCTGGCCCATAAGGCCCTCGGCCGGAAGCTCCGC TTTCTCTTCTGCTCTCCATCATG <b>CACCATCACCATCACCATCACCATGACTAC</b> <b>AAAGACGATGACGACAAG</b> GCGGTGAGTAGCTGGGACCTGGATTGCTTTCT TTATCCGTCGCCATCCATGGCAGGCCGAGCCTGCGGGGGCTA
RPL11_PCR_F	TCTCTGTGGTTAGCTGGGA
RPL11_PCR_R	TTGCGGGCTCCATATTCCTC

**Table 2: List of oligos**

### *Viruses*

The pT7-SVmCherry plasmid encoding the SINV genome with a deduplicated promoter expressing mCherry was a gift from Emmanuel Garcia-Moreno (Garcia-Moreno et al., 2019). The pT7-SVmCherry plasmid was first linearized with XhoI and used as a template for in vitro RNA transcription with HiScribe T7 ARCA mRNA kit (New England Biolabs, catalog no. E2065S). Transcribed genomic RNA was transfected into BHK-21 using Lipofectamine 2000 reagent (Invitrogen, catalog no. 11668027). Viruses were collected 24h after transfection and further amplified in BHK-21 for 24h. Cell supernatant was cleaned by centrifugation for 15 min at 3000g at RT, aliquoted and stored at -80°C. Viruses titration was performed on 6 well plates seeded at 60% confluency with HEK293T cells. 18h post-infection, cells were collected and fixed using paraformaldehyde (Sigma, catalog no. 158127) and mCherry fluorescence was analyzed by fluorescent flow-cytometry using MACSQuant (Milteny Biotech) and quantified using FlowJo. All infections were performed at an MOI of 3-5 to guarantee >90% cells infected.

### *Measurement of protein synthesis using O-propargyl-puromycin (OPP)*

Cells were treated with 10 µM OPP (Imagina Biotechnology, catalog no. OP001-26) for 30 minutes at 37°C. The cells were then fixed in PBS-paraformaldehyde 4% (w/v) for 20 minutes, then permeabilized with PBS-0.5% Triton X-100 for 20 minutes. Fluorescent labelling of the OPP was made with the Click-IT™ Plus Alexa Fluor™488 Picolyl Azide (Thermo Fisher Scientific,

catalog no. C10641), according to the manufacturer's instructions. Finally, cells were analyzed with the MACSQuant VYB cytometer and results were analyzed using FlowJo (FlowJo LLC).

### *Polysome gradients analysis*

10-50% sucrose gradients were made using stock 10% and 50% (w/v) sucrose stock solutions (sucrose, 10mM HEPES pH7.4, 100 mM KCl, 5 mM MgCl<sub>2</sub>, 1mM DTT, 100µg/mL cycloheximide (Sigma, catalog no. 01810). 5.6 mL of 10% sucrose was layered in a 13.2 mL, Thinwall Polypropylene Tube (Beckmann, catalog no. 331362) then 5.6 mL 50% sucrose was layered at the bottom of the tube using a glass pipet. Gradients were made using Gradient Master 108 (Serlabo Technologies) and stored at 4°C before use.

Cells supernatant was removed and replaced with ice-cold PBS supplemented with 100µg/mL cycloheximide. In case cells were crosslinked before lysis, cell supernatant was removed and replaced with ice-cold PBS supplemented with 100µg/mL cycloheximide and 0.1% formaldehyde (w/v) and placed immediately at 4°C for 10 min. Supernatant was then removed and crosslinking was quenched with ice-cold PBS supplemented with 250 mM glycine at 4°C for 10 min.

Cells were scraped, collected in 1.5mL centrifuge tube and centrifuged for 5 min at 4°C at 500g. Cells were lysed in Lysis buffer (25mM Tris pH7.4, 150mM NaCl, 15mM MgCl<sub>2</sub>, 1mM DTT, 100µg/mL cycloheximide, 1% Triton X-100) on ice for 10 min. Lysates were cleared by centrifugation for 10 min at 4°C at 1,500g and supernatants were layered on 10-50% sucrose gradients. Polysomes were separated by ultra-centrifugation on a SW 41 Ti rotor at 35,000 rpm for 2h40min at 4°C. Gradients were analyzed by measuring 254 nm OD and 1 mL fractions were collected for Western Blot analysis.

### *Western Blot and silver-staining analysis*

AP eluates and gradients fractions, samples were precipitated using Methanol-Chloroform precipitation Briefly, 3 volumes of methanol, 1 volume of chloroform and 4 volumes of water were added. Aqueous and organic phases were separated by centrifugation at RT and the organic phase was discarded. The aqueous phase was precipitated by 4 volumes of methanol and protein pellets were collected at the bottom of the tube by centrifugation. Protein pellets were dried at RT and resuspended in Loading buffer (1X Bolt Sample Reducing Agent(ThermoFischer, catalog no. B0009), 1XBolt LDS Buffer (ThermoFischer, catalog no. B0008). Other samples were mixed directly with Bolt Sample Reducing Agent and Bolt LDS Buffer without precipitation. Samples were migrated in pre-cast Bolt 4-12% gels (ThermoFischer, catalog no. NW04122BOX) using MES

buffer (ThermoFischer, catalog no. B0002) and transferred to methanol-activated PVDF membranes (Dutscher, catalog no. 10600101). Membranes were blotted with primary antibodies diluted in 1X TBS, 0.1% Tween (v/v), 3% BSA (w/v). All antibodies (Table 3) were used at their recommended dilution. Silver-staining was performed using Pierce Silver Stain Kit (ThermoFischer, catalog no. 24612)



Targets	Manufacturer	Catalog no.
DDX18	ProteinTech	28502-1-AP
DDX21	ProteinTech	10528-1-AP
DDX27	ProteinTech	17087-1-AP
BYSL	ProteinTech	28319-1-AP
ZNF622	ProteinTech	20804-1-AP
EIF6	ProteinTech	10291-1-AP
ASCC3	ProteinTech	17627-1-AP
ASCC2	ProteinTech	11529-1-AP
ASCC1	ProteinTech	12301-1-AP
HNRNPM	ProteinTech	26897-1-AP
BRX1	ProteinTech	17295-1-AP
Flag	Sigma	F3165
eIF3a	Cell Signaling	3411
eIF3e	N/A	(Morris-Desbois et al., 1999)
RPL30	Abcam	ab170930
RPS3a	Abcam	ab176342
ACTB	Sigma	A1978

**Table 3: List of antibodies**

### *Tandem affinity purification of 0.1%FA crosslinked ribosomes*

Only the final protocol of the ribosome affinity purification methods is described here, including the formaldehyde crosslinking step. For modifications made during optimization of the method, please refer to the Results section. 8XHis-Flag-RPS5, 8xHis-Flag-RPL11 and WT HEK293T cells were seeded into 15 cm plates so that confluency was 80% at the time of harvesting. If applicable, cells were infected at an MOI of 3-5 or mock infected at different time points before harvesting. For each infection time-point, two 80% confluent 15 cm plates were used. At the time of recovery, cell supernatant was removed and replaced with ice-cold PBS supplemented with 100µg/mL

cycloheximide and 0.1% formaldehyde (w/v) and placed immediately at 4°C for 10 min. Supernatant was then removed and crosslinking was quenched with ice-cold PBS supplemented with 250 mM glycine at 4°C for 10 min. Cells were collected and pelleted by centrifugation at 500g for 5 min at 4°C. The equivalent of two 15 cm plate were lysed in 50 mL of Lysis/Binding buffer (25mM Tris pH7.4, 150mM NaCl, 15mM MgCl<sub>2</sub>, 10mM CaCl<sub>2</sub>, 1mM DTT, 8U/mL Nuclease S7 (Sigma, catalog no. 10107921001), 100µg/mL cycloheximide, 0.2X cOmplete EDTA-free Protease Inhibitor Cocktail (Sigma, catalog no. 11873580001), 0.2X PhosSTOP (Sigma, catalog no. 4906837001), 1% Triton X-100) for 10 min at 4°C. Lysates were cleared by centrifugation at 3,000g for 15 min at 4°C. 50 mL lysates were then mixed with 300µL Anti-FLAG M2 Affinity Agarose Gel (Sigma, catalog no. A2220) pre-washed with Washing buffer (25mM Tris pH7.4, 150mM NaCl, 15mM MgCl<sub>2</sub>, 1% Triton X-100), and incubated for 1h at 4°C on a rotating wheel. Samples were loaded on a 14 cm Econo-Pac Chromatography Column (Bio-Rad, catalog no. 7321011) and the supernatant was removed. Beads were then washed 4 times with 25mL of Washing buffer. Beads were recovered and transferred to a 2mL Protein LoBind tubes (Eppendorf, catalog no. 0030108450), and washed 3 times with 1mL of Washing buffer. Beads were resuspended in Washing buffer supplemented with 500µg/mL final DYKDDDDK peptide (GeneScript, catalog no. A00170-40) and ribosomes were eluted for 1h at 4°C on a rotating wheel in a new 2mL Protein LoBind tube. 8xHis-Flag-ribosome eluates were cleaned from agarose beads using Mini Bio-Spin Chromatography Columns (Bio-Rad, catalog no. #7326207) 8xHis-Flag-ribosome eluates were then added to 50µL pre-washed Dynabeads His-Tag Isolation and Pulldown (ThermoFischer, catalog no. 10104D), and incubated for 30 min at 4°C on a rotating wheel. Supernatant was discarded, beads were resuspended in 400µL of Washing buffer, transferred to a new 2mL Protein LoBind tube before washing for 5 min at 4°C on a rotating wheel. Washing solution was removed and beads were washed 4 additional times. Beads were transferred to a new 2mL Protein LoBind tube and washed a final time in Washing buffer with no Triton X-100. Beads were transferred to a new 2mL Protein LoBind tube and 8xHis-Flag-ribosomes were eluted using His Elution buffer (500mM Imidazole pH6, 500mM NaCl) for 30 min at RT on a rotating wheel. Eluates were kept at 20°C until LC-MS/MS analysis.

### *Tandem affinity purification of 0.1%FA crosslinked polysomes*

Polysomes were first isolated by polysome gradient fractionation before submitted to tandem affinity purification. 8xHis-Flag-RPS5 and WT HEK293T cells were mock infected or infected for 12h before harvesting. To compensate for the decrease in polysomes amount in infected cells, three

15cm plates at 80% confluency were used whereas one 15cm plate was used for mock infected cells. Cells were crosslinked, quenched and recovered as described before. Cells were lysed in 1mL Lysis buffer (25mM Tris pH7.4, 150mM NaCl, 15mM MgCl<sub>2</sub>, 1mM DTT, 100µg/mL cycloheximide, 0.2X cOmplete EDTA-free Protease Inhibitor Cocktail, 0.2X PhosSTOP, 1% Triton X-100) and loaded on 10-50% gradients. 800µL fractions were collected and fractions 8 to 14 corresponding to disomes and upwards were pooled. Volume was adjusted to 50mL using Binding buffer (25mM Tris pH7.4, 150mM NaCl, 15mM MgCl<sub>2</sub>, 10mM CaCl<sub>2</sub>, 1mM DTT, 8U/mL Nuclease S7, 100µg/mL cycloheximide, 0.2X cOmplete EDTA-free Protease Inhibitor Cocktail, 0.2X PhosSTOP, 1% Triton X-100) and tandem affinity purification was performed as described earlier.

### *Mass spectrometry*

Mass spectrometry sample preparation and LC/MS-MS quantification has been described earlier(Sysoev et al., 2016).

### *Proteomic quantitative analysis*

Proteomic quantitative analysis has been described earlier(Sysoev et al., 2016). Because RAPs may be entirely lost during infection, or only present after infection as is the case for viral proteins, the ribosome interactome was determined independently for each infection time point using 8XHis-Flag-RPS5 and WT samples at each time point. In case proteins were not detected in samples, missing values were replaced by pseudo-values equal to the noise intensity of corresponding peptides to allow for calculation of a pseudo-Fold-Change. Protein log-intensity were tested against the null hypothesis that log-intensity-ratios are equal to zero using a moderated t-test(Lönnstedt and Speed, 2002) implemented in the R/Bioconductor package limma(Smyth, 2005). Adjusted p-values were corrected for multiple testing by using the method of Benjamini-Hochberg(Benjamini and Hochberg, 1995). The same strategy has been applied to determine the changes in RAPs during infection, with comparison with 8xHis-Flag-RPS5 samples at different time points. Because proteins with low abundant RAPs are more likely to be missed by mass-spectrometry analysis, they are more subject to missing values than highly associated RAPs. This increases the likelihood of low abundant RAPs to be miss-reported as differentially associated despite the use of pseudo-values. Also, low abundant RAPs are more difficult to detect by Western Blot analysis to confirm their changes in association. Thus, rather than filtering proteins based on the number of missing values, which would remove all viral proteins from the analysis, we filtered proteins based on their 8xHis-

Flag-RPS5 average abundance. Thus, only proteins with an average log-intensity value of 22 are reported in the graphs. All graphs were made using the R ggplot2 package(Wickham, 2009).

## Part II: Investigating alphavirus nsP2-RPS6/eS6 interaction using quantitative yeast two-hybrid

### Introduction

While waiting for the mass-spectrometry results presented earlier, we sought out to confirm previously described interaction of Alphavirus proteins with the ribosome. A number of Alphavirus proteins have been suggested to interact with the ribosome in infected cells. The capsid protein C of SINV and SFV has been shown to cosediment with 80S translating ribosomes (Glanville and Ulmanen, 1976; Ulmanen et al., 1976, 1979; Wengler and Wengler, 1984). This was later postulated to be related to ribosome-assisted particle assembly and dis-assembly (Wengler, 1987, 2009; Wengler and Wengler, 1984, 2002; Wengler et al., 1984). Additionally, nsP2 of SFV, VEE and SINV have been reported to either cosediment and/or copurify with ribosomes (Atasheva et al., 2007; Montgomery et al., 2006; Ranki et al., 1979). In particular, RPS6/eS6-Flag immunoprecipitation copurifies VEE nsP2 (Montgomery et al., 2006). Co-expression of nsP2 of VEE, SINV and SFV and RPS6 from human in a cell-free translation system shows copurification of the two proteins as well, meaning that this interaction exists independently of RPS6 integration into ribosomes, and suggesting that RPS6 is the direct site of interaction for nsP2. Finally, VEE nsP2 is able to interact with *Aedes albopictus* RPS6, and as such, RPS6-nsP2 interaction appears to be conserved with different Alphaviruses in different hosts (Montgomery et al., 2006). More recently, yeast two-hybrid screening of CHIKV nsP2 interactions gave a positive signal for RPS6 and RPL4/uL4 interaction, suggesting again that RPS6 is nsP2 interaction site on the ribosome (Bourai et al., 2012).

Interestingly, RPS6 becomes highly phosphorylated during mTOR activation, the effect of which leads to translation repression (Meyuhas, 2015b). As such, RPS6 phosphorylation has been postulated to participate translation inhibition, but this remains largely unclear (Meyuhas, 2015b). Whether mTOR is activated during *Alphavirus* infection remains somewhat unclear. Conflicting results report that SFV does induced RPS6 phosphorylation (Thaa et al., 2015) while other reports that it does not (Montgomery et al., 2006), with CHIKV only moderately activating mTOR (Thaa et al., 2015). As for SINV, SINV infection does not induce RPS6 phosphorylation in mammalian cells (Mohankumar et al., 2011) yet does so in arthropod cells (Patel and Hardy, 2012). This is

extremely intriguing, as the vast majority of viral infection give rise to RPS6 phosphorylation, essentially through modulation of the mTOR pathway(Li, 2019).

Five clustered residues of RPS6 - S<sub>235</sub>, S<sub>236</sub>, S<sub>240</sub>, S<sub>244</sub>, and S<sub>247</sub> – are subject to phosphorylation. Phosphorylation happens in an ordered fashion starting with S<sub>236</sub>, then from N-to-C direction. The five residues are present at the end of a long solvent-accessible alpha-helix and are unresolved on recent structures of the human 80S ribosomes(Khatter et al., 2015). This suggest that that the C-terminus, where phoshorylation sites reside, is unstructured or highly flexible. The recently released AlphaFold2 prediction of RPS6 structure gives a similar information (<https://alphafold.ebi.ac.uk/entry/P62753>). RPS6 C-terminus is predicted to adopt a long alpha-helix conformation from amino acid R183 to K249, yet the confidence score of the predicted structures falls off towards the C-terminus, with the decrease starting at R231 (Figure 23). Based on this information, we reasoned that eS6 phosphorylation could enhance RPS6 C-terminus to fold as an alpha-helix. This would point to a role in RPS6 phosphorylation in regulating folding, and potentially allow for the recruitment of cellular or viral interacting proteins.

We investigated whether that was likely using Waggawagga, an online tool for alpha-helix prediction based on multiple prediction algorithms(Simm et al., 2015). Using the phoshomimetic conversions S → E, and S → D all algorithms used by Waggawagga suggest that RPS6 phosphorylation extends alpha-helix stability in the C-direction, as shown by Marcoil calculations of coiled-coil scores for WT (Figure 24A), S → D (Figure 24B) and S → E (Figure 24C) phosphomimetic mutants for all five residues. Thus, we sought out to investigate the relationship between RPS6 phosphorylation and nsP2 binding.

David Cluet, a recent addition to our lab, has developed a quantitative fluorescent based yeast two-hybrid system(Cluet et al., 2020). Classical two-hybrid methods rely on expression a B-galactosidase reporter, but because Bait and Prey expression levels are not investigated using these methods, they are prone to false-negative, typically when one partner is lowly expressed(Cluet et al., 2020). Similarly, these methods are unable to investigate the strength of protein interactions, and only provide a yes/no answer. The quantitative approach mentioned earlier relies on single-cell co-measurement levels of Bait, Prey and Reporter, each colored by a different fluorescent protein (Figure 25A). Reporter expression can be put in perspective with both Bait and Prey levels, and allows for a quantitative measure of the interaction strength. We reasoned that this approach could

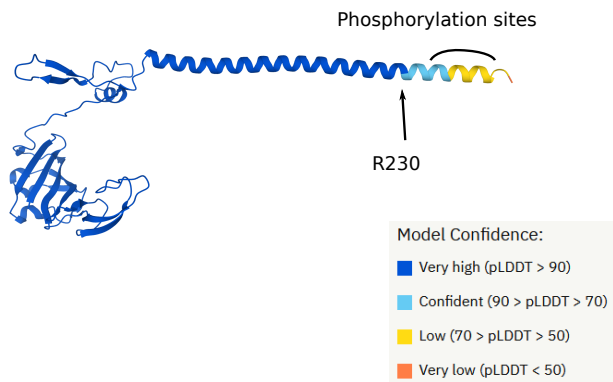


**Figure 23: AlphaFold prediction of RPS6 structure**

AlphaFold prediction of the RPS6 structures shows a drop in the C-terminal structure confidence where RPS6 phosphorylation sites reside.

be used to evaluate the strength of nsP2-RPS6 interaction, especially in relation RPS6 phosphorylation levels.

## Results

We investigated human RPS6 and SINV nsP2 interaction, using ribosomal RPS10/eS10 and NPM1, a ribosome-interacting protein with unknown ribosomal binding site, as controls. We also included Barnase H102A prey coupled with Barnstar Y29F, D35A and D39A baits of known 117 pM, 11-77 pM (estimated), and 420nM KD values respectively, as a reference for interaction strength(Cluet et al., 2020). RPS6 and RPS10 showed high level of auto-activation of the reporter when used as baits and paired with an empty prey plasmid, and hence cannot be used in this configuration for determination of KD values (Figure 25B). When RPS6 was used as prey however, it did not give rise to auto-activation and RPS6-nsP2 pairing showed limited BFP expression, a potential suggesting interaction. However, BFP expression was lower than that of the Barnase H102A/Barnstar D39A and close to the detection limit of this method(Cluet et al., 2020).

We sought out to replicated this result, while incorporating new prey and bait partners to the experiment. We reasoned that splitting RPS6 and nsP2 in parts would be beneficial for our analysis. This could help increase expression levels of baits and preys, facilitate accessibility for interaction(Bourai et al., 2012), and allow the identification of domains involved in the interaction. Given that RPS6 accessibility to solvent is restricted to the C-terminal region(Khatter et al., 2015), we generated C-terminal and N-terminal truncations of RPS6 corresponding to fragments 1-182 (N-ter) and 183-249 (C-ter). nsP2 features two annotated helicase and protease domains, in between the unannotated N-terminal and C-terminal regions. Thus, we constructed SINV nsP2 truncations based on nsP2 domains named N-ter (1-183), helicase (184-431), protease (432-638), and C-ter (639-805). Finally, the RPS6-nsP2 interaction has been reported for different Alphaviruses nsP2 and vector/host RPS6/(Montgomery et al., 2006), and which prompted us to explore this interaction using RPS6/eS6 from *Gallus gallus* (chicken, host), *Aedes albopictus* (mosquito, vector), *Aedes aegypti* (mosquito, vector), as well as nsP2 from two other alphaviruses SFV, and CHIKV.

This time however, we were not able to detect the RPS6-nsP2 interaction (Figure 25C). N-ter and C-ter truncations were not able to induce BFP expression when paired nsP2 either, and RPS6 from chicken and mosquitoes all gave the same result, despite a reasonable expression level. Weirdly, nsP2 truncations all showed modest to high level of auto-activation of the BFP reporter when paired



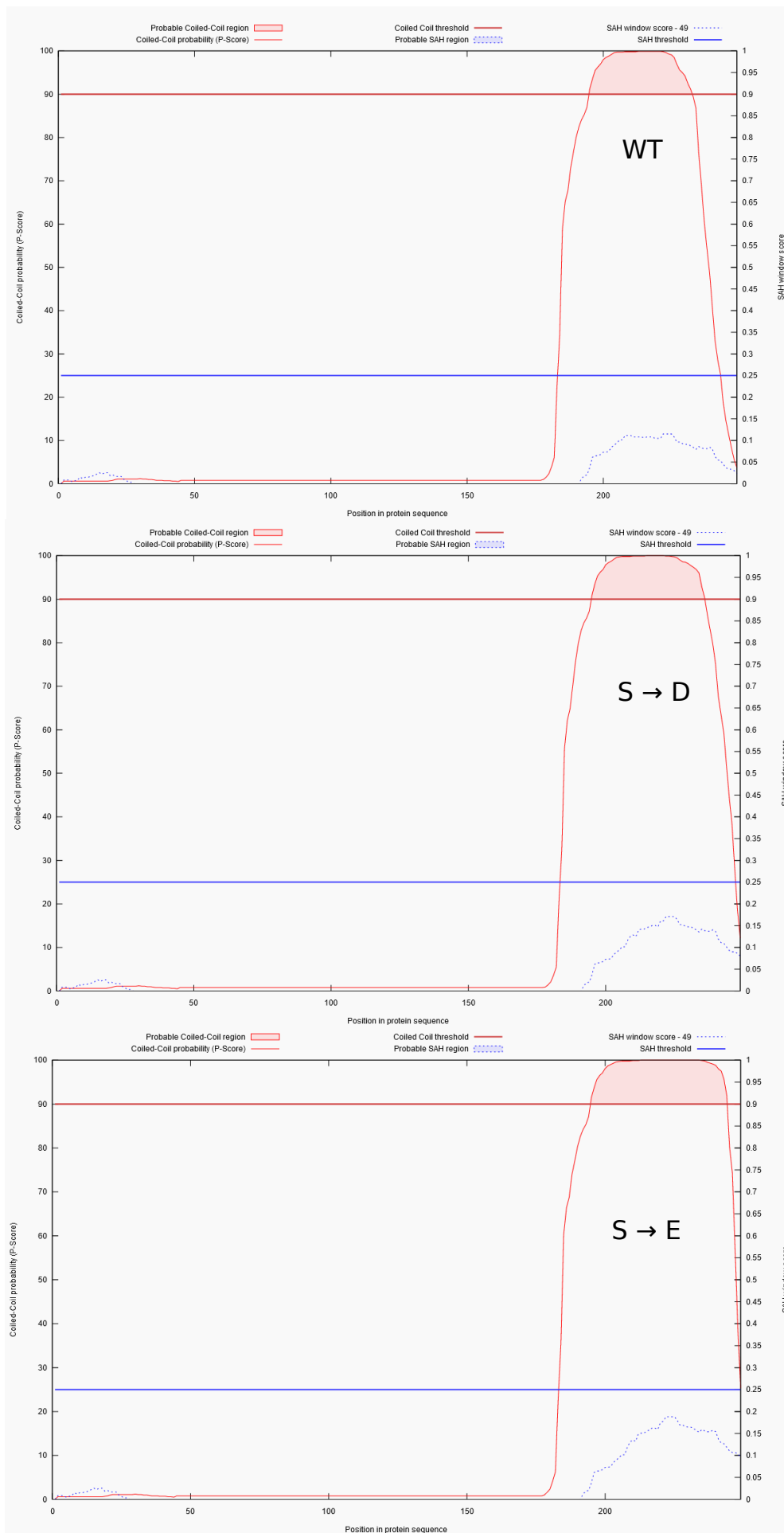


**Figure 24: Marcoil analysis of RPS6 amino acid sequence**

Marcoil analysis was performed on WT RPS6 (A), S → D phosphomimetic RPS6 mutant (B), and S → E phosphomimetic mutant (C). Calculations of the coiled-coil probably score suggests that phosphorylation of RPS6 stabilizes the C-terminal alpha-helix

with the empty prey vector. This was surprising given that full-length nsP2 did not behave similarly. Finally, CHIKV and SFV nsP2 both auto-activated BFP expression even in the absence of prey expression.

## Discussion

Protein-protein interactions are governed by kinetic and thermodynamic parameters, whose measure helps understanding how fast and for how long interactions form in cells. Yet, quantitative measures of this interactions is often restricted to *in vitro* experiments such as Surface Plasmon Resonance or switchSENSE(Cléry et al., 2017, 2019). These experiments require protein production and purification and are thus cumbersome to use for the screening and measure of many interaction at a time. Classical yeast two-hybrid strategies provide higher flexibility, throughput and involve *in cell* rather than *in vitro* interactions but are only qualitative, and prone to false-negatives and false-positives. Finally, *in cell* fluorescent complementation experiments(Miller et al., 2015) allow for examination of protein-protein interactions in mammalian cells but suffer from the same drawbacks than yeast two-hybrid.

We reasoned that the method developed by David Cluet and colleagues (Cluet et al., 2020)was promising for the investigation of the role of ribosomal protein RPS6 phosphorylation. Given than the C-terminal phosphorylated region of RPS6 is the only RPS6 solvent accessible region, we postulated that RPS6 phosphorylation might modify RPS6 ability to fold and/or to interact with partners. Thus we investigated the interaction of *Alphaviruses* nsP2 with RPS6, an interaction that has been reported several time.

We were unable to detect this interaction using this method. First, the ribosomal proteins studied here, including RPS6/eS6, produced high level of auto-activation of the BFP reporter when used as Baits. This might be related to their ability to tightly bind rRNA in context of the ribosome, as many RNA binding protein also show some level of DNA binding, especially in the case of double-stranded RNA binding proteins(Bourgeois et al., 2016). This limits the analysis, as interaction strength can be influenced depending on the Bait/Prey orientation chosen(Cluet et al., 2020). Secondly, RPS6/eS6 expression was quite low. Interaction strength measurements are optimal when restricted to a particular window of Bait and Prey expression, because this provides an ideal

dynamic range of BFP reporter expression(Cluet et al., 2020). Finally, nsP2 from CHIKV and SFV showed auto-activation of the BFP reporter as well. This could be related to their RNA binding properties, and suggests that their helicase domain is able to somewhat bind DNA. Why this was not the case with SINV nsP2 remains unclear. We received our mass-spectrometry results shortly after this last experiment, and concentrated on the main part of my PhD thesis until then.

We were able however to confirm the previously reported interaction of nsP2 with the ribosome using our newly developed ribosome affinity purification (see Part I). To date, the role of the nsP2-ribosome interaction has not been unveiled. Interestingly though, RPS6 sits at the entrance of the mRNA channel(Khatter et al., 2015) and thus, an interaction between nsP2 and the 40S ribosomal subunit would put the nsP2 helicase in a convincing position for a role in sgRNA unwinding. In fact, the DSH downstream the C AUG codon very likely requires the participation of an helicase, given its very long 28 nucleotide stem. More work is required to properly locate the nsP2 binding site onto the ribosome and investigate the role of phosphorylated residues. One alternative to the two-hybrid strategy described here could be to perform GST-pulldown involving nsP2 and RPS6. This strategy would allow to investigate whether phosphorylation of RPS6 affects nsP2 binding using phosphomimetic mutants, although only to a semi-quantitative degree. Alternatively, we are working in collaboration with Yohan Couté from the EdyP lab, Grenoble, France to implement ribosome interactant binding site discovery by crosslinking/mass-spectrometry (XL-MS). This strategy involves crosslinking of purified ribosomes using the MS cleavable crosslinker agent DSBU, followed by trypsin digestion and identification of crosslinked peptides. This method involves highly purified ribosomes using our new method and would allow for pan-discovery of RAPs binding sites onto the ribosome. A proof of concept using commercial *E. coli* ribosomes was recently released and authors were able to identify inter-molecular crosslinks that are coherent with the known structure of the ribosome(Tüting et al., 2020). So far, our own work has shown promising result, with detection of both intra- and inter- molecular crosslinking events for ribosomal proteins. However, few crosslinking events with ribosome associated proteins were detected and more work is required to enrich for RAPs-originating crosslinked peptides.

# Materials & Methods

## Plasmid construction

pSB\_1Bait\_RFP-X (X being the protein of interest) plasmids were constructed by linearization of pSB\_1Bait\_RFP-Empty using XhoI, and subsequent yeast recombination-based cloning using cDNAs detailed below. pSB\_1Prey\_yEGFP-X plasmids were constructed by linearization of pSB\_1Prey\_yEGFP-Empty using XhoI, and subsequent yeast recombination-based cloning using cDNAs detailed earlier. All plasmids were validated by Sanger sequencing.

## cDNA amplification

Bait and Prey plasmids(Cluet et al., 2020) were prepared as follows. All cDNAs were amplified using Phusion High-Fidelity DNA polymerase (NEB) using primers complementary to the targets, and additional appropriate overhangs for yeast recombination-based cloning into pSB\_1Bait\_RFP and pSB\_1Prey\_yEGFP plasmid backbones(Cluet et al., 2020). SINV nsP2 was amplified from pT7-SINV-mCherry(Garcia-Moreno et al., 2019), CHIKV nsP2 was amplified from from pCHIKV-GFP (pCHIKV-GFP was a gift from Marlène Dreux), SFV nsP2 was amplified from pSFV3 (pSFV3 was a gift from Henrik Garoff (Addgene plasmid # 92072 ; <http://n2t.net/addgene:92072> ; RRID:Addgene\_92072)). Human RPS6 was amplified from HEK293T cells (ATCC CRL-3216 ) cDNA. Chicken RPS6 was amplified from primary T2EC cells(Gandrillon et al., 1999). *Aedes aegypti* RPS6 was amplified from Aag-2 cells (ATCC CCL-125). *Aedes albopictus* was amplified from U4.4 cells (ATCC CCL-126). Human RPS6 N-ter (1-182) and C-ter (183-249) Prey plasmids were constructed by amplifications of the desired region from previously constructed pSB\_1Prey\_yEGFP-RPS6, and re-cloned by yeast recombination-based cloning into linearized pSB\_1Prey\_yEGFP-Empty. SINV nsP2 N-ter (1-183), helicase (184-431), protease (432-638), and C-ter (639-805) Bait plasmids were constructed by amplifications of the desired region from previously constructed pSB\_1Bait\_RFP-nsP2, and re-cloned by yeast recombination-based cloning into linearized pSB\_1Bait\_RFP-Empty.

## Quantitative two-hybrid assay

Quantitative two-hybrid assay was performed as previously described (Cluet et al., 2020). Briefly, chemo-competent EGY42a-pBFP2 yeast cells were transformed with Bait vectors and TB50 $\alpha$  yeast cells were transformed with Prey vectors. Haploid cells were selected, mated, and amplified to generate diploid cells transformed with pBFP2 reporter plasmid, Bait plasmid, and Prey plasmid. Cells were transferred into Galactose/Raffinose medium to induce expression of the Prey cassette, and consequently authorize reporter expression. Expression was then stopped by paraformaldehyde fixation. Finally, cells were run through flow cytometry analysis and BFP, RFP and yEGFP intensity levels were measured.

## Quantitative two-hybrid analysis

FCS files were opened using R package flowCore, and analysed using an home-made R script. Briefly, to account for differences in expression levels of Baits and Preys, only cells falling into 700-900 A.U. RFP intensity and 3500-4500 A.U. yEGFP intensity gates were kept for the analysis. The average BFP intensity was calculated on gated cells, and number of cells analysed reported.

Abdullah, S.W., Wu, J., Zhang, Y., Bai, M., Guan, J., Liu, X., Sun, S., and Guo, H. (2021). DDX21, a Host Restriction Factor of FMDV IRES-Dependent Translation and Replication. *Viruses* 13, 1765.

Abu Bakar, F., and Ng, L.F.P. (2018). Nonstructural Proteins of Alphavirus—Potential Targets for Drug Development. *Viruses* 10, 71.

Ahola, T., and Kääriäinen, L. (1995). Reaction in alphavirus mRNA capping: formation of a covalent complex of nonstructural protein nsP1 with 7-methyl-GMP. *PNAS* 92, 507–511.

Ahola, T., Kujala, P., Tuittila, M., Blom, T., Laakkonen, P., Hinkkanen, A., and Auvinen, P. (2000). Effects of palmitoylation of replicase protein nsP1 on alphavirus infection. *J Virol* 74, 6725–6733.

Akhrymuk, I., Kulemzin, S.V., and Frolova, E.I. (2012). Evasion of the innate immune response: the Old World alphavirus nsP2 protein induces rapid degradation of Rpb1, a catalytic subunit of RNA polymerase II. *J Virol* 86, 7180–7191.

Aliperti, G., and Schlesinger, M.J. (1978). Evidence for an autoprotease activity of sindbis virus capsid protein. *Virology* 90, 366–369.

Ameismeier, M., Cheng, J., Berninghausen, O., and Beckmann, R. (2018). Visualizing late states of human 40S ribosomal subunit maturation. *Nature* 558, 249–253.

Ameismeier, M., Zemp, I., van den Heuvel, J., Thoms, M., Berninghausen, O., Kutay, U., and Beckmann, R. (2020). Structural basis for the final steps of human 40S ribosome maturation. *Nature* 587, 683–687.

- Archer, S.K., Shirokikh, N.E., Beilharz, T.H., and Preiss, T. (2016). Dynamics of ribosome scanning and recycling revealed by translation complex profiling. *Nature* 535, 570–574.
- Atasheva, S., Gorchakov, R., English, R., Frolov, I., and Frolova, E. (2007). Development of Sindbis Viruses Encoding nsP2/GFP Chimeric Proteins and Their Application for Studying nsP2 Functioning. *J. Virol.* 81, 5046–5057.
- Atasheva, S., Fish, A., Fornerod, M., and Frolova, E.I. (2010). Venezuelan Equine Encephalitis Virus Capsid Protein Forms a Tetrameric Complex with CRM1 and Importin  $\alpha/\beta$  That Obstructs Nuclear Pore Complex Function. *Journal of Virology* 84, 4158–4171.
- Avey, D., Tepper, S., Li, W., Turpin, Z., and Zhu, F. (2015). Phosphoproteomic Analysis of KSHV-Infected Cells Reveals Roles of ORF45-Activated RSK during Lytic Replication. *PLOS Pathogens* 11, e1004993.
- Aviner, R., Li, K.H., Frydman, J., and Andino, R. (2021). Cotranslational prolyl hydroxylation is essential for flavivirus biogenesis. *Nature* 1–7.
- Bablanian, R., Esteban, M., Baxt, B., and Sonnabend, J.A. (1978). Studies on the Mechanisms of Vaccinia Virus Cytopathic Effects: I. Inhibition of Protein Synthesis in Infected Cells is Associated with Virus-induced RNA Synthesis. *Journal of General Virology* 39, 391–402.
- Bachelier, J.-P., Cavallé, J., and Hüttenhofer, A. (2002). The expanding snoRNA world. *Biochimie* 84, 775–790.
- Baggen, J., Persoons, L., Vanstreels, E., Jansen, S., Van Looveren, D., Boeckx, B., Geudens, V., De Man, J., Jochmans, D., Wauters, J., et al. (2021). Genome-wide CRISPR screening identifies TMEM106B as a proviral host factor for SARS-CoV-2. *Nat Genet* 53, 435–444.
- Balinsky, C.A., Schmeisser, H., Wells, A.I., Ganesan, S., Jin, T., Singh, K., and Zoon, K.C. IRAV (FLJ11286), an Interferon-Stimulated Gene with Antiviral Activity against Dengue Virus, Interacts with MOV10. *Journal of Virology* 91, e01606-16.
- Ballesta, J.P.G., and Remacha, M. (1996). The Large Ribosomal Subunit Stalk as a Regulatory Element of the Eukaryotic Translational Machinery. In *Progress in Nucleic Acid Research and Molecular Biology*, W.E. Cohn, and K. Moldave, eds. (Academic Press), pp. 157–193.
- Banerjee, A.K., Blanco, M.R., Bruce, E.A., Honson, D.D., Chen, L.M., Chow, A., Bhat, P., Ollikainen, N., Quinodoz, S.A., Loney, C., et al. (2020). SARS-CoV-2 Disrupts Splicing, Translation, and Protein Trafficking to Suppress Host Defenses. *Cell* 183, 1325-1339.e21.
- Banham, A.H., Leader, D.P., and Smith, G.L. (1993). Phosphorylation of ribosomal proteins by the vaccinia virus B1R protein kinase. *FEBS Lett.* 321, 27–31.
- Barnhart, M.D., Moon, S.L., Emch, A.W., Wilusz, C.J., and Wilusz, J. (2013). Changes in cellular mRNA stability, splicing, and polyadenylation through HuR protein sequestration by a cytoplasmic RNA virus. *Cell Rep* 5, 909–917.
- Basore, K., Kim, A.S., Nelson, C.A., Zhang, R., Smith, B.K., Uranga, C., Vang, L., Cheng, M., Gross, M.L., Smith, J., et al. (2019). Cryo-EM Structure of Chikungunya Virus in Complex with the Mxra8 Receptor. *Cell* 177, 1725-1737.e16.

- Basu, A., Das, P., Chaudhuri, S., Bevilacqua, E., Andrews, J., Barik, S., Hatzoglou, M., Komar, A.A., and Mazumder, B. (2011). Requirement of rRNA Methylation for 80S Ribosome Assembly on a Cohort of Cellular Internal Ribosome Entry Sites. *Mol. Cell. Biol.* *31*, 4482–4499.
- Beaud, G., Masse, T., Madjar, J.-J., and Leader, D.P. (1989). Identification of induced protein kinase activities specific for the ribosomal proteins uniquely phosphorylated during infection of HeLa cells with vaccinia virus. *FEBS Lett.* *259*, 10–14.
- Beaud, G., Sharif, A., Topa-Massé, A., and Leader, D.P. (1994). Ribosomal protein S2/Sa kinase purified from HeLa cells infected with vaccinia virus corresponds to the B1R protein kinase and phosphorylates in vitro the viral ssDNA-binding protein. *J. Gen. Virol.* *75* ( Pt 2), 283–293.
- Begik, O., Lucas, M.C., Prysycz, L.P., Ramirez, J.M., Medina, R., Milenkovic, I., Cruciani, S., Liu, H., Vieira, H.G.S., Sas-Chen, A., et al. (2021). Quantitative profiling of pseudouridylation dynamics in native RNAs with nanopore sequencing. *Nat Biotechnol* 1–14.
- Ben-Hamida, F., and Beaud, G. (1978). In vitro inhibition of protein synthesis by purified cores from vaccinia virus. *PNAS* *75*, 175–179.
- Ben-Hamida, F., Person, A., and Beaud, G. (1983). Solubilization of a protein synthesis inhibitor from vaccinia virions. *J. Virol.* *45*, 452–455.
- Benjamini, Y., and Hochberg, Y. (1995). Controlling the False Discovery Rate: A Practical and Powerful Approach to Multiple Testing. *Journal of the Royal Statistical Society. Series B (Methodological)* *57*, 289–300.
- Berlanga, J.J., Ventoso, I., Harding, H.P., Deng, J., Ron, D., Sonenberg, N., Carrasco, L., and de Haro, C. (2006). Antiviral effect of the mammalian translation initiation factor 2alpha kinase GCN2 against RNA viruses. *EMBO J* *25*, 1730–1740.
- Beura, L.K., Dinh, P.X., Osorio, F.A., and Pattnaik, A.K. (2011). Cellular Poly(C) Binding Proteins 1 and 2 Interact with Porcine Reproductive and Respiratory Syndrome Virus Nonstructural Protein 1β and Support Viral Replication. *Journal of Virology* *85*, 12939–12949.
- Birkedal, U., Christensen-Dalsgaard, M., Krogh, N., Sabarinathan, R., Gorodkin, J., and Nielsen, H. (2015). Profiling of Ribose Methylations in RNA by High-Throughput Sequencing. *Angewandte Chemie International Edition* *54*, 451–455.
- Blau, L., Knirsh, R., Ben-Dror, I., Oren, S., Kuphal, S., Hau, P., Proescholdt, M., Bosserhoff, A.-K., and Vardimon, L. (2012). Aberrant expression of c-Jun in glioblastoma by internal ribosome entry site (IRES)-mediated translational activation. *PNAS* *109*, E2875–E2884.
- Boersma, S., Khuperkar, D., Verhagen, B.M.P., Sonneveld, S., Grimm, J.B., Lavis, L.D., and Tanenbaum, M.E. (2019). Multi-Color Single-Molecule Imaging Uncovers Extensive Heterogeneity in mRNA Decoding. *Cell* *0*.
- Boersma, S., Rabouw, H.H., Bruurs, L.J.M., Pavlovič, T., van Vliet, A.L.W., Beumer, J., Clevers, H., van Kuppeveld, F.J.M., and Tanenbaum, M.E. (2020). Translation and Replication Dynamics of Single RNA Viruses. *Cell* *183*, 1930-1945.e23.
- Bohlen, J., Fenzl, K., Kramer, G., Bukau, B., and Teleman, A.A. (2020). Selective 40S Footprinting Reveals Cap-Tethered Ribosome Scanning in Human Cells. *Molecular Cell* *79*, 561-574.e5.

- Bonaventure, B., Rebendenne, A., Gracia, F.G. de, McKellar, J., Gracias, S., Labaronne, E., Tauziet, M., Valadão, A.L.C., Bernard, E., Briant, L., et al. (2021). A genome-wide CRISPR/Cas9 knock-out screen identifies the DEAD box RNA helicase DDX42 as a broad antiviral inhibitor.
- Bonderoff, J.M., LaRey, J.L., and Lloyd, R.E. (2008). Cleavage of Poly(A)-Binding Protein by Poliovirus 3C Proteinase Inhibits Viral Internal Ribosome Entry Site-Mediated Translation. *Journal of Virology* 82, 9389–9399.
- Bonneville, J.M., Sanfaçon, H., Fütterer, J., and Hohn, T. (1989). Posttranscriptional trans-activation in cauliflower mosaic virus. *Cell* 59, 1135–1143.
- Bourai, M., Lucas-Hourani, M., Gad, H.H., Drosten, C., Jacob, Y., Tafforeau, L., Cassonnet, P., Jones, L.M., Judith, D., Couderc, T., et al. (2012). Mapping of Chikungunya Virus Interactions with Host Proteins Identified nsP2 as a Highly Connected Viral Component. *J. Virol.* 86, 3121–3134.
- Bourgeois, C.F., Mortreux, F., and Auboeuf, D. (2016). The multiple functions of RNA helicases as drivers and regulators of gene expression. *Nat. Rev. Mol. Cell Biol.* 17, 426–438.
- Braack, L., Gouveia de Almeida, A.P., Cornel, A.J., Swanepoel, R., and de Jager, C. (2018). Mosquito-borne arboviruses of African origin: review of key viruses and vectors. *Parasit Vectors* 11, 29.
- Brass, A.L., Dykxhoorn, D.M., Benita, Y., Yan, N., Engelman, A., Xavier, R.J., Lieberman, J., and Elledge, S.J. (2008). Identification of Host Proteins Required for HIV Infection Through a Functional Genomic Screen. *Science*.
- Brito Querido, J., Sokabe, M., Kraatz, S., Gordiyenko, Y., Skehel, J.M., Fraser, C.S., and Ramakrishnan, V. (2020). Structure of a human 48S translational initiation complex. *Science* 369, 1220–1227.
- Buendia, B., Person-Fernandez, A., Beaud, G., and Madjar, J.-J. (1987). Ribosomal protein phosphorylation in vivo and in vitro by vaccinia virus. *Eur. J. Biochem.* 162, 95–103.
- Bukrinskaya, A.G., Bykovsky, A.Ph., and Zhdanov, V.M. (1969). The participation of Sendai virus ribonucleoprotein in virus-specific polysome formation. *Virology* 39, 705–720.
- Calviello, L., Venkataramanan, S., Rogowski, K.J., Wyler, E., Wilkins, K., Tejura, M., Thai, B., Krol, J., Filipowicz, W., Landthaler, M., et al. (2021). DDX3 depletion represses translation of mRNAs with complex 5' UTRs. *Nucleic Acids Research* 49, 5336–5350.
- Campos, R.K., Wong, B., Xie, X., Lu, Y.-F., Shi, P.-Y., Pompon, J., Garcia-Blanco, M.A., and Bradrick, S.S. (2017). RPLP1 and RPLP2 Are Essential Flavivirus Host Factors That Promote Early Viral Protein Accumulation. *J. Virol.* 91.
- Cao, S., Dhungel, P., and Yang, Z. (2017). Going against the Tide: Selective Cellular Protein Synthesis during Virally Induced Host Shutoff. *J. Virol.* 91, e00071-17.
- Carrasco, L., Sanz, M., and González-Almela, E. (2018). The Regulation of Translation in Alphavirus-Infected Cells. *Viruses* 10, 70.
- Carvajal, F., Vallejos, M., Walters, B., Contreras, N., Hertz, M.I., Olivares, E., Cáceres, C.J., Pino, K., Letelier, A., Thompson, S.R., et al. (2016). Structural domains within the HIV-1 mRNA and the



- ribosomal protein S25 influence cap-independent translation initiation. *The FEBS Journal* **283**, 2508–2527.
- Cassady, K.A., Gross, M., and Roizman, B. (1998). The herpes simplex virus US11 protein effectively compensates for the gamma1(34.5) gene if present before activation of protein kinase R by precluding its phosphorylation and that of the alpha subunit of eukaryotic translation initiation factor 2. *J. Virol.* **72**, 8620–8626.
- Castelló, A., Sanz, M.A., Molina, S., and Carrasco, L. (2006). Translation of Sindbis virus 26S mRNA does not require intact eukaryotic initiation factor 4G. *J Mol Biol* **355**, 942–956.
- Chapat, C., Jafarnejad, S.M., Matta-Camacho, E., Hesketh, G.G., Gelbart, I.A., Attig, J., Gkogkas, C.G., Alain, T., Stern-Ginossar, N., Fabian, M.R., et al. (2017). Cap-binding protein 4EHP effects translation silencing by microRNAs. *PNAS* **114**, 5425–5430.
- Chaudhari, H.V., Inamdar, M.M., and Kondabagil, K. (2021). Scaling relation between genome length and particle size of viruses provides insights into viral life history. *IScience* **24**, 102452.
- Chaudhuri, S., Vyas, K., Kapasi, P., Komar, A.A., Dinman, J.D., Barik, S., and Mazumder, B. (2007). Human ribosomal protein L13a is dispensable for canonical ribosome function but indispensable for efficient rRNA methylation. *RNA* **13**, 2224–2237.
- Chen, B., Brown, K.A., Lin, Z., and Ge, Y. (2018). Top-Down Proteomics: Ready for Prime Time? *Anal. Chem.* **90**, 110–127.
- Chen, Z., Wang, C., Feng, X., Nie, L., Tang, M., Zhang, H., Xiong, Y., Swisher, S.K., Srivastava, M., and Chen, J. (2021). Comprehensive analysis of the host-virus interactome of SARS-CoV-2. *BioRxiv* 2020.12.31.424961.
- Cheng, E., Haque, A., Rimmer, M.A., Hussein, I.T.M., Sheema, S., Little, A., and Mir, M.A. (2011). Characterization of the Interaction between Hantavirus Nucleocapsid Protein (N) and Ribosomal Protein S19 (RPS19). *J. Biol. Chem.* **286**, 11814–11824.
- Choi, H.K., Tong, L., Minor, W., Dumas, P., Boege, U., Rossmann, M.G., and Wengler, G. (1991). Structure of Sindbis virus core protein reveals a chymotrypsin-like serine proteinase and the organization of the virion. *Nature* **354**, 37–43.
- Chretien, J.-P., Anyamba, A., Bedno, S.A., Breiman, R.F., Sang, R., Sergon, K., Powers, A.M., Onyango, C.O., Small, J., Tucker, C.J., et al. (2007). DROUGHT-ASSOCIATED CHIKUNGUNYA EMERGENCE ALONG COASTAL EAST AFRICA. *The American Journal of Tropical Medicine and Hygiene* **76**, 405–407.
- Cléry, A., Sohier, T.J.M., Welte, T., Langer, A., and Allain, F.H.T. (2017). switchSENSE: A new technology to study protein-RNA interactions. *Methods* **118–119**, 137–145.
- Cléry, A., Gillioz, L., Nguyen, C.K.X., and Allain, F.H.-T. (2019). A Step-by-Step Guide to Study Protein–RNA Interactions. *CHIMIA International Journal for Chemistry* **73**, 406–414.
- Cluet, D., Amri, I., Vergier, B., Léault, J., Audibert, A., Grosjean, C., Calabrési, D., and Spichty, M. (2020). A Quantitative Tri-fluorescent Yeast Two-hybrid System: From Flow Cytometry to In cellula Affinities. *Molecular & Cellular Proteomics* **19**, 701–715.

- Collart, M.A., and Weiss, B. (2020). Ribosome pausing, a dangerous necessity for co-translational events. *Nucleic Acids Research* *48*, 1043–1055.
- Compans, R.W. (1973). Influenza virus proteins: II. Association with components of the cytoplasm. *Virology* *51*, 56–70.
- Contu, L., Balistreri, G., Domanski, M., Uldry, A.-C., and Mühlemann, O. (2021). Characterisation of the Semliki Forest Virus-host cell interactome reveals the viral capsid protein as an inhibitor of nonsense-mediated mRNA decay. *PLOS Pathogens* *17*, e1009603.
- Cristea, I.M., Carroll, J.-W.N., Rout, M.P., Rice, C.M., Chait, B.T., and MacDonald, M.R. (2006). Tracking and elucidating alphavirus-host protein interactions. *J Biol Chem* *281*, 30269–30278.
- Cristea, I.M., Rozjabek, H., Molloy, K.R., Karki, S., White, L.L., Rice, C.M., Rout, M.P., Chait, B.T., and MacDonald, M.R. (2010). Host factors associated with the Sindbis virus RNA-dependent RNA polymerase: role for G3BP1 and G3BP2 in virus replication. *J Virol* *84*, 6720–6732.
- Cross, R.K. (1983). Identification of a unique guanine-7-methyltransferase in Semliki forest virus (SFV) infected cell extracts. *Virology* *130*, 452–463.
- Cullot, G., Boutin, J., Toutain, J., Prat, F., Pennamen, P., Rooryck, C., Teichmann, M., Rousseau, E., Lamrissi-Garcia, I., Guyonnet-Duperat, V., et al. (2019). CRISPR-Cas9 genome editing induces megabase-scale chromosomal truncations. *Nat Commun* *10*, 1136.
- Daniloski, Z., Jordan, T.X., Wessels, H.-H., Hoagland, D.A., Kasela, S., Legut, M., Maniatis, S., Mimitou, E.P., Lu, L., Geller, E., et al. (2021). Identification of Required Host Factors for SARS-CoV-2 Infection in Human Cells. *Cell* *184*, 92-105.e16.
- Darzynkiewicz, E., Stepinski, J., Ekiel, I., Jin, Y., Haber, D., Sijuwade, T., and Tahara, S.M. (1988).  $\beta$ -globin mRNAs capped with m 7 G, m 22.7 G or m 32.2.7 G differ in intrinsic translation efficiency. *Nucleic Acids Research* *16*, 8953–8962.
- Das, P.K., Merits, A., and Lulla, A. (2014). Functional cross-talk between distant domains of chikungunya virus non-structural protein 2 is decisive for its RNA-modulating activity. *J Biol Chem* *289*, 5635–5653.
- De Caluwé, L., Ariën, K.K., and Bartholomeeusen, K. (2021). Host Factors and Pathways Involved in the Entry of Mosquito-Borne Alphaviruses. *Trends in Microbiology* *29*, 634–647.
- Deffrasnes, C., Marsh, G.A., Foo, C.H., Rootes, C.L., Gould, C.M., Grusovin, J., Monaghan, P., Lo, M.K., Tompkins, S.M., Adams, T.E., et al. (2016). Genome-wide siRNA Screening at Biosafety Level 4 Reveals a Crucial Role for Fibrillar in Henipavirus Infection. *PLOS Pathogens* *12*, e1005478.
- Delang, L., Li, C., Tas, A., Quérat, G., Albulescu, I.C., De Burghgraeve, T., Guerrero, N.A.S., Gigante, A., Piorkowski, G., Decroly, E., et al. (2016). The viral capping enzyme nsP1: a novel target for the inhibition of chikungunya virus infection. *Sci Rep* *6*, 31819.
- Dhungel, P., Cantu, F.M., Molina, J.A., and Yang, Z. (2020). Vaccinia Virus as a Master of Host Shutoff Induction: Targeting Processes of the Central Dogma and Beyond. *Pathogens* *9*, 400.

- Dickson, A.M., Anderson, J.R., Barnhart, M.D., Sokoloski, K.J., Oko, L., Opyrchal, M., Galanis, E., Wilusz, C.J., Morrison, T.E., and Wilusz, J. (2012). Dephosphorylation of HuR protein during alphavirus infection is associated with HuR relocalization to the cytoplasm. *J Biol Chem* 287, 36229–36238.
- DiGiacomo, V., and Meruelo, D. (2016). Looking into laminin receptor: critical discussion regarding the non-integrin 37/67-kDa laminin receptor/RPSA protein. *Biological Reviews* 91, 288–310.
- DiGiuseppe, S., Rollins, M.G., Astar, H., Khalatyan, N., Savas, J.N., and Walsh, D. (2020). Proteomic and mechanistic dissection of the poxvirus-customized ribosome. *Journal of Cell Science* 134.
- Ding, M.X., and Schlesinger, M.J. (1989). Evidence that Sindbis virus NSP2 is an autoprotease which processes the virus nonstructural polyprotein. *Virology* 171, 280–284.
- Dmitriev, S.E., Terenin, I.M., Andreev, D.E., Ivanov, P.A., Dunaevsky, J.E., Merrick, W.C., and Shatsky, I.N. (2010). GTP-independent tRNA Delivery to the Ribosomal P-site by a Novel Eukaryotic Translation Factor\*. *Journal of Biological Chemistry* 285, 26779–26787.
- Domashevskiy, A.V., Miyoshi, H., and Goss, D.J. (2012). Inhibition of Pokeweed Antiviral Protein (PAP) by Turnip Mosaic Virus Genome-linked Protein (VPg)\*. *Journal of Biological Chemistry* 287, 29729–29738.
- Doyle, J.P., Dougherty, J.D., Heiman, M., Schmidt, E.F., Stevens, T.R., Ma, G., Bupp, S., Shrestha, P., Shah, R.D., Doughty, M.L., et al. (2008). Application of a translational profiling approach for the comparative analysis of CNS cell types. *Cell* 135, 749–762.
- Duan, Y., Du, A., Gu, J., Duan, G., Wang, C., Gui, X., Ma, Z., Qian, B., Deng, X., Zhang, K., et al. (2019). PARYlation regulates stress granule dynamics, phase separation, and neurotoxicity of disease-related RNA-binding proteins. *Cell Res* 29, 233–247.
- Dubin, D.T., Stollar, V., Hsueh, C.-C., Timko, K., and Guild, G.M. (1977). Sindbis virus messenger RNA: the 5'-termini and methylated residues of 26 and 42 S RNA. *Virology* 77, 457–470.
- Dubin, D.T., Timko, K., Gillies, S., and Stollar, V. (1979). The extreme 5'-terminal sequences of sindbis virus 26 and 42 S RNA. *Virology* 98, 131–141.
- van Duijn, L.P., Kasperaitis, M., Ameling, C., and Voorma, H.O. (1986). Additional methylation at the N(2)-position of the cap of 26S Semliki Forest virus late mRNA and initiation of translation. *Virus Research* 5, 61–66.
- Dunham, W.H., Mullin, M., and Gingras, A.-C. (2012). Affinity-purification coupled to mass spectrometry: Basic principles and strategies. *PROTEOMICS* 12, 1576–1590.
- Emmott, E., Munday, D., Bickerton, E., Britton, P., Rodgers, M.A., Whitehouse, A., Zhou, E.-M., and Hiscox, J.A. (2013). The Cellular Interactome of the Coronavirus Infectious Bronchitis Virus Nucleocapsid Protein and Functional Implications for Virus Biology. *J. Virol.* 87, 9486–9500.
- Erales, J., Marchand, V., Panthu, B., Gillot, S., Belin, S., Ghayad, S.E., Garcia, M., Laforêts, F., Marcel, V., Baudin-Baillieu, A., et al. (2017). Evidence for rRNA 2'-O-methylation plasticity:

- Control of intrinsic translational capabilities of human ribosomes. *Proc. Natl. Acad. Sci. U.S.A.* *114*, 12934–12939.
- Esteban, M., and Metz, D.H. (1973). Early Virus Protein Synthesis in Vaccinia Virus-infected Cells. *Journal of General Virology* *19*, 201–216.
- Etchison, D., and Fout, S. (1985). Human rhinovirus 14 infection of HeLa cells results in the proteolytic cleavage of the p220 cap-binding complex subunit and inactivates globin mRNA translation in vitro. *Journal of Virology* *54*, 634–638.
- Etchison, D., Milburn, S.C., Edery, I., Sonenberg, N., and Hershey, J.W. (1982). Inhibition of HeLa cell protein synthesis following poliovirus infection correlates with the proteolysis of a 220,000-dalton polypeptide associated with eucaryotic initiation factor 3 and a cap binding protein complex. *J Biol Chem* *257*, 14806–14810.
- Feoktistova, K., Tuvshintogs, E., Do, A., and Fraser, C.S. (2013). Human eIF4E promotes mRNA restructuring by stimulating eIF4A helicase activity. *PNAS* *110*, 13339–13344.
- Fernández, I.S., Bai, X.-C., Murshudov, G., Scheres, S.H.W., and Ramakrishnan, V. (2014). Initiation of Translation by Cricket Paralysis Virus IRES Requires Its Translocation in the Ribosome. *Cell* *157*, 823–831.
- Ferretti, M.B., and Karbstein, K. (2019). Does functional specialization of ribosomes really exist? *RNA* *25*, 521–538.
- Firth, A.E., and Brierley, I. (2012). Non-canonical translation in RNA viruses. *J. Gen. Virol.* *93*, 1385–1409.
- Firth, A.E., Chung, B.Y., Fleeton, M.N., and Atkins, J.F. (2008). Discovery of frameshifting in Alphavirus 6K resolves a 20-year enigma. *Virology Journal* *5*, 108.
- Fonseca, B.D., Zakaria, C., Jia, J.-J., Graber, T.E., Svitkin, Y., Tahmasebi, S., Healy, D., Hoang, H.-D., Jensen, J.M., Diao, I.T., et al. (2015). La-related Protein 1 (LARP1) Represses Terminal Oligopyrimidine (TOP) mRNA Translation Downstream of mTOR Complex 1 (mTORC1)\*. *Journal of Biological Chemistry* *290*, 15996–16020.
- Forrester, N.L., Palacios, G., Tesh, R.B., Savji, N., Guzman, H., Sherman, M., Weaver, S.C., and Lipkin, W.I. (2012). Genome-Scale Phylogeny of the Alphavirus Genus Suggests a Marine Origin. *Journal of Virology* *86*, 2729–2738.
- Frolov, I., and Schlesinger, S. (1994). Translation of Sindbis virus mRNA: effects of sequences downstream of the initiating codon. *J Virol* *68*, 8111–8117.
- Frolov, I., and Schlesinger, S. (1996). Translation of Sindbis virus mRNA: analysis of sequences downstream of the initiating AUG codon that enhance translation. *J Virol* *70*, 1182–1190.
- Frolova, E., Gorchakov, R., Garmashova, N., Atasheva, S., Vergara, L.A., and Frolov, I. (2006). Formation of nsP3-specific protein complexes during Sindbis virus replication. *J Virol* *80*, 4122–4134.
- Fros, J.J., and Pijlman, G.P. (2016). Alphavirus Infection: Host Cell Shut-Off and Inhibition of Antiviral Responses. *Viruses* *8*.

- Fros, J.J., Domeradzka, N.E., Baggen, J., Geertsema, C., Flipse, J., Vlak, J.M., and Pijlman, G.P. (2012). Chikungunya virus nsP3 blocks stress granule assembly by recruitment of G3BP into cytoplasmic foci. *J Virol* *86*, 10873–10879.
- Fuller, S.D. (1987). The T=4 envelope of sindbis virus is organized by interactions with a complementary T=3 capsid. *Cell* *48*, 923–934.
- Fütterer, J., and Hohn, T. (1991). Translation of a polycistronic mRNA in the presence of the cauliflower mosaic virus transactivator protein. *EMBO J.* *10*, 3887–3896.
- Gaglia Marta Maria, Covarrubias Sergio, Wong Wesley, and Glaunsinger Britt A. (2012). A Common Strategy for Host RNA Degradation by Divergent Viruses. *Journal of Virology* *86*, 9527–9530.
- Ganaie, S.S., Haque, A., Cheng, E., Bonny, T.S., Salim, N.N., and Mir, M.A. (2014). Ribosomal protein S19-binding domain provides insights into hantavirus nucleocapsid protein-mediated translation initiation mechanism. *Biochem. J.* *464*, 109–121.
- Gandrillon, O., Schmidt, U., Beug, H., and Samarut, J. (1999). TGF-beta cooperates with TGF-alpha to induce the self-renewal of normal erythrocytic progenitors: evidence for an autocrine mechanism. *EMBO J* *18*, 2764–2781.
- Garcia-Moreno, M., Sanz, M.A., Pelletier, J., and Carrasco, L. (2013). Requirements for eIF4A and eIF2 during translation of Sindbis virus subgenomic mRNA in vertebrate and invertebrate host cells. *Cellular Microbiology* *15*, 823–840.
- Garcia-Moreno, M., Sanz, M.A., and Carrasco, L. (2015). Initiation codon selection is accomplished by a scanning mechanism without crucial initiation factors in Sindbis virus subgenomic mRNA. *RNA* *21*, 93–112.
- Garcia-Moreno, M., Noerenberg, M., Ni, S., Järvelin, A.I., González-Almela, E., Lenz, C.E., Bach-Pages, M., Cox, V., Avolio, R., Davis, T., et al. (2019). System-wide Profiling of RNA-Binding Proteins Uncovers Key Regulators of Virus Infection. *Mol. Cell* *74*, 196–211.e11.
- Garcin, D., Lezzi, M., Dobbs, M., Elliott, R.M., Schmaljohn, C., Kang, C.Y., and Kolakofsky, D. (1995). The 5' ends of Hantaan virus (Bunyaviridae) RNAs suggest a prime-and-realign mechanism for the initiation of RNA synthesis. *J Virol* *69*, 5754–5762.
- Garmashova, N., Atasheva, S., Kang, W., Weaver, S.C., Frolova, E., and Frolov, I. (2007a). Analysis of Venezuelan Equine Encephalitis Virus Capsid Protein Function in the Inhibition of Cellular Transcription. *Journal of Virology* *81*, 13552–13565.
- Garmashova, N., Gorchakov, R., Volkova, E., Paessler, S., Frolova, E., and Frolov, I. (2007b). The Old World and New World alphaviruses use different virus-specific proteins for induction of transcriptional shutoff. *J Virol* *81*, 2472–2484.
- Garoff, H., Huylebroeck, D., Robinson, A., Tillman, U., and Liljeström, P. (1990). The signal sequence of the p62 protein of Semliki Forest virus is involved in initiation but not in completing chain translocation. *Journal of Cell Biology* *111*, 867–876.

- des Georges, A., Dhote, V., Kuhn, L., Hellen, C.U.T., Pestova, T.V., Frank, J., and Hashem, Y. (2015). Structure of mammalian eIF3 in the context of the 43S preinitiation complex. *Nature* 525, 491–495.
- Ghulam, M.M., Catala, M., and Abou Elela, S. (2020). Differential expression of duplicated ribosomal protein genes modifies ribosome composition in response to stress. *Nucleic Acids Res* 48, 1954–1968.
- Glanville, N., and Ulmanen, I. (1976). Biological activity of invitro synthesised protein: Binding of Semliki Forest virus capsid protein to the large ribosomal subunit. *Biochem. Biophys. Res. Commun.* 71, 393–399.
- Göertz, G.P., McNally, K.L., Robertson, S.J., Best, S.M., Pijlman, G.P., and Fros, J.J. (2018). The methyltransferase-like domain of chikungunya virus nsP2 inhibits the interferon response by promoting the nuclear export of STAT1. *Journal of Virology* 92, e01008.
- Gomez de Cedrón, M., Ehsani, N., Mikkola, M.L., García, J.A., and Kääriäinen, L. (1999). RNA helicase activity of Semliki Forest virus replicase protein NSP2. *FEBS Lett* 448, 19–22.
- González-Almela, E., Sanz, M.A., García-Moreno, M., Northcote, P., Pelletier, J., and Carrasco, L. (2015). Differential action of pateamine A on translation of genomic and subgenomic mRNAs from Sindbis virus. *Virology* 484, 41–50.
- González-Almela, E., Williams, H., Sanz, M.A., and Carrasco, L. (2018). The Initiation Factors eIF2, eIF2A, eIF2D, eIF4A, and eIF4G Are Not Involved in Translation Driven by Hepatitis C Virus IRES in Human Cells. *Frontiers in Microbiology* 9, 207.
- Gorchakov, R., Frolova, E., Williams, B.R.G., Rice, C.M., and Frolov, I. (2004). PKR-Dependent and -Independent Mechanisms Are Involved in Translational Shutoff during Sindbis Virus Infection. *Journal of Virology* 78, 8455–8467.
- Gorchakov, R., Garmashova, N., Frolova, E., and Frolov, I. (2008). Different types of nsP3-containing protein complexes in Sindbis virus-infected cells. *J Virol* 82, 10088–10101.
- Gordon, D.E., Jang, G.M., Bouhaddou, M., Xu, J., Obernier, K., White, K.M., O’Meara, M.J., Rezelj, V.V., Guo, J.Z., Swaney, D.L., et al. (2020). A SARS-CoV-2 protein interaction map reveals targets for drug repurposing. *Nature* 583, 459–468.
- Götte, B., Liu, L., and McInerney, G.M. (2018). The Enigmatic Alphavirus Non-Structural Protein 3 (nsP3) Revealing Its Secrets at Last. *Viruses* 10, E105.
- Grandadam, M., Caro, V., Plumet, S., Thiberge, J.-M., Souarès, Y., Failloux, A.-B., Tolou, H.J., Budelot, M., Cosserat, D., Leparç-Goffart, I., et al. Chikungunya Virus, Southeastern France - Volume 17, Number 5—May 2011 - Emerging Infectious Diseases journal - CDC.
- Greenwood, E.J., Matheson, N.J., Wals, K., Boomen, D.J. van den, Antrobus, R., Williamson, J.C., and Lehner, P.J. (2016). Temporal proteomic analysis of HIV infection reveals remodelling of the host phosphoproteome by lentiviral Vif variants. *ELife*.
- Gressner, A.M., and Wool, I.G. (1974). The Phosphorylation of Liver Ribosomal Proteins in Vivo: Evidence That Only a Single Small Subunit Protein (s6) Is Phosphorylated. *J. Biol. Chem.* 249, 6917–6925.

- de Groot, R.J., Hardy, W.R., Shirako, Y., and Strauss, J.H. (1990). Cleavage-site preferences of Sindbis virus polyproteins containing the non-structural proteinase. Evidence for temporal regulation of polyprotein processing in vivo. *EMBO J* 9, 2631–2638.
- Gross, L., Vicens, Q., Einhorn, E., Noireterre, A., Schaeffer, L., Kuhn, L., Imler, J.-L., Eriani, G., Meignin, C., and Martin, F. (2017). The IRES5'UTR of the dicistrovirus cricket paralysis virus is a type III IRES containing an essential pseudoknot structure. *Nucleic Acids Res* 45, 8993–9004.
- Guo, H. (2018). Specialized ribosomes and the control of translation. *Biochem. Soc. Trans.* BST20160426.
- Hafirassou, M.L., Meertens, L., Umaña-Díaz, C., Labeau, A., Dejarnac, O., Bonnet-Madin, L., Kümmerer, B.M., Delaugerre, C., Roingard, P., Vidalain, P.-O., et al. (2017). A Global Interactome Map of the Dengue Virus NS1 Identifies Virus Restriction and Dependency Host Factors. *Cell Reports* 21, 3900–3913.
- Hahn, C.S., Strauss, E.G., and Strauss, J.H. (1985). Sequence analysis of three Sindbis virus mutants temperature-sensitive in the capsid protein autoprotease. *Proc Natl Acad Sci U S A* 82, 4648–4652.
- Hahn, Y.S., Strauss, E.G., and Strauss, J.H. (1989). Mapping of RNA- temperature-sensitive mutants of Sindbis virus: assignment of complementation groups A, B, and G to nonstructural proteins. *J Virol* 63, 3142–3150.
- Halstead, S.B. (2015). Reappearance of chikungunya, formerly called dengue, in the Americas. *Emerg Infect Dis* 21, 557–561.
- Hammon, W.M., Rundnick, A., and Sather, G.E. (1960). Viruses Associated with Epidemic Hemorrhagic Fevers of the Philippines and Thailand. *Science* 131, 1102–1103.
- Hanke, T., Szawlowski, P., and Randall, R.E.Y. 1992 Construction of solid matrix-antibody-antigen complexes containing simian immunodeficiency virus p27 using tag-specific monoclonal antibody and tag-linked antigen. *Journal of General Virology* 73, 653–660.
- Haque, A., and Mir, M.A. (2010). Interaction of Hantavirus Nucleocapsid Protein with Ribosomal Protein S19. *J. Virol.* 84, 12450–12453.
- Hardy, W.R., and Strauss, J.H. (1989). Processing the nonstructural polyproteins of sindbis virus: nonstructural proteinase is in the C-terminal half of nsP2 and functions both in cis and in trans. *J Virol* 63, 4653–4664.
- Hashem, Y., des Georges, A., Dhote, V., Langlois, R., Liao, H.Y., Grassucci, R.A., Pestova, T.V., Hellen, C.U.T., and Frank, J. (2013). Hepatitis-C-virus-like internal ribosome entry sites displace eIF3 to gain access to the 40S subunit. *Nature* 503, 539–543.
- Hefti, E., Bishop, D.H.L., Dubin, D.T., and Stollar, V. (1976). 5' Nucleotide Sequence of Sindbis Viral RNA. *J Virol* 17, 149–159.
- Heiman, M., Schaefer, A., Gong, S., Peterson, J.D., Day, M., Ramsey, K.E., Suárez-Fariñas, M., Schwarz, C., Stephan, D.A., Surmeier, D.J., et al. (2008). A translational profiling approach for the molecular characterization of CNS cell types. *Cell* 135, 738–748.

- Hernández-Díaz, T., Valiente-Echeverría, F., and Soto-Rifo, R. (2021). RNA Helicase DDX3: A Double-Edged Sword for Viral Replication and Immune Signaling. *Microorganisms* 9, 1206.
- Hertz, M.I., Landry, D.M., Willis, A.E., Luo, G., and Thompson, S.R. (2013). Ribosomal Protein S25 Dependency Reveals a Common Mechanism for Diverse Internal Ribosome Entry Sites and Ribosome Shunting. *Mol. Cell. Biol.* 33, 1016–1026.
- Heyer, E.E., and Moore, M.J. (2016). Redefining the Translational Status of 80S Monosomes. *Cell* 164, 757–769.
- Hickey, K.L., Dickson, K., Cogan, J.Z., Replogle, J.M., Schoof, M., D’Orazio, K.N., Sinha, N.K., Hussmann, J.A., Jost, M., Frost, A., et al. (2020). GIGYF2 and 4EHP Inhibit Translation Initiation of Defective Messenger RNAs to Assist Ribosome-Associated Quality Control. *Molecular Cell* 79, 950-962.e6.
- Hirsch, A.J. (2010). The use of RNAi-based screens to identify host proteins involved in viral replication. *Future Microbiology* 5, 303–311.
- Hiscox, J.A. (2007). RNA viruses: hijacking the dynamic nucleolus. *Nat Rev Microbiol* 5, 119–127.
- Hoang, H.-D., Graber, T.E., and Alain, T. (2018). Battling for Ribosomes: Translational Control at the Forefront of the Antiviral Response. *J. Mol. Biol.* 430, 1965–1992.
- Hsieh, P., and Robbins, P.W. (1984). Regulation of asparagine-linked oligosaccharide processing. Oligosaccharide processing in *Aedes albopictus* mosquito cells. *Journal of Biological Chemistry* 259, 2375–2382.
- Hsieh, P., Rosner, M.R., and Robbins, P.W. (1983). Host-dependent variation of asparagine-linked oligosaccharides at individual glycosylation sites of Sindbis virus glycoproteins. *Journal of Biological Chemistry* 258, 2548–2554.
- Hsueh, C.-C., and Dubin, D.T. (1976). Di- and trimethylated congeners of 7-methylguanine in Sindbis virus mRNA. *Nature* 264, 190–191.
- Huang, C., Lokugamage, K.G., Rozovics, J.M., Narayanan, K., Semler, B.L., and Makino, S. (2011). SARS coronavirus nsp1 protein induces template-dependent endonucleolytic cleavage of mRNAs: viral mRNAs are resistant to nsp1-induced RNA cleavage. *PLoS Pathog* 7, e1002433.
- Hussain, T., Llácer, J.L., Fernández, I.S., Munoz, A., Martin-Marcos, P., Savva, C.G., Lorsch, J.R., Hinnebusch, A.G., and Ramakrishnan, V. (2014). Structural changes enable start codon recognition by the eukaryotic translation initiation complex. *Cell* 159, 597–607.
- Imami, K., Milek, M., Bogdanow, B., Yasuda, T., Kastelic, N., Zauber, H., Ishihama, Y., Landthaler, M., and Selbach, M. (2018). Phosphorylation of the Ribosomal Protein RPL12/uL11 Affects Translation during Mitosis. *Molecular Cell*.
- Ingolia, N.T., Brar, G.A., Stern-Ginossar, N., Harris, M.S., Talhouarne, G.J.S., Jackson, S.E., Wills, M.R., and Weissman, J.S. (2014a). Ribosome Profiling Reveals Pervasive Translation Outside of Annotated Protein-Coding Genes. *Cell Rep* 8, 1365–1379.



- Ingolia, N.T., Brar, G.A., Stern-Ginossar, N., Harris, M.S., Talhouarne, G.J.S., Jackson, S.E., Wills, M.R., and Weissman, J.S. (2014b). Ribosome Profiling Reveals Pervasive Translation Outside of Annotated Protein-Coding Genes. *Cell Reports* 8, 1365–1379.
- Ivanova, L., and Schlesinger, M.J. (1993). Site-directed mutations in the Sindbis virus E2 glycoprotein identify palmitoylation sites and affect virus budding. *J Virol* 67, 2546–2551.
- Iyer-Bierhoff, A., Krogh, N., Tessarz, P., Ruppert, T., Nielsen, H., and Grummt, I. (2018). SIRT7-Dependent Deacetylation of Fibrillarin Controls Histone H2A Methylation and rRNA Synthesis during the Cell Cycle. *Cell Rep* 25, 2946-2954.e5.
- Jaafar, Z.A., Oguro, A., Nakamura, Y., and Kieft, J.S. (2016). Translation initiation by the hepatitis C virus IRES requires eIF1A and ribosomal complex remodeling. *ELife* 5, e21198.
- Jack, K., Bellodi, C., Landry, D.M., Niederer, R.O., Meskauskas, A., Musalgaonkar, S., Kopmar, N., Krasnykh, O., Dean, A.M., Thompson, S.R., et al. (2011). rRNA Pseudouridylation Defects Affect Ribosomal Ligand Binding and Translational Fidelity from Yeast to Human Cells. *Mol. Cell* 44, 660–666.
- Jackson, R.J., Hellen, C.U.T., and Pestova, T.V. (2010). The mechanism of eukaryotic translation initiation and principles of its regulation. *Nat. Rev. Mol. Cell Biol.* 11, 113–127.
- Jäger, S., Cimermancic, P., Gulbahce, N., Johnson, J.R., McGovern, K.E., Clarke, S.C., Shales, M., Mercenne, G., Pache, L., Li, K., et al. (2012). Global landscape of HIV–human protein complexes. *Nature* 481, 365–370.
- Jan, E., Mohr, I., and Walsh, D. (2016). A Cap-to-Tail Guide to mRNA Translation Strategies in Virus-Infected Cells. *Annu. Rev. Virol.* 3, 283–307.
- Jayabalan, A.K., Adivarahan, S., Koppula, A., Abraham, R., Batish, M., Zenklusen, D., Griffin, D.E., and Leung, A.K.L. (2021). Stress granule formation, disassembly, and composition are regulated by alphavirus ADP-ribosylhydrolase activity. *PNAS* 118.
- Jemielity, S., Wang, J.J., Chan, Y.K., Ahmed, A.A., Li, W., Monahan, S., Bu, X., Farzan, M., Freeman, G.J., Umetsu, D.T., et al. (2013). TIM-family Proteins Promote Infection of Multiple Enveloped Viruses through Virion-associated Phosphatidylserine. *PLOS Pathogens* 9, e1003232.
- Jha, S., Rollins, M.G., Fuchs, G., Procter, D.J., Hall, E.A., Cozzolino, K., Sarnow, P., Savas, J.N., and Walsh, D. (2017). Trans-kingdom mimicry underlies ribosome customization by a poxvirus kinase. *Nature* 546, 651–655.
- Jin, H., and Elliott, R.M. (1993). Characterization of Bunyamwera virus S RNA that is transcribed and replicated by the L protein expressed from recombinant vaccinia virus. *Journal of Virology* 67, 1396–1404.
- Jones, R., Bragagnolo, G., Arranz, R., and Reguera, J. (2021). Capping pores of alphavirus nsP1 gate membranous viral replication factories. *Nature* 589, 615–619.
- Jose, J., Snyder, J.E., and Kuhn, R.J. (2009). A structural and functional perspective of alphavirus replication and assembly. *Future Microbiol* 4, 837–856.

- Joshi, B., Cameron, A., and Jagus, R. (2004). Characterization of mammalian eIF4E-family members. *European Journal of Biochemistry* 271, 2189–2203.
- Juszkiewicz, S., Slodkowicz, G., Lin, Z., Freire-Pritchett, P., Peak-Chew, S.-Y., and Hegde, R.S. (2020a). Ribosome collisions trigger cis-acting feedback inhibition of translation initiation. *ELife* 9.
- Juszkiewicz, S., Speldewinde, S.H., Wan, L., Svejstrup, J.Q., and Hegde, R.S. (2020b). The ASC-1 Complex Disassembles Collided Ribosomes. *Molecular Cell* 79, 603-614.e8.
- Kaerlein, M., and Horak, I. (1976a). Phosphorylation of ribosomal proteins in HeLa cells infected with vaccinia virus. *Nature* 259, 150–151.
- Kaerlein, M., and Horak, I. (1976b). Phosphorylation of ribosomal proteins in HeLa cells infected with vaccinia virus. *Nature* 259, 150–151.
- Kaerlein, M., and Horak, I. (1978). Identification and Characterization of Ribosomal Proteins Phosphorylated in Vaccinia-Virus-Infected HeLa Cells. *Eur. J. Biochem.* 90, 463–469.
- Kalkkinen, N., Jörnvall, H., Söderlund, H., and Kääriäinen, L. (1980). Analysis of Semliki-Forest-virus structural proteins to illustrate polyprotein processing of alpha viruses. *Eur J Biochem* 108, 31–37.
- Kamel, W., Noerenberg, M., Cerikan, B., Chen, H., Järvelin, A.I., Kammoun, M., Lee, J.Y., Shuai, N., Garcia-Moreno, M., Andrejeva, A., et al. (2021). Global analysis of protein-RNA interactions in SARS-CoV-2-infected cells reveals key regulators of infection. *Molecular Cell* 81, 2851-2867.e7.
- Kamitani, W., Huang, C., Narayanan, K., Lokugamage, K.G., and Makino, S. (2009). A two-pronged strategy to suppress host protein synthesis by SARS coronavirus Nsp1 protein. *Nat. Struct. Mol. Biol.* 16, 1134–1140.
- Kariuki Njenga, M., Nderitu, L., Ledermann, J.P., Ndirangu, A., Logue, C.H., Kelly, C.H.L., Sang, R., Sergon, K., Breiman, R., and Powers, A.M.Y. 2008 Tracking epidemic Chikungunya virus into the Indian Ocean from East Africa. *Journal of General Virology* 89, 2754–2760.
- Karlas, A., Machuy, N., Shin, Y., Pleissner, K.-P., Artarini, A., Heuer, D., Becker, D., Khalil, H., Ogilvie, L.A., Hess, S., et al. (2010). Genome-wide RNAi screen identifies human host factors crucial for influenza virus replication. *Nature* 463, 818–822.
- Karlas, A., Berre, S., Couderc, T., Varjak, M., Braun, P., Meyer, M., Gangneux, N., Karo-Astover, L., Weege, F., Raftery, M., et al. (2016). A human genome-wide loss-of-function screen identifies effective chikungunya antiviral drugs. *Nat Commun* 7, 11320.
- Kedersha, N., Panas, M.D., Achorn, C.A., Lyons, S., Tisdale, S., Hickman, T., Thomas, M., Lieberman, J., McInerney, G.M., Ivanov, P., et al. (2016). G3BP-Caprin1-USP10 complexes mediate stress granule condensation and associate with 40S subunits. *J Cell Biol* 212, 845–860.
- Khatter, H., Myasnikov, A.G., Natchiar, S.K., and Klaholz, B.P. (2015). Structure of the human 80S ribosome. *Nature* 520, 640–645.
- Kim, D.Y., Reynaud, J.M., Rasaloukaya, A., Akhrymuk, I., Mobley, J.A., Frolov, I., and Frolova, E.I. (2016). New World and Old World Alphaviruses Have Evolved to Exploit Different

Components of Stress Granules, FXR and G3BP Proteins, for Assembly of Viral Replication Complexes. *PLoS Pathog* 12, e1005810.

Kimple, M.E., Brill, A.L., and Pasker, R.L. (2013). Overview of Affinity Tags for Protein Purification. *Current Protocols in Protein Science* 73, 9.9.1-9.9.23.

Kinast, V., Plociennikowska, A., Anggakusuma, Bracht, T., Todt, D., Brown, R.J.P., Boldanova, T., Zhang, Y., Brüggemann, Y., Friesland, M., et al. (2020). C19orf66 is an interferon-induced inhibitor of HCV replication that restricts formation of the viral replication organelle. *Journal of Hepatology* 73, 549–558.

King, H.A., Cobbold, L.C., and Willis, A.E. (2010). The role of IRES trans-acting factors in regulating translation initiation. *Biochem. Soc. Trans.* 38, 1581–1586.

Klimstra, W.B., Nangle, E.M., Smith, M.S., Yurochko, A.D., and Ryman, K.D. (2003). DC-SIGN and L-SIGN can act as attachment receptors for alphaviruses and distinguish between mosquito cell- and mammalian cell-derived viruses. *J Virol* 77, 12022–12032.

Knight, R.L., Schultz, K.L.W., Kent, R.J., Venkatesan, M., and Griffin, D.E. (2009). Role of N-Linked Glycosylation for Sindbis Virus Infection and Replication in Vertebrate and Invertebrate Systems. *Journal of Virology* 83, 5640–5647.

Knoener, R.A., Becker, J.T., Scalf, M., Sherer, N.M., and Smith, L.M. (2017). Elucidating the in vivo interactome of HIV-1 RNA by hybridization capture and mass spectrometry. *Sci Rep* 7, 16965.

Knudsen, A.B. (1995). Global distribution and continuing spread of *Aedes albopictus*. *Parassitologia* 37, 91–97.

Komar, A.A., and Merrick, W.C. (2020). A Retrospective on eIF2A—and Not the Alpha Subunit of eIF2. *International Journal of Molecular Sciences* 21, 2054.

König, R., Zhou, Y., Elleder, D., Diamond, T.L., Bonamy, G.M.C., Irelan, J.T., Chiang, C., Tu, B.P., De Jesus, P.D., Lilley, C.E., et al. (2008). Global Analysis of Host-Pathogen Interactions that Regulate Early-Stage HIV-1 Replication. *Cell* 135, 49–60.

König, R., Stertz, S., Zhou, Y., Inoue, A., Hoffmann, H.-H., Bhattacharyya, S., Alamares, J.G., Tscherne, D.M., Ortigoza, M.B., Liang, Y., et al. (2010). Human host factors required for influenza virus replication. *Nature* 463, 813–817.

Kozak, M. (1987). An analysis of 5'-noncoding sequences from 699 vertebrate messenger RNAs. *Nucleic Acids Research* 15, 8125–8148.

Kozak, M. (1990). Downstream secondary structure facilitates recognition of initiator codons by eukaryotic ribosomes. *PNAS* 87, 8301–8305.

Krasnopolsky, S., Kuzmina, A., and Taube, R. (2020). Genome-wide CRISPR knockout screen identifies ZNF304 as a silencer of HIV transcription that promotes viral latency. *PLOS Pathogens* 16, e1008834.

Krishnan, M.N., Ng, A., Sukumaran, B., Gilfoy, F.D., Uchil, P.D., Sultana, H., Brass, A.L., Adametz, R., Tsui, M., Qian, F., et al. (2008). RNA interference screen for human genes associated with West Nile virus infection. *Nature* 455, 242–245.

- Krogh, N., Jansson, M.D., Häfner, S.J., Tehler, D., Birkedal, U., Christensen-Dalsgaard, M., Lund, A.H., and Nielsen, H. (2016). Profiling of 2'-O-Me in human rRNA reveals a subset of fractionally modified positions and provides evidence for ribosome heterogeneity. *Nucleic Acids Res.* *44*, 7884–7895.
- Kulsuptrakul, J., Wang, R., Meyers, N.L., Ott, M., and Puschnik, A.S. (2021). A genome-wide CRISPR screen identifies UFMylation and TRAMP-like complexes as host factors required for hepatitis A virus infection. *Cell Reports* *34*, 108859.
- Kumar, P., Hellen, C.U.T., and Pestova, T.V. (2016). Toward the mechanism of eIF4F-mediated ribosomal attachment to mammalian capped mRNAs. *Genes Dev.* *30*, 1573–1588.
- Laakkonen, P., Hyvönen, M., Peränen, J., and Kääriäinen, L. (1994). Expression of Semliki Forest virus nsP1-specific methyltransferase in insect cells and in *Escherichia coli*. *J Virol* *68*, 7418–7425.
- Laakkonen, P., Ahola, T., and Kääriäinen, L. (1996). The Effects of Palmitoylation on Membrane Association of Semliki Forest Virus RNA Capping Enzyme\*. *Journal of Biological Chemistry* *271*, 28567–28571.
- Lafontaine, D.L.J. (2015). Noncoding RNAs in eukaryotic ribosome biogenesis and function. *Nat. Struct. Mol. Biol.* *22*, 11–19.
- LaFontaine, E., Miller, C.M., Permaul, N., Martin, E.T., and Fuchs, G. (2020). Ribosomal protein RACK1 enhances translation of poliovirus and other viral IRESs. *Virology* *545*, 53–62.
- Lahr, R.M., Fonseca, B.D., Ciotti, G.E., Al-Ashtal, H.A., Jia, J.-J., Niklaus, M.R., Blagden, S.P., Alain, T., and Berman, A.J. (2017). La-related protein 1 (LARP1) binds the mRNA cap, blocking eIF4F assembly on TOP mRNAs. *ELife* *6*, e24146.
- Lamper, A.M., Fleming, R.H., Ladd, K.M., and Lee, A.S.Y. (2020). A phosphorylation-regulated eIF3d translation switch mediates cellular adaptation to metabolic stress. *Science* *370*, 853–856.
- Lancaster, C., Pristatsky, P., Hoang, V.M., Casimiro, D.R., Schwartz, R.M., Rustandi, R., and Ha, S. (2016). Characterization of N-glycosylation profiles from mammalian and insect cell derived chikungunya VLP. *Journal of Chromatography B* *1032*, 218–223.
- Landers, V.D., Wilkey, D.W., Merchant, M.L., Mitchell, T.C., and Sokoloski, K.J. (2021). The Alphaviral Capsid Protein Inhibits IRAK1-Dependent TLR Signaling. *Viruses* *13*, 377.
- Landry, D.M., Hertz, M.I., and Thompson, S.R. (2009). RPS25 is essential for translation initiation by the Dicistroviridae and hepatitis C viral IRESs. *Genes Dev.* *23*, 2753–2764.
- LaStarza, M.W., Lemm, J.A., and Rice, C.M. (1994). Genetic analysis of the nsP3 region of Sindbis virus: evidence for roles in minus-strand and subgenomic RNA synthesis. *J Virol* *68*, 5781–5791.
- Lee, A.S.-Y., Burdeinick-Kerr, R., and Whelan, S.P.J. (2013). A ribosome-specialized translation initiation pathway is required for cap-dependent translation of vesicular stomatitis virus mRNAs. *Proc. Natl. Acad. Sci. U.S.A.* *110*, 324–329.
- Lee, A.S.Y., Kranzusch, P.J., and Cate, J.H.D. (2015). eIF3 targets cell-proliferation messenger RNAs for translational activation or repression. *Nature* *522*, 111–114.

- Lee, A.S.Y., Kranzusch, P.J., Doudna, J.A., and Cate, J.H.D. (2016). eIF3d is an mRNA cap-binding protein that is required for specialized translation initiation. *Nature* 536, 96–99.
- Lee, K.-M., Chen, C.-J., and Shih, S.-R. (2017). Regulation Mechanisms of Viral IRES-Driven Translation. *Trends in Microbiology* 25, 546–561.
- Lee, K.-M., Wu, C.-C., Wu, S.-E., Lin, Y.-H., Wang, L.-T., Chang, C.-R., Huang, P.-N., Shih, S.-R., and Kuo, R.-L. (2020). The RNA-dependent RNA polymerase of enterovirus A71 associates with ribosomal proteins and positively regulates protein translation. *RNA Biology* 17, 608–622.
- Lee, S., Owen, K.E., Choi, H.K., Lee, H., Lu, G., Wengler, G., Brown, D.T., Rossmann, M.G., and Kuhn, R.J. (1996). Identification of a protein binding site on the surface of the alphavirus nucleocapsid and its implication in virus assembly. *Structure* 4, 531–541.
- Lee, S., Lee, Y., Choi, Y., Son, A., Park, Y., Lee, K.-M., Kim, J., Kim, J.-S., and Kim, V.N. (2021a). The SARS-CoV-2 RNA interactome. *Molecular Cell* 81, 2838-2850.e6.
- Lee, S., Lee, Y., Choi, Y., Son, A., Park, Y., Lee, K.-M., Kim, J., Kim, J.-S., and Kim, V.N. (2021b). The SARS-CoV-2 RNA interactome. *Molecular Cell* 81, 2838-2850.e6.
- Lefkowitz, E.J., Dempsey, D.M., Hendrickson, R.C., Orton, R.J., Siddell, S.G., and Smith, D.B. (2018). Virus taxonomy: the database of the International Committee on Taxonomy of Viruses (ICTV). *Nucleic Acids Research* 46, D708–D717.
- Lemm, J.A., and Rice, C.M. (1993a). Assembly of functional Sindbis virus RNA replication complexes: requirement for coexpression of P123 and P34. *J Virol* 67, 1905–1915.
- Lemm, J.A., and Rice, C.M. (1993b). Roles of nonstructural polyproteins and cleavage products in regulating Sindbis virus RNA replication and transcription. *Journal of Virology* 67, 1916–1926.
- Lemm, J.A., Rümenapf, T., Strauss, E.G., Strauss, J.H., and Rice, C.M. (1994). Polypeptide requirements for assembly of functional Sindbis virus replication complexes: a model for the temporal regulation of minus- and plus-strand RNA synthesis. *EMBO J* 13, 2925–2934.
- Leung, A.K.L., Vyas, S., Rood, J.E., Bhutkar, A., Sharp, P.A., and Chang, P. (2011a). Poly(ADP-ribose) regulates stress responses and microRNA activity in the cytoplasm. *Mol Cell* 42, 489–499.
- Leung, J.Y.-S., Ng, M.M.-L., and Chu, J.J.H. (2011b). Replication of alphaviruses: a review on the entry process of alphaviruses into cells. *Adv Virol* 2011, 249640.
- Levy, S., Avni, D., Hariharan, N., Perry, R.P., and Meyuhas, O. (1991). Oligopyrimidine tract at the 5' end of mammalian ribosomal protein mRNAs is required for their translational control. *PNAS* 88, 3319–3323.
- Li, S. (2019). Regulation of Ribosomal Proteins on Viral Infection. *Cells* 8, 508.
- Li, G., and Rice, C.M. (1993). The signal for translational readthrough of a UGA codon in Sindbis virus RNA involves a single cytidine residue immediately downstream of the termination codon. *J Virol* 67, 5062–5067.
- Li, Z., and Nagy, P.D. (2011). Diverse roles of host RNA binding proteins in RNA virus replication. *RNA Biology* 8, 305–315.

- Li, B., Clohisey, S.M., Chia, B.S., Wang, B., Cui, A., Eisenhaure, T., Schweitzer, L.D., Hoover, P., Parkinson, N.J., Nachshon, A., et al. (2020). Genome-wide CRISPR screen identifies host dependency factors for influenza A virus infection. *Nat Commun* *11*, 164.
- Li, Y., Treffers, E.E., Naphine, S., Tas, A., Zhu, L., Sun, Z., Bell, S., Mark, B.L., van Veelen, P.A., van Hemert, M.J., et al. (2014). Transactivation of programmed ribosomal frameshifting by a viral protein. *Proc. Natl. Acad. Sci. U.S.A.* *111*, E2172-2181.
- Li, Y., Firth, A.E., Brierley, I., Cai, Y., Naphine, S., Wang, T., Yan, X., Kuhn, J.H., and Fang, Y. (2019a). Programmed-2/-1 Ribosomal Frameshifting in Simariteriviruses: an Evolutionarily Conserved Mechanism. *J. Virol.* *93*, e00370-19.
- Li, Y., Muffat, J., Javed, A.O., Keys, H.R., Lungjangwa, T., Bosch, I., Khan, M., Virgilio, M.C., Gehrke, L., Sabatini, D.M., et al. (2019b). Genome-wide CRISPR screen for Zika virus resistance in human neural cells. *PNAS* *116*, 9527–9532.
- Liljas, A., and Sanyal, S. (2018). The enigmatic ribosomal stalk. *Quarterly Reviews of Biophysics* *51*.
- Link, A.J., Eng, J., Schieltz, D.M., Carmack, E., Mize, G.J., Morris, D.R., Garvik, B.M., Yates, J.R., and Iii (1999). Direct analysis of protein complexes using mass spectrometry. *Nat. Biotechnol.* *17*, 676–682.
- Lloyd, R.E., Jense, H.G., and Ehrenfeld, E. (1987). Restriction of translation of capped mRNA in vitro as a model for poliovirus-induced inhibition of host cell protein synthesis: relationship to p220 cleavage. *Journal of Virology* *61*, 2480–2488.
- Lobigs, M., and Garoff, H. (1990). Fusion function of the Semliki Forest virus spike is activated by proteolytic cleavage of the envelope glycoprotein precursor p62. *Journal of Virology* *64*, 1233–1240.
- Lobigs, M., Zhao, H.X., and Garoff, H. (1990). Function of Semliki Forest virus E3 peptide in virus assembly: replacement of E3 with an artificial signal peptide abolishes spike heterodimerization and surface expression of E1. *J Virol* *64*, 4346–4355.
- Locker, N., Easton, L.E., and Lukavsky, P.J. (2007). HCV and CSFV IRES domain II mediate eIF2 release during 80S ribosome assembly. *EMBO J* *26*, 795–805.
- Lokugamage, K.G., Narayanan, K., Huang, C., and Makino, S. (2012). Severe Acute Respiratory Syndrome Coronavirus Protein nsp1 Is a Novel Eukaryotic Translation Inhibitor That Represses Multiple Steps of Translation Initiation. *Journal of Virology* *86*, 13598–13608.
- Lokugamage, K.G., Narayanan, K., Nakagawa, K., Terasaki, K., Ramirez, S.I., Tseng, C.-T.K., and Makino, S. (2015). Middle East Respiratory Syndrome Coronavirus nsp1 Inhibits Host Gene Expression by Selectively Targeting mRNAs Transcribed in the Nucleus while Sparing mRNAs of Cytoplasmic Origin. *Journal of Virology* *89*, 10970–10981.
- Lönnstedt, I., and Speed, T. (2002). REPLICATED MICROARRAY DATA. *Statistica Sinica* *12*, 31–46.
- Loughran, G., Firth, A.E., and Atkins, J.F. (2011). Ribosomal frameshifting into an overlapping gene in the 2B-encoding region of the cardiovirus genome. *PNAS* *108*, E1111–E1119.

- Lukavsky, P.J. (2009). Structure and function of HCV IRES domains. *Virus Research* 139, 166–171.
- Lumsden, W.H.R. (1955). An epidemic of virus disease in Southern Province, Tanganyika territory, in 1952–1953 II. General description and epidemiology. *Transactions of the Royal Society of Tropical Medicine and Hygiene* 49, 33–57.
- Lundström, J.O., Hesson, J.C., Schäfer, M.L., Östman, Ö., Semmler, T., Bekaert, M., Weidmann, M., Lundkvist, Å., and Pfeffer, M. (2019). Sindbis virus polyarthritis outbreak signalled by virus prevalence in the mosquito vectors. *PLoS Negl Trop Dis* 13, e0007702.
- Lyon, K., Aguilera, L.U., Morisaki, T., Munsky, B., and Stasevich, T.J. (2019). Live-Cell Single RNA Imaging Reveals Bursts of Translational Frameshifting. *Molecular Cell*.
- Majzoub, K., Hafirassou, M.L., Meignin, C., Goto, A., Marzi, S., Fedorova, A., Verdier, Y., Vinh, J., Hoffmann, J.A., Martin, F., et al. (2014). RACK1 Controls IRES-Mediated Translation of Viruses. *Cell* 159, 1086–1095.
- Marceau, C.D., Puschnik, A.S., Majzoub, K., Ooi, Y.S., Brewer, S.M., Fuchs, G., Swaminathan, K., Mata, M.A., Elias, J.E., Sarnow, P., et al. (2016). Genetic dissection of Flaviviridae host factors through genome-scale CRISPR screens. *Nature* 535, 159–163.
- Marchand, V., Blanloeil-Oillo, F., Helm, M., and Motorin, Y. (2016). Illumina-based RiboMethSeq approach for mapping of 2'-O-Me residues in RNA. *Nucleic Acids Res* 44, e135–e135.
- Martinez-Azorin, F., Remacha, M., and Ballesta, J.P.G. (2008). Functional characterization of ribosomal P1/P2 proteins in human cells. *Biochemical Journal* 413, 527–534.
- Martínez-Salas, E., Lozano, G., Fernandez-Chamorro, J., Francisco-Velilla, R., Galan, A., and Diaz, R. (2013). RNA-Binding Proteins Impacting on Internal Initiation of Translation. *Int. J. Mol. Sci.* 14, 21705–21726.
- Martínez-Salas, E., Francisco-Velilla, R., Fernandez-Chamorro, J., Lozano, G., and Diaz-Toledano, R. (2015). Picornavirus IRES elements: RNA structure and host protein interactions. *Virus Res.* 206, 62–73.
- Martinez-Salas, E., Francisco-Velilla, R., Fernandez-Chamorro, J., and Embarek, A.M. (2018). Insights into Structural and Mechanistic Features of Viral IRES Elements. *Frontiers in Microbiology* 8, 2629.
- Mathiot, C.C., Grimaud, G., Garry, P., Bouquety, J.C., Mada, A., Daguisy, A.M., and Georges, A.J. (1990). An outbreak of human Semliki Forest virus infections in Central African Republic. *Am J Trop Med Hyg* 42, 386–393.
- Matsuki, H., Takahashi, M., Higuchi, M., Makokha, G.N., Oie, M., and Fujii, M. (2013). Both G3BP1 and G3BP2 contribute to stress granule formation. *Genes Cells* 18, 135–146.
- Mattijssen, S., Kozlov, G., Fonseca, B.D., Gehring, K., and Maraia, R.J. (2021). LARP1 and LARP4: up close with PABP for mRNA 3' poly(A) protection and stabilization. *RNA Biology* 18, 259–274.
- Mayer, D., Molawi, K., Martínez-Sobrido, L., Ghanem, A., Thomas, S., Baginsky, S., Grossmann, J., García-Sastre, A., and Schwemmle, M. (2007). Identification of Cellular Interaction Partners of

the Influenza Virus Ribonucleoprotein Complex and Polymerase Complex Using Proteomic-Based Approaches. *J. Proteome Res.* 6, 672–682.

Mayne, J.T., Rice, C.M., Strauss, E.G., Hunkapiller, M.W., and Strauss, J.H. (1984). Biochemical studies of the maturation of the small Sindbis virus glycoprotein E3. *Virology* 134, 338–357.

Mazumder, B., Sampath, P., Seshadri, V., Maitra, R.K., DiCorleto, P.E., and Fox, P.L. (2003). Regulated release of L13a from the 60S ribosomal subunit as a mechanism of transcript-specific translational control. *Cell* 115, 187–198.

Mazumder, B., Poddar, D., Basu, A., Kour, R., Verbovetskaya, V., and Barik, S. (2014). Extraribosomal l13a is a specific innate immune factor for antiviral defense. *J. Virol.* 88, 9100–9110.

McCormick, C., and Khapersky, D.A. (2017). Translation inhibition and stress granules in the antiviral immune response. *Nat Rev Immunol* 17, 647–660.

McInerney, G.M., Kedersha, N.L., Kaufman, R.J., Anderson, P., and Liljeström, P. (2005). Importance of eIF2alpha phosphorylation and stress granule assembly in alphavirus translation regulation. *Mol Biol Cell* 16, 3753–3763.

McMahon, M., Contreras, A., Holm, M., Uechi, T., Forester, C.M., Pang, X., Jackson, C., Calvert, M.E., Chen, B., Quigley, D.A., et al. (2019). A single H/ACA small nucleolar RNA mediates tumor suppression downstream of oncogenic RAS. *ELife* 8, e48847.

Meade, N., Furey, C., Li, H., Verma, R., Chai, Q., Rollins, M.G., DiGiuseppe, S., Naghavi, M.H., and Walsh, D. (2018). Poxviruses Evade Cytosolic Sensing through Disruption of an mTORC1-mTORC2 Regulatory Circuit. *Cell* 174, 1143-1157.e17.

Meade, N., King, M., Munger, J., and Walsh, D. (2019). mTOR Dysregulation by Vaccinia Virus F17 Controls Multiple Processes with Varying Roles in Infection. *J Virol* 93, e00784-19.

Meertens, L., Hafirassou, M.L., Couderc, T., Bonnet-Madin, L., Kril, V., Kümmerer, B.M., Labeau, A., Brugier, A., Simon-Loriere, E., Burlaud-Gaillard, J., et al. (2019). FHL1 is a major host factor for chikungunya virus infection. *Nature* 574, 259–263.

Melancon, P., and Garoff, H. (1987). Processing of the Semliki Forest virus structural polyprotein: role of the capsid protease. *J Virol* 61, 1301–1309.

Mellacheruvu, D., Wright, Z., Couzens, A.L., Lambert, J.-P., St-Denis, N.A., Li, T., Miteva, Y.V., Hauri, S., Sardi, M.E., Low, T.Y., et al. (2013). The CRAPome: a contaminant repository for affinity purification-mass spectrometry data. *Nat. Methods* 10, 730–736.

Mendes, A., and Kuhn, R.J. (2018). Alphavirus Nucleocapsid Packaging and Assembly. *Viruses* 10, E138.

Meyuhas, O. (2015a). Ribosomal Protein S6 Phosphorylation: Four Decades of Research. *Int. Rev. Cell. Mol. Biol.* 320, 41–73.

Meyuhas, O. (2015b). Chapter Two - Ribosomal Protein S6 Phosphorylation: Four Decades of Research. In *International Review of Cell and Molecular Biology*, K.W. Jeon, ed. (Academic Press), pp. 41–73.



- Miller, C.M., Selvam, S., and Fuchs, G. (2021). Fatal attraction: The roles of ribosomal proteins in the viral life cycle. *WIREs RNA* 12, e1613.
- Miller, K.E., Kim, Y., Huh, W.-K., and Park, H.-O. (2015). Bimolecular Fluorescence Complementation (BiFC) Analysis: Advances and Recent Applications for Genome-Wide Interaction Studies. *Journal of Molecular Biology* 427, 2039–2055.
- Mills, E.W., and Green, R. (2017). Ribosomopathies: There's strength in numbers. *Science* 358.
- Mir, M.A., and Panganiban, A.T. (2004). Trimeric Hantavirus Nucleocapsid Protein Binds Specifically to the Viral RNA Panhandle. *Journal of Virology* 78, 8281–8288.
- Mir, M.A., and Panganiban, A.T. (2008). A protein that replaces the entire cellular eIF4F complex. *EMBO J.* 27, 3129–3139.
- Mir, M.A., and Panganiban, A.T. (2010). The Triplet Repeats of the Sin Nombre Hantavirus 5' Untranslated Region Are Sufficient in cis for Nucleocapsid-Mediated Translation Initiation. *J. Virol.* 84, 8937–8944.
- Mir, M.A., Duran, W.A., Hjelle, B.L., Ye, C., and Panganiban, A.T. (2008). Storage of cellular 5' mRNA caps in P bodies for viral cap-snatching. *PNAS* 105, 19294–19299.
- Mohankumar, V., Dhanushkodi, N.R., and Raju, R. (2011). Sindbis virus replication, is insensitive to rapamycin and torin1, and suppresses Akt/mTOR pathway late during infection in HEK cells. *Biochemical and Biophysical Research Communications* 406, 262–267.
- Mohl, B.-P., Emmott, E., and Roy, P. (2017). Phosphoproteomic Analysis Reveals the Importance of Kinase Regulation During Orbivirus Infection. *Molecular & Cellular Proteomics* 16, 1990–2005.
- Moller-Tank, S., Kondratowicz, A.S., Davey, R.A., Rennert, P.D., and Maury, W. (2013). Role of the Phosphatidylserine Receptor TIM-1 in Enveloped-Virus Entry. *Journal of Virology* 87, 8327–8341.
- Montgomery, S.A., Berglund, P., Beard, C.W., and Johnston, R.E. (2006). Ribosomal protein S6 associates with alphavirus nonstructural protein 2 and mediates expression from alphavirus messages. *J. Virol.* 80, 7729–7739.
- Moorman, N.J., Cristea, I.M., Terhune, S.S., Rout, M.P., Chait, B.T., and Shenk, T. (2008). Human Cytomegalovirus Protein UL38 Inhibits Host Cell Stress Responses by Antagonizing the Tuberos Sclerosis Protein Complex. *Cell Host & Microbe* 3, 253–262.
- Morris-Desbois, C., Bochar, V., Reynaud, C., and Jalinot, P. (1999). Interaction between the Ret finger protein and the Int-6 gene product and co-localisation into nuclear bodies. *Journal of Cell Science* 112, 3331–3342.
- Moss, B. (1968). Inhibition of HeLa Cell Protein Synthesis by the Vaccinia Virion. *J Virol* 2, 1028–1037.
- Moss, B., and Filler, R. (1970). Irreversible Effects of Cycloheximide During the Early Period of Vaccinia Virus Replication. *J Virol* 5, 99–108.

- Muhs, M., Yamamoto, H., Ismer, J., Takaku, H., Nashimoto, M., Uchiumi, T., Nakashima, N., Mielke, T., Hildebrand, P.W., Nierhaus, K.H., et al. (2011). Structural basis for the binding of IRES RNAs to the head of the ribosomal 40S subunit. *Nucleic Acids Res.* 39, 5264–5275.
- Muhs, M., Hilal, T., Mielke, T., Skabkin, M.A., Sanbonmatsu, K.Y., Pestova, T.V., and Spahn, C.M.T. (2015). Cryo-EM of Ribosomal 80S Complexes with Termination Factors Reveals the Translocated Cricket Paralysis Virus IRES. *Molecular Cell* 57, 422–432.
- Napthine, S., Treffers, E.E., Bell, S., Goodfellow, I., Fang, Y., Firth, A.E., Snijder, E.J., and Brierley, I. (2016). A novel role for poly(C) binding proteins in programmed ribosomal frameshifting. *Nucleic Acids Research* 44, 5491–5503.
- Napthine, S., Ling, R., Finch, L.K., Jones, J.D., Bell, S., Brierley, I., and Firth, A.E. (2017). Protein-directed ribosomal frameshifting temporally regulates gene expression. *Nat Commun* 8, 15582.
- Napthine, S., Bell, S., Hill, C.H., Brierley, I., and Firth, A.E. (2019). Characterization of the stimulators of protein-directed ribosomal frameshifting in Theiler's murine encephalomyelitis virus. *Nucleic Acids Research* 47, 8207–8223.
- Natchiar, S.K., Myasnikov, A.G., Kratzat, H., Hazemann, I., and Klaholz, B.P. (2017). Visualization of chemical modifications in the human 80S ribosome structure. *Nature* 551, 472–477.
- Ng, T.I., Mo, H., Pilot-Matias, T., He, Y., Koev, G., Krishnan, P., Mondal, R., Pithawalla, R., He, W., Dekhtyar, T., et al. (2007). Identification of host genes involved in hepatitis C virus replication by small interfering RNA technology. *Hepatology* 45, 1413–1421.
- Nishiyama, T., Yamamoto, H., Uchiumi, T., and Nakashima, N. (2007). Eukaryotic ribosomal protein RPS25 interacts with the conserved loop region in a dicistroviral intergenic internal ribosome entry site. *Nucleic Acids Res.* 35, 1514–1521.
- Noton, S.L., and Fearn, R. (2015). Initiation and regulation of paramyxovirus transcription and replication. *Virology* 479–480, 545–554.
- Oberstein, A., Perlman, D.H., Shenk, T., and Terry, L.J. (2015). Human cytomegalovirus pUL97 kinase induces global changes in the infected cell phosphoproteome. *PROTEOMICS* 15, 2006–2022.
- Okumura, F., Zou, W., and Zhang, D.-E. (2007). ISG15 modification of the eIF4E cognate 4EHP enhances cap structure-binding activity of 4EHP. *Genes Dev.* 21, 255–260.
- Olivares, E., Landry, D.M., Cáceres, C.J., Pino, K., Rossi, F., Navarrete, C., Huidobro-Toro, J.P., Thompson, S.R., and López-Lastra, M. (2014). The 5' Untranslated Region of the Human T-Cell Lymphotropic Virus Type 1 mRNA Enables Cap-Independent Translation Initiation. *Journal of Virology* 88, 5936–5955.
- Oliveira, S., Rocha, J., Sousa, C.A., and Capinha, C. (2021). Wide and increasing suitability for *Aedes albopictus* in Europe is congruent across distribution models. *Sci Rep* 11, 9916.
- Ooi, Y.S., Stiles, K.M., Liu, C.Y., Taylor, G.M., and Kielian, M. (2013). Genome-Wide RNAi Screen Identifies Novel Host Proteins Required for Alphavirus Entry. *PLOS Pathogens* 9, e1003835.

- Osborne, M.J., Volpon, L., Kornblatt, J.A., Culjkovic-Kraljacic, B., Baguet, A., and Borden, K.L.B. (2013). eIF4E3 acts as a tumor suppressor by utilizing an atypical mode of methyl-7-guanosine cap recognition. *PNAS* *110*, 3877–3882.
- Panas, M.D., Varjak, M., Lulla, A., Eng, K.E., Merits, A., Karlsson Hedestam, G.B., and McInerney, G.M. (2012). Sequestration of G3BP coupled with efficient translation inhibits stress granules in Semliki Forest virus infection. *Mol Biol Cell* *23*, 4701–4712.
- Panas, M.D., Ahola, T., and McInerney, G.M. (2014). The C-terminal repeat domains of nsP3 from the Old World alphaviruses bind directly to G3BP. *J Virol* *88*, 5888–5893.
- Panas, M.D., Schulte, T., Thaa, B., Sandalova, T., Kedersha, N., Achour, A., and McInerney, G.M. (2015). Viral and cellular proteins containing FGDF motifs bind G3BP to block stress granule formation. *PLoS Pathog* *11*, e1004659.
- Panda, D., Rose, P.P., Hanna, S.L., Gold, B., Hopkins, K.C., Lyde, R.B., Marks, M.S., and Cherry, S. (2013). Genome-wide RNAi Screen Identifies SEC61A and VCP as Conserved Regulators of Sindbis Virus Entry. *Cell Reports* *5*, 1737–1748.
- Parikh, B.A., and Tumer, N.E. (2004). Antiviral activity of ribosome inactivating proteins in medicine. *Mini Rev Med Chem* *4*, 523–543.
- Park, H.-S., Himmelbach, A., Browning, K.S., Hohn, T., and Ryabova, L.A. (2001). A Plant Viral “Reinitiation” Factor Interacts with the Host Translational Machinery. *Cell* *106*, 723–733.
- Parsyan, A., Shahbazian, D., Martineau, Y., Petroulakis, E., Alain, T., Larsson, O., Mathonnet, G., Tettweiler, G., Hellen, C.U., Pestova, T.V., et al. (2009). The helicase protein DHX29 promotes translation initiation, cell proliferation, and tumorigenesis. *PNAS* *106*, 22217–22222.
- Patel, R.K., and Hardy, R.W. (2012). Role for the phosphatidylinositol 3-kinase-Akt-TOR pathway during sindbis virus replication in arthropods. *J Virol* *86*, 3595–3604.
- Patel, A., Treffers, E.E., Meier, M., Patel, T.R., Stetefeld, J., Snijder, E.J., and Mark, B.L. (2020). Molecular characterization of the RNA-protein complex directing  $-2/-1$  programmed ribosomal frameshifting during arterivirus replicase expression. *Journal of Biological Chemistry* *295*, 17904–17921.
- Patton, R.D., Sanjeev, M., Woodward, L.A., Mabin, J.W., Bundschuh, R., and Singh, G. (2020). Chemical crosslinking enhances RNA immunoprecipitation for efficient identification of binding sites of proteins that photo-crosslink poorly with RNA. *RNA* *26*, 1216–1233.
- Pelletier, J., Schmeing, T.M., and Sonenberg, N. (2021). The multifaceted eukaryotic cap structure. *WIREs RNA* *12*, e1636.
- Penzo, M., Carnicelli, D., Montanaro, L., and Brigotti, M. (2016). A reconstituted cell-free assay for the evaluation of the intrinsic activity of purified human ribosomes. *Nat Protoc* *11*, 1309–1325.
- Peränen, J., Rikkinen, M., Liljeström, P., and Kääriäinen, L. (1990). Nuclear localization of Semliki Forest virus-specific nonstructural protein nsP2. *J Virol* *64*, 1888–1896.

- Peränen, J., Laakkonen, P., Hyvönen, M., and Kääriäinen, L. (1995). The alphavirus replicase protein nsP1 is membrane-associated and has affinity to endocytic organelles. *Virology* 208, 610–620.
- Person, A., and Beaud, G. (1978). Inhibition of host protein synthesis in vaccinia virus-infected cells in the presence of cordycepin (3'-deoxyadenosine). *J Virol* 25, 11–18.
- Person, A., and Beaud, G. (1980). Shut-Off of Host Protein Synthesis in Vaccinia-Virus-Infected Cells Exposed to Cordycepin. *Eur. J. Biochem.* 103, 85–93.
- Person, A., Ben-Hamida, F., and Beaud, G. (1980). Inhibition of 40S–Met–tRNA f Met ribosomal initiation complex formation by vaccinia virus. *Nature* 287, 355–357.
- Person-Fernandez, A., and Beaud, G. (1986). Purification and characterization of a protein synthesis inhibitor associated with vaccinia virus. *J. Biol. Chem.* 261, 8283–8289.
- Pestova, T.V., Lomakin, I.B., Lee, J.H., Choi, S.K., Dever, T.E., and Hellen, C.U.T. (2000). The joining of ribosomal subunits in eukaryotes requires eIF5B. *Nature* 403, 332–335.
- Pestova, T.V., de Breyne, S., Pisarev, A.V., Abaeva, I.S., and Hellen, C.U.T. (2008). eIF2-dependent and eIF2-independent modes of initiation on the CSFV IRES: a common role of domain II. *EMBO J* 27, 1060–1072.
- Petitjean, O., Girardi, E., Ngondo, R.P., Lupashin, V., and Pfeffer, S. (2020). Genome-Wide CRISPR-Cas9 Screen Reveals the Importance of the Heparan Sulfate Pathway and the Conserved Oligomeric Golgi Complex for Synthetic Double-Stranded RNA Uptake and Sindbis Virus Infection. *MSphere* 5.
- Pettersson, R.F., Söderlund, H., and Kääriäinen, L. (1980). The Nucleotide Sequences of the 5'-Terminal T1 Oligonucleotides of Semliki-Forest-Virus 42-S and 26-S RNAs are Different. *European Journal of Biochemistry* 105, 435–443.
- Philippe, L., Elzen, A.M.G. van den, Watson, M.J., and Thoreen, C.C. (2020). Global analysis of LARP1 translation targets reveals tunable and dynamic features of 5' TOP motifs. *PNAS* 117, 5319–5328.
- Picard, D., Kao, C.C., and Hudak, K.A. (2005). Pokeweed Antiviral Protein Inhibits Brome Mosaic Virus Replication in Plant Cells\*. *Journal of Biological Chemistry* 280, 20069–20075.
- Pietilä, M.K., Hellström, K., and Ahola, T. (2017). Alphavirus polymerase and RNA replication. *Virus Research* 234, 44–57.
- Pietilä, M.K., van Hemert, M.J., and Ahola, T. (2018). Purification of Highly Active Alphavirus Replication Complexes Demonstrates Altered Fractionation of Multiple Cellular Membranes. *J Virol* 92, e01852-17.
- Pisarev, A.V., Kolupaeva, V.G., Pisareva, V.P., Merrick, W.C., Hellen, C.U.T., and Pestova, T.V. (2006). Specific functional interactions of nucleotides at key -3 and +4 positions flanking the initiation codon with components of the mammalian 48S translation initiation complex. *Genes Dev.* 20, 624–636.

- Pisareva, V.P., and Pisarev, A.V. (2016). DHX29 and eIF3 cooperate in ribosomal scanning on structured mRNAs during translation initiation. *RNA* 22, 1859–1870.
- Poblete-Durán, N., Prades-Pérez, Y., Vera-Otarola, J., Soto-Rifo, R., and Valiente-Echeverría, F. (2016). Who Regulates Whom? An Overview of RNA Granules and Viral Infections. *Viruses* 8.
- Pooggin, M.M., and Ryabova, L.A. (2018). Ribosome Shunting, Polycistronic Translation, and Evasion of Antiviral Defenses in Plant Pararetroviruses and Beyond. *Front. Microbiol.* 9.
- Quade, N., Boehringer, D., Leibundgut, M., van den Heuvel, J., and Ban, N. (2015a). Cryo-EM structure of Hepatitis C virus IRES bound to the human ribosome at 3.9-Å resolution. *Nat Commun* 6, 7646.
- Quade, N., Boehringer, D., Leibundgut, M., van den Heuvel, J., and Ban, N. (2015b). Cryo-EM structure of Hepatitis C virus IRES bound to the human ribosome at 3.9-Å resolution. *Nat. Commun.* 6, 7646.
- Ramsey, J., and Mukhopadhyay, S. (2017). Disentangling the Frames, the State of Research on the Alphavirus 6K and TF Proteins. *Viruses* 9, E228.
- Ramsey, J., Renzi, E.C., Arnold, R.J., Trinidad, J.C., and Mukhopadhyay, S. Palmitoylation of Sindbis Virus TF Protein Regulates Its Plasma Membrane Localization and Subsequent Incorporation into Virions. *Journal of Virology* 91, e02000-16.
- Ran, F.A., Hsu, P.D., Wright, J., Agarwala, V., Scott, D.A., and Zhang, F. (2013). Genome engineering using the CRISPR-Cas9 system. *Nat. Protocols* 8, 2281–2308.
- Ranki, M., Ulmanen, I., and Kääriäinen, L. (1979). Semliki Forest virus-specific nonstructural protein is associated with ribosomes. *FEBS Lett.* 108, 299–302.
- Rao, S., Lungu, C., Crespo, R., Steijaert, T.H., Gorska, A., Palstra, R.-J., Prins, H.A.B., van Ijcken, W., Mueller, Y.M., van Kampen, J.J.A., et al. (2021). Selective cell death in HIV-1-infected cells by DDX3 inhibitors leads to depletion of the inducible reservoir. *Nat Commun* 12, 2475.
- Rebendenne, A., Roy, P., Bonaventure, B., Valadão, A.L.C., Desmarests, L., Rouillé, Y., Tauziet, M., Arnaud-Arnould, M., Giovannini, D., Lee, Y., et al. (2021). Bidirectional genome-wide CRISPR screens reveal host factors regulating SARS-CoV-2, MERS-CoV and seasonal coronaviruses.
- Reineke, L.C., and Lloyd, R.E. (2013). Diversion of stress granules and P-bodies during viral infection. *Virology* 436, 255–267.
- Remacha, M., Jimenez-Diaz, A., Bermejo, B., Rodriguez-Gabriel, M.A., Guarinos, E., and Ballesta, J.P. (1995). Ribosomal acidic phosphoproteins P1 and P2 are not required for cell viability but regulate the pattern of protein expression in *Saccharomyces cerevisiae*. *Molecular and Cellular Biology* 15, 4754–4762.
- Reschke, M., Clohessy, J.G., Seitzer, N., Goldstein, D.P., Breitkopf, S.B., Schmolze, D.B., Ala, U., Asara, J.M., Beck, A.H., and Pandolfi, P.P. (2013). Characterization and Analysis of the Composition and Dynamics of the Mammalian Riboproteome. *Cell Reports* 4, 1276–1287.

- Rezza, G., Nicoletti, L., Angelini, R., Romi, R., Finarelli, A., Panning, M., Cordioli, P., Fortuna, C., Boros, S., Magurano, F., et al. (2007). Infection with chikungunya virus in Italy: an outbreak in a temperate region. *The Lancet* 370, 1840–1846.
- Ricci, E.P., Kucukural, A., Cenik, C., Mercier, B.C., Singh, G., Heyer, E.E., Ashar-Patel, A., Peng, L., and Moore, M.J. (2014). Staufen1 senses overall transcript secondary structure to regulate translation. *Nat. Struct. Mol. Biol.* 21, 26–35.
- Richardson, C.D., Ray, G.J., DeWitt, M.A., Curie, G.L., and Corn, J.E. (2016). Enhancing homology-directed genome editing by catalytically active and inactive CRISPR-Cas9 using asymmetric donor DNA. *Nature Biotechnology* 34, 339–344.
- Rikkinen, M. (1996). Functional significance of the nuclear-targeting and NTP-binding motifs of Semliki Forest virus nonstructural protein nsP2. *Virology* 218, 352–361.
- Rikkinen, M., Peranen, J., and Kaariainen, L. (1992). Nuclear and nucleolar targeting signals of semliki forest virus nonstructural protein nsP2. *Virology* 189, 462–473.
- Rikkinen, M., Peränen, J., and Kääriäinen, L. (1994). ATPase and GTPase activities associated with Semliki Forest virus nonstructural protein nsP2. *Journal of Virology* 68, 5804–5810.
- Rodriguez, W., Srivastav, K., and Muller, M. C19ORF66 Broadly Escapes Virus-Induced Endonuclease Cleavage and Restricts Kaposi's Sarcoma-Associated Herpesvirus. *Journal of Virology* 93, e00373-19.
- Roller, R.J., and Roizman, B. (1992). The herpes simplex virus 1 RNA binding protein US11 is a virion component and associates with ribosomal 60S subunits. *J. Virol.* 66, 3624–3632.
- Rose, P.P., Hanna, S.L., Spiridigliozzi, A., Wannissorn, N., Beiting, D.P., Ross, S.R., Hardy, R.W., Bambina, S.A., Heise, M.T., and Cherry, S. (2011). Natural resistance-associated macrophage protein is a cellular receptor for sindbis virus in both insect and mammalian hosts. *Cell Host Microbe* 10, 97–104.
- Rosemond-Hornbeak, H., and Moss, B. (1975). Inhibition of host protein synthesis by vaccinia virus: fate of cell mRNA and synthesis of small poly (A)-rich polyribonucleotides in the presence of actinomycin D. *J Virol* 16, 34–42.
- Rupp, J.C., Sokoloski, K.J., Gebhart, N.N., and Hardy, R.W. (2015). Alphavirus RNA synthesis and non-structural protein functions. *J Gen Virol* 96, 2483–2500.
- Sagot, J., and Beaud, G. (1979). Phosphorylation in vivo of a vaccinia-virus structural protein found associated with the ribosomes from infected cells. *Eur. J. Biochem.* 98, 131–140.
- Salonen, A., Vasiljeva, L., Merits, A., Magden, J., Jokitalo, E., and Kääriäinen, L. (2003). Properly Folded Nonstructural Polyprotein Directs the Semliki Forest Virus Replication Complex to the Endosomal Compartment. *Journal of Virology* 77, 1691–1702.
- Salveti, A., and Greco, A. (2014). Viruses and the nucleolus: The fatal attraction. *Biochimica et Biophysica Acta (BBA) - Molecular Basis of Disease* 1842, 840–847.

- Sampath, P., Mazumder, B., Seshadri, V., Gerber, C.A., Chavatte, L., Kinter, M., Ting, S.M., Dignam, J.D., Kim, S., Driscoll, D.M., et al. (2004). Noncanonical function of glutamyl-prolyl-tRNA synthetase: gene-specific silencing of translation. *Cell* 119, 195–208.
- Sanz, M.A., and Carrasco, L. (2001). Sindbis Virus Variant with a Deletion in the 6K Gene Shows Defects in Glycoprotein Processing and Trafficking: Lack of Complementation by a Wild-Type 6K Gene intrans. *Journal of Virology* 75, 7778–7784.
- Sanz, E., Yang, L., Su, T., Morris, D.R., McKnight, G.S., and Amieux, P.S. (2009a). Cell-type-specific isolation of ribosome-associated mRNA from complex tissues. *Proc. Natl. Acad. Sci. U.S.A.* 106, 13939–13944.
- Sanz, M.A., Castelló, A., and Carrasco, L. (2007). Viral translation is coupled to transcription in Sindbis virus-infected cells. *J Virol* 81, 7061–7068.
- Sanz, M.Á., Castelló, A., Ventoso, I., Berlanga, J.J., and Carrasco, L. (2009b). Dual Mechanism for the Translation of Subgenomic mRNA from Sindbis Virus in Infected and Uninfected Cells. *PLOS ONE* 4, e4772.
- Sanz, M.Á., Castelló, A., Ventoso, I., Berlanga, J.J., and Carrasco, L. (2009c). Dual Mechanism for the Translation of Subgenomic mRNA from Sindbis Virus in Infected and Uninfected Cells. *PLOS ONE* 4, e4772.
- Sanz, M.A., Welnowska, E., Redondo, N., and Carrasco, L. (2010). Translation driven by picornavirus IRES is hampered from Sindbis virus replicons: rescue by poliovirus 2A protease. *J Mol Biol* 402, 101–117.
- Sanz, M.A., García-Moreno, M., and Carrasco, L. (2015). Inhibition of host protein synthesis by Sindbis virus: correlation with viral RNA replication and release of nuclear proteins to the cytoplasm. *Cellular Microbiology* 17, 520–541.
- Sanz, M.A., González Almela, E., and Carrasco, L. (2017a). Translation of Sindbis Subgenomic mRNA is Independent of eIF2, eIF2A and eIF2D. *Sci Rep* 7, 43876.
- Sanz, M.A., González Almela, E., and Carrasco, L. (2017b). Translation of Sindbis Subgenomic mRNA is Independent of eIF2, eIF2A and eIF2D. *Sci Rep* 7, 43876.
- Sanz, M.A., Almela, E.G., García-Moreno, M., Marina, A.I., and Carrasco, L. (2019). A viral RNA motif involved in signaling the initiation of translation on non-AUG codons. *RNA* 25, 431–452.
- Saxena, T., Tandon, B., Sharma, S., Chameettachal, S., Ray, P., Ray, A.R., and Kulshreshtha, R. (2013). Combined miRNA and mRNA Signature Identifies Key Molecular Players and Pathways Involved in Chikungunya Virus Infection in Human Cells. *PLoS One* 8, e79886.
- Schepetilnikov, M., Kobayashi, K., Geldreich, A., Caranta, C., Robaglia, C., Keller, M., and Ryabova, L.A. (2011). Viral factor TAV recruits TOR/S6K1 signalling to activate reinitiation after long ORF translation. *The EMBO Journal* 30, 1343–1356.
- Schmid-Burgk, J.L., Höning, K., Ebert, T.S., and Hornung, V. (2016). CRISPaint allows modular base-specific gene tagging using a ligase-4-dependent mechanism. *Nature Communications* 7, 12338.

- Schmidt, N., Lareau, C.A., Keshishian, H., Ganskih, S., Schneider, C., Hennig, T., Melanson, R., Werner, S., Wei, Y., Zimmer, M., et al. (2021a). The SARS-CoV-2 RNA–protein interactome in infected human cells. *Nat Microbiol* 6, 339–353.
- Schmidt, N., Lareau, C.A., Keshishian, H., Ganskih, S., Schneider, C., Hennig, T., Melanson, R., Werner, S., Wei, Y., Zimmer, M., et al. (2021b). The SARS-CoV-2 RNA–protein interactome in infected human cells. *Nat Microbiol* 6, 339–353.
- Schmidt, T.G.M., Batz, L., Bonet, L., Carl, U., Holzapfel, G., Kiem, K., Matulewicz, K., Niermeier, D., Schuchardt, I., and Stanar, K. (2013). Development of the Twin-Strep-tag® and its application for purification of recombinant proteins from cell culture supernatants. *Protein Expression and Purification* 92, 54–61.
- Schneider, W.M., Luna, J.M., Hoffmann, H.-H., Sánchez-Rivera, F.J., Leal, A.A., Ashbrook, A.W., Le Pen, J., Ricardo-Lax, I., Michailidis, E., Peace, A., et al. (2021). Genome-Scale Identification of SARS-CoV-2 and Pan-coronavirus Host Factor Networks. *Cell* 184, 120-132.e14.
- Scholthof, H.B., Gowda, S., Wu, F.C., and Shepherd, R.J. (1992). The full-length transcript of a caulimovirus is a polycistronic mRNA whose genes are trans activated by the product of gene VI. *J. Virol.* 66, 3131–3139.
- Schubert, K., Karousis, E.D., Jomaa, A., Scaiola, A., Echeverria, B., Gurzeler, L.-A., Leibundgut, M., Thiel, V., Mühlemann, O., and Ban, N. (2020). SARS-CoV-2 Nsp1 binds the ribosomal mRNA channel to inhibit translation. *Nature Structural & Molecular Biology* 27, 959–966.
- Schüler, M., Connell, S.R., Lescoute, A., Giesebrecht, J., Dabrowski, M., Schroerer, B., Mielke, T., Penczek, P.A., Westhof, E., and Spahn, C.M.T. (2006). Structure of the ribosome-bound cricket paralysis virus IRES RNA. *Nat. Struct. Mol. Biol.* 13, 1092–1096.
- Sefton, B.M. (1977). Immediate glycosylation of Sindbis virus membrane proteins. *Cell* 10, 659–668.
- Sessions, O.M., Barrows, N.J., Souza-Neto, J.A., Robinson, T.J., Hershey, C.L., Rodgers, M.A., Ramirez, J.L., Dimopoulos, G., Yang, P.L., Pearson, J.L., et al. (2009). Discovery of insect and human dengue virus host factors. *Nature* 458, 1047–1050.
- Sharma, S., and Lafontaine, D.L.J. (2015). “View From A Bridge”: A New Perspective on Eukaryotic rRNA Base Modification. *Trends Biochem. Sci.* 40, 560–575.
- Sharma, U., Conine, C.C., Shea, J.M., Boskovic, A., Derr, A.G., Bing, X.Y., Belleannee, C., Kucukural, A., Serra, R.W., Sun, F., et al. (2016). Biogenesis and function of tRNA fragments during sperm maturation and fertilization in mammals. *Science* 351, 391–396.
- Shatkin, A.J. (1963). Actinomycin D and Vaccinia Virus Infection of Hela Cells. *Nature* 199, 357–358.
- Shen, L., and Pelletier, J. (2020). General and Target-Specific DExD/H RNA Helicases in Eukaryotic Translation Initiation. *International Journal of Molecular Sciences* 21, 4402.
- Shen, Z., Ye, G., Deng, F., Wang, G., Cui, M., Fang, L., Xiao, S., Fu, Z.F., and Peng, G. (2018). Structural Basis for the Inhibition of Host Gene Expression by Porcine Epidemic Diarrhea Virus nsp1. *Journal of Virology* 92.



- Shi, Y., Yang, Y., Hoang, B., Bardeleben, C., Holmes, B., Gera, J., and Lichtenstein, A. (2016). Therapeutic potential of targeting IRES-dependent c-myc translation in multiple myeloma cells during ER stress. *Oncogene* 35, 1015–1024.
- Shi, Z., Fujii, K., Kovary, K.M., Genuth, N.R., Röst, H.L., Teruel, M.N., and Barna, M. (2017). Heterogeneous Ribosomes Preferentially Translate Distinct Subpools of mRNAs Genome-wide. *Mol. Cell* 67, 71-83.e7.
- Shirako, Y., and Strauss, J.H. (1994). Regulation of Sindbis virus RNA replication: uncleaved P123 and nsP4 function in minus-strand RNA synthesis, whereas cleaved products from P123 are required for efficient plus-strand RNA synthesis. *J Virol* 68, 1874–1885.
- Shirokikh, N.E., and Spirin, A.S. (2008). Poly(A) leader of eukaryotic mRNA bypasses the dependence of translation on initiation factors. *Proc. Natl. Acad. Sci. U.S.A.* 105, 10738–10743.
- Simm, D., Hatje, K., and Kollmar, M. (2015). Waggawagga: comparative visualization of coiled-coil predictions and detection of stable single  $\alpha$ -helices (SAH domains). *Bioinformatics* 31, 767–769.
- Simsek, D., Tiu, G.C., Flynn, R.A., Byeon, G.W., Leppek, K., Xu, A.F., Chang, H.Y., and Barna, M. (2017). The Mammalian Ribo-interactome Reveals Ribosome Functional Diversity and Heterogeneity. *Cell* 169, 1051-1065.e18.
- Singh, I., and Helenius, A. (1992). Role of ribosomes in Semliki Forest virus nucleocapsid uncoating. *J. Virol.* 66, 7049–7058.
- Singh, N., and Bhalla, N. (2020). Moonlighting Proteins. 21.
- Sivan, G., Martin, S.E., Myers, T.G., Buehler, E., Szymczyk, K.H., Ormanoglu, P., and Moss, B. (2013). Human genome-wide RNAi screen reveals a role for nuclear pore proteins in poxvirus morphogenesis. *PNAS* 110, 3519–3524.
- Sjöberg, M., Lindqvist, B., and Garoff, H. (2011). Activation of the Alphavirus Spike Protein Is Suppressed by Bound E3. *Journal of Virology* 85, 5644–5650.
- Skabkin, M.A., Skabkina, O.V., Dhote, V., Komar, A.A., Hellen, C.U.T., and Pestova, T.V. (2010). Activities of Ligatin and MCT-1/DENR in eukaryotic translation initiation and ribosomal recycling. *Genes Dev* 24, 1787–1801.
- Smith, R.W.P., Graham, S.V., and Gray, N.K. (2008). Regulation of translation initiation by herpesviruses. *Biochem Soc Trans* 36, 701–707.
- Smyth, G.K. (2005). limma: Linear Models for Microarray Data. In *Bioinformatics and Computational Biology Solutions Using R and Bioconductor*, R. Gentleman, V.J. Carey, W. Huber, R.A. Irizarry, and S. Dudoit, eds. (New York, NY: Springer), pp. 397–420.
- Söderholm, S., Kainov, D.E., Öhman, T., Denisova, O.V., Schepens, B., Kuleskiy, E., Imanishi, S.Y., Corthals, G., Hintsanen, P., Aittokallio, T., et al. (2016). Phosphoproteomics to Characterize Host Response During Influenza A Virus Infection of Human Macrophages. *Molecular & Cellular Proteomics* 15, 3203–3219.

- Sokoloski, K.J., Dickson, A.M., Chaskey, E.L., Garneau, N.L., Wilusz, C.J., and Wilusz, J. (2010). Sindbis Virus Usurps the Cellular HuR Protein to Stabilize Its Transcripts and Promote Productive Infections in Mammalian and Mosquito Cells. *Cell Host & Microbe* 8, 196–207.
- Sommer, C.L., Barrows, N.J., Bradrick, S.S., Pearson, J.L., and Garcia-Blanco, M.A. (2012). G Protein-Coupled Receptor Kinase 2 Promotes Flaviviridae Entry and Replication. *PLOS Neglected Tropical Diseases* 6, e1820.
- Song, S.-K., Choi, Y., Moon, Y.H., Kim, S.-G., Choi, Y.D., and Lee, J.S. (2000). Systemic induction of a *Phytolacca insularis* antiviral protein gene by mechanical wounding, jasmonic acid, and abscisic acid. *Plant Mol Biol* 43, 439–450.
- Song, W., Joo, M., Yeom, J.-H., Shin, E., Lee, M., Choi, H.-K., Hwang, J., Kim, Y.-I., Seo, R., Lee, J.E., et al. (2019a). Divergent rRNAs as regulators of gene expression at the ribosome level. *Nat Microbiol* 4, 515–526.
- Song, Y., Mugavero, J., Stauff, C.B., and Wimmer, E. (2019b). Dengue and Zika Virus 5' Untranslated Regions Harbor Internal Ribosomal Entry Site Functions. *MBio* 10, e00459-19.
- Soto-Rifo, R., and Ohlmann, T. (2013). The role of the DEAD-box RNA helicase DDX3 in mRNA metabolism. *Wiley Interdiscip Rev RNA* 4, 369–385.
- Soto-Rifo, R., Rubilar, P.S., Limousin, T., de Breyne, S., Décimo, D., and Ohlmann, T. (2012). DEAD-box protein DDX3 associates with eIF4F to promote translation of selected mRNAs. *EMBO J.* 31, 3745–3756.
- Soto-Rifo, R., Rubilar, P.S., and Ohlmann, T. (2013). The DEAD-box helicase DDX3 substitutes for the cap-binding protein eIF4E to promote compartmentalized translation initiation of the HIV-1 genomic RNA. *Nucl. Acids Res.* 41, 6286–6299.
- Spuul, P., Salonen, A., Merits, A., Jokitalo, E., Kääriäinen, L., and Ahola, T. (2007). Role of the Amphipathic Peptide of Semliki Forest Virus Replicase Protein nsP1 in Membrane Association and Virus Replication. *Journal of Virology* 81, 872–883.
- van Steeg, H., van Grinsven, M., van Mansfeld, F., Voorma, H.O., and Benne, R. (1981a). Initiation of protein synthesis in neuroblastoma cells infected by Semliki Forest Virus. A decreased requirement of late viral mRNA for eIF-4B and cap binding protein. *FEBS Lett* 129, 62–66.
- van Steeg, H., Thomas, A., Verbeek, S., Kasperaitis, M., Voorma, H.O., and Benne, R. (1981b). Shutoff on Neuroblastoma Cell Protein Synthesis by Semliki Forest Virus: Loss of Ability of Crude Initiation Factors to Recognize Early Semliki Forest Virus and Host mRNA's. *J Virol* 38, 728–736.
- Stern-Ginossar, N., Thompson, S.R., Mathews, M.B., and Mohr, I. (2019). Translational Control in Virus-Infected Cells. *Cold Spring Harb Perspect Biol* 11, a033001.
- Strauss, J.H., and Strauss, E.G. (1994). The alphaviruses: gene expression, replication, and evolution. *Microbiol Rev* 58, 491–562.
- Strauss, E.G., Rice, C.M., and Strauss, J.H. (1983). Sequence coding for the alphavirus nonstructural proteins is interrupted by an opal termination codon. *PNAS* 80, 5271–5275.

- Strauss, E.G., De Groot, R.J., Levinson, R., and Strauss, J.H. (1992). Identification of the active site residues in the nsP2 proteinase of Sindbis virus. *Virology* 191, 932–940.
- Strnadova, P., Ren, H., Valentine, R., Mazzon, M., Sweeney, T.R., Brierley, I., and Smith, G.L. (2015). Inhibition of Translation Initiation by Protein 169: A Vaccinia Virus Strategy to Suppress Innate and Adaptive Immunity and Alter Virus Virulence. *PLOS Pathog.* 11, e1005151.
- Sutherland, B.W., Toews, J., and Kast, J. (2008). Utility of formaldehyde cross-linking and mass spectrometry in the study of protein–protein interactions. *Journal of Mass Spectrometry* 43, 699–715.
- Suzuki, Y., Chin, W.-X., Han, Q., Ichiyama, K., Lee, C.H., Eyo, Z.W., Ebina, H., Takahashi, H., Takahashi, C., Tan, B.H., et al. (2016). Characterization of RyDEN (C19orf66) as an Interferon-Stimulated Cellular Inhibitor against Dengue Virus Replication. *PLOS Pathogens* 12, e1005357.
- Sysoev, V.O., Fischer, B., Frese, C.K., Gupta, I., Krijgsveld, J., Hentze, M.W., Castello, A., and Ephrussi, A. (2016). Global changes of the RNA-bound proteome during the maternal-to-zygotic transition in *Drosophila*. *Nat Commun* 7, 12128.
- Tai, A.W., Benita, Y., Peng, L.F., Kim, S.-S., Sakamoto, N., Xavier, R.J., and Chung, R.T. (2009). A Functional Genomic Screen Identifies Cellular Cofactors of Hepatitis C Virus Replication. *Cell Host & Microbe* 5, 298–307.
- Takkinen, K., Peränen, J., and Kääriäinen, L. (1991). Proteolytic processing of Semliki Forest virus-specific non-structural polyprotein. *J Gen Virol* 72 ( Pt 7), 1627–1633.
- Tanaka, T., Kamitani, W., DeDiego, M.L., Enjuanes, L., and Matsuura, Y. (2012). Severe acute respiratory syndrome coronavirus nsp1 facilitates efficient propagation in cells through a specific translational shutoff of host mRNA. *J Virol* 86, 11128–11137.
- Tang, J., Jose, J., Chipman, P., Zhang, W., Kuhn, R.J., and Baker, T.S. (2011). Molecular links between the E2 envelope glycoprotein and nucleocapsid core in Sindbis virus. *J Mol Biol* 414, 442–459.
- Taylor, T.J., and Knipe, D.M. (2004). Proteomics of herpes simplex virus replication compartments: association of cellular DNA replication, repair, recombination, and chromatin remodeling proteins with ICP8. *J Virol* 78, 5856–5866.
- Tayri-Wilk, T., Slavin, M., Zamel, J., Blass, A., Cohen, S., Motzik, A., Sun, X., Shalev, D.E., Ram, O., and Kalisman, N. (2020). Mass spectrometry reveals the chemistry of formaldehyde cross-linking in structured proteins. *Nature Communications* 11, 3128.
- Tcherkezian, J., Cargnello, M., Romeo, Y., Huttlin, E.L., Lavoie, G., Gygi, S.P., and Roux, P.P. (2014). Proteomic analysis of cap-dependent translation identifies LARP1 as a key regulator of 5'TOP mRNA translation. *Genes Dev.* 28, 357–371.
- Tessarz, P., Santos-Rosa, H., Robson, S.C., Sylvestersen, K.B., Nelson, C.J., Nielsen, M.L., and Kouzarides, T. (2014). Glutamine methylation in histone H2A is an RNA-polymerase-I-dedicated modification. *Nature* 505, 564–568.
- Thaa, B., Biasiotto, R., Eng, K., Neuvonen, M., Götte, B., Rheinemann, L., Mutso, M., Utt, A., Varghese, F., Balistreri, G., et al. (2015). Differential Phosphatidylinositol-3-Kinase-Akt-mTOR

- Activation by Semliki Forest and Chikungunya Viruses Is Dependent on nsP3 and Connected to Replication Complex Internalization. *J Virol* 89, 11420–11437.
- Thiébeauld, O., Schepetilnikov, M., Park, H.-S., Geldreich, A., Kobayashi, K., Keller, M., Hohn, T., and Ryabova, L.A. (2009). A new plant protein interacts with eIF3 and 60S to enhance virus-activated translation re-initiation. *The EMBO Journal* 28, 3171–3184.
- Thoms, M., Buschauer, R., Ameisemeier, M., Koepke, L., Denk, T., Hirschenberger, M., Kratzat, H., Hayn, M., Mackens-Kiani, T., Cheng, J., et al. (2020). Structural basis for translational shutdown and immune evasion by the Nsp1 protein of SARS-CoV-2. *Science* 369, 1249–1255.
- Toribio, R., Díaz-López, I., and Ventoso, I. (2016a). New insights into the topology of the scanning ribosome during translation initiation: Lessons from viruses. *RNA Biology* 13, 1223–1227.
- Toribio, R., Díaz-López, I., Boskovic, J., and Ventoso, I. (2016b). An RNA trapping mechanism in Alphavirus mRNA promotes ribosome stalling and translation initiation. *Nucleic Acids Research* 44, 4368–4380.
- Tourrière, H., Chebli, K., Zekri, L., Courselaud, B., Blanchard, J.M., Bertrand, E., and Tazi, J. (2003). The RasGAP-associated endoribonuclease G3BP assembles stress granules. *J Cell Biol* 160, 823–831.
- Trendel, J., Schwarzl, T., Horos, R., Prakash, A., Bateman, A., Hentze, M.W., and Krijgsveld, J. (2018). The Human RNA-Binding Proteome and Its Dynamics during Translational Arrest. *Cell*.
- Tumer, N.E., Hwang, D.-J., and Bonness, M. (1997). C-terminal deletion mutant of pokeweed antiviral protein inhibits viral infection but does not depurinate host ribosomes. *PNAS* 94, 3866–3871.
- Tüting, C., Iacobucci, C., Ihling, C.H., Kastritis, P.L., and Sinz, A. (2020). Structural analysis of 70S ribosomes by cross-linking/mass spectrometry reveals conformational plasticity. *Sci Rep* 10, 12618.
- Ulmanen, I., Söderlund, H., and Kääriäinen, L. (1976). Semliki Forest virus capsid protein associates with the 60S ribosomal subunit in infected cells. *J. Virol.* 20, 203–210.
- Ulmanen, I., Söderlund, H., and Kääriäinen, L. (1979). Role of protein synthesis in the assembly of semliki forest virus nucleocapsid. *Virology* 99, 265–276.
- Valášek, L., Szamecz, B., Hinnebusch, A.G., and Nielsen, K.H. (2007). Chapter Eight - In Vivo Stabilization of Preinitiation Complexes by Formaldehyde Cross-Linking. In *Methods in Enzymology*, J. Lorsch, ed. (Academic Press), pp. 163–183.
- Vancini, R., Wang, G., Ferreira, D., Hernandez, R., and Brown, D.T. (2013). Alphavirus Genome Delivery Occurs Directly at the Plasma Membrane in a Time- and Temperature-Dependent Process. *Journal of Virology* 87, 4352–4359.
- Vandenbussche, F., Desmyter, S., Ciani, M., Proost, P., Peumans, W.J., and Damme, E.J.M.V. (2004). Analysis of the in planta antiviral activity of elderberry ribosome-inactivating proteins. *European Journal of Biochemistry* 271, 1508–1515.

- Vasiljeva, L., Merits, A., Auvinen, P., and Kääriäinen, L. (2000). Identification of a novel function of the alphavirus capping apparatus. RNA 5'-triphosphatase activity of Nsp2. *J Biol Chem* 275, 17281–17287.
- Vasiljeva, L., Merits, A., Golubtsov, A., Sizemskaja, V., Kääriäinen, L., and Ahola, T. (2003). Regulation of the sequential processing of Semliki Forest virus replicase polyprotein. *J Biol Chem* 278, 41636–41645.
- Vasudevan, D., Neuman, S.D., Yang, A., Lough, L., Brown, B., Bashirullah, A., Cardozo, T., and Ryoo, H.D. (2020). Translational induction of ATF4 during integrated stress response requires noncanonical initiation factors eIF2D and DENR. *Nat Commun* 11, 4677.
- Vattem, K.M., and Wek, R.C. (2004). Reinitiation involving upstream ORFs regulates ATF4 mRNA translation in mammalian cells. *PNAS* 101, 11269–11274.
- Vazeille, M., Moutailler, S., Coudrier, D., Rousseaux, C., Khun, H., Huerre, M., Thiria, J., Dehecq, J.-S., Fontenille, D., Schuffenecker, I., et al. (2007). Two Chikungunya Isolates from the Outbreak of La Reunion (Indian Ocean) Exhibit Different Patterns of Infection in the Mosquito, *Aedes albopictus*. *PLOS ONE* 2, e1168.
- Ventoso, I., Sanz, M.A., Molina, S., Berlanga, J.J., Carrasco, L., and Esteban, M. (2006). Translational resistance of late alphavirus mRNA to eIF2 $\alpha$  phosphorylation: a strategy to overcome the antiviral effect of protein kinase PKR. *Genes Dev.* 20, 87–100.
- Voss, J.E., Vaney, M.-C., Duquerroy, S., Vonrhein, C., Girard-Blanc, C., Crublet, E., Thompson, A., Bricogne, G., and Rey, F.A. (2010). Glycoprotein organization of Chikungunya virus particles revealed by X-ray crystallography. *Nature* 468, 709–712.
- Wada, M., Lokugamage, K.G., Nakagawa, K., Narayanan, K., and Makino, S. (2018). Interplay between coronavirus, a cytoplasmic RNA virus, and nonsense-mediated mRNA decay pathway. *Proceedings of the National Academy of Sciences of the United States of America* 115, E10157–E10166.
- Walker, M.J., Shortridge, M.D., Albin, D.D., Cominsky, L.Y., and Varani, G. (2020). Structure of the RNA Specialized Translation Initiation Element that Recruits eIF3 to the 5'-UTR of c-Jun. *Journal of Molecular Biology* 432, 1841–1855.
- Walsh, D., and Mohr, I. (2011). Viral subversion of the host protein synthesis machinery. *Nat. Rev. Microbiol.* 9, 860–875.
- Walsh, D., Mathews, M.B., and Mohr, I. (2013). Tinkering with Translation: Protein Synthesis in Virus-Infected Cells. *Cold Spring Harb Perspect Biol* 5, a012351.
- Wang, X., and Huang, L. (2008). Identifying Dynamic Interactors of Protein Complexes by Quantitative Mass Spectrometry. *Molecular & Cellular Proteomics* 7, 46–57.
- Wang, K.S., Kuhn, R.J., Strauss, E.G., Ou, S., and Strauss, J.H. (1992). High-affinity laminin receptor is a receptor for Sindbis virus in mammalian cells. *J Virol* 66, 4992–5001.
- Wang, L., He, Q., Gao, Y., Guo, X., Ge, X., Zhou, L., and Yang, H. (2012). Interaction of cellular poly(C)-binding protein 2 with nonstructural protein 1 $\beta$  is beneficial to Chinese highly pathogenic porcine reproductive and respiratory syndrome virus replication. *Virus Research* 169, 222–230.

- Wang, L., Fu, B., Li, W., Patil, G., Liu, L., Dorf, M.E., and Li, S. (2017a). Comparative influenza protein interactomes identify the role of plakophilin 2 in virus restriction. *Nat Commun* 8, 13876.
- Wang, R., Simoneau, C.R., Kulsuptrakul, J., Bouhaddou, M., Travisano, K.A., Hayashi, J.M., Carlson-Stevermer, J., Zengel, J.R., Richards, C.M., Fozouni, P., et al. (2021). Genetic Screens Identify Host Factors for SARS-CoV-2 and Common Cold Coronaviruses. *Cell* 184, 106-119.e14.
- Wang, X., Chemmama, I.E., Yu, C., Huszagh, A., Xu, Y., Viner, R., Block, S.A., Cimermancic, P., Rychnovsky, S.D., Ye, Y., et al. (2017b). The Proteasome-Interacting Ecm29 Protein Disassembles the 26S Proteasome in Response to Oxidative Stress. *J. Biol. Chem.* jbc.M117.803619.
- Wang, X., Xuan, Y., Han, Y., Ding, X., Ye, K., Yang, F., Gao, P., Goff, S.P., and Gao, G. (2019). Regulation of HIV-1 Gag-Pol Expression by Shiftless, an Inhibitor of Programmed -1 Ribosomal Frameshifting. *Cell* 176, 625-635.e14.
- Wang, Y.F., Sawicki, S.G., and Sawicki, D.L. (1994). Alphavirus nsP3 functions to form replication complexes transcribing negative-strand RNA. *J Virol* 68, 6466–6475.
- Waterbeemd, M. van de, Tamara, S., Fort, K.L., Damoc, E., Franc, V., Bieri, P., Itten, M., Makarov, A., Ban, N., and Heck, A.J.R. (2018). Dissecting ribosomal particles throughout the kingdoms of life using advanced hybrid mass spectrometry methods. *Nat. Commun.* 9, 2493.
- Weaver, S.C., and Forrester, N.L. (2015). Chikungunya: Evolutionary history and recent epidemic spread. *Antiviral Res* 120, 32–39.
- Wei, J., Alfajaro, M.M., DeWeirdt, P.C., Hanna, R.E., Lu-Culligan, W.J., Cai, W.L., Strine, M.S., Zhang, S.-M., Graziano, V.R., Schmitz, C.O., et al. (2021). Genome-wide CRISPR Screens Reveal Host Factors Critical for SARS-CoV-2 Infection. *Cell* 184, 76-91.e13.
- Weirich, C.S., Erzberger, J.P., and Barral, Y. (2008). The septin family of GTPases: architecture and dynamics. *Nat Rev Mol Cell Biol* 9, 478–489.
- Wengler, G. (1987). The mode of assembly of alphavirus cores implies a mechanism for the disassembly of the cores in the early stages of infection. *Arch. Virol.* 94, 1–14.
- Wengler, G. (2009). The regulation of disassembly of alphavirus cores. *Arch. Virol.* 154, 381–390.
- Wengler, G., and Wengler, G. (1984). Identification of a transfer of viral core protein to cellular ribosomes during the early stages of alphavirus infection. *Virology* 134, 435–442.
- Wengler, G., and Wengler, G. (2002). In vitro analysis of factors involved in the disassembly of Sindbis virus cores by 60S ribosomal subunits identifies a possible role of low pH. *J. Gen. Virol.* 83, 2417–2426.
- Wengler, G., Wengler, G., Boege, U., and Wahn, K. (1984). Establishment and analysis of a system which allows assembly and disassembly of alphavirus core-like particles under physiological conditions in vitro. *Virology* 132, 401–412.
- Wickham, H. (2009). *ggplot2: Elegant Graphics for Data Analysis* (New York: Springer-Verlag).

- Wild, T., Horvath, P., Wyler, E., Widmann, B., Badertscher, L., Zemp, I., Kozak, K., Csucs, G., Lund, E., and Kutay, U. (2010). A Protein Inventory of Human Ribosome Biogenesis Reveals an Essential Function of Exportin 5 in 60S Subunit Export. *PLOS Biology* 8, e1000522.
- Wilkinson, T.A., Tellinghuisen, T.L., Kuhn, R.J., and Post, C.B. (2005). Association of sindbis virus capsid protein with phospholipid membranes and the E2 glycoprotein: implications for alphavirus assembly. *Biochemistry* 44, 2800–2810.
- Willems, W.R., Kaluza, G., Boschek, C.B., Bauer, H., Hager, H., Schütz, H.J., and Feistner, H. (1979). Semliki forest virus: cause of a fatal case of human encephalitis. *Science* 203, 1127–1129.
- Wright, P.J., and Cooper, P.D. (1974). Poliovirus proteins associated with ribosomal structures in infected cells. *Virology* 59, 1–20.
- Wu, Y., Yang, X., Yao, Z., Dong, X., Zhang, D., Hu, Y., Zhang, S., Lin, J., Chen, J., An, S., et al. (2020). C19orf66 interrupts Zika virus replication by inducing lysosomal degradation of viral NS3. *PLOS Neglected Tropical Diseases* 14, e0008083.
- Wurth, L., Gribbling-Burrer, A.-S., Verheggen, C., Leichter, M., Takeuchi, A., Baudrey, S., Martin, F., Krol, A., Bertrand, E., and Allmang, C. (2014). Hypermethylated-capped selenoprotein mRNAs in mammals. *Nucleic Acids Research* 42, 8663–8677.
- Yamada, S.B., Gendron, T.F., Niccoli, T., Genuth, N.R., Grosely, R., Shi, Y., Glaria, I., Kramer, N.J., Nakayama, L., Fang, S., et al. (2019). RPS25 is required for efficient RAN translation of C9orf72 and other neurodegenerative disease-associated nucleotide repeats. *Nat Neurosci* 22, 1383–1388.
- Yang, Y., and Wang, Z. (2019a). IRES-mediated cap-independent translation, a path leading to hidden proteome. *Journal of Molecular Cell Biology* 11, 911–919.
- Yang, Y., and Wang, Z. (2019b). IRES-mediated cap-independent translation, a path leading to hidden proteome. *Journal of Molecular Cell Biology* 11, 911–919.
- Yángüez, E., Hunziker, A., Dobay, M.P., Yildiz, S., Schading, S., Elshina, E., Karakus, U., Gehrig, P., Grossmann, J., Dijkman, R., et al. (2018). Phosphoproteomic-based kinase profiling early in influenza virus infection identifies GRK2 as antiviral drug target. *Nature Communications* 9, 3679.
- Yoo, D., Wootton, S.K., Li, G., Song, C., and Rowland, R.R. (2003). Colocalization and interaction of the porcine arterivirus nucleocapsid protein with the small nucleolar RNA-associated protein fibrillarin. *J Virol* 77, 12173–12183.
- Yoon, A., Peng, G., Brandenburger, Y., Brandenburg, Y., Zollo, O., Xu, W., Rego, E., and Ruggero, D. (2006). Impaired control of IRES-mediated translation in X-linked dyskeratosis congenita. *Science* 312, 902–906.
- Yoshimi, K., Kunihiro, Y., Kaneko, T., Nagahora, H., Voigt, B., and Mashimo, T. (2016). ssODN-mediated knock-in with CRISPR-Cas for large genomic regions in zygotes. *Nat Commun* 7, 10431.
- Zhang, H., Fang, L., Zhu, X., Wang, D., and Xiao, S. (2018a). Global analysis of ubiquitome in PRRSV-infected pulmonary alveolar macrophages. *Journal of Proteomics* 184, 16–24.
- Zhang, N., Zhao, H., and Zhang, L. (2019). Fatty Acid Synthase Promotes the Palmitoylation of Chikungunya Virus nsP1. *J Virol* 93, e01747-18.

Zhang, R., Kim, A.S., Fox, J.M., Nair, S., Basore, K., Klimstra, W.B., Rimkunas, R., Fong, R.H., Lin, H., Poddar, S., et al. (2018b). Mxra8 is a receptor for multiple arthritogenic alphaviruses. *Nature* 557, 570–574.

Zhang, X., Fugère, M., Day, R., and Kielian, M. (2003). Furin processing and proteolytic activation of Semliki Forest virus. *J Virol* 77, 2981–2989.

Zhu, F., Zhou, Y.-K., Ji, Z.-L., and Chen, X.-R. (2018). The Plant Ribosome-Inactivating Proteins Play Important Roles in Defense against Pathogens and Insect Pest Attacks. *Front. Plant Sci.* 9.

Zhu, Y., Feng, F., Hu, G., Wang, Y., Yu, Y., Zhu, Y., Xu, W., Cai, X., Sun, Z., Han, W., et al. (2021). A genome-wide CRISPR screen identifies host factors that regulate SARS-CoV-2 entry. *Nat Commun* 12, 961.



## Annex 1

### Genome editing in primary cells and *in vivo* using viral-derived Nanoblades loaded with Cas9-sgRNA ribonucleoproteins

CRISPR-Cas9 systems – and derivatives – have revolutionized biology in the last decades. The RNA-guided Cas9 endonuclease has proved itself to be a fantastic tool for genome editing, and allows precise and specific genome manipulation such as knock-out, homologous-directed-recombination (HDR) assisted mutation corrections, and HDR assisted protein tagging. Since its first release in 2013, the toolbox of RNA-guided endonucleases has expanded and is not restricted to genome manipulation anymore. Cas9 (and other related nucleases) can be fused with transcriptional activators, transcriptional repressors, epigenetic modifiers to permit gene expression levels alteration.

A second major direction in which this toolbox was improved concerns the delivery of the system. The transfection of plasmids encoding for Cas9 and the sgRNA has proved very efficient in cells that can be easily transfected, yet it is unusable with a large number of cell lines, and more so in primary cells and *in vivo*. Now the most widely used strategies rely on gene delivery of the CRISPR-Cas9 system by lentiviral vector, as well as electroporation of the Cas9-sgRNA ribonucleoprotein (RNP) complex. Although they have increased the number of cell lines that can be targeted by CRISPR-Cas9 related systems, these strategy still suffer major hurdles. Lentiviral vector delivery induces random gene insertion of the CRISPR-Cas9 cassette and continuous expression of the Cas9 and the sgRNA. This leads to accumulation of unwanted editing in cells at off-target sites, owing to the limited specificity of Cas9. Because electroporation of the RNP leads to time-limited presence of the complex, offtargets are strongly reduced. Yet, not all cell type support electroporation and it is inapplicable *in vivo*.

This works describe the development of *Nanoblades*, a method that provides the benefits of the two strategies detailed earlier without their limitations. *Nanoblades* are viral-like particles based on Murine Leukemia Virus, that deliver the RNP into recipient cells, without relying on genetic material transfer. In this system, the Cas9 is fused to MLV Gag by proteolytic peptide, which

addresses Cas9 to the membrane. There, a pair of two envelope proteins induce the formation of viral-like particles, that can later fuse with the recipient cell membrane. Because of the high affinity of Cas9 for its gRNA, the latter is similarly picked up by the particles. Once encapsulated, the Gag-Cas9 fusion is cleaved by MLV protease, and Cas9 is delivered into the recipient cells to accomplish genome editing. We show that this method is highly-efficient in a wide number of cell lines, as well as primary cells, and show that it allows *in vivo* genome editing as well. Thanks to the transient presence of the Cas9-gRNA RNP, off-targets are strongly decreased as well.





My contribution to this work can be found on Figure 3. I designed the strategy for DDX3X Flag tagging and optimized it in transfected cells before it was adapted to *Nanoblade*-assisted tagging. I also designed and performed the experiment of gene expression activation of the TTN gene by the *Nanoblade* variant delivering the Cas9-VPR transcription activation complex.

ARTICLE

<https://doi.org/10.1038/s41467-018-07845-z>

OPEN

# Genome editing in primary cells and in vivo using viral-derived Nanoblades loaded with Cas9-sgRNA ribonucleoproteins

Philippe E. Mangeot<sup>1</sup>, Valérie Risson<sup>2</sup>, Floriane Fusil<sup>1</sup>, Aline Marnef<sup>3</sup>, Emilie Laurent<sup>1</sup>, Juliana Blin <sup>1</sup>, Virginie Mournetas<sup>4</sup>, Emmanuelle Massouridès <sup>4</sup>, Thibault J.M. Sohier <sup>1</sup>, Antoine Corbin<sup>1</sup>, Fabien Aubé<sup>5</sup>, Marie Teixeira<sup>6</sup>, Christian Pinset<sup>4</sup>, Laurent Schaeffer<sup>2</sup>, Gaëlle Legube<sup>3</sup>, François-Loïc Cosset<sup>1</sup>, Els Verhoeyen<sup>1,7</sup>, Théophile Ohlmann<sup>1</sup> & Emiliano P. Ricci <sup>1,5</sup>

Programmable nucleases have enabled rapid and accessible genome engineering in eukaryotic cells and living organisms. However, their delivery into target cells can be technically challenging when working with primary cells or in vivo. Here, we use engineered murine leukemia virus-like particles loaded with Cas9-sgRNA ribonucleoproteins (Nanoblades) to induce efficient genome-editing in cell lines and primary cells including human induced pluripotent stem cells, human hematopoietic stem cells and mouse bone-marrow cells. Transgene-free Nanoblades are also capable of in vivo genome-editing in mouse embryos and in the liver of injected mice. Nanoblades can be complexed with donor DNA for “all-in-one” homology-directed repair or programmed with modified Cas9 variants to mediate transcriptional up-regulation of target genes. Nanoblades preparation process is simple, relatively inexpensive and can be easily implemented in any laboratory equipped for cellular biology.

<sup>1</sup>CIRI, Centre International de Recherche en Infectiologie Univ Lyon, Inserm, U1111, Université Claude Bernard Lyon 1, CNRS, UMR5308, ENS de Lyon, F-69007 Lyon, France. <sup>2</sup>Institut NeuroMyoGène, CNRS 5310, INSERM U121, Université Lyon 1, Faculté de Médecine Lyon Est, Lyon 69008, France. <sup>3</sup>LBCMCP, Centre de Biologie Intégrative (CBI), CNRS, Université de Toulouse, UT3, 118 Route de Narbonne, 31062 Toulouse, France. <sup>4</sup>I-STEM/CECS, Inserm, UMR861 28 rue Henri Desbrières, 91100 Corbeil Essonnes, France. <sup>5</sup>LBMC, Laboratoire de Biologie et Modélisation de la Cellule Univ Lyon, ENS de Lyon, Université Claude Bernard Lyon 1, CNRS, UMR 5239, INSERM, U1210, Lyon 69007, France. <sup>6</sup>SFR BioSciences, Plateau de Biologie Expérimentale de la Souris (AniRA-PBES), Ecole Normale Supérieure de Lyon, Université Lyon1, CNRS UMS3444 INSERM US8, 69007 Lyon, France. <sup>7</sup>Present address: CIRI, Université Côte d’Azur, INSERM, C3M, 06204 Nice, France. These authors contributed equally: Valérie Risson, Floriane Fusil, Aline Marnef. Correspondence and requests for materials should be addressed to P.E.M. (email: [philippe.mangeot@inserm.fr](mailto:philippe.mangeot@inserm.fr)) or to E.P.R. (email: [emiliano.ricci@ens-lyon.org](mailto:emiliano.ricci@ens-lyon.org))

Targeted genome editing tools, such as meganucleases (MGN), zinc-finger nucleases (ZFN), transcription activator-like effector nucleases (TALENs) and more recently the clustered regularly interspaced short palindromic repeats (CRISPR) have revolutionized most biomedical research fields. Such tools allow to precisely edit the genome of eukaryotic cells by inducing double-stranded DNA (dsDNA) breaks at specific loci. Relying on the cell endogenous repair pathways, dsDNA breaks can then be repaired by non-homologous end-joining (NHEJ) or homology-directed repair (HDR) allowing the removal or insertion of new genetic information at a desired locus.

Among the above-mentioned tools, CRISPR-Cas9 is currently the most simple and versatile method for genome engineering. Indeed, in the two-component system, the bacterial-derived nuclease Cas9 (for CRISPR-associated protein 9) associates with a single-guide RNA (sgRNA) to target a complementary DNA sequence and induce a dsDNA break<sup>1</sup>. Therefore, by the simple modification of the sgRNA sequence, users can specify the genomic locus to be targeted. Consistent with the great promises of CRISPR-Cas9 for genome engineering and gene therapy, considerable efforts have been made in developing efficient tools to deliver the Cas9 and the sgRNA into target cells *ex vivo* either by transfection of plasmids coding for the nucleases, transduction with viral-derived vectors coding for the nucleases or by direct injection or electroporation of Cas9-sgRNA complexes into cells.

Here, we have designed Nanoblades, a protein-delivery vector based on friend murine leukemia virus (MLV) that allows the transfer of Cas9-sgRNA ribonucleoproteins (RNPs) to cell lines and primary cells *in vitro* and *in vivo*. Nanoblades deliver the ribonucleoprotein cargo in a transient and rapid manner without delivering a transgene and can mediate knock-in in cell lines when complexed with a repair template. Nanoblades can also be programmed with modified Cas9 proteins to mediate transient transcriptional activation of targeted genes.

## Results

**Cas9-sgRNA RNP delivery through MLV virus-like particles (VLPs).** Assembly of retroviral particles relies on the viral structural Gag polyprotein, which multimerizes at the cell membrane and is sufficient, when expressed in cultured cells, to induce release of VLPs into the cell supernatant<sup>2</sup>. When Gag is coexpressed together with a fusogenic viral envelope, pseudotyped VLPs are produced that lack a viral genome but still retain their capacity to fuse with target cells and deliver the Gag protein into their cytoplasm. As previously investigated<sup>3,4</sup>, we took advantage of the structural role of Gag and designed an expression vector coding for the MLV Gag polyprotein fused, at its C-terminal end, to a flag-tagged version of *Streptococcus pyogenes* Cas9 protein (Gag::Cas9, Fig. 1a). The two fused proteins are separated by a proteolytic site which can be cleaved by the MLV protease to release the Flag-tagged Cas9 (Fig. 1a). By cotransfecting HEK-293T cells with plasmids coding for Gag::Cas9, Gag-Pro-Pol, a sgRNA, and viral envelopes, fusogenic VLPs are produced and released in the culture medium (herein described as Nanoblades). Biochemical and imaging analysis of purified particles (Supplementary Figure 1a, 1b, 1c and 1d) indicates that Nanoblades (150 nm) are slightly larger than wild-type MLV (Supplementary Figure 1b) but sediment at a density of 1.17 g/ml (Supplementary Figure 1c) as described for MLV VLPs<sup>5</sup>. As detected by western blot, Northern blot, mass-spectrometry, and deep-sequencing, Nanoblades contain the Cas9 protein and sgRNA (Supplementary Figure 1 and 2 and Supplementary Data 1). In addition to Gag, Cas9 and envelope proteins,

mass-spectrometry analysis of Nanoblades identified several cellular proteins, mostly membrane-associated proteins (Supplementary Figure 2a and Supplementary Data 1). Interestingly, the packaging of sgRNA depends on the presence of the Gag::Cas9 fusion protein, since Nanoblades produced from cells that only express the Gag protein fail to incorporate detectable amounts of sgRNA (Supplementary Figure 1d). Furthermore, Cas9-dependent loading of the sgRNA within Nanoblades is not limited by the efficiency of the interaction between the Cas9 and the sgRNA, since expressing an optimized version of the sgRNA that improves binding to Cas9<sup>6</sup> does not appear to increase sgRNA levels within purified VLPs (Supplementary Figure 1d see sgRNA(F+E)).

To assess for Cas9-sgRNA RNP delivery efficiency in target cells and induction of genomic dsDNA breaks, we designed Nanoblades with a sgRNA targeting the 45S rDNA loci. Human 45S rDNA genes are present in hundreds of tandem repeats across five autosomes, locate in the nucleolus and are transcribed exclusively by RNA polymerase (Pol) I<sup>7</sup>. Using immunofluorescence microscopy, it is therefore possible to follow the occurrence of dsDNA breaks at rDNA loci with single-cell resolution by monitoring the nucleolus using the nucleolar marker RNA Pol I and the well-established dsDNA break-marker, histone variant  $\gamma$ -H2AX<sup>8</sup>, that localizes at the nucleolar periphery after dsDNA break induction within rDNA<sup>9</sup>. U2OS (osteosarcoma cell line) cells transduced for 24 h with Nanoblades programmed with a sgRNA targeting rDNA display the typical  $\gamma$ -H2AX distribution at the nucleolar periphery with RNA Pol I, indicative of rDNA breaks, whilst cells transduced with Nanoblades with control sgRNAs do not (Fig. 1b, top panel). Interestingly, this distribution of  $\gamma$ -H2AX at the nucleolar periphery can be observed as early as 4 h after transduction in 60% of cells with a maximum effect observed at 16 h after transduction, where almost 100% of observed cells display this  $\gamma$ -H2AX distribution (Fig. 1b, bottom panel and quantification below). In comparison, only 60% of cells transfected with a plasmid coding for Cas9 and the sgRNA display the perinucleolar  $\gamma$ -H2AX/RNA Pol I localization 24 h after transfection. Similar results were obtained in human primary fibroblasts with more than 85% cells displaying this distribution after 16 h (Supplementary Figure 1e). These results suggest that Nanoblade-mediated delivery of the Cas9-sgRNA RNP is both efficient and rapid in cell lines and primary human cells. To further confirm these results, we designed and dosed Nanoblades (by ELISA assay using anti-Cas9 antibodies) programmed with a sgRNA widely used in the literature<sup>10</sup> that targets the human *EMX1* gene to induce dsDNA cleavage at a single locus. HEK-293T cells were then transduced with increasing amounts of Nanoblades and gene editing was measured from the bulk population 48 h after transduction (Fig. 1c). Under these conditions, we observed a dose-dependent effect of Nanoblades ranging from 35% of *EMX1* (at 4 pmol of Cas9) editing to 77% of editing at the highest dose (20 pmol) of Cas9 (Fig. 1c).

Because Nanoblades carry cellular proteins from producer cells in addition to Cas9 (Supplementary Data 1), we tested whether these proteins could also be delivered to recipient cells. For this, we over-expressed the firefly luciferase in producer cells and collected Nanoblades targeting *EMX1* from the supernatant. Luciferase-loaded Nanoblades were then used to transduce HEK293T cells for 24 h. Cells were then washed twice in PBS and incubated in fresh medium for 4, 8, 24, and 48 h. Luciferase activity was measured at each time point, as well as in input Nanoblades (Supplementary Figure 2c). As observed, we could detect a mild luciferase signal (4–6% of input) at 4 and 8 h upon transduction. However, the signal rapidly faded at 24 h (2% of input) and

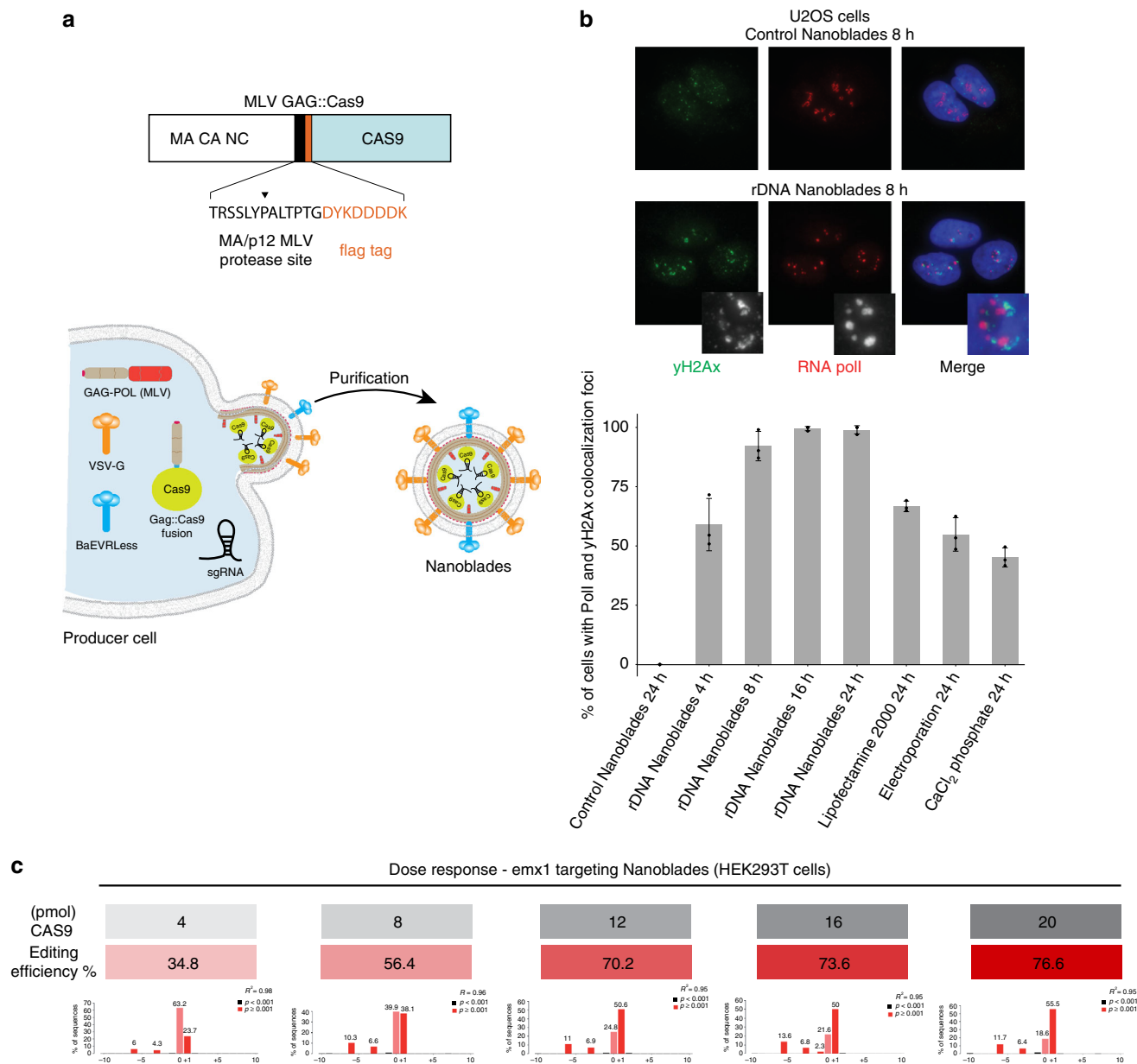
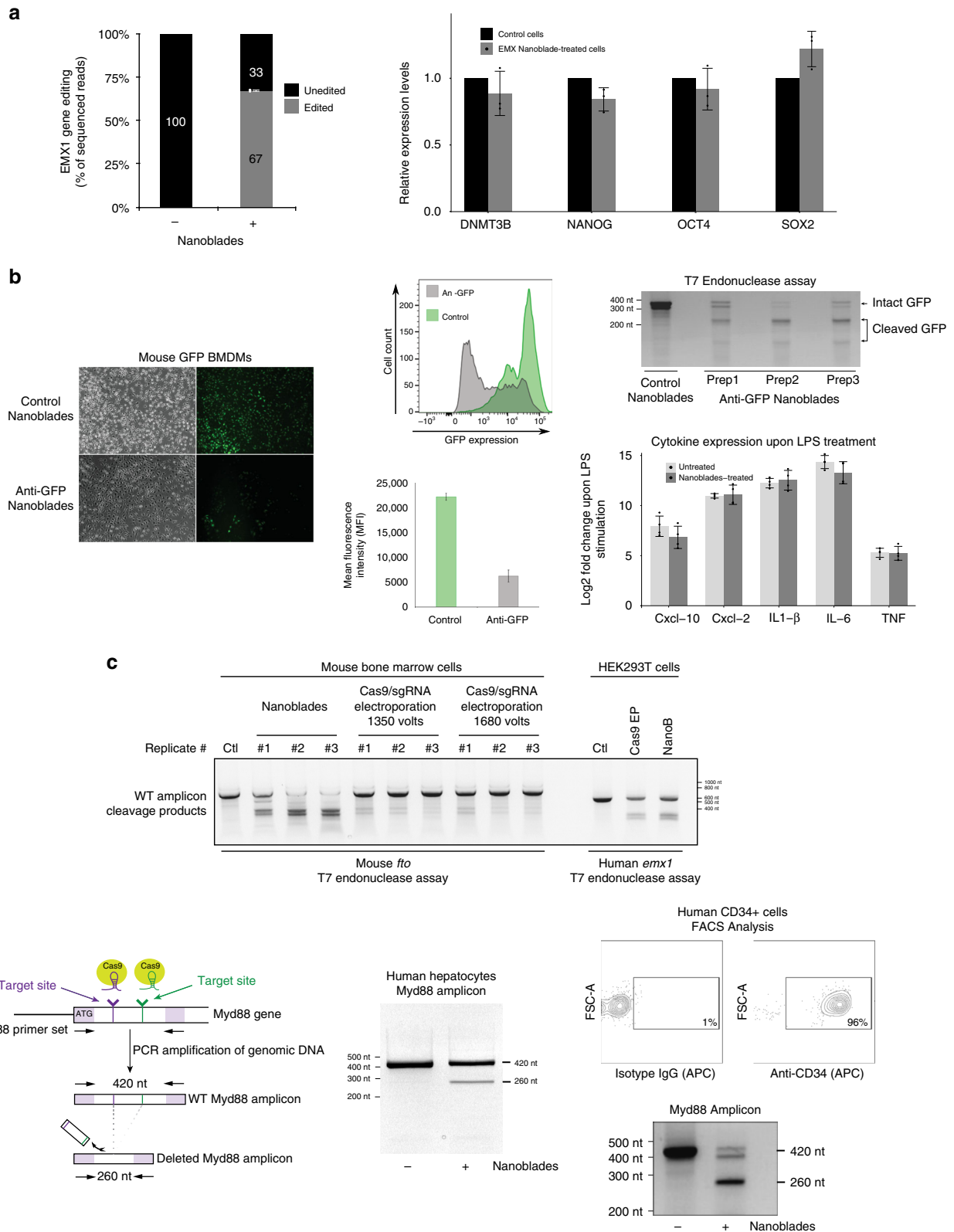


**Fig. 1** Nanoblade-mediated genome editing. **a** Scheme describing the MLV Gag::Cas9 fusion and the Nanoblade production protocol based on the transfection of HEK-293T cells by plasmids coding for Gag-Pol, Gag::Cas9, VSV-G, BaEVRLess, and the sgRNA. **b** Top panel, immunofluorescence analysis of  $\gamma$ -H2AX (green), RNA poll (red) in U2OS cells 8 h after being transduced with control Nanoblades or with Nanoblades targeting ribosomal DNA genes. Bottom panel, quantification of  $\gamma$ -H2AX and RNA poll colocalization foci in U2OS cells at different times after Nanoblades transduction or after classical DNA transfection methods ( $n = 3$ , error bars correspond to standard deviation). **c** Dose response of Nanoblades. HEK-293T cells were transduced with increasing amounts of Nanoblades targeting human *EMX1* ( $n = 1$  displayed). The exact amount of Cas9 used for transduction was measured by dot blot (in gray). Genome editing was assessed by Sanger sequencing and Tide analysis (in red)

was almost undetectable at 48 h (Supplementary Figure 2c). In addition to the ectopically expressed firefly luciferase, we also investigated transmission of the CD81 cell-surface protein, which is highly expressed in HEK293T producer cells and is present in Nanoblades as revealed by mass spectrometry (Supplementary Data 1). HepG2 cells, a hepatic cell line that lacks CD81 expression<sup>11</sup>, were transduced for 24 h with Nanoblades targeting *EMX1* and then washed twice with PBS before monitoring CD81 residual signal immediately after the washes or 8 and 48 h after incubation with fresh medium (Supplementary Figure 2d). As observed, even though CD81 was very abundant at the cell surface of producer cells

and completely absent in recipient cells (Supplementary Figure 2d, left and middle panels), we could only detect a mild CD81 signal immediately after transduction (see Supplementary Figure 2d, right panel). Later time points (8 and 48 h) did not show any specific CD81 labeling in recipient HepG2 cells. The impact of cellular proteins delivered by Nanoblades into recipient cells appears therefore limited and restricted to a short time frame.

Taken together, our results indicate that Nanoblades can be efficiently used to mediate genome editing in a rapid and dose-dependent manner with limited impact on the proteome of target cells.



**Nanoblades-mediated genome editing in primary cells.** Genome editing in primary cells and patient-derived pluripotent cells represents a major interest both for basic science and therapeutical applications. However, primary cells are often refractory to DNA transfection and other gene delivery methods. Because Nanoblades were capable of efficient delivery of functional Cas9-sgRNA RNPs into primary fibroblasts, we tested whether they

were effective in other primary cells for genome editing. To this aim, Nanoblades targeting *EMX1* were used to transduce human-induced pluripotent stem cells (hiPSCs). Genome editing at the *EMX1* locus was assessed in the bulk cellular population 48 h after transduction by deep-sequencing of the *EMX1* locus (Fig. 2a, left panel). As observed, Nanoblades were capable of mediating 67% genome editing at the *EMX1* locus in hiPSCs. Notably, hiPSCs



**Fig. 2** Genome editing in primary cells transduced with Nanoblades. **a** Left panel, editing efficiency at the *EMX1* locus (measured by high-throughput sequencing on the Illumina Miseq platform) of human-induced pluripotent stem cells (hiPSCs) transduced with Nanoblades targeting human *EMX1* ( $n = 3$ ). Right panel, expression of pluripotency markers measured by qPCR in control cells and cells transduced with Nanoblades targeting *EMX1* ( $n = 3$ ). **b** Left and middle panels, fluorescence microscopy and FACS analysis of GFP expressing BMDMs transduced at the bone marrow stage (day 0 after bone marrow collection) with control Nanoblades or Nanoblades targeting the *GFP*-coding sequence ( $n = 3$ ). Right top panel, T7 endonuclease assay against the GFP sequence from Nanoblades-treated BMDMs. Right bottom panel, cytokine expression levels (measured by qPCR) in untreated or Nanoblade-treated cells upon LPS stimulation ( $n = 4$ ). **c** T7 endonuclease assay against mouse *Fto* or human *EMX1* genomic sequences amplified by PCR from primary mouse bone marrow cells transduced with Nanoblades or electroporated with recombinant Cas9-sgRNA RNPs. For bone marrow cells, two electroporation settings were tested. Lanes numbered #1–#3 correspond to biological replicates. Editing efficiencies were calculated by TIDE<sup>13</sup> analysis of the Sanger sequencing electropherograms for each PCR amplicon **d** Left panel, excision of a 160 bp DNA fragment of *MYD88* using Nanoblades. Middle panel PCR results obtained in human primary hepatocytes transduced with Nanoblades. Right-panel (top), FACS analysis of CD34+ cells purified from human cord-blood. Bottom, genome editing at the *MYD88* locus assessed by PCR in untreated and Nanoblades-treated CD34+ cells. Error bars in all figures correspond to standard deviation

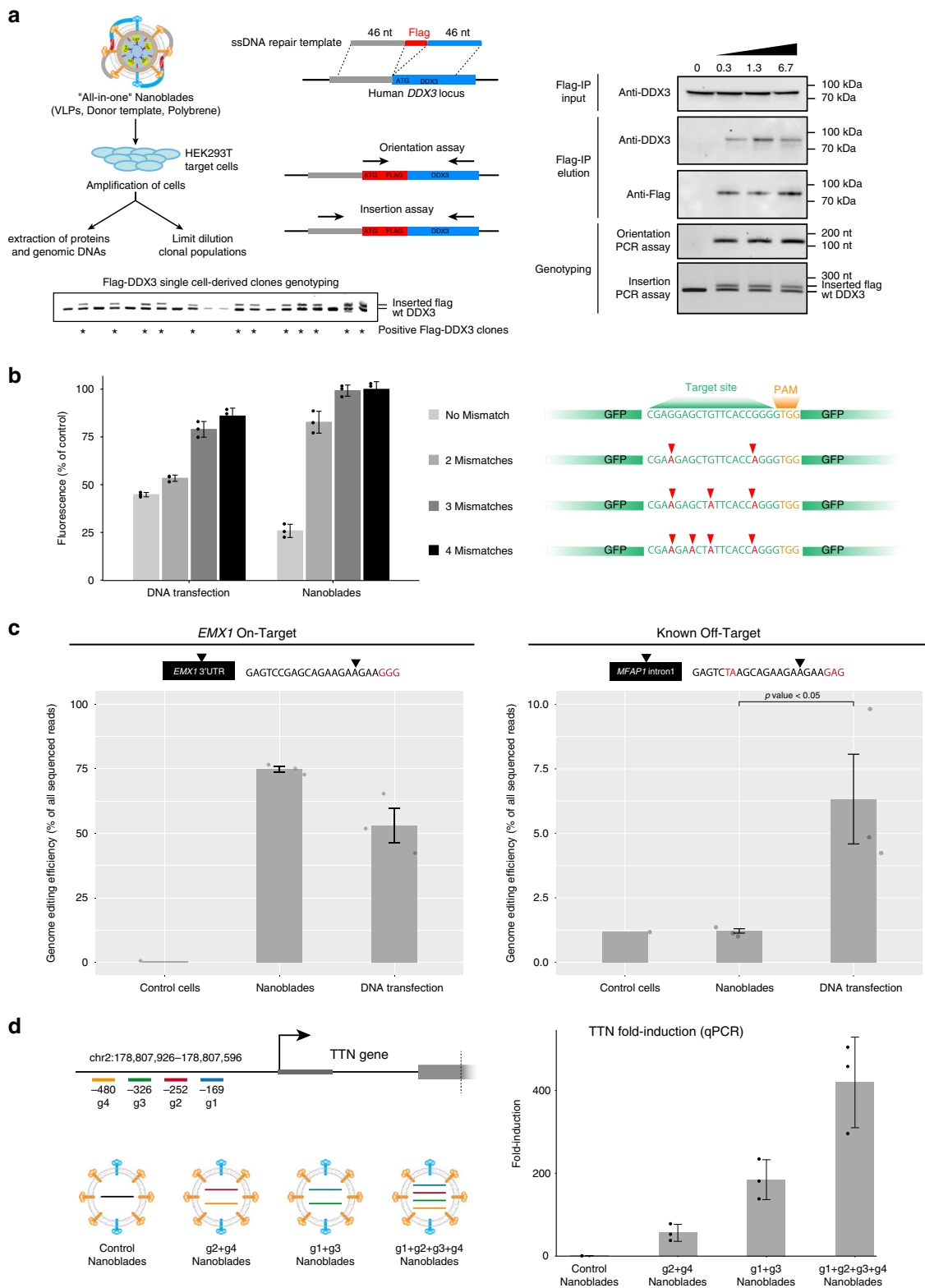
treated with *EMX1* Nanoblades maintained constant levels of pluripotency markers compared to control cells (Fig. 2a, right panel) thus indicating that their multipotent status did not appear to be affected.

Similarly to hiPSCs, mouse bone marrow (BM) cells can be collected and differentiated in vitro into various hematopoietic cell types, such as macrophages (bone marrow-derived macrophages or BMDMs) and dendritic cells. Efficient genome editing of specific genes in BM cells would therefore allow for the corresponding pre-existing protein to be degraded during differentiation and obtain a functional knockout. To test this hypothesis, BM cells obtained from GFP transgenic mice<sup>12</sup> were transduced with Nanoblades programmed with a sgRNA targeting the *GFP* coding sequence. 6 h after transduction, cells were washed and incubated in presence of macrophage colony-stimulating factor (M-CSF) for 1 week. After this, cells were collected to monitor GFP levels by fluorescence microscopy, FACS and genome editing by T7 endonuclease assay (Fig. 2b). We consistently obtained close to 75% reduction of GFP expression as measured by FACS analysis and around 60–65% genome editing at the *GFP* locus as measured by T7 endonuclease assays (Fig. 2b). Importantly, genome editing through Nanoblades did not affect the capacity of BMDMs to respond to LPS as their cytokine expression remains identical to that of untreated control cells (Fig. 2b bottom right panel). Nanoblades can therefore be used to inactivate genes in BM cells and study their function in differentiated cells. To further complement these results, we compared the efficiency of Nanoblades to that of recombinant Cas9-sgRNA RNP electroporation in targeting an endogenous gene in primary mouse BM cells. For this, Nanoblades or Cas9-sgRNA RNPs programmed to target the *Fto* gene were used, respectively, to transduce or electroporate primary BM cells freshly extracted from mice. As a control, Nanoblades or Cas9-sgRNA RNPs programmed to target human *EMX1* were also tested in HEK293T cells. In both cases, the efficiency of genome editing was assessed 24 h after transduction or electroporation. As observed (Fig. 2c), both Nanoblades and Cas9-sgRNA electroporation mediate efficient genome editing in HEK293T at 71% (Nanoblades) and 44% (Electroporation) of editing efficiency at the *EMX1* locus. Interestingly, in primary BM cells, while Nanoblades achieve highly efficient genome editing of the *Fto* locus (up to 76% as measured by TIDE<sup>13</sup> analysis), Cas9 electroporation was much less efficient at both conditions that we tested (1350 and 1680 V) yielding a mild but visible signal in the T7 endonuclease assay which was nevertheless below the detection limit for TIDE analysis. Interestingly both protocols (Nanoblades and protein electroporation) did not have an important impact on cell viability 24 h after Cas9 delivery (Supplementary Figure 2e).

Nanoblades efficiency was also investigated in human cells that represent a major interest in research and gene therapy like human primary hepatocytes and human hematopoietic stem cells (HSCs) that both have the capacity to colonize and regenerate fully functional tissues. For both these cell types, Nanoblades programmed with two sgRNAs targeting the human *Myd88* gene were prepared and achieved significant cleavage efficiencies, as revealed by flanking PCR assays (Fig. 2d). Interestingly, HSCs are difficult to transduce with classic VSV-G pseudotyped lentiviral vectors (LVs) because they lack the LDL receptor<sup>14</sup>, a limitation that can be alleviated by the use of the baboon retroviral envelope glycoprotein (BaEV)<sup>15</sup>. This prompted us to equip Nanoblades with both BaEV and VSV G-envelopes for these cells and finally in all our study as the combination of both envelopes improved Cas9 delivery in most cells (Supplementary Figure 6a and b). As observed, Nanoblades were also able to induce genome editing in these cells (50% genome editing based on T7 endonuclease assay, Fig. 2d) thus expanding the catalog of primary cells that can be edited using Nanoblades.

Taken together, our results indicate that Nanoblades are an efficient delivery system to induce rapid and effective genome editing in murine and human primary cells of high therapeutic value that are notoriously difficult to transfect.

**“All-in-one” Nanoblades for homology directed repair.** Precise insertion of genetic material (also known as Knock-in) using CRISPR-Cas9 can be achieved through HDR. This occurs when a donor DNA template with sequence homology to the region surrounding the targeted genomic locus is provided to cells together with the Cas9-sgRNA RNP. Based on a previous finding showing that retroviral-particles can be complexed with DNA in the presence of polybrene to allow for virus-dependent DNA transfection<sup>16</sup>, we tested whether Nanoblades could be directly complexed with a DNA template to mediate HDR in target cells. To test this approach, Nanoblades programmed to target a locus close to the AUG start codon of the human *DDX3* gene were complexed to a single-stranded DNA oligomer bearing the FLAG-tag sequence flanked with 46 nucleotide (nt) homology arms corresponding to the region surrounding the start-codon of *DDX3* (Fig. 3a, left panel). HEK293T were transduced with these “All-in-one” Nanoblades and passed 6 times before assessing HDR efficiency in the bulk cellular population both by PCR and by Flag-immunoprecipitation followed by western-blotting (using a *DDX3* and FLAG-antibody). As observed (Fig. 3a, right panel), cells transduced with “All-in-one” Nanoblades showed incorporation of the FLAG-tag at the *DDX3* locus both genetically and at the level of protein expression (Fig. 3a right panel, see Flag-IP elution and Genotyping panels). In parallel, single-cell



clones were derived from the Flag-DDX3 bulk population and tested for Flag incorporation by PCR. As shown (Fig. 3a left bottom panel), 12 out of 20 isolated clones displayed incorporation of the Flag-sequence at the DDX3 locus thus suggesting a knock-in efficiency of more than 50% of cells using “all-in-one” Nanoblades.

Knock-in assisted by “All-in-one” Nanoblades was also obtained at the AAVS1 locus which has been described as a safe

harbor for transgene insertion<sup>17</sup>. For this we designed a dsDNA template of 4 kb bearing the puromycin resistance gene with homology arms to the AAVS1 locus. After transduction of HEK-293T cells with Nanoblades complexed with this template using polybrene, single-cell-derived clones were selected with puromycin. Out of  $1 \times 10^5$  transduced cells, we obtained 47 puromycin-resistant clones (Supplementary Figure 3b, c and d). A PCR-assay revealed that 42 out of 47 puromycin-resistant clones tested had



**Fig. 3** “All-in-one” Nanoblades for knock-in experiments and assessment of Nanoblades off-target activity. **a** Left panel, Nanoblades targeting human *DDX3* close to its start codon were complexed with a donor ssDNA bearing homology arms to the targeted locus and a Flag-tag sequence in the presence of polybrene. HEK293T cells were then transduced with these “All-in-one” Nanoblades. After cell amplification, a fraction of cells were collected to extract genomic DNA and total proteins while the remaining cells were cultured to obtain single-cell clonal populations. Right panel, insertion of the Flag-tag in HEK-293T cells transduced with “all-in-one” Nanoblades complexed with increasing amounts of donor ssDNA was assessed by Flag-immunoprecipitation followed by western-blot using anti-flag or anti-DDX3 antibodies in the input and Flag-immunoprecipitation elution fractions. Flag insertion was also assessed by PCR using a forward primer in the flag-sequence and a reverse primer in the *DDX3* locus (Orientation PCR assay) or using primers flanking the Flag sequence (Insertion PCR assay). Bottom panel, Flag-insertion in 20 different single-cell-derived clones was assessed by PCR using primers flanking the Flag-sequence. **b** Left panel, off-target monitoring in immortalized mouse macrophages stably expressing *GFP* transgenes bearing silent mutations in the region targeted by the sgRNA. Right panel, cells were transfected with plasmids coding for Cas9 and the sgRNA or transduced with Nanoblades. GFP expression was measured by FACS 72 h after transfection/transduction ( $n = 3$ ). **c** Left and right panels, gene-editing at the *EMX1* on-target site and the *MFAP1* intronic off-target site measured by high-throughput sequencing in untreated cells (control cells) and cells transduced with *EMX1* Nanoblades (Nanoblades) or transfected with plasmids coding for Cas9 and the *EMX1* sgRNA (DNA transfection) ( $n = 3$ ). Statistical significance of the Nanoblades and DNA transfection comparison at the on-target site was computed using a two-tail Student test. **d** Left panel, position of sgRNAs targeting the promoter of *TTN* and VLPs with different combination of sgRNAs produced for the experiment. Right-panel, *TTN* mRNA expression levels (normalized to Control) as measured by qPCR in MCF7 transduced with VLPs ( $n = 3$ ). Error bars in all figures correspond to standard deviation

the puromycin cassette inserted at the *AAVS1* locus (Supplementary Figure 3d).

Taken together, our results show that Nanoblades can be used for the precise insertion of genetic material through HDR both with ssDNA and dsDNA donor DNA template and no requirement for any transfection reagent.

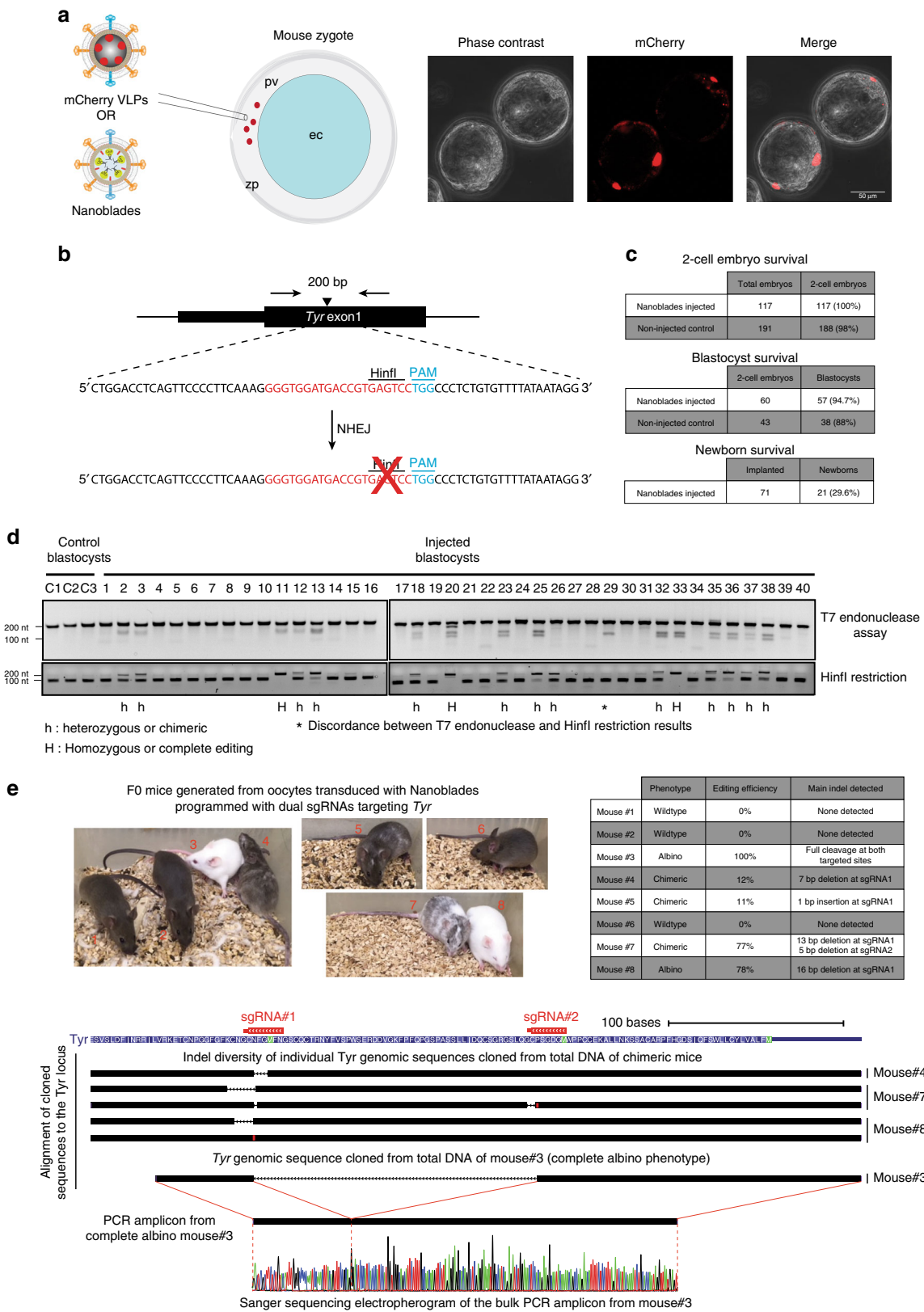
**Nanoblades confer low off-target genome-editing.** A major concern related to the use of CRISPR/Cas9-mediated gene editing are the potential off-target effects that can occur at genomic loci that are similar in sequence to the original target. Interestingly, several reports have shown that transient delivery of the Cas9-sgRNA complex by injection or RNP transfection generally leads to reduced off-target effects as compared to constitutive expression of Cas9 and sgRNA from DNA transfection experiments<sup>18</sup>. Since Nanoblades deliver the Cas9-sgRNA complex in a dose-dependent and transient fashion, we tested whether they could also lead to reduced off-target effects when compared to classical DNA transfection. For this, we developed an approach similar to that described by Fu and colleagues<sup>19</sup> by creating a series of HEK-293T reporter cell lines transduced with different versions of a *GFP* transgene bearing silent point mutations located in the sgRNA target site (Fig. 3b, right panel). These cells were either transfected with plasmids coding for Cas9 and the sgRNA targeting the *GFP* or transduced with Nanoblades programmed with the same sgRNA. 96 h after transfection/transduction, cells were collected and GFP expression was monitored by FACS (Fig. 3b, left panel). As expected, GFP expression from cells bearing the wild-type *GFP* sequence (No Mismatch) was efficiently repressed both after Nanoblades transduction (close to 80% repression) and DNA transfection (close to 60% repression) (Fig. 3b, left panel “No Mismatch”). When two mismatches were introduced in the target site, Nanoblades were no longer able to efficiently repress GFP expression (20% compared to control) while GFP expression from transfected cells was still reduced to levels similar to that of the *GFP* bearing a perfect match with the sgRNA. Interestingly, the presence of three or four mismatches completely abolished *GFP* editing in Nanoblades-treated cells while cells transfected with the Cas9 and sgRNA plasmids still displayed a mild inhibition of GFP expression (Fig. 3b see 3 and 4 Mismatches).

To complement these results, we further tested for genomic off-target effects using the well-characterized sgRNA targeting human *EMX1*. Off-targets for this sgRNA have been extensively studied using T7 endonuclease assays and high-throughput sequencing approaches<sup>10</sup>. We PCR-amplified the *EMX1* locus and one of the previously described *EMX1* genomic off-target loci occurring at the intron of *MFAP1*<sup>10</sup> in cells treated for 72 h with

Nanoblades programmed with the *EMX1* sgRNA or transfected with a DNA construct coding for Cas9 and the *EMX1* sgRNA. We then assessed genome-editing on each sample by high-throughput sequencing (Fig. 3c)<sup>13</sup>. Editing at the on-target site was efficient in Nanoblade-treated cells (75% in average) and to a less extent in cells transfected with the DNA coding for Cas9 and the sgRNA (53% in average) (Fig. 3c, left panel). As expected, small INDELS (insertions and deletions) occurred close to the expected Cas9 cleavage site located 3nt upstream the PAM sequence both in Nanoblades treated and in DNA-transfected cells (Supplementary Figure 4). Surprisingly, in spite of the higher editing efficiency at the on-target site, we could not detect any significant editing at the *MFAP1* off-target site in Nanoblades-treated cells (Fig. 3c, right panel). In contrast, cells transfected with the DNA coding for Cas9 and the sgRNA displayed significant editing (close 6%) at the off-target site (Fig. 3c, right panel) and had INDELS at the expected cut site (Supplementary Figure 4).

Taken together, our results indicate that similarly to other protocols that lead to transient delivery of the Cas9-sgRNA RNP, Nanoblades display low off-target effects.

**Targeted transcriptional activation through Nanoblades.** Having shown efficient genome editing using Nanoblades loaded with the catalytically active Cas9, we tested whether Nanoblades could also deliver Cas9 variant proteins for applications, such as targeted transcriptional activation. To this aim, we fused the Cas9-derived transcriptional activator (SP-dCas9-VPR)<sup>20</sup> to Gag from MLV and expressed the fusion protein in producer cells together with a control sgRNA or different combinations of sgRNAs targeting the promoter region of human Titin (*TTN*) as previously described<sup>20</sup> (Fig. 3d, left panel). Nanoblades loaded with SP-dCas9-VPR were then incubated with MCF-7 cells and induction of *TTN* measured by quantitative RT-PCR (normalized to GAPDH expression). As observed (Fig. 3d, right panel), when two different sgRNAs were used in combination, *TTN* transcription was stimulated from 50 to 200 fold compared to the control situation. Interestingly, when combining the four different sgRNAs in a single VLP, we obtained up to 400-fold transcription stimulation of *TTN* after 4 h of transduction. Our results therefore suggest that in spite of the large molecular size of the SP-dCas9-VPR (predicted at 224 kDa alone and 286 kDa when fused to MLV Gag), neither its encapsidation within VLPs nor its delivery and function within target cells are impaired. The use of Cas9 variants could therefore expand the toolbox of potential applications of Nanoblades in immortalized and primary cells.



**Nanoblades-mediated transduction of mouse zygotes.** CRISPR-Cas9 has been extensively used to generate transgenic animals through microinjection of zygotes with DNA coding for Cas9 and the sgRNA or with the synthetic sgRNA and a Cas9 coding mRNA or directly with the preassembled Cas9-sgRNA RNP<sup>21</sup>. However, some of these options usually require injection into the

pronucleus or the cytoplasm of zygotes, which can significantly impact their viability. Moreover, in some species, pronucleus and even cytoplasmic microinjection can be technically challenging.

Because Nanoblades are programmed to fuse with their target cells, we reasoned that they could also transduce murine zygotes without requiring intracellular microinjection. To test this

**Fig. 4** Generation of transgenic mice using Nanoblades. **a** Left panel, scheme describing injection of mCherry VLPs or Nanoblades in the perivitelline space of mouse 1-cell embryos. Right panel, fluorescence microscopy of mouse blastocysts injected with mCherry VLPs at the single-cell stage. **b** Scheme of the design strategy to target the mouse *Tyr* locus (adapted from ref. 22). Upon editing and NHEJ repair, the *Hin*I restriction site becomes inactive. **c** Survival rates of injected embryos at two-cell, blastocyst, and newborn stage (the latter obtained from experiments presented in Supplementary figure 5). **d** T7 endonuclease (top panel) and *Hin*I restrictions (bottom panel) assays on PCR fragments amplified from the *Tyr* locus of Control or Nanoblades-injected embryos. **e** Top left panel, photographs of F0 mice generated from embryos injected with Nanoblades programmed with two sgRNAs targeting the *Tyr* locus. Top-right panel, phenotype, editing efficiency (as measured by TIDE analysis of the Sanger-sequencing electropherograms) and the main INDEL type as detected by Sanger sequencing of individual PCR clones. Bottom-panel, alignment of individual PCR clones obtained from the *Tyr* locus of F0 mice against the mouse mm10 genome indicating the main observed INDELS in chimeric mice (mouse #4, #7, and #8) and total excision of the *Tyr* sequence between the sgRNA1 and sgRNA2 targeting loci for the complete albino mouse (mouse #3). The Sanger sequencing electropherogram from the bulk PCR amplicon obtained from mouse #3 indicates complete editing at both targeted sites

hypothesis, VLPs loaded with the mCherry protein (instead of Cas9) were produced and injected in the perivitelline space of mouse zygotes (Fig. 4a, top panel). Embryos were harvested 80 h after injection (blastocyst stage) and visualized by fluorescence microscopy, showing mCherry protein delivery within embryo cells (Fig. 4a, right panel).

Nanoblades programmed with a sgRNA targeting the first exon of the tyrosinase (*Tyr*) gene previously described in ref. 22 were produced and injected in the perivitelline space of mouse zygotes. This particular sgRNA was specifically designed to target a *Hin*I restriction site in the *Tyr* gene that should be disrupted upon dsDNA cleavage and NHEJ repair<sup>22</sup> (Fig. 4b). 80 h after injection, blastocysts were harvested and genomic DNA extracted to monitor genome-editing by PCR amplification followed by T7 endonuclease assay or *Hin*I restriction. As observed (Fig. 4d), 16 out of 40 blastocysts were positive for genome-editing at the *Tyr* gene both for the T7 endonuclease and the *Hin*I restriction assays. Interestingly, three blastocysts (#11, #20, and #33) appeared to bear complete *Tyr* editing as we could not detect any residual *Hin*I restriction products (Fig. 4d). In the remaining 13 blastocysts that were positive for genome editing at the *Tyr* locus, we observed different editing efficiencies thus arguing for variable levels of mosaicism between individuals (Fig. 4d). Interestingly, injection of Nanoblades in the perivitelline was not associated with embryo mortality as we did not obtain any significant difference in survival rates between injected and non-inject embryos (Fig. 4c). To further validate these results, we produced Nanoblades programmed with two sgRNAs targeting the *Tyr* locus (see Fig. 4e bottom scheme) that were injected in the perivitelline space of single-cell embryos, which were then implanted into pseudopregnant females and carried to term. In this case, five out of eight F0 mice obtained carried detectable *Tyr* editing both at the phenotype and genotype level as assayed by PCR amplification of the *Tyr* locus from genomic DNA extracted from the fingers of each animal (Fig. 4e). Interestingly, one of the two fully albino mice carried a complete deletion of the DNA segment between the two sgRNA-targeted loci in all tested cells (as assayed by Sanger sequencing of the bulk PCR product and Sanger sequencing of single clone PCR fragments (Fig. 4e bottom panels)). The remaining F0 mice that displayed a partial *Tyr* disruption phenotype had an editing efficiency ranging from 11% up to 78% of all *Tyr* alleles (Fig. 4e see table). Sanger sequencing of individual PCR clones amplified from these mice indicated that one of the two sgRNAs (sgRNA1) was more efficient in inducing INDELS (Fig. 4e bottom scheme). Moreover, we also detected some degree of mosaicism within each individual mouse (with the exception of mouse #3 which had complete bi-allelic excision of the *Tyr* sequence between the two target loci) with at least two types of INDELS detected in mice 7 and 8 (Fig. 4e, see genomic alignment scheme). This, however, is very similar to the degree of mosaicism found in other approaches<sup>22,23</sup>. Taken together, these results validate the use of

Nanoblades to generate transgenic mice upon perivitelline injection of single-cell embryos.

To further confirm the ability of Nanoblades to mediate genome-editing in mouse embryos and transmission of the edited locus to the offspring, we designed a sgRNA targeting the loxP sequence that could mimic the action of the Cre recombinase by removing a loxP flanked cassette (Supplementary Figure 5, left panel). These Nanoblades were first tested in primary BM cells derived from R26R-EYFP transgenic mice bearing a single-copy of the YFP transgene under control of a “lox-stop-lox” cassette<sup>24</sup> (Supplementary Figure 5, top right panel). Nanoblades were then injected in the perivitelline space of heterozygous R26R-EYFP 1-cell embryos which were then implanted into pseudopregnant females and carried to term. In this case, 1 out of 14 founder animals was YFP positive under ultraviolet (UV) light and displayed efficient excision of the “lox-stop-lox” cassette as confirmed by PCR<sup>25</sup> (Supplementary Figure 5, bottom left panel). Consistent with our previous results, the F1 progeny obtained after mating the loxed F0 mouse with a wild-type mouse contained the “loxed” version of the YFP allele and displayed YFP expression in tails and muscle fibers (Supplementary Figure 5, bottom right panel), indicating efficient transmission of the loxed allele from the F0 founder to its progeny.

Taken together, Nanoblades can represent a viable alternative to classical microinjection experiments for the generation of transgenic animals, in particular for species with fragile embryos or with poorly visible pronuclei.

#### In vivo editing of *Hpd* in the liver of tyrosinaemic FRG mice.

Hereditary tyrosinemia type I (HT1) is a metabolic disease caused by disruption of fumarylacetoacetate hydrolase (*Fah*), which is an enzyme required in the tyrosine catabolic pathway. *Fah*<sup>-/-</sup> mice recapitulate many phenotypic characteristics of HT1 in humans, such as hypertyrosinemia and liver failure and have to be treated with nitisinone for their survival. Disruption of hydroxyphenylpyruvate dioxygenase (HPD), the enzyme targeted by nitisinone) through hydrodynamic tail vein injection in *Fah*<sup>-/-</sup> mice was recently shown to restore their survival in the absence of nitisinone thanks to the selective advantage of *Hpd* negative hepatocytes<sup>26</sup>. We therefore reasoned that Nanoblades could represent a non-invasive method to inactivate the *Hpd* gene in NRG (NOD<sup>Fah</sup><sup>-/-</sup>/Rag2<sup>-/-</sup>/Il2rg<sup>-/-</sup>) mice<sup>27</sup>. To this aim, we designed a sgRNA directed against the fourth exon of *Hpd*, which should disrupt the reading frame through the INDELS caused by NHEJ (see Methods section for the sequence). Nanoblades directed against *Hpd* or against human *EMX1* (control) were introduced in NRG mice through retro-orbital injection (Fig. 5a). Upon injection, mice were weaned off nitisinone until they reached a 20% loss of their body weight, in which case nitisinone was subsequently administered punctually. Two weeks after injection, all mice injected with Nanoblades targeting *Hpd* displayed detectable editing in the liver (between 7% and 13%

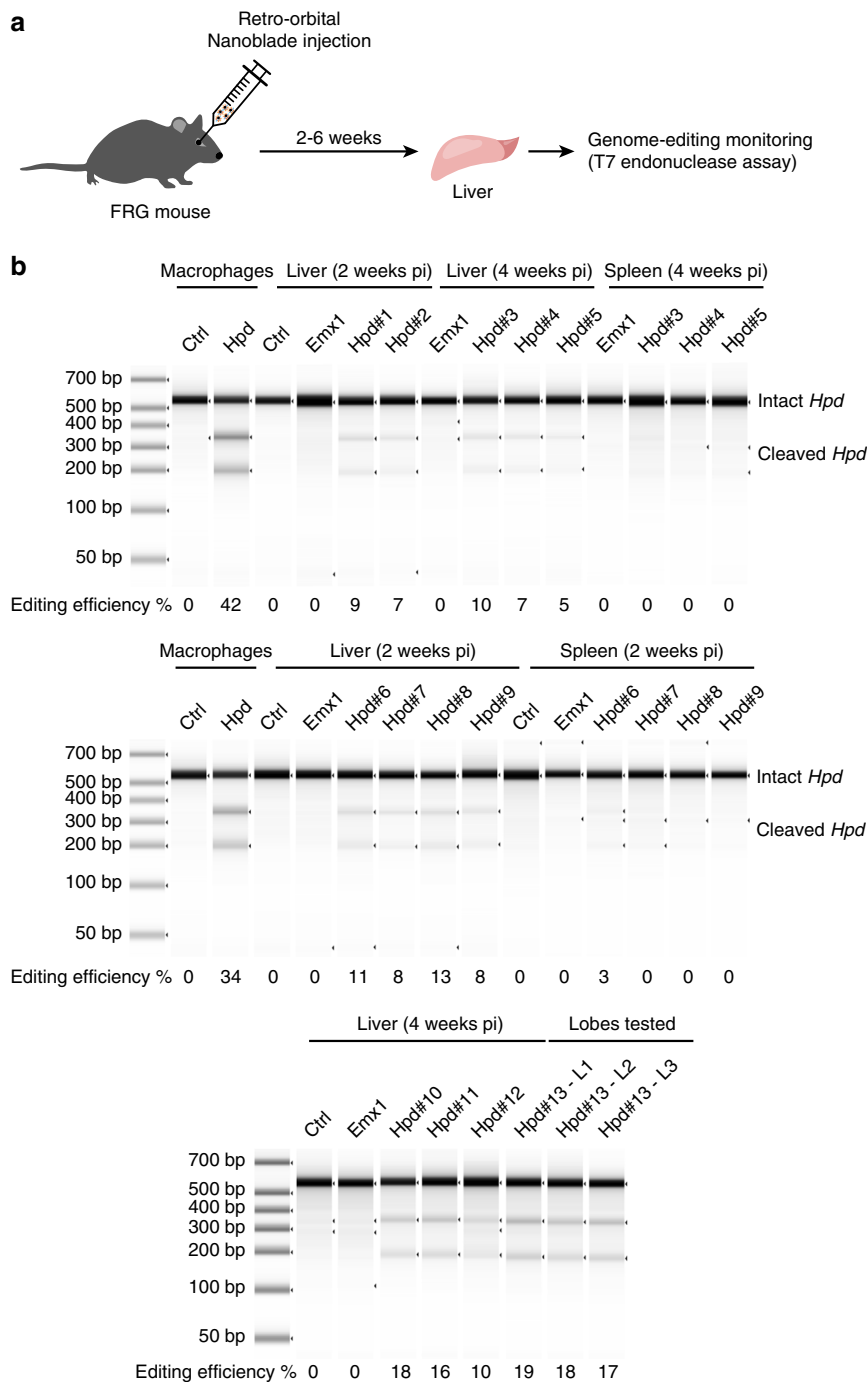


**Fig. 5** Inactivation of *Hpd* in the liver of tyrosinaemic FRG mice. **a** Scheme of the experimental approach to target the liver of FRG mice. **b** T7 endonuclease assay to monitor genome editing at the *Hpd* gene in immortalized mouse macrophages and in the liver or spleen of injected mice. Samples were quantified using a TapeStation chip

efficiency, Fig. 5b). On the contrary, no editing was detected in control (uninjected) mice or in mice injected with Nanoblades targeting human *EMX1* (Fig. 5b). Similar results were obtained 4 weeks post-injection where all mice injected with Nanoblades targeting *Hpd* displayed genome editing in the liver (Fig. 5b). Furthermore, genome-editing occurred in a homogenous fashion across the liver as shown by T7 endonuclease assay from biopsies recovered from three different lobes of a single animal (Fig. 5b, bottom panel). In contrast, editing in other organs, such as spleen was weak or not detectable (Fig. 5b).

Interestingly, we observed a small overall increase in editing levels at 4 weeks post-injection compared to 2 weeks post-

injection suggesting that cells with *Hpd* editing could have a selective advantage over non-edited cells (Fig. 5b compare middle and bottom panel). Because we did not monitor genome editing earlier than 2 weeks post injection, we cannot rule out that a similar selective advantage of edited cells might have occurred during this incubation time. Nevertheless, based on the weak increase of the editing efficiency observed between 2 and 4 weeks after injection, we do not expect this selective advantage to significantly improve the observed editing efficiency during the first 2 weeks after injection. Importantly, Nanoblades injection was not associated with any signs of morbidity.



## Discussion

Genome editing should ideally be achieved in a fast and precise fashion to limit toxicity and possible off-target effects due to a sustained expression of effectors. In this regard, extensive efforts have been recently described to vehicle Cas9-sgRNA RNPs in cultured cells and in vivo by non-coding material including Nanocarriers<sup>28</sup>, optimized transfection reagents<sup>18</sup>, or lentivirus-derived particles<sup>29</sup>.

This work describes and characterizes VLPs to efficiently vectorize the CRISPR-Cas9 system into primary cells, embryos, and animals. These non-coding agents—we called herein Nanoblades—incorporate the Cas9 endonuclease into their internal structure. The molecular basis of this technology is the fusion of Cas9 from *Streptococcus pyogenes* to Gag from MLV. Expressed with other components of viral assembly and construct encoding gRNA(s), this molecule can bind sgRNAs into producer cells, forms RNP complexes and cohabit with Gag and Gag-Pol within particles. We indeed show that robust packaging of sgRNAs into Nanoblades depends on their interaction with Gag::Cas9 (Supplementary Figure 1d).

When compared to other methods of delivery such as lipofection or electroporation, Nanoblades were more efficient and rapid in inducing dsDNA breaks both in immortalized U2OS cells, primary fibroblasts (Fig. 1b, Supplementary Figure 1e). Nanoblades are also functional in primary cells that are known to be difficult to transfect and transduce using classical delivery methods, such as human iPS cells, human CD34+ and primary mouse bone-marrow cells (Fig. 2) reaching efficiencies comparable or even superior to other recent methods<sup>30,31</sup>, such as Cas9-sgRNA ribonucleoprotein electroporation (Fig. 2c), together with low off-target effects (Fig. 3b and c). Furthermore, Nanoblades achieve genome editing in a dose-dependent manner (Fig. 1c). Beyond delivery of Cas9-sgRNA complexes, we also show that Nanoblades can be complexed with DNA repair templates to mediate homologous recombination-based knock-in cultured cells in the absence of any transfection reagent. Our results also validate the use of Nanoblades in vivo for generating transgenic mice upon embryo injection in the perivitelline space (Fig. 4 and Supplementary Figure 5) or in the liver of injected animals (Fig. 5). Although, other recent methods for in vivo genome editing of zygotes and animals have reached higher editing rates<sup>22,23,32–34</sup>, Nanoblades represent a viable, inexpensive, and accessible alternative that can still benefit from further improvements.

Similarly to other cell-derived particles (including most viral vectors), Nanoblades incorporate RNAs and proteins from producer cells that could be responsible for the transmission of undesired effects. Mass spectrometry analysis of the content of Nanoblades revealed that plasma membrane terms were particularly enriched, which is consistent with the vesicular nature of Nanoblades (Supplementary Figure 2a and Supplementary Data 1). As previously described for retroviral-VLPs<sup>35</sup>, characterization of the RNA content revealed that Nanoblades contain thousands of individual cellular mRNA species, most of these being encapsidated stochastically, in proportion to their abundance in the producer cell. We found that transcripts overexpressed for production purposes (GAG, VSV-G, etc.) represent <0.4% of Nanoblades RNAs (Supplementary Figure 2b) supporting the notion that their delivery to recipient cells is marginal. Confirming this observation, transfer of cellular proteins loaded in Nanoblades from producer cells to recipient cells appears to be minimal and restricted to a short time window between 8 and 24 h after transduction (Supplementary Figure 2c and d). While we cannot exclude the fact that VLPs may be responsible for some cellular responses, depending on the nature of recipient cells, efficient doses of Nanoblades were globally harmless for most

primary cells we tested and in injected animals. In our effort to exploit the retroviral nature of Nanoblades, we explored diverse pseudotyping options (Supplementary Figure 6) and finally focused on the use of an original mixture of two envelopes (VSV-G plus BRL), a recipe that we have optimized (Supplementary Figure 6) and which systematically displayed the best cleavage results in most recipient cells. Depending on the cellular target, it may be possible to pseudotype Nanoblades with envelopes from Measles virus<sup>36</sup>, influenza virus<sup>37</sup>, or other targeting systems<sup>38,39</sup> to restrict or improve Cas9 delivery to certain cell types (Supplementary Figure 6a).

Next generation Nanoblades may also benefit from the continual evolutions of Cas9-derivatives that can support fusion with Gag from MLV (Fig. 3) and could be adapted to other gene-editing targetable nucleases like Cpf1 nucleases<sup>40</sup> or even the latest generation of programmable base editors<sup>41</sup>. We also noted that Nanoblades can be engineered to accommodate other proteins/RNAs in addition to Cas9-RNPs and serve as multi-functional agents. Nanoblades capable of delivering both Cas9-RNPs and a reverse-transcribed template that can serve for reparation by homologous-recombination could therefore be envisioned. Furthermore, multiple sgRNAs can be incorporated within Nanoblades thus allowing gene excisions or multiple genes to be targeted. Multiplexing of sgRNAs may also allow the introduction of an additional sgRNA targeting a specific gene that will allow selection of cells efficiently edited by Nanoblade-mediated CRISPR<sup>42</sup>.

This versatility allows any laboratory equipped with BSL2 facilities to generate its own batches of particles. Beyond cell lines, our VLP-based technique provides a powerful tool to mediate gene editing in hiPSCs and primary cells including macrophages, human hematopoietic progenitors and primary hepatocytes. We have shown that Nanoblades injection into the perivitelline space of mouse-zygotes was particularly harmless for the recipient cells, since none of the injected zygotes were affected in their development after treatment. Generation of transgenic animals upon perivitelline space injection of VLPs could be adapted to other species, including larger animals for which the number of zygotes is limited. Finally, we achieved significant gene-editing in the liver of injected adult mice with no consequences on their viability. Nanoblades, could therefore represent an interesting route for the delivery of Cas9 in vivo to inactivate gene expression but also used in combination with other viral delivery tools carrying a donor DNA template (such as Adeno-associated virus (AAV)) to perform in vivo HDR experiments as recently shown<sup>32</sup>.

Considering the examples provided in our work, we believe that the Nanoblade technology will facilitate gene editing in academic laboratories working with primary cells and could represent a viable alternative for therapeutical purposes and the rapid generation of primary cell-types harboring genetic diseases, humanized-liver mouse models and transgenic animal models.

## Methods

**Plasmids.** SP-dCas9-VPR was a gift from George Church (Addgene plasmid #63798). Lenti CRISPR was a gift from F. Zhang (Addgene plasmid #49535). The GagMLV-CAS9 fusion was constructed by sequential insertions of PCR-amplified fragments in an eukaryotic expression plasmid harboring the human cytomegalovirus early promoter (CMV), the rabbit Beta-globin intron and polyadenylation signals. The MA-CA-NC sequence from Friend MLV (Accession Number: M93134) was fused to the MA/p12 protease-cleavage site (9 aa) and the Flag-nls-spCas9 amplified from pLenti CRISPR.

**Cell culture.** Gesicle Producer 293T (Clontech 632617), U2OS cells, and primary human fibroblasts (Coriell Institute, GM00312) were grown in DMEM supplemented with 10% fetal calf serum (FCS).

hiPSCs were obtained and cultured as described in ref. <sup>43</sup>.

Bone marrow-derived macrophages (BMDMs) were differentiated from BM cells obtained from wild-type C57BL/6 mice. Cells were grown in DMEM

supplemented with 10% FCS and 20% L929 supernatant containing MCSF as described in ref. 44. Macrophages were stimulated for the indicated times with LPS (Invivogen) at a final concentration of 100 ng/ml.

**CD34+ cell sample collection, isolation, and transduction.** Cord blood (CB) samples were collected in sterile tubes containing the anti-coagulant, citrate-dextrose (ACD, Sigma, France) after informed consent and approval was obtained by the institutional review board (Centre international d'inféctiologie (CIRI), Lyon, France) according to the Helsinki declaration. Low-density cells were separated over, Ficoll-Hypaque. CD34+ isolation was performed by means of positive selection using magnetic cell separation (Miltenyi MACs) columns according to the manufacturer's instructions (Miltenyi Biotec, Bergisch Gladbach, Germany). Purity of the selected CD34+ fraction was assessed by FACS analysis with a phycoerythrin (PE)-conjugated anti-CD34 antibody (Miltenyi Biotec, Bergisch Gladbach, Germany) and exceeded 95% for all experiments. Human CD34+ cells were incubated for 18–24 h in 24-well plates in serum-free medium (CellGro, CellGenix, Germany) supplemented with human recombinant: SCF (100 ng/ml), TPO (20 ng/ml), Flt3-L (100 ng/ml) (Miltenyi, France).  $5 \times 10^4$  prestimulated CD34+ cells were then incubated with nanoblades in 48-well plates in serum-free medium.

**sgRNA design and sequences (+PAM).** sgRNAs targeting *MYD88*, *DDX3*, *GFP*, *Hpd*, *Fto*, *Tyr*, and the *LoxP* sequence were designed using CRISPRseek<sup>45</sup>.

Human AAVS1: 5' ACCCCACAGTGGGGCCACTAggg 3'  
 Human DDX3: 5' AGGGATGATGCATGTGGCAGTgg 3'  
 Human EMX1: 5' GAGTCCGAGCAGAAGAAGAagg 3'  
 Human MYD88 #1: 5' GAGACCTCAAGGGTAGAGGTggg 3'  
 Human MYD88 #2: 5' GCAGCCATGGCGGGCGGTCCtgg 3'  
 Human rDNA: 5' CCTTCTTAGCGATCTGAGagg 3'  
 Human TTN -169: 5' CCTTGGTGAAGTCTCCTTTgagg 3'  
 Human TTN -252: 5' ATGTTAAATCCGAAAATGcagg 3'  
 Human TTN -326: 5' GGGCACAGTCTCAGGTTTgggg 3'  
 Human TTN -480: 5' ATGAGCTCTCTCAACGTTAagg 3'  
 Mouse Fto: 5' CATGAAGCGCGTCCAGACCgagg 3'  
 Mouse Hpd: 5' GAGTTTCTATAGGTGGTGGTGGTgggg 3'  
 Mouse Tyr: 5' GGGTGGATACCGTGAAGTCCtgg 3' obtained from Chen et al. 22  
 Mouse Tyr: 5' AACTTCATGGGTTTCAACTGcgg 3' obtained from Yoon et al. 23  
 Mouse Tyr: 5' ATGGGTGATGGGAGTCCCTGcgg 3' this study  
 LoxP: 5' CATTATACGAAGTTATATTAagg 3'  
 GFP: 5' CGAGGAGCTGTTACCAGGGTggg 3'

**Production of Nanoblades.** Nanoblades were produced from transfected gestic producer 293T cells plated at  $5 \times 10^6$  cells/10 cm plate 24 h before transfection with the JetPrime reagent (Polyplus). Plasmids encoding the GagMLV-CAS9 fusion (1.7 µg), Gag-POLMLV (2.8 µg), gRNA expressing plasmid(s) (4.4 µg), VSV-G (0.4 µg), the Baboon Endogenous retrovirus Rless glycoprotein (BaEVRless)<sup>15</sup> (0.7 µg) were cotransfected and supernatants were collected from producer cells after 40 h. For production of serum-free particles, medium was replaced 24 h after transfection by 10 ml of Optimum (Gibco) supplemented with penicillin–streptomycin. Nanoblade-containing medium was clarified by a short centrifugation ( $500 \times g$  5 min) and filtered through a 0.8 µm pore-size filter before ultracentrifugation (1h30 at  $96,000 \times g$ ). Pellet was resuspended by gentle agitation in 100 µl of cold 1X PBS. Nanoblades were classically concentrated 100-fold. X-Nanoblades referred as Nanoblades loaded with gRNA(s) targeting the x-gene.

To dose Cas9 packaged into particles, Nanoblades or recombinant Cas9 (New England Biolabs) were diluted in 1X PBS and serial dilutions were spotted onto a Nitrocellulose membrane. After incubation with a blocking buffer (nonfat Milk 5% w/v in TBST), membrane was stained with a Cas9 antibody (7A9-3A3 clone, Cell signaling) and revealed by a secondary anti-mouse antibody coupled to horseradish peroxidase. Cas9 spots were quantified by Chemidoc touch imaging system (Biorad).

**Transduction procedure.** Transductions with Nanoblades were performed in a minimal volume to optimize cell/particles interactions for at least 2 h before supplementing with fresh medium. When specified, polybrene was used at a final concentration of 4 µg/ml in the transduction medium. After dosing Cas9 amount in each Nanoblades preparation, we typically used 10 pmol of encapsidated Cas9 for  $1 \times 10^5$  adherent cells.

**sgRNA in vitro transcriptions.** sgRNAs were in vitro transcribed using the EnGen sgRNA Synthesis kit, *S. pyogenes* (New England Biolabs; E3322S) following the manufacturer's protocol with the following oligonucleotides:

Human EMX1: 5' TTCTAATACGACTCACTATAgatccgag cagaagaagaaGTTTTAGAGCTAGA 3'  
 Mouse Fto: 5' TTCTAATACGACTCACTATAgatcaagcgcgtc cagaccgGTTTTAGAGCTAGA 3'

After transcription, sgRNAs were purified by acidic phenol/chloroform extraction and precipitated using 2.5 volumes of 100% ethanol. sgRNA integrity was then assessed by denaturing urea polyacrylamide gel electrophoresis.

**Cas9-sgRNA RNP electroporation procedure.** Cas9-sgRNA RNP electroporation was performed as described in the manufacturer's protocol. Briefly, 12 pmol of recombinant Cas9 (EnGen Cas9 NLS, *S. pyogenes*; New England Biolabs; M0646T) were incubated with 12 pmol of in vitro transcribed sgRNAs in the presence of Resuspension Buffer R (Neon Transfection System; ThermoFisher Scientific; MPK1025) for 20 min at room temperature. After this,  $1 \times 10^5$  cells resuspended in 5 µl of resuspension buffer R (for HEK293T cells) or resuspension buffer T (for primary mouse BM cells) are added to the Cas9-sgRNA mix and the whole mixture electroporated with the following settings:

-1700 V, 20 ms, 1 pulse (HEK293T cells)  
 -1350 V, 10 ms, 4 pulses (mouse BM cells)  
 -1680 V, 20 ms, 1 pulse (mouse BM cells)

Upon electroporation, cells were incubated in their corresponding medium (DMEM complemented with 10% FCS for HEK293T cells and DMEM complemented with 10% FCS and 20% L929 supernatant containing MCSF for 24 h before extracting their genomic DNA to assess genome editing.

**Combination of Nanoblades with ssDNA and dsDNA.** Nanoblades programmed to target the AUG codon of *DDX3* were resuspended in PBS 2% FBS and combined with ssDNA donor repair template (see the sequence of "Flag-DDX3 primer" below) at a final concentration of 0.3, 1.3 or 6.7 µM in 30 µl of PBS supplemented with polybrene (Sigma) at 4 µg/ml. Complexes were let 15 min on ice before addition to  $7 \times 10^4$  HEK293T cells plated 6 h before in 400 µl of complete medium supplemented with polybrene (4 µg/ml). 24 h later, transduction medium was supplemented with 1 ml of fresh medium (10% FCS) and cells were passed the day after into six-well plates for amplification. Cells were amplified in 10 cm dishes and passed six times during 3 weeks before extraction of proteins and genomic DNAs.

Sequence of the Flag-DDX3 primer (HPLC-purified):

5'-ACTCGCTTAGCAGCGGAAGACTCCGagTTCTCGGTA CTCTTCAGGGATGGA  
 CTACAAGGACGACGATGACAAgagTCATGTGGCAGTG  
 GAAAATGCGCTCGGGCTGGACCAGCAGGTGA-3'

DDX3 amplification was performed using the following primers: DDX3-Forward 5'-CTTCGCGGTGGAACAAACAC-3' and DDX3-Reverse1 5'-CGCCATTAGCCAGGTTAGGT-3' for the "Insertion PCR assay" and Flag-Forward 5'-GACTACAAGG  
 ACGACGATGACAAG-3' and DDX3-Reverse2 5'-CGCCATTA GCCAGGTTAGGT-3' for the "Orientation PCR assay". PCR conditions were performed as follows: 94 °C 5 min, followed by three cycles (94 °C 30 s, 64 °C 30 s, 72 °C 30 s), followed by 25 cycles (94 °C 30 s, 57 °C 30 s, 72 °C 30 s), followed by 5 min at 72 °C.

dsDNA (AAVS1): 10 µl of concentrated Nanoblades were complexed with 650 ng of dsDNA in a total volume of 30 µl of PBS with polybrene at a final concentration of 4 µg/ml. After 15 min of incubation on ice, complexes were used to transduce  $1 \times 10^5$  HEK293T cells in a 24-well plate containing medium supplemented with polybrene (4 µg/ml). Two days later cells were reseeded in a 10 cm dish before puromycin selection (0.5 µg/ml). Single-cell-derived clones were next isolated and cultivated in a 12-well plates before PCR analysis performed on genomic DNAs (500 ng).

Primers used to assess the presence of the puromycin cassette are:

Puromycin-forward 1: 5'-GGCAGTCTGCTGTTCTCTGAC-3'  
 Puromycin-reverse 1: 5'-GATCCAGATCTGGTGTGGCGCG  
 TGGCGGGGTAG-3'

Followed by a nested-PCR using the following primers:

Puromycin-forward 2: 5'-GATATACGCGTCCCAGGGCCGG  
 TTAATGTGGCTC-3'  
 Puromycin-reverse 1: 5'-GATCCAGATCTGGTGTGGCGCG  
 TGGCGGGGTAG-3'

Primers used to assess correct integration of the cassette at the AAVS1 locus are:

AAVS1-forward: 5'-CGAACTCTGCCCTCTAACGCTG-3'  
 Puromycin reverse 2: 5'-GATCCAGATCTGGTGTGGCGCG  
 TGGCGGGGTAG-3'

Followed by a nested-PCR using the following primers:

AAVS1-forward: 5'-GGCAGGTCCTGCTTCTCTGAC-3'  
 Puromycin reverse 3: 5'-CACCGTGGCTGTACTCGGT  
 CAT-3'

**Flag-immunoprecipitation and western-blotting.** For Flag-immunoprecipitation,  $5 \times 10^6$  cells were lysed in 500 µl of lysis buffer (NaCl 300 mM, MgCl<sub>2</sub> 6 mM, Tris-HCl 15 mM, 0.5% NP40). 250 µl of the cell lysate (1 mg of total proteins) was incubated with 40 µl of M2-antiFlag magnetic beads (Sigma M8823) equilibrated in TBS. After incubation for 2 h at 4 °C, beads were washed four times in lysis buffer and proteins eluted in 60 µl of TBS supplemented with Flag-peptide (120 µg/ml final) for 2 h at 4 °C. The supernatant (without beads) was then collected and used for western-blot analyses.

Western-blotting against Flag-DDX3 and endogenous DDX3 was performed using the following antibodies: anti-DDX3 (rabbit, Sigma 19B4, 1/1000 dilution), Flag-M2 Antibody (mouse, Sigma F3165, 1/2000 dilution), and actin antibody (mouse, Sigma A1978, 1/10,000 dilution). The uncropped images for

Supplementary Figs. 1a, 2d, 3d and 2b–d, 3a, 4d are provided in Supplementary Fig. 7.

**T7 endonuclease assay.** Genomic DNA was extracted from VLP-treated cells using the Nucleospin gDNA extraction kit (Macherey-Nagel). 150 ng of genomic DNA was then used for PCR amplification. PCR products were diluted by a factor 2 and complemented with Buffer 2 (New England Biolabs) to a final concentration of 1×. Diluted PCR amplicons were then heat denatured at 95 °C and cooled down to 20 °C with a 0.1 °C/s ramp. Heteroduplexes were incubated for 30 min at 37 °C in presence of 10 units of T7 Endonuclease I (NEB). Samples were finally run on a 2.5% agarose gel or on a BioAnalyzer chip (Agilent) to assess editing efficiency.

**Reverse-transcription and quantitative PCR.** Total RNAs were extracted using TriPure Isolation Reagent (Roche, 11667165001) following the manufacturer's instructions. 1.5 µg of total RNA was treated with DNase and reverse-transcribed using Maxima First Strand cDNA Synthesis Kit for RT-qPCR (Thermo Scientific, K1672) following the manufacturer's instructions. qPCR experiments were performed on a LightCycler 480 (ROCHE) in technical triplicates in 10 µl reaction volume as follows: 5 µl of 2X SYBR qPCR Premix Ex Taq (Thi RNaseH Plus) (TAKARA, TAKRR420W); forward and reverse primers (0.5 µM each final); 7.5 µg of cDNA.

**Immunofluorescence and imaging.** Cells were fixed in 1X PBS supplemented with 4% of paraformaldehyde (PFA) for 20 min, washed three times with 1X PBS and permeabilized with 0.5% Triton X-100 for 4.5 min. Cells were incubated with primary antibodies overnight at 4 °C. Primary antibodies used are: rabbit yH2AX (1:1000; Abcam 81299) and mouse RNA pol I RPA194 (1:500; Santacruz sc48385). Cells were washed three times in 1X PBS, followed by incubation of the secondary antibodies conjugated to Alexa 488 or 594 used at a 1:1000 dilution (Life Technologies) for 1 h at room temperature. After three 1X PBS washes, nucleus were stained with Hoechst 33342 at 1 µg/ml for 5 min. The coverslips were mounted in Citifluor medium (AF1, Citifluor, London, UK). Cells were observed under a Leica DM6000. At least 100 cells were counted in each indicated experiment. Averages and standard deviation values were obtained from three independent biological replicates.

**Flow cytometry analysis of CD81 expression.**  $1 \times 10^6$  HepG2 or HEK293T cells were detached from the cell culture plate using Accutase (Stemcell technologies #07920) and washed twice in PBS + 2%BSA. Cells were then incubated in 100 µl of PBS + 2%BSA + Anti-CD81 (BD Biosciences #555675, clone JS-81, 1/200 dilution) for 30 min at 4 °C. Cells were then washed three times in PBS + 2% BSA and incubated in 100 µl of PBS + 2 %BSA + anti-mouse FITC (Biolenged # 406001, 1/2000 dilution) for 30 min at 4 °C in the dark. Cells were then washed three times in PBS + 2%BSA and fixed with 4% of paraformaldehyde (PFA) for 15 min and washed in PBS + 2%BSA before flow cytometry analysis on a BD FACSCanto II.

**Northern-blot of sgRNAs.** 2 µg of total RNA extracted from Nanoblades or Nanoblade-producing cells were run on a 10% acrylamide, 8 M Urea, 0.5X TBE gel for 1 h at 35 W. RNAs were then transferred onto a Nitrocellulose membrane (Hybond Amersham) by semi-dry transfert for 1 h at 300 mA in 0.5X TBE. The membrane was UV-irradiated for 1 min using a stratalinker 1800 and then baked at 80 °C for 30 min. The membrane was then incubated in 50 ml of Church buffer (125 mM Na<sub>2</sub>HPO<sub>4</sub>, 0.085% phosphoric acid, 1 mM EDTA, 7% SDS, 1% BSA) and washed twice in 10 ml of Church buffer. The 5' P32-labeled ( $1 \times 10^7$  cpm total) and heat-denatured ssDNA probe directed against the constant sequence of the guideRNA (sequence of the sgRNA antisense probe: 5'GCACCGACTCGGTGCCA CTTTTCAGTTGATAACGGACTAGCCTTATTTAACCTTGCTATTCTA GCTCTA3') was diluted in 10 ml of Church buffer and incubated with the membrane overnight at 37 °C. The membrane was washed four times in 50 ml of wash buffer (1X SSC + 0.1% SDS) before proceeding to phosphorimaging.

**Transmission electron microscopy (TEM) and mass spectrometry (MS).** Nanoblades programmed to target the YFP were prepared and processed for TEM and MS as previously described<sup>46</sup>. Briefly, Nanoblades were produced from transfected Gesicles Producer 293T cells plated at  $5 \times 10^6$  cells/10 cm plate 24 h before transfection with the JetPrime reagent (Polyplus) and supernatants were collected from producer cells after 40 h, passed through a 0.45 µm filter and concentrated 100-fold by overnight centrifugation at  $3800 \times g$ . This preparation was next laid overlaid on a continuous optiprep gradient and ultracentrifuged to obtain density fractions. Fractions containing Nanoblades were next pooled and centrifuged overnight at  $3800 \times g$  before PBS resuspension to obtain a  $6000 \times$ -concentrated sample.

For electron microscopy, after a flash-fixation in glutaraldehyde, staining was amplified using the R-Gent Kit (Biovalley, Marne-la-Vallée, France) before the negative coloration (phosphotungstic acid 2%). Specimen were observed under a JEM-1400 microscope (Jeol, Tokyo, Japan) coupled with the Orius-600 camera (Gatan, Pleasanton, CA).

**High-throughput sequencing of RNAs extracted from Nanoblades.** Total RNA was extracted from purified Nanoblades programmed to target the YFP using Trizol. RNAs were then fragmented to 100nt and used as input for the preparation of cDNA libraries following the protocol described in ref. <sup>47</sup>. Briefly, RNA fragments with a 3'-OH were ligated to a preadenylated DNA adaptor. Following this, ligated RNAs were reverse transcribed with Superscript III (Invitrogen) with a barcoded reverse-transcription primer that anneals to the preadenylated adaptor. After reverse transcription, cDNAs were resolved in a denaturing gel (10% acrylamide and 8 M urea) for 1 h and 45 min at 35 W. Gel-purified cDNAs were then circularized with CircLigase I (Epicentre) and PCR-amplified with Illumina's paired-end primers 1.0 and 2.0.

Analysis of high-throughput sequencing data was performed as previously described<sup>48</sup>. Briefly, reads were split with respect to their 5'-barcode sequence. After this, 5'-barcode and 3'-adaptor sequences were removed from reads. Reads were mapped to a custom set of sequences including 18S, 28S, 45S, 5S, and 5.8S rRNA, tRNAs, the sgRNA directed against the GFP sequence and all transcripts coding for Nanoblades components (Envelopes, Gag and Pol, Cas9) using Bowtie<sup>49</sup>. Reads that failed to map to this custom set of sequences were next aligned to University of California, Santa Cruz (UCSC) human hg18 assembly using TopHat2<sup>50</sup>. Read counts on all transcripts of interest were obtained using the HTSeq count package<sup>51</sup>.

**High-throughput sequencing of Emx1 On-target and Off-target loci.** Genomic DNA was extracted from Nanoblades-treated cells using the Nucleospin gDNA extraction kit (Macherey-Nagel). 150 ng of genomic DNA was then used for PCR amplification using primers specific for the *EMX1* On-target locus (*EMX1*-Forward 5'-ACACTCTTTCCCTACACGACGCTCTTCCGATCTGTTCCAGAACCGG AGGACAAAGTAC-3' and *EMX1*-Reverse 5'-GTGACTGGAGTCCCTCTCTAT GGGCAGTCGGTGAAGCCCATTTGCTTCCCTCTGTCAATG-3') and the previously described Off-target locus in the intron of *MFAP1* (*MFAP1*-Forward 5'-ACACTCTTTCCCTACACGACGCTCTTCCGATCTCCATCACGGCCTTTG CAAATAGAGCCC-3' and *MFAP1*-Reverse 5'-GTGACTGGAGTCCCTCTCTA TGGCAGTCGGTGACAGAGGGAACACTACAAGATCGCTGAGC-3') bearing adapters sequencing for Illumina's Miseq platform. Obtained PCR products were purified and PCR amplified with a second set of primers bearing specific barcodes for multiplex sequencing. Final PCR products were sequenced on the Miseq platform using a custom sequencing primer (Miseq-Custom 1: 5' ATCACCGACTGCCCATAGAGAGGACTCCAGTCAC 3') and a custom index sequencing primer (Miseq-Custom 2: 5' GTGACTGGAGTCCCTCTCTATGGGC AGTCGGTGAT 3').

**Animal experimentation.** All animal experiments were approved by a local ethics committee of the Université de Lyon (CECCAPP, registered as CEEA015 by the French ministry of research) and subsequently authorized by the French ministry of research (APAFIS#8154-2016112814462837 v2 for the generation of transgenic animals and C 69 123 0303 for the usage of Nanoblades in vivo). All procedures were in accordance with the European Community Council Directives of September 22, 2010 (2010/63/EU) regarding the protection of animals used for scientific purposes.

**Mouse oocyte injection.** Four or five weeks old FVB/NRj female mice (Janvier Labs, France) were superovulated by intraperitoneal (i.p.) administration of 5 IU of pregnant mare serum gonadotropin (PMSG, Alcyon, France), followed by an additional i.p. injection of 5 IU human chorion gonadotropin 48 h later (hCG, Alcyon, France). Superovulated females were mated with B6D2F1 adult males (1 male/2 females) and euthanized at 0.5 day post coitum (usually between 10 and 11 a.m.). Oviduct were dissected, and the ampulla nicked to release zygotes associated with surrounding cumulus cells into a 200 µl droplet of hyaluronidase (Sigma) in M2 solution (300 µg/ml, Sigma) under a stereomicroscope (Olympus SZX9). Zygotes were incubated for 1 min at room temperature and passed with a mouth pipette through three washes of M2 medium to remove cumulus cells. Zygotes were kept in M16 medium (Sigma) in a water jacketed CO<sub>2</sub> incubator (5% CO<sub>2</sub>, 37 °C) until microinjection with Nanoblades. Micro-injection were carried-out under a stereomicroscope (Olympus SZX9) using a FemtoJet 4i (Eppendorf) microinjector. Briefly, 1 pl of Nanoblades were injected in the perivitelline space of oocytes. Zygotes were then transferred into M16 medium and kept overnight in incubator. The embryos that reached the two-cell stage were transferred into the oviduct of B6CBAF1 (Charles River, France) pseudopregnant females (15–20 embryos per female).

**Retro-orbital injection of Nanoblades.** All experiments were performed in accordance with the European Union guidelines for approval of the protocols by the local ethics committee (Authorization Agreement C2EA 15, "Comité Rhône-Alpes d'Ethique pour l'Expérimentation Animale", Lyon, France). The highly Immunosuppressed NOD FRG mice (Fah<sup>-/-</sup>/Rag2<sup>-/-</sup>/Il2rg<sup>-/-</sup>) (Yecuris coaration), deficient for T-cell, B-cell, and NK-cell are maintained in pathogen-free facility. Retro-orbital injection (SRO) were performed under isoflurane anesthesia.

Genomic DNA from each mouse (treated either by control or *Hpd* targeting Nanoblades) was extracted from three distinct liver lobes and pooled together.



Following this, a two-step PCR was performed on 300 ng of gDNA template, the first PCR using primers Hpd-Forward 1: 5'-CTTAGGAGGTTCAGCAAGATG GGAG-3' and Hpd-Reverse 1: 5'-TCTAGTCTCTATCCAGGGTCCAGCC-3' to amplify the *Hpd* gene (94 °C 5 min, 3 cycles 94 °C, 64 °C, 72 °C, and 20 cycles 94 °C, 58 °C, 72 °C, 5 min 72 °C). The second nested-PCR used primers Hpd-Forward 2: 5'-GAACTGGGATTGGCTAGTGCG-3' and Hpd-Reverse 2: 5'-CACCCAG CACCACCTATAGAAACTC-3' (94 °C 5 min, 3 cycles 94 °C, 64 °C, 72 °C and 30 cycles 94 °C, 57 °C, 72 °C, 5 min 72 °C). Amplicons were next analyzed by T7-endonuclease assay as described.

**Raw data files.** Uncropped scans of ethidium bromide gels and western-blotting figures are displayed in Supplementary Figure 7.

### Data availability

Gene Expression Omnibus: [GSE107035](https://www.ncbi.nlm.nih.gov/geo/query/acc.cgi?acc=GSE107035). The following plasmids will be available from Addgene: Gag::Cas9 fusion (BIC-Gag-CAS9, Plasmid ID: 119942), the Gag::Cas9-VPR fusion (BICstim-Gag-dCAS9-VPR, Plasmid ID: 120922) and the Gag::Cre fusion (GAG-CRErec, Plasmid ID: 119971).

Received: 11 December 2017 Accepted: 30 November 2018

Published online: 03 January 2019

### References

- Jinek, M. et al. A programmable dual-RNA-guided DNA endonuclease in adaptive bacterial immunity. *Sci. N. Y. NY* **337**, 816–821 (2012).
- Gheysens, D., Jacobs, E., de Foresta, F. & Thiriart, C. Assembly and release of HIV-1 precursor Pr55gag virus-like particles from recombinant baculovirus-infected insect cells. *Cell* **59**, 103–112 (1989).
- Kaczmarczyk, S. J., Sitaraman, K., Young, H. A., Hughes, S. H. & Chatterjee, D. K. Protein delivery using engineered virus-like particles. *Proc. Natl Acad. Sci. USA* **108**, 16998–17003 (2011).
- Voelkel, C. et al. Protein transduction from retroviral Gag precursors. *Proc. Natl Acad. Sci. USA* **107**, 7805–7810 (2010).
- O'Connor, T. E., Rauscher, F. J. & Zeigel, R. F. Density gradient centrifugation of a murine leukemia virus. *Sci. N. Y. NY* **144**, 1144–1147 (1964).
- Chen, B. et al. Dynamic imaging of genomic loci in living human cells by an optimized CRISPR/Cas system. *Cell* **155**, 1479–1491 (2013).
- Gibbons, J. G., Branco, A. T., Yu, S. & Lemos, B. Ribosomal DNA copy number is coupled with gene expression variation and mitochondrial abundance in humans. *Nat. Commun.* **5**, 4850 (2014).
- Kinner, A., Wu, W., Staudt, C. & Iliakis, G. Gamma-H2AX in recognition and signaling of DNA double-strand breaks in the context of chromatin. *Nucleic Acids Res.* **36**, 5678–5694 (2008).
- van Sluis, M. & McStay, B. A localized nucleolar DNA damage response facilitates recruitment of the homology-directed repair machinery independent of cell cycle stage. *Genes Dev.* **29**, 1151–1163 (2015).
- Tsai, S. Q. et al. GUIDE-seq enables genome-wide profiling of off-target cleavage by CRISPR-Cas nucleases. *Nat. Biotechnol.* **33**, 187–197 (2015).
- Zhang, J. et al. CD81 is required for hepatitis C virus glycoprotein-mediated viral infection. *J. Virol.* **78**, 1448–1455 (2004).
- Okabe, M., Ikawa, M., Kominami, K. & Nakanishi, T. Green mice as a source of ubiquitous green cells. *FEBS Lett.* **407**, 313–319 (1997).
- Brinkman, E. K., Chen, T., Amendola, M. & van Steensel, B. Easy quantitative assessment of genome editing by sequence trace decomposition. *Nucleic Acids Res.* **42**, e168 (2014).
- Amirache, F. et al. Mystery solved: VSV-G-LVs do not allow efficient gene transfer into unstimulated T cells, B cells, and HSCs because they lack the LDL receptor. *Blood* **123**, 1422–1424 (2014).
- Girard-Gagnepain, A. et al. Baboon envelope pseudotyped LVs outperform VSV-G-LVs for gene transfer into early-cytokine-stimulated and resting HSCs. *Blood* **124**, 1221–1231 (2014).
- Okimoto, T., Friedmann, T. & Miyano, A. VSV-G envelope glycoprotein forms complexes with plasmid DNA and MLV retrovirus-like particles in cell-free conditions and enhances DNA transfection. *Mol. Ther. J. Am. Soc. Gene Ther.* **4**, 232–238 (2001).
- Sadelain, M., Papapetrou, E. P. & Bushman, F. D. Safe harbours for the integration of new DNA in the human genome. *Nat. Rev. Cancer* **12**, 51 (2012).
- Zuris, J. A., Thompson, D. B., Shu, Y. & Guilinger, J. P. Efficient delivery of genome-editing proteins in vitro and in vivo. *Nature* **33**, 73–80 (2015).
- Fu, Y. et al. High-frequency off-target mutagenesis induced by CRISPR-Cas nucleases in human cells. *Nat. Biotechnol.* **31**, 822–826 (2013).
- Chavez, A. et al. Highly efficient Cas9-mediated transcriptional programming. *Nat. Methods* **12**, 326–328 (2015).
- Hori, T. et al. Validation of microinjection methods for generating knockout mice by CRISPR/Cas-mediated genome engineering. *Sci. Rep.* **4**, 4513 (2014).
- Chen, S., Lee, B., Lee, A. Y.-F., Modzelewski, A. J. & He, L. Highly efficient mouse genome editing by CRISPR ribonucleoprotein electroporation of zygotes. *J. Biol. Chem.* **291**, 14457–14467 (2016).
- Yoon, Y. et al. Streamlined ex vivo and in vivo genome editing in mouse embryos using recombinant adeno-associated viruses. *Nat. Commun.* **9**, 412 (2018).
- Srinivas, S., Watanabe, T. & Lin, C. S. Cre reporter strains produced by targeted insertion of EYFP and ECFP into the ROSA26 locus. *BMC Ldts* **1**, 4 (2001).
- Zhang, D. J. et al. Selective expression of the Cre Recombinase in late-stage thymocytes using the distal promoter of the Lck gene. *J. Immunol.* **174**, 6725–6731 (2005).
- Pankowicz, F. P. et al. Reprogramming metabolic pathways in vivo with CRISPR-Cas9 genome editing to treat hereditary tyrosinaemia. *Nat. Commun.* **7**, 12642 (2016).
- Azuma, H. et al. Robust expansion of human hepatocytes in Fah<sup>-/-</sup>/Rag2<sup>-/-</sup>/Il2rg<sup>-/-</sup> mice. *Nat. Biotechnol.* **25**, 903–910 (2007).
- Qazi, S. et al. Programmed self-assembly of an active P22-Cas9 nanocarrier system. *Mol. Pharm.* **13**, 1191–1196 (2016).
- Choi, J. G. et al. Lentivirus pre-packed with Cas9 protein for safer gene editing. *Gene Ther.* **23**, 627–634 (2016).
- Wang, G. et al. Efficient, footprint-free human iPSC genome editing by consolidation of Cas9/CRISPR and piggyBac technologies. *Nat. Protoc.* **12**, 88–103 (2017).
- Modarai, S. R. et al. Efficient delivery and nuclear uptake is not sufficient to detect gene editing in CD34<sup>+</sup> cells directed by a ribonucleoprotein complex. *Mol. Ther.—Nucleic Acids* **11**, 116–129 (2018).
- Yin, H. et al. Therapeutic genome editing by combined viral and non-viral delivery of CRISPR system components in vivo. *Nat. Biotechnol.* **34**, 328–333 (2016).
- Lau, C.-H. & Suh, Y. In vivo genome editing in animals using AAV-CRISPR system: applications to translational research of human disease. *F1000Res.* **6**, 2153 (2017).
- Yin, H. et al. Structure-guided chemical modification of guide RNA enables potent non-viral in vivo genome editing. *Nat. Biotechnol.* **35**, 1179–1187 (2017).
- Rulli, S. J. et al. Selective and nonselective packaging of cellular RNAs in retrovirus particles. *J. Virol.* **81**, 6623–6631 (2007).
- Frecha, C. et al. Stable transduction of quiescent T cells without induction of cycle progression by a novel lentiviral vector pseudotyped with measles virus glycoproteins. *Blood* **112**, 4843–4852 (2008).
- Szécsi, J. et al. Targeted retroviral vectors displaying a cleavage site-engineered hemagglutinin (HA) through HA-protease interactions. *Mol. Ther. J. Am. Soc. Gene Ther.* **14**, 735–744 (2006).
- Morizono, K. et al. Lentiviral vector retargeting to P-glycoprotein on metastatic melanoma through intravenous injection. *Nat. Med.* **11**, 346–352 (2005).
- Morizono, K. et al. Redirecting lentiviral vectors pseudotyped with Sindbis virus-derived envelope proteins to DC-SIGN by modification of N-linked glycans of envelope proteins. *J. Virol.* **84**, 6923–6934 (2010).
- Zetsche, B. et al. Cpf1 is a single RNA-guided endonuclease of a class 2 CRISPR-Cas system. *Cell* **163**, 759–771 (2015).
- Gaudelli, N. M. et al. Programmable base editing of A•T to G•C in genomic DNA without DNA cleavage. *Nature* **551**, 464–471 (2017).
- Agudelo, D. et al. Marker-free coselection for CRISPR-driven genome editing in human cells. *Nat. Methods* **14**, 615–620 (2017).
- Massouridès, E. et al. Dp412e: a novel human embryonic dystrophin isoform induced by BMP4 in early differentiated cells. *Skelet. Muscle* **5**, 40 (2015).
- Carpenter, S. et al. A long noncoding RNA mediates both activation and repression of immune response genes. *Sci. N. Y. NY* **341**, 789–792 (2013).
- Zhu, L. J., Holmes, B. R., Aronin, N. & Brodsky, M. H. CRISPRseek: a bioconductor package to identify target-specific guide RNAs for CRISPR-Cas9 genome-editing systems. *PLoS ONE* **9**, e108424 (2014).
- Mangeot, P.-E. et al. Protein transfer into human cells by VSV-G-induced nanovesicles. *Mol. Ther. J. Am. Soc. Gene Ther.* **19**, 1656–1666 (2011).
- Heyer, E. E., Ozadam, H., Ricci, E. P., Cenik, C. & Moore, M. J. An optimized kit-free method for making strand-specific deep sequencing libraries from RNA fragments. *Nucleic Acids Res.* **43**, e2 (2015).
- Ricci, E. P. et al. Staufeni senses overall transcript secondary structure to regulate translation. *Nat. Struct. Mol. Biol.* **21**, 26–35 (2014).
- Langmead, B., Trapnell, C., Pop, M. & Salzberg, S. L. Ultrafast and memory-efficient alignment of short DNA sequences to the human genome. *Genome Biol.* **10**, R25 (2009).



50. Kim, D. et al. TopHat2: accurate alignment of transcriptomes in the presence of insertions, deletions and gene fusions. *Genome Biol.* **14**, R36 (2013).
51. Anders, S., Pyl, P. T. & Huber, W. HTSeq—a Python framework to work with high-throughput sequencing data. *Bioinformatics* **31**, 166–169 (2015).

### Acknowledgements

Sequencing was performed by the IGBMC Microarray and Sequencing platform, a member of the 'France Génomique' consortium (ANR-10-INBS-0009). We acknowledge the contribution of SFR Biosciences (UMS3444/CNRS, US8/Inserm, ENS de Lyon, UCBL) facilities: Platim and PBES (Celphedia, AniRA). We also thank J.F. Henry, N. Aguilera, and J.L. Thoumas from the animal facility (PBES, Plateau de Biologie Expérimentale de la Souris, ENS de Lyon), as well as A. Ollivier for their technical help in handling mice. We thank Claire Lionnet from Platim for technical assistance in taking confocal fluorescence images. We thank Elisabeth Errazuriz-Cerda and the CeCIL-facility (Lyon, France) for the preparation and the observation of samples by TEM and Yohann Couté and the edyp-service (Grenoble, France) for the proteomic analysis. We thank Gérard Benoît for his help in preparing final figures. This work was funded by Labex Ecofect (ANR-11-LABX-0048) of the Université de Lyon, within the program Investissements d'Avenir (ANR-11-IDEX-0007) operated by the French National Research Agency (ANR), Fondation FINOVI and Agence Nationale des Recherches sur le SIDA et les Hépatites Virales (ANRS—ECTZ3306) to E.P.R. Open access fees were funded by the European Research Council (ERC-StG-LS6-805500 to E.P.R.) under the European Union's Horizon 2020 research and innovation programs.

### Author contributions

P.E.M. and E.P.R. conceived the study and designed most experiments. P.E.M., E.P.R., V.R., A.M., E.L., F.F., E.V., F.L.C., T.S. and F.A. designed experiments. P.E.M., E.P.R., E.L., V.R., A.M., F.F., T.S., F.A., J.B., E.V., V.M., M.T., and E.M. performed experiments and analyzed data. P.E.M. and E.P.R. wrote the paper with contributions from all authors.

### Additional information

**Supplementary Information** accompanies this paper at <https://doi.org/10.1038/s41467-018-07845-z>.

**Competing interests:** P.E.M., T.O., and E.P.R. are named as inventors on a patent relating to the Nanoblades technology (patent applicants: Institut National de la Santé et de la Recherche Médicale (INSERM), Centre National de la Recherche Scientifique (CNRS), Ecole Normale Supérieure de Lyon, Université Claude Bernard Lyon 1, Villeurbanne Cedex; name of inventors: Theophile Ohlmann, Mathieu Misery, Philippe Mangeot, Emiliano Ricci; application number: WO 2017/068077 A1; patent status: published, 27th April 2017; all aspects of the manuscript are covered by the patent application. The remaining authors declare no competing interests.

**Reprints and permission** information is available online at <http://npg.nature.com/reprintsandpermissions/>

**Journal peer review information:** *Nature Communications* thanks the anonymous reviewers for their contribution to the peer review of this work. Peer reviewer reports are available.

**Publisher's note:** Springer Nature remains neutral with regard to jurisdictional claims in published maps and institutional affiliations.



**Open Access** This article is licensed under a Creative Commons Attribution 4.0 International License, which permits use, sharing, adaptation, distribution and reproduction in any medium or format, as long as you give appropriate credit to the original author(s) and the source, provide a link to the Creative Commons license, and indicate if changes were made. The images or other third party material in this article are included in the article's Creative Commons license, unless indicated otherwise in a credit line to the material. If material is not included in the article's Creative Commons license and your intended use is not permitted by statutory regulation or exceeds the permitted use, you will need to obtain permission directly from the copyright holder. To view a copy of this license, visit <http://creativecommons.org/licenses/by/4.0/>.

© The Author(s) 2019

## Annex 2

# System-wide Profiling of RNA-Binding Protein Uncovers Key Regulators of Virus Infection

RNA binding (RBP) proteins are key regulatory partners of all kinds of RNAs in the cell. When assembled with small RNAs, RNP guide the maturation, editing and cleavage of numerous other RNAs. In the case of mRNAs, RBPs participate in the production, maturation, splicing, export, stability, and translation of mRNAs. As such, RBPs dictate the fate of all transcripts of the cell, and are key determinants in gene expression levels. In recent years, the atlas of RNA binding proteins and their RNA binding sites have largely expanded, thanks to mass-spectrometry analysis of RNA crosslinked proteins. But the dynamics of the compendium of RBPs (RBPome) are largely unexplored. In particular, strong modifications of the cell metabolism are likely to induce major changes in RBPome. Conversely, these changes are likely to highlight their participation in major pathways related to gene expression.

To investigate how dynamic the mRNA RBPome is, our co-authors used comparative RNA-interactome Capture (cRIC) a method that relies on UV crosslinking of RBP-RNA interactions, followed by oligo(dT) purification of mRNAs, and quantification of proteins. cRIC was applied to SINV infection, which leads to host-cell shut-off, and major shuffling of RBP between the cytoplasm and the nucleus. cRIC identified drastic remodelling of the mRNA RBPome during SINV infection. Differences were shown to not originate from protein abundance in the cell, but rather by the changes in the transcriptome of the infected cells. Notably, viral mRNAs represent up to 50% of the mRNAs after 18 hours post infection, and their abundance drives the changes in the overall RBPome. RBPs whose presence was increased in the RBPome were shown to relocate in viral replication factories and to be critical for viral replication. This work shows that the RBPome is highly dynamic and that this remodeling highlights critical regulation happening in the cell.

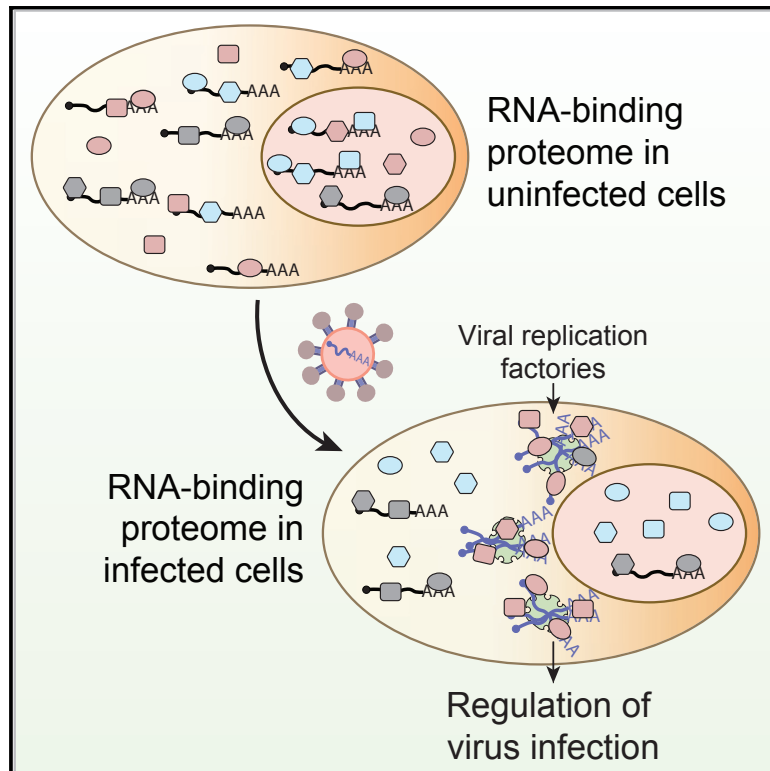
My contribution to this work was fairly modest as I designed, cloned and produced plasmids encoding gRNAs. They were used to knock-out genes of regulated RBPs, and investigate their role in viral replication.

I have since been implicated in many projects with different members of the Castello lab, having designed and produced dozens of gRNA encoding plasmids, as well as producing as many *Nanoblades* equipped with these gRNAs. I have also assisted these members in designing their own gRNAs, designing the screening procedures for CRISPR/Cas9 experiments, and taught them how to make *Nanoblades* and use them. This long-standing collaboration is expected to translate into many more papers to come.

# Molecular Cell

## System-wide Profiling of RNA-Binding Proteins Uncovers Key Regulators of Virus Infection

### Graphical Abstract



### Authors

Manuel Garcia-Moreno,  
Marko Noerenberg, Shuai Ni, ...,  
Bernd Fischer, Shabaz Mohammed,  
Alfredo Castello

### Correspondence

alfredo.castellopalomares@  
bioch.ox.ac.uk

### In Brief

Garcia-Moreno, Noerenberg, Ni, and colleagues developed “comparative RNA-interactome capture” to analyze the RNA-bound proteome during virus infection. More than 200 cellular RNA-binding proteins change their binding activity in response to this challenge, mainly driven by transcript availability. Many of these RNA-binding proteins regulate viral replication and can be targeted to influence infection outcome.

### Highlights

- A quarter of the RBPome changes upon SINV infection
- Alterations in RBP activity are largely explained by changes in RNA availability
- Altered RBPs are crucial for viral infection efficacy
- GEMIN5 binds to the 5' end of SINV RNAs and regulates viral gene expression

# System-wide Profiling of RNA-Binding Proteins Uncovers Key Regulators of Virus Infection

Manuel Garcia-Moreno,<sup>1,12</sup> Marko Noerenberg,<sup>1,12</sup> Shuai Ni,<sup>3,4,12</sup> Aino I. Järvelin,<sup>1</sup> Esther González-Almela,<sup>5</sup> Caroline E. Lenz,<sup>1</sup> Marcel Bach-Pages,<sup>1</sup> Victoria Cox,<sup>1</sup> Rosario Avolio,<sup>1,6</sup> Thomas Davis,<sup>1</sup> Svenja Hester,<sup>1</sup> Thibault J.M. Sohier,<sup>7</sup> Bingnan Li,<sup>8</sup> Gregory Heikel,<sup>9,10</sup> Gracjan Michlewski,<sup>9,10,11</sup> Miguel A. Sanz,<sup>5</sup> Luis Carrasco,<sup>5</sup> Emiliano P. Ricci,<sup>7</sup> Vicent Pelechano,<sup>8</sup> Ilan Davis,<sup>1</sup> Bernd Fischer,<sup>3,13</sup> Shabaz Mohammed,<sup>1,2</sup> and Alfredo Castello<sup>1,14,\*</sup>

<sup>1</sup>Department of Biochemistry, University of Oxford, OX1 3QU Oxford, UK

<sup>2</sup>Department of Chemistry, Chemistry Research Laboratory, University of Oxford, Mansfield Road, Oxford OX1 3TA, UK

<sup>3</sup>German Cancer Research Center (DKFZ), 69120 Heidelberg, Germany

<sup>4</sup>Faculty of Biosciences, Heidelberg University, Heidelberg, Germany

<sup>5</sup>Centro de Biología Molecular “Severo Ochoa,” Universidad Autónoma de Madrid, 28049 Madrid, Spain

<sup>6</sup>Department of Molecular Medicine and Medical Biotechnology, University of Naples Federico II, Naples, Italy

<sup>7</sup>Université de Lyon, ENSL, UCBL, CNRS, INSERM, LBMC, 46 Allée d'Italie, 69007 Lyon, France

<sup>8</sup>SciLifeLab, Department of Microbiology, Tumor, and Cell Biology, Karolinska Institutet, 17165 Solna, Sweden

<sup>9</sup>Wellcome Centre for Cell Biology, University of Edinburgh, Michael Swann Building, Edinburgh EH9 3BF, UK

<sup>10</sup>Division of Infection and Pathway Medicine, University of Edinburgh, The Chancellor's Building, 49 Little France Crescent, Edinburgh EH16 4SB, UK

<sup>11</sup>Zhejiang University-University of Edinburgh Institute, Zhejiang University, 718 East Haizhou Road, Haining, Zhejiang 314400, People's Republic of China

<sup>12</sup>These authors contributed equally

<sup>13</sup>Deceased

<sup>14</sup>Lead Contact

\*Correspondence: [alfredo.castello@bioch.ox.ac.uk](mailto:alfredo.castello@bioch.ox.ac.uk)  
<https://doi.org/10.1016/j.molcel.2019.01.017>

## SUMMARY

The compendium of RNA-binding proteins (RBPs) has been greatly expanded by the development of RNA-interactome capture (RIC). However, it remained unknown if the complement of RBPs changes in response to environmental perturbations and whether these rearrangements are important. To answer these questions, we developed “comparative RIC” and applied it to cells challenged with an RNA virus called sindbis (SINV). Over 200 RBPs display differential interaction with RNA upon SINV infection. These alterations are mainly driven by the loss of cellular mRNAs and the emergence of viral RNA. RBPs stimulated by the infection redistribute to viral replication factories and regulate the capacity of the virus to infect. For example, ablation of XRN1 causes cells to be refractory to SINV, while GEMIN5 moonlights as a regulator of SINV gene expression. In summary, RNA availability controls RBP localization and function in SINV-infected cells.

## INTRODUCTION

RNA-binding proteins (RBPs) assemble with RNA forming ribonucleoproteins (RNPs) that dictate RNA fate (Glisovic et al., 2008). Historically, most of the known RBPs were characterized by the presence of well-established RNA-binding domains

(RBDs), which include the RNA recognition motif, K-homology domain, and others (Lunde et al., 2007). However, stepwise identification of unconventional RBPs evoked the existence of a broader universe of protein-RNA interactions than previously anticipated (Castello et al., 2015). Recently, a system-wide approach termed RNA-interactome capture (RIC) has greatly expanded the compendium of RBPs (RBPome) (Hentze et al., 2018). RIC employs UV crosslinking, oligo(dT) capture under denaturing conditions, and quantitative proteomics to identify the complement of proteins interacting with polyadenylated (poly(A)) RNA in living cells (Baltz et al., 2012; Castello et al., 2012). RIC uncovered hundreds of unconventional RBPs, several of which are now known to play crucial roles in cell biology (Hentze et al., 2018). Recent work has suggested that cells can adapt to physiological cues through discrete alterations in the RBPome (Perez-Perri et al., 2018; Sysoev et al., 2016). However, it remains unknown to what extent the RBPome can be remodeled, how RBP responses are triggered, and what are the biological consequences of this plasticity. For example, RIC reported changes in the composition of the RBPome during fruit fly embryo development that could be explained by matching alterations in protein abundance (Sysoev et al., 2016). However, several RBPs did not follow this trend, displaying protein-level independent changes in RNA binding and raising the question of whether physiological perturbations can induce such responsive behavior more widely. To address this possibility, we developed a “comparative RIC” (cRIC) approach to profile with high accuracy RBP dynamics in cells infected with sindbis virus (SINV) (Figures 1A and 1B).

Viruses have been fundamental for the discovery and characterization of important steps of cellular RNA metabolism such as

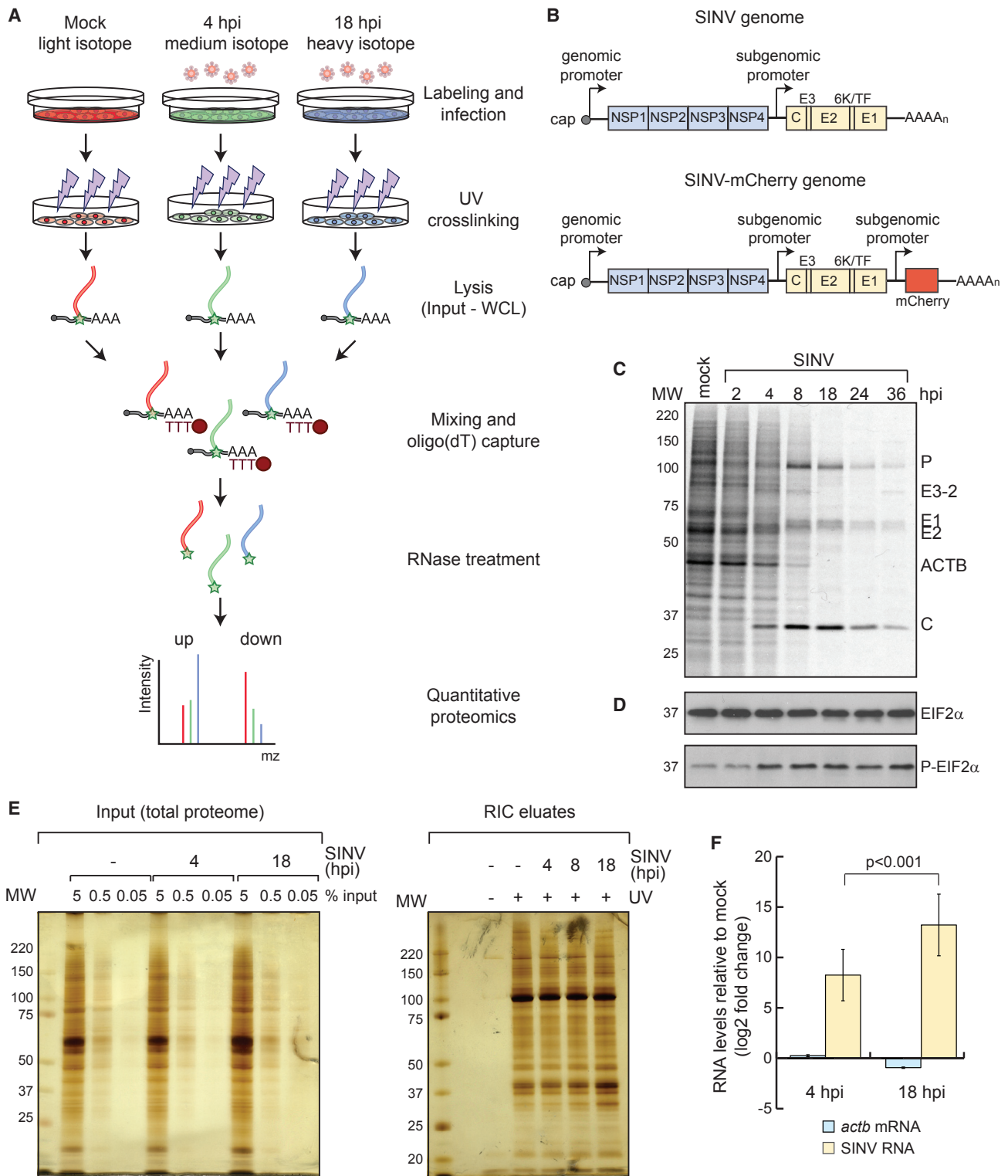


**Figure 1. Application of RIC to HEK293 Cells Infected with SINV**

(A) Schematic representation of cRIC.

(B) Schematic representation of SINV and chimeric SINV-mCherry genomes.

(C) Analysis of the proteins synthesized in uninfected and SINV-infected HEK293 cells by [<sup>35</sup>S]-Met/Cys incorporation for 1 h followed by autoradiography.

(D) Analysis of total and phosphorylated eIF2 $\alpha$  by western blotting.

(legend continued on next page)

RNA splicing, nuclear export, and translation initiation. This is due to their ability to hijack key cellular pathways by interfering with the activity of master regulatory proteins (Akusjarvi, 2008; Carrasco et al., 2018; Castelló et al., 2011; Garcia-Moreno et al., 2018; Lloyd, 2015). Furthermore, specialized RBPs are at the frontline of cellular antiviral defenses, detecting pathogen-associated molecular patterns (PAMPs) such as double-stranded RNA (dsRNA) or RNAs with 5' triphosphate ends (Barbalat et al., 2011; Vladimer et al., 2014). Hence, virus infected cells represent an optimal scenario to assess the RBPome rearrangements.

Our data show that the complement of active cellular RBPs strongly changes in response to SINV infection, mainly due to deep variations in RNA availability. Importantly, “altered” RBPs are critical, as their perturbation affects viral fitness or/and the ability of the cell to counteract the infection. We envision that these RBPs represent novel targets for host-based antiviral therapies.

## RESULTS AND DISCUSSION

### Applying RIC to Cells Infected with SINV

To study the dynamics of cellular RBPs in response to physiological cues, we challenged cells with a cytoplasmic RNA virus and applied RIC. We chose SINV and HEK293 cells as viral and cellular models, respectively. SINV is a highly tractable virus that is transmitted from mosquito to vertebrates, causing high fever, arthralgia, malaise, and rash in humans. SINV replicates in the cytoplasm of the infected cell and produces three viral RNAs (Figures 1B and S1A): genomic RNA (gRNA), subgenomic RNA (sgRNA), and negative-stranded RNA. gRNA is packaged into the viral capsid and is translated to produce the nonstructural proteins (NSPs) that form the replication complex. The sgRNA is synthesized from an internal promoter and encodes the structural proteins (SPs), which are required to generate the viral particles. The negative strand serves as a template for replication. Both gRNA and sgRNA have cap and poly(A) tail.

HEK293 cells are an excellent cellular model to study SINV, as its infection exhibits all the expected molecular signatures, including (1) active viral replication (Figures 1C, S1B, and S1C), (2) host protein synthesis shutoff while viral proteins are massively produced (Figures 1C and S1B), (3) phosphorylation of the eukaryotic initiation factor 2 subunit alpha (EIF2 $\alpha$ ) (Figure 1D), and (4) formation of cytoplasmic foci enriched in viral RNA and proteins, commonly known as viral replication factories (Figures S1C and S1D). SINV infection causes a strong induction of the antiviral program, including  $\beta$ -interferon ( $\beta$ -IFN), which reflects the existence of active antiviral sensors and effectors (Figure S1E). Importantly, SINV achieves infection in a high proportion of cells (~85%) with relatively low number of viral particles (MOI) (Figure S1F), reducing cell-to-cell variability and biological noise.

Pilot RIC experiments in uninfected and SINV-infected cells revealed the isolation of a protein pool matching that previously observed for human RBPs (Castello et al., 2012), which strongly differed from the total proteome (Figure 1E). No proteins were detected in nonirradiated samples, demonstrating the UV dependency of RIC. Infection did not induce major alterations in the protein pattern observed by silver staining, which correspond to the most abundant housekeeping RBPs (Figure 1E). However, other less predominant bands displayed substantial differences, calling for in-depth proteomic analysis. Oligo(dT) capture led to the isolation of both host and SINV RNAs in infected cells (Figure 1F), which is expected as gRNA and sgRNA are polyadenylated.

### SINV Infection Alters the Activity of Hundreds of RBPs

To allow accurate quantification of RBPs associated with poly(A) RNA under different physiological conditions, we developed a cRIC approach by combining the original protocol (Castello et al., 2013) with stable isotope labeling by amino acids in cell culture (SILAC) (Figure 1A). In brief, cells were grown in presence of light, medium, or heavy amino acids with incorporation efficiency >98%. Labeled cells were infected with SINV and irradiated with UV light at 4 and 18 h post-infection (hpi), using uninfected cells as a control (Figure 1A). These times correlate with key states in the SINV biological cycle; i.e., at 4 hpi, viral gene expression coexists with host protein synthesis, while the proteins synthesized at 18 hpi are almost exclusively viral (Figure 1C). SILAC labels were permuted among uninfected, 4 hpi, and 18 hpi in the three biological replicates to correct for possible isotope-dependent effects. After lysis, aliquots were stored for parallel transcriptomic and whole-proteome analyses. We combined equal amounts of the lysates from the three conditions prior to the oligo(dT) capture, and eluates were analyzed by quantitative proteomics (Figure 1A). Protein intensity ratios between condition pairs were computed, and the significance of each protein intensity change was estimated using a moderated t test (Figures 2A–2D, S2A, and S2B). We used a semiquantitative method for the cases in which an intensity value was missing (“zero”) in one of the two conditions leading to “infinite” or zero ratios (Sysoev et al., 2016).

We identified a total of 794 proteins, 91% of which were already annotated by the Gene Ontology term “RNA-binding” or/and previously reported to be RBPs in eukaryotic cells by RIC (Hentze et al., 2018). Hence, the protein composition of our dataset largely resembles that of previously established RBPomes. Only 17 proteins displayed differential interaction with RNA at 4 hpi (Figures 2A, 2B, and S2A; Table S1). Fifteen of these were detected exclusively by the semiquantitative method due to the lack of intensity value in one condition, reflecting possible “on-off” and “off-on” states (Table S1). By contrast, 236 RBPs displayed altered RNA-binding activities at 18 hpi (Figures 2C, 2D, and S2B; Table S1). A total of 247 RBPs displayed

(E) Silver staining analysis of the “inputs” (i.e., total proteome, left) and eluates (i.e., RBPome, right) of a representative RIC experiment in SINV-infected cells. (F) qRT-PCR analysis of the eluates of a representative RIC experiment using specific primers against SINV RNAs, *actb* and *gapdh* (for normalization) mRNAs. Error bars represent SE.

hpi, hours post-infection; MW, molecular weight.

See also Figure S1.



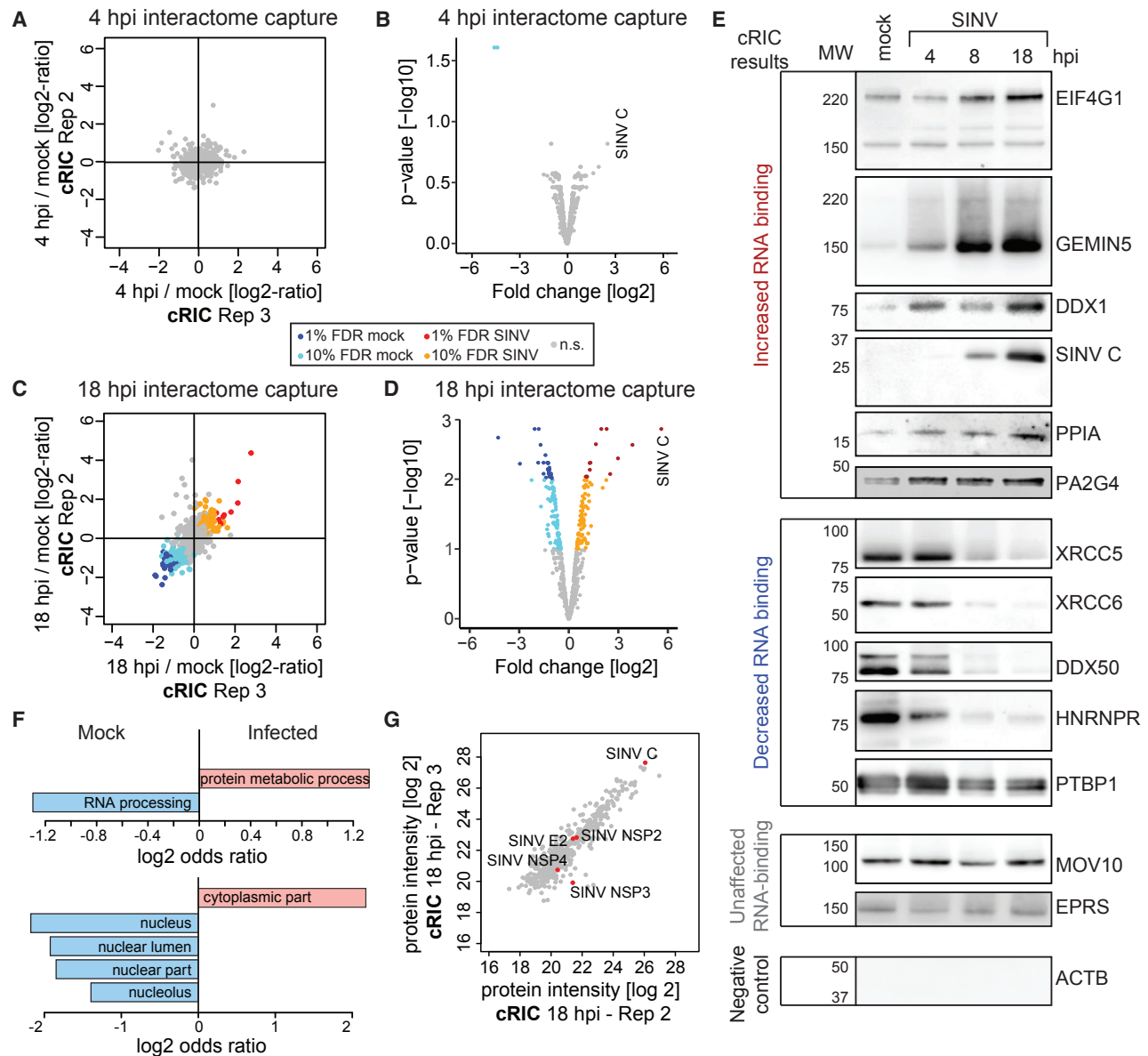


**Figure 2. Analysis of the RNA-Bound Proteome in SINV-Infected HEK293 Cells by cRIC**

(A) Scatterplot showing the intensity ratio between 4 hpi and uninfected conditions of each protein (dots) in the eluates of two biological replicates of cRIC. (B) Volcano plot showing the log<sub>2</sub> fold change and the significance (p value) of each protein between 4 hpi and uninfected conditions using data from three biological replicates. (C) As in (A) but for 18 hpi. (D) As in (B) but for 18 hpi. (E) Western blotting analysis with specific antibodies of the eluates of a representative RIC experiment in SINV-infected HEK293 cells. (F) Molecular function (top) and cellular component (bottom) Gene Ontology (GO) term enrichment analysis of the stimulated (salmon) against inhibited (blue) RBPs (18 hpi). (G) Representative scatterplot comparing the raw intensity of each protein in the eluates of two cRIC replicates at 18 hpi. FDR, false discovery rate; n.s., non-significant. See also [Figure S2](#) and [Table S1](#).

differential binding in infected cells (4 and 18 hpi) and are referred to here as “altered RBPs.” Interestingly, 181 of these lack classical RBDs, highlighting the importance of unconventional RBPs in virus infection.

To validate these results, we applied RIC to cells infected with SINV but, in this case, the eluates were analyzed by western blotting. We selected nine altered RBPs falling into three statistical categories; i.e., four with 1% false discovery rate (FDR), four



with 10% FDR, and one with nonsignificant changes. We included a positive control (the viral RBP SINV capsid [C]), two “non-altered” RBPs (MOV10 and EPRS), and a negative control ( $\beta$ -actin [ACTB]). Strikingly, the RNA-binding behavior of each protein fully matched the proteomic outcome, including those classified with 10% FDR (Figure 2E). Changes in RNA binding increased progressively throughout the infection. The proteomic data assigned a nonsignificant downregulation to HNRNPR (Table S1); however, the reduced activity of this protein was apparent by western blotting (Figure 2E), suggesting that our dataset may contain false negatives. Nonetheless, the excellent agreement between the proteomic and western blotting data supports the high quality of our results.

### Determination of the RBP Networks Altered by SINV Infection

Among the 247 altered RBPs, 133 presented reduced and 114 increased association with RNA, and they are here referred to as “inhibited” and “stimulated” RBPs, respectively. Most of the inhibited RBPs were linked to nuclear processes such as RNA processing and export (Figures 2F and S2C). While cytoplasmic viruses are known to hamper nuclear RNA metabolism, the mechanisms by which this occurs remain poorly understood (Castelló et al., 2011; Gorchakov et al., 2005; Lloyd, 2015). Whether the inhibition of nuclear RBPs contributes to this phenomenon should be further investigated. Conversely, a large proportion of the stimulated RBPs are cytoplasmic and are linked to protein synthesis, 5' to 3' RNA degradation, RNA transport, protein metabolism, and antiviral response (Figures 2F and S2D).

Interestingly, several RBPs involved in translation were stimulated at 18 hpi despite the shutoff of host protein synthesis (Figure 1C), including 9 eukaryotic initiation factors, 3 elongation factors, and 12 ribosomal proteins. This enhancement is likely due to the high translational activity of SINV RNAs (Figure 1C) (Frolov and Schlesinger, 1996). The core components of the cap-binding complex EIF4A1 and EIF4E were not stimulated by the infection despite the activation of their protein partner, EIF4G1 (Table S1). In agreement, EIF4A1 and EIF4E do not participate in SINV sgRNA translation (Carrasco et al., 2018). A recent report showed that EIF3D is a cap-binding protein that controls the translation of specific mRNA pools (Lee et al., 2016). EIF3D is stimulated by SINV, and thus its potential contribution to SINV RNA translation deserves further consideration. Importantly, 88 altered RBPs associate with ribosomes in mouse cells (Table S2) (Simsek et al., 2017). The existence of “specialized ribosomes” has been proposed; however, experimental evidence is sparse (Au and Jan, 2014). Our results indicate that the composition of ribosomes and the scope of proteins associated with them may strongly differ between infected and uninfected cells, possibly resulting in differential translational properties.

cRIC uncovered 16 altered RNA helicases (Table S2), 13 of which were inhibited upon infection. RNA helicases are fundamental at virtually every stage of RNA metabolism (Chen and Shyu, 2014), and their inhibition is expected to have important consequences in RNA metabolism. Only 3 helicases were stimulated by SINV (DDX1, DHX57, and DHX29) (Figure 2E; Table S2). DHX29 enhances 48S complex formation on SINV sgRNA

in reconstituted *in vitro* systems (Skabkin et al., 2010), and its stimulation supports its regulatory role in infected cells.

Notably, a defined subset of antiviral RBPs is stimulated upon SINV infection, including IFI16, IFIT5, TRIM25, TRIM56, and ZC3HAV1 (ZAP) (Table S1). IFI16 was previously described to bind dsDNA in cells infected with DNA viruses (Ni et al., 2016). Our data reveal that IFI16 also binds RNA, and it is activated early after SINV infection (4 hpi). This agrees with the recently described ability of IFI16 to restrict RNA virus infection (Thompson et al., 2014). These findings highlight the capacity of cRIC to identify antiviral factors responding virus infection.

Interestingly, cRIC also identified viral RBPs associated with poly(A) RNA, including the known viral RBPs (i.e., RNA helicase NSP2, the RNA polymerase NSP4, and capsid) and, unexpectedly, also NSP3 and E2 (Figures 2G and S2E). NSP3 was only quantified in two replicates (Figure S2E), and thus its interaction with RNA requires experimental confirmation. The identification of E2 in cRIC eluates was unexpected. In the viral particle of the related VEEV, E2 interacts with the capsid protein nearby cavities that communicate with the inner part of the virion where the gRNA density resides (Zhang et al., 2011), potentially enabling transitory or stochastic interactions with viral RNA.

### RBP Responses to SINV Are Not Caused by Changes in Protein Abundance

Changes detected by cRIC can be a consequence of matching alterations in protein abundance (Sysoev et al., 2016). To assess this possibility globally, we analyzed the total proteome by quantitative proteomics (cRIC inputs; Figure 1A). Importantly, SINV infection did not cause noticeable changes in host RBP levels, including 129 RBPs with altered RNA-binding activity (Figures 3A–3C and S3A–S3C; Table S3). In agreement, silver and Coomassie staining did not show noticeable protein fluctuations except for the viral capsid (Figure 1E and 3D). The lack of changes in protein levels, even for altered RBPs, was confirmed by western blotting (Figure 3E; Table S3). It is not wholly unexpected that RBPs are unaffected in spite of the shutoff of cellular protein synthesis. Analogous to siRNA experiments, detectable decreases in protein abundance may require hours or even days after translational suppression, especially for relatively stable proteins.

### The Transcriptome Undergoes Pervasive Changes in SINV-Infected Cells

Mechanistically, the activity of host RBPs can also be dictated by changes in the availability of their target RNAs. To test this possibility, we analyzed by RNA sequencing (RNA-seq) the total RNA isolated from cRIC input samples (Figure 1A). 4 h of SINV infection had a relatively minor impact on the host transcriptome (Figure 3F). By contrast, deep changes were observed at 18 hpi, with 12,372 differentially expressed RNAs ( $p < 0.1$ ; Figures 3G and S3E–S3G). Only 1,448 RNAs were upregulated, and these were enriched in the Gene Ontology (GO) term “antiviral response.” By contrast, 10,924 RNAs were downregulated, including many housekeeping genes (Table S4).

To validate these results by an orthogonal approach, we used qRT-PCR focusing on 20 mRNAs randomly chosen across the whole variation range. Importantly, data obtained

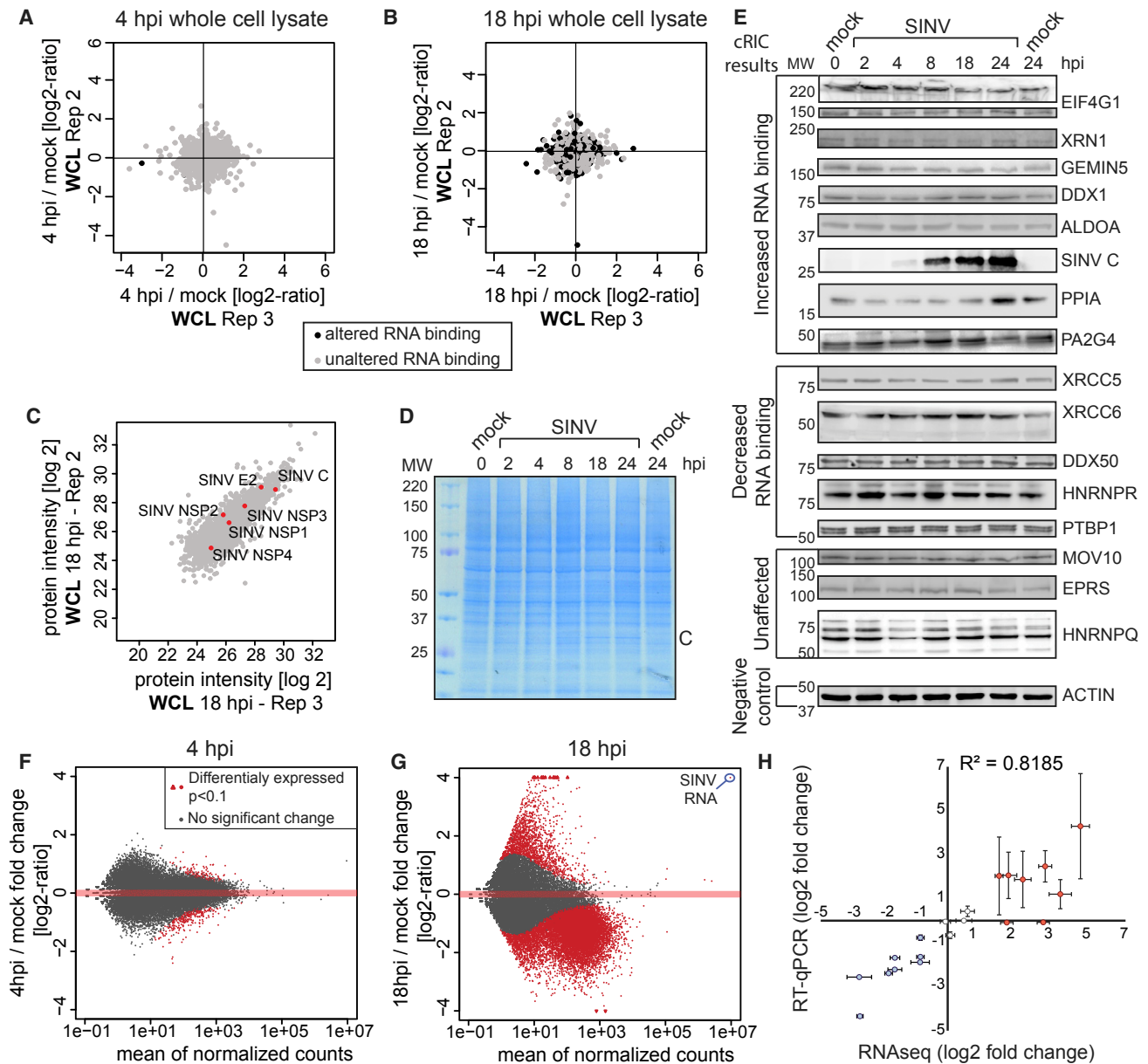


**Figure 3. Proteomic and Transcriptomic Analyses of Whole SINV-Infected Cell Lysates**

(A) Scatterplot comparing the intensity ratio between 4 hpi and uninfected conditions of each protein (dots) in the inputs (total proteome) of two biological replicates of cRIC. Black dots represent proteins significantly enriched in either 4 hpi or uninfected conditions in Figure 2A.

(B) As in (A) but for 18 hpi.

(C) Scatterplot comparing the intensity of each protein in the inputs of two cRIC replicates at 18 hpi.

(D) Representative Coomassie blue staining of cells infected with SINV.

(E) Western blotting analysis of lysates of cells infected with SINV (see Table S3 for quantification).

(F) MA plot comparing the read coverage and the log<sub>2</sub> fold change between 4 hpi and uninfected cells of each gene detected in the RNA sequencing (RNA-seq) experiment. Red dots represent RNAs enriched with  $p < 0.1$ .

(G) As in (F) but for 18 hpi.

(H) Correlation of the RNA-seq and RT-qPCR data by plotting the log<sub>2</sub> fold change for randomly selected transcripts by the two methods. Error bars represent SE of three independent experiments.

See also Figure S3 and Tables S3 and S4.

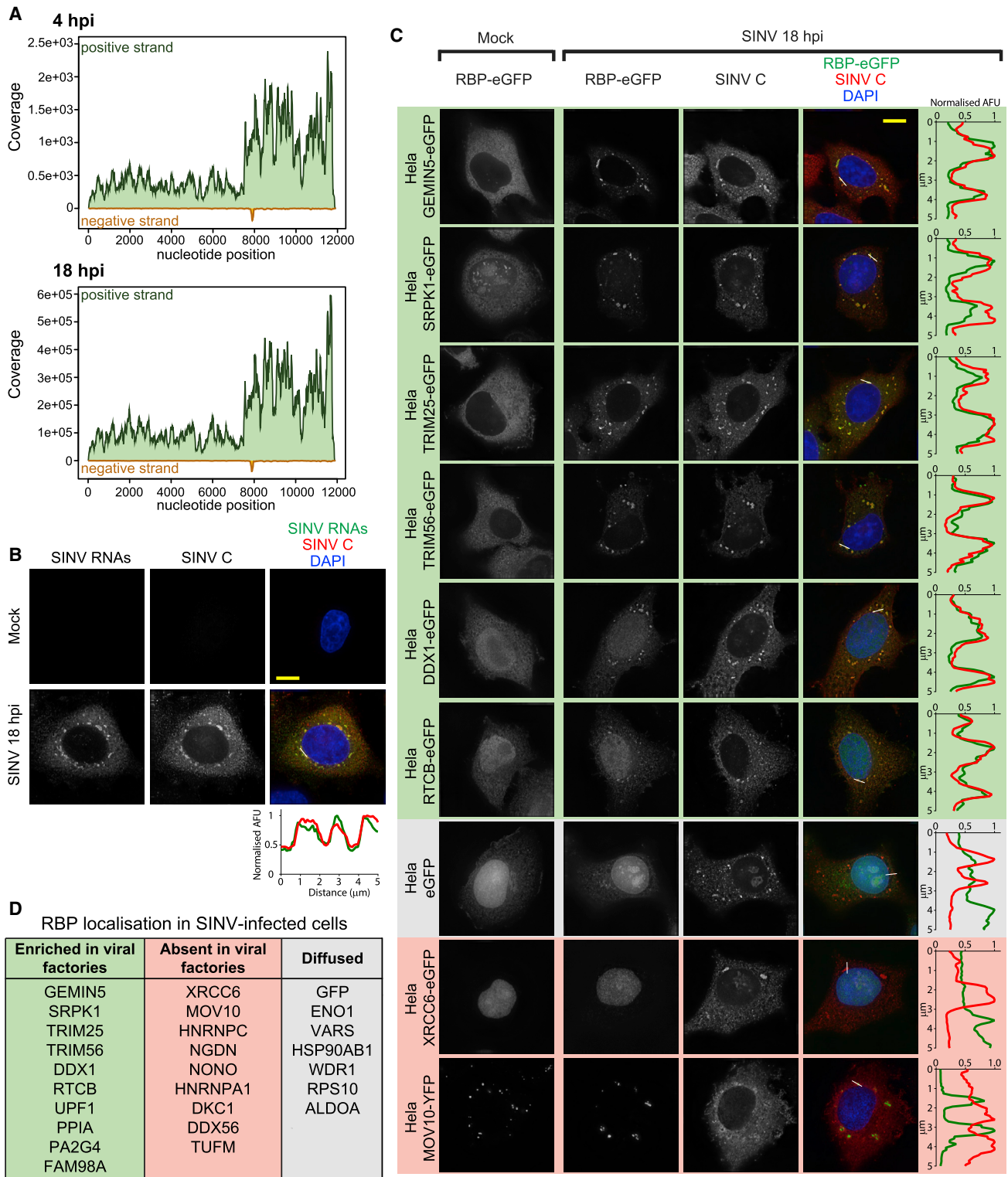


**Figure 4. Host RBP Localization in SINV-Infected Cells**

(A) RNA-seq read coverage of the positive and negative RNA strand of SINV. Note that the y axes in both plots have different scales.

(B) Localization analysis of SINV RNA and capsid protein in infected HeLa cells at 18 hpi by combined *in situ* hybridization and immunofluorescence.

(legend continued on next page)

with both techniques strongly correlated ( $R^2 = 0.82$ ) (Figure 3H), confirming the RNA-seq results. The decreased availability of cellular RNA could explain why 133 RBPs display reduced association with poly(A) RNA in infected cells (Table S1). In addition, inhibited RBPs could exchange poly(A) mRNA for non-poly(A) RNAs, which are not captured by the oligo(dT) beads.

### Stimulated RBPs Are Relocated to the Viral Replication Factories

SINV produces two overlapping mRNAs, gRNA and sgRNA (Figures 1B and S1A), and, consequently, the read coverage was substantially higher in the last third of the gRNA, where both transcripts overlap (Figure 4A). Both sgRNA and gRNA have poly(A) and thus should contribute to the cRiC results (Figures 4A and S4A). Conversely, the negative strand has low abundance and lacks a poly(A) tail. Importantly, SINV RNAs become the most abundant RNA species, after rRNA, at 18 hpi (Figures 3G and S3G). The emergence of such abundant RNA substrates likely induces cellular RBPs to exchange the “declining” cellular mRNAs for “emerging” viral RNAs, driving the remodeling of the RBPome. Alternatively, “dormant” RBPs could be “awakened” by the recognition of signatures within the viral RNA, analogous to known antiviral RBPs (Vladimer et al., 2014). We thus hypothesized that RBPs displaying enhanced binding should co-localize with viral RNA.

SINV RNA and capsid accumulate in cytoplasmic foci that correspond to the viral factories (Figures S1D, 4B, and S4A). To test whether stimulated RBPs relocate to these foci, we generated 26 tetracycline-inducible cell lines expressing host RBPs fused to EGFP. These included 16 lines expressing stimulated RBPs and 8 expressing inhibited RBPs. The non-altered RBP, MOV10, and unfused EGFP were used as controls. Strikingly, 9 out of the 16 stimulated RBPs (56%) accumulated at viral factories demarcated by SINV C (Figures 4C, 4D, and S4B). Five additional stimulated RBPs (29%) showed diffuse localization in cytoplasm but were also present at the capsid-containing foci (Figure S4B). *In situ* hybridization analysis confirmed that SINV RNA co-localized with a representative stimulated RBP, GEMIN5, supporting the potential interplay between stimulated RBPs and viral RNA (Figure S4C). Among the stimulated RBPs, only NGDN, HNRNPA1 and the mitochondrial translation elongation factor TUFM (3 out of 16; 17%) were absent in the viral factories, which suggests that their function is restricted to host RNAs. HNRNPA1 was shown to bind SINV RNA (LaPointe et al., 2018; Lin et al., 2009), while in our analysis, it strictly displays nuclear localization (Figure S4B). We cannot rule out that a small pool of HNRNPA1 is present in the viral factories at undetectable levels or, alternatively, that the EGFP tag is affecting HNRNPA1 localization.

In contrast to stimulated RBPs, only one (out of 8; 12.5%) inhibited RBP was enriched in the viral factories (Figures 4D and

S4B). This protein, called UPF1, is a helicase involved in the nonsense-mediated decay pathway and is known to inhibit infection of alphaviruses (Balistreri et al., 2014). Conversely, 5 out of 8 (62.5%) virus-inhibited RBPs are nuclear and remained nuclear after infection (Figures 4C, 4D, and S4B). These results indicate that, with exceptions, inhibited RBPs do not redistribute to the viral factories.

### The Exonuclease XRN1 Is Essential for SINV Infection

The loss of cellular mRNAs is likely contributing to the remodeling of the RBPome by diminishing substrate availability. However, it is unclear how this phenomenon is triggered and whether it benefits or hampers viral infection. Changes in RNA levels can globally be a consequence of reduced transcription and/or increased RNA degradation. To explore which of these pathways contribute the most to RNA loss in SINV-infected cells, we compared the fold change of each mRNA in our dataset to the rate of synthesis, processing, and degradation of each individual transcript (Mukherjee et al., 2017). Transcription could explain most of the differences at 4 hpi, whereas RNA degradation accounted for more than 50% of the explained variance at 18 hpi (Figures 5A and S5A). We reasoned that this phenomenon can be a combined effect of the activation of the 5' to 3' RNA degradation machinery, as the exonuclease XRN1 and its interactor, PATL1, are stimulated at 18 hpi (Table S1), and a reduced transcriptional activity (Gorchakov et al., 2005).

XRN1 is broadly considered as an antiviral factor that erases viral RNA (Molleston and Cherry, 2017). RNA pseudoknots present in several viral RNAs are able to stall XRN1, leading to the production of sgRNAs (Chapman et al., 2014; Pijlman et al., 2008). In dengue virus (DENV), XRN1-derived sgRNAs can benefit infection by interfering with the antiviral response (Manokaran et al., 2015).

In SINV-infected cells, XRN1 and MOV10 foci (corresponding to P-bodies) are juxtaposed to the viral replication factories, suggesting that the exonuclease could attack viral RNA (Figures 4C, S4C, and 5B). To our surprise, XRN1 knockout (KO) cells were refractory to SINV infection, while partial KO led to an intermediate phenotype (Figure 5C). These results suggest that XRN1 activity is instead essential for SINV infection. XRN1 KO cells did not exhibit any defect in cell morphology, proliferation rate, or viability, and they supported efficiently the replication of HIV-1 (Figures 5D and S5C–S5F). These results indicate that XRN1 KO lines are not metabolically deficient or subjected to a heavy stress incompatible with virus infection.

To determine if XRN1 activity involves the generation of RNA degradation products, we analyzed our RNA-seq data. However, we did not find any increase in read coverage compatible with XRN1-derived degradation products, suggesting that XRN1 role in SINV infection differs from that described for DENV.

(C) Localization by immunofluorescence of the EGFP-fused RBPs and SINV C. Green and red fluorescence intensity profiles in a representative 5- $\mu$ m section (white line) are plotted in (B) and (C).

(D) Summary of the observed localization of the 26 proteins tested in (C) and Figure S4B.

Scale bars represent 10  $\mu$ m. AFU, arbitrary fluorescence units.

See also Figure S4.



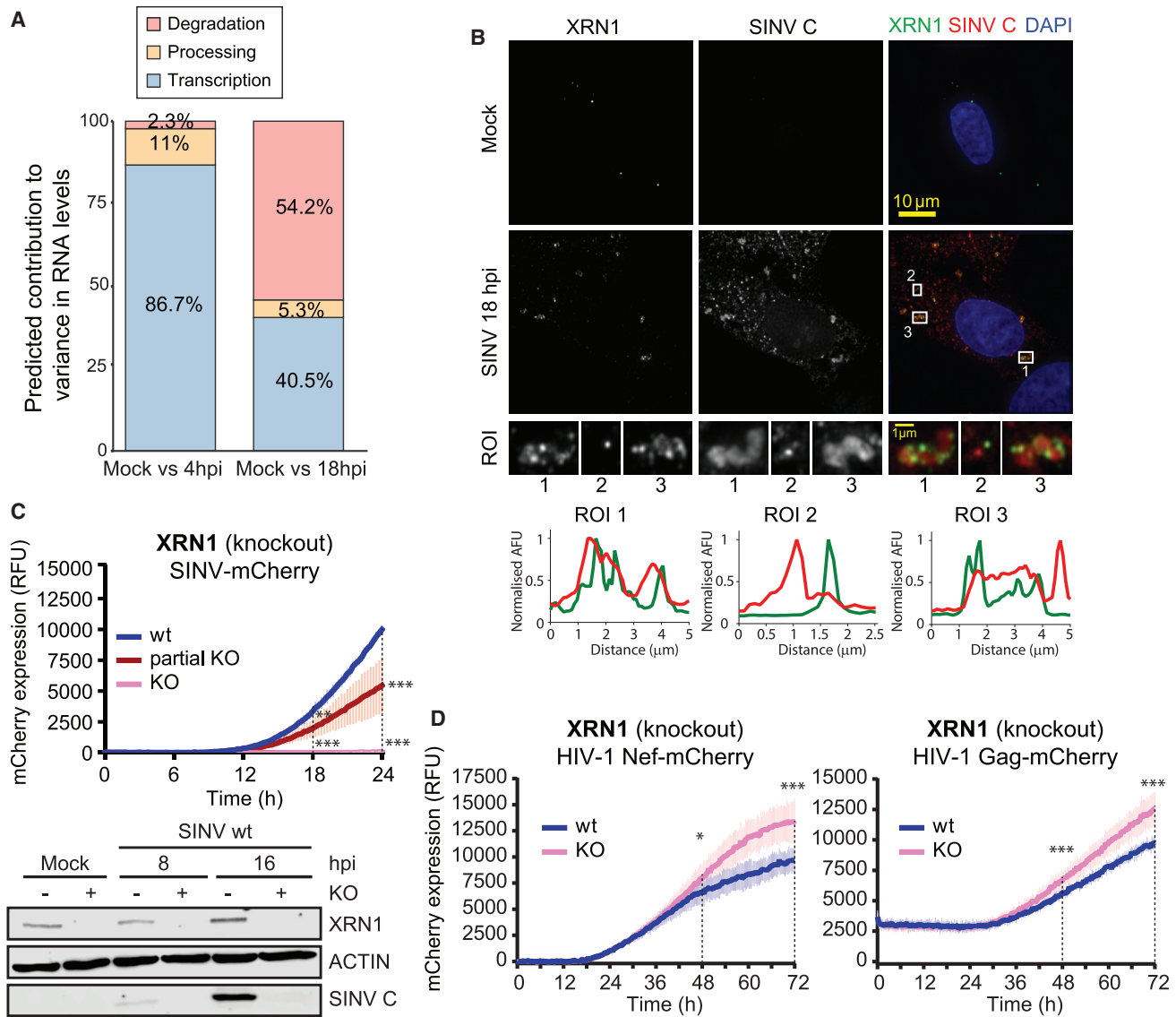


**Figure 5. The Exonuclease XRN1 in Cells Infected with SINV**

(A) Contribution of transcription, processing, and degradation to the transcriptomic changes induced by SINV. We compared our RNA-seq data to available data estimating these parameters (Mukherjee et al., 2017). ANOVA was used to predict the contribution of each RNA biological process to the variance in RNA levels. (B) Immunolocalization of XRN1 and SINV C. Green and red fluorescence profiles for regions of interest (ROI) are displayed.

(C) Top: mCherry fluorescence in XRN1 KO and control cells infected with SINV-mCherry measured every 15 min in a plate reader with atmospheric control (5% CO<sub>2</sub> and 37°C). RFU, relative fluorescence units. Western blot of XRN1 and SINV C (bottom).

(D) Infection fitness of HIV-1<sub>Nef-mCherry</sub> and HIV-1<sub>Gag-mCherry</sub> pseudotyped viruses in XRN1 KO cells. mCherry expression was measured as in (C). mCherry fluorescence is represented as mean ± SD of three independent infections in each of the three biological replicates (n = 9). \*\*\*p < 0.001; \*\*p < 0.01; \*p < 0.05.

See also Figure S5.

### RBPome Responses Are Biologically Important

To determine to a broader extent whether RBP responses are functionally important, we sought to study the impact of altered RBPs on virus infection. The ligase RTCB, together with DDX1, FAM98A, and other RBPs, forms the tRNA ligase complex (TRLIC) (Popow et al., 2011). RTCB and DDX1 were stimulated by SINV (Table S1), and these and FAM98A accumulated in the viral factories (Figures 4C and S4B). TRLIC mediates the un-

usual ligation of 3'-phosphate or 2',3'-cyclic phosphate to a 5'-hydroxyl and these molecule ends are generated by a limited repertoire of cellular endonucleases, which include the endoplasmic reticulum resident protein IRE1α (Popow et al., 2011). SINV has been proposed to cause unfolded protein response (Rathore et al., 2013), which is compatible with the activation of IRE1α and TRLIC in infected cells (Jurkin et al., 2014). Notably, inhibition of IRE1α with 4μ8C strongly reduced viral fitness in low,

non-cytotoxic concentrations (Figures 6A and S6A), suggesting that IRE1 $\alpha$  and TRLC are positively contributing to SINV infection.

PPIA (also cyclophilin A) has also been classified as an RBP by RIC studies (Hentze et al., 2018). It switches proline conformation-modulating protein activity, which plays a crucial role in hepatitis C virus infection (Rupp and Bartenschlager, 2014). PPIA is also important for the infection of other viruses, such as HIV-1 (Li et al., 2007). PPIA RNA-binding activity is stimulated by SINV infection and is recruited to the viral factories (Figures 2E and S4B). Interestingly, SINV-mCherry infection is delayed by PPIA loss of function (KO and inhibition; Figures 6B, S6A, and S6B). Overexpression had no effect in SINV-mCherry fitness (Figure 6B, bottom).

The heat shock chaperone HSP90AB1 is stimulated by SINV (Table S1). HSP90AB1 has been classified as an RBP by RIC (Hentze et al., 2018), and its RBD has been located in a discrete region at its C-terminal domain (Figure S6C) (Castello et al., 2016). Chaperones from the HSP90 family are important in the remodeling of RNPs and are linked to virus infection (Geller et al., 2012; Iwasaki et al., 2010). Notably, SINV-mCherry infection was significantly delayed in HSP90AB1 KO cells, even though four homologs of this protein exist (Figures 6C and S6B). Moreover, the pro-viral activity of HSP90AB1 was confirmed by treatment with specific inhibitors (Figures 6C and S6A). Again, overexpression had no effect in SINV-mCherry fitness (Figure 6C). The implication of PPIA and HSP90 in the biological cycle of a variety of unrelated viruses highlights these proteins as master regulators of infection (Garcia-Moreno et al., 2018).

PA2G4 RNA-binding activity was also enhanced by SINV (Table S1). It associates with ribosomes (Table S2) (Simsek et al., 2017) and regulates the cap-independent translation of foot-and-mouth disease virus (FMDV) RNA (Monie et al., 2007). Treatment with its specific inhibitor WS6 hampered SINV-mCherry fitness (Figures 6D and S6A), suggesting that this protein promotes SINV infection. Overexpression did not cause any effect, as with previous examples (Figure 6D). The possibility that PA2G4 contributes to the non-canonical, cap-dependent translation of SINV RNAs should be further investigated.

SRPK1 is a kinase that phosphorylates the RS repeats present in SR proteins, which are involved in alternative splicing regulation, RNA export, and stability (Howard and Sanford, 2015). SINV infection stimulates SRPK1 RNA-binding activity (Table S1) and causes its relocation to viral replication factories (Figure 4C). Inhibition of SRPK1 hampers SINV and HIV-1 infection (Fukuhara et al., 2006), and we show here that overexpression of SRPK1 enhances SINV fitness (Figure 6E). This suggests that SRPK1 positively contributes to SINV infection. Future work should determine if SRPK1 kinase activity is involved in infection, and if so, which proteins it phosphorylates.

We tested the effects of overexpression of nine additional stimulated or inhibited RBPs fused to EGFP (Figures S6D and S6E). Phenotypes in viral fitness ranged from nonexistent (ALDOA, XRCC6, RPS10, MOV10, NGDN, and CSTF2) to mild (RPS27, NONO, and DKC1). The lack of phenotypic effects in

overexpression experiments does not rule out that the protein actually participates in SINV infection (see above). Nevertheless, RBPs whose overexpression affects infection fitness have potential as regulatory proteins.

The family of tripartite-motif-containing (TRIM) proteins comprises more than 75 members endowed with E3 ubiquitin ligase activity, and few of them have been classified as RBPs by RIC (Hentze et al., 2018). Notably, SINV infection enhanced TRIM25 and TRIM56 interaction with RNA (Table S1), correlating with their redistribution to viral replication factories (Figure 4C). TRIM25 was proposed to interact with DENV RNA (Manokaran et al., 2015); however, this analysis employed native immunoprecipitation (IP) that cannot distinguish between direct and indirect protein-RNA interactions. To test if TRIM25 interacts directly with SINV RNA, we immunoprecipitated under stringent conditions TRIM25-EGFP from SINV-infected cells irradiated with UV light. Co-precipitated RNA was analyzed by RT-PCR using specific primers against SINV RNA. A band with the expected size was detected in TRIM25-EGFP IPs, but not in the negative controls (Figure 7A), confirming that TRIM25 interacts with SINV RNA directly. TRIM25 interaction with RNA enhances its E3 ubiquitin ligase activity (Choudhury et al., 2017). TRIM25-EGFP overexpression inhibited SINV-mCherry infection (Figure 7B), which agrees with its ability to activate the key antiviral factors RIG-I and ZC3HAV1 through ubiquitination (Gack et al., 2007; Li et al., 2017). It is known that TRIM56 binds double-stranded DNA. However, it enhances the antiviral response in cells infected with both DNA and RNA viruses (Seo et al., 2018; Tsuchida et al., 2010). cRIC thus complements these results, revealing that TRIM56 interacts directly with RNA (Table S1). As with TRIM25, overexpression of TRIM56-EGFP reduced SINV fitness (Figure 7B), confirming its capacity to restrict the infection of the RNA virus, SINV.

Importantly, 160 out of the 247 altered RBPs lack previous connections to virus infection (Garcia-Moreno et al., 2018). Hence, our dataset likely contains numerous pro- and antiviral RBPs yet to be uncovered.

### **GEMIN5 Binds to the 5' UTR of SINV RNAs and Regulates Viral Protein Expression**

GEMIN5 is a member of the survival motor neuron (SMN) complex, which mediates the assembly of the small nuclear RNPs (snRNPs) (Gubitz et al., 2002). It is strongly stimulated by SINV infection and redistributed to the viral factories co-localizing with SINV RNA (Figures 2E, 4C, and S4C). To our surprise, none of the known molecular partners of GEMIN5 (i.e., GEMIN and SMN proteins) were stimulated by SINV (Table S1), implying a GEMIN5-specific response that agrees with the existence of a free pool of GEMIN5 (Battle et al., 2007). In SINV-infected cells, overexpression of GEMIN5-EGFP caused a moderate but significant delay of mCherry production and strongly inhibited capsid synthesis (Figure 7B). These results align well with the described role of GEMIN5 in translational control (Francisco-Velilla et al., 2018; Piñeiro et al., 2015).

Protein-protein interaction analysis of GEMIN5-EGFP revealed that, in our experimental settings, it interacts with the ribosome, especially with the 60S subunit (Figure 7C, pink

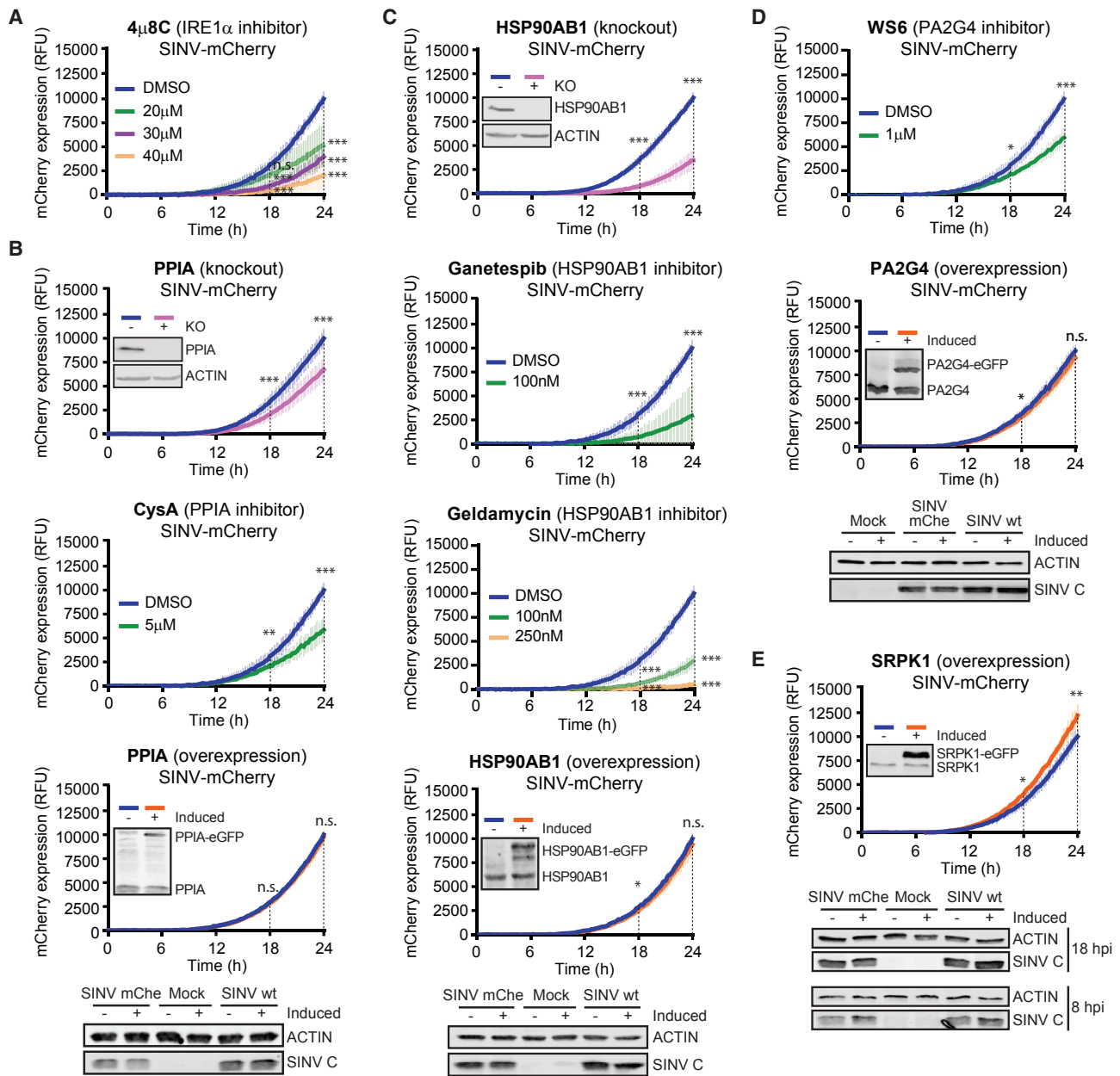


**Figure 6. Impact of Stimulated RBPs in SINV Infection**

(A) Expression of mCherry in HEK293 cells infected with SINV-mCherry and treated or not with the IRE1α inhibitor 4μ8C. Red fluorescence was measured as in Figure 5C.

(B) As in (A) but with PPIA KO cells (top), the PPIA inhibitor cyclosporine A (CysA) (middle), and cells overexpressing PPIA-EGFP (bottom). KO and overexpression of PPIA and SINV C accumulation (18 hpi) were assessed by western blotting.

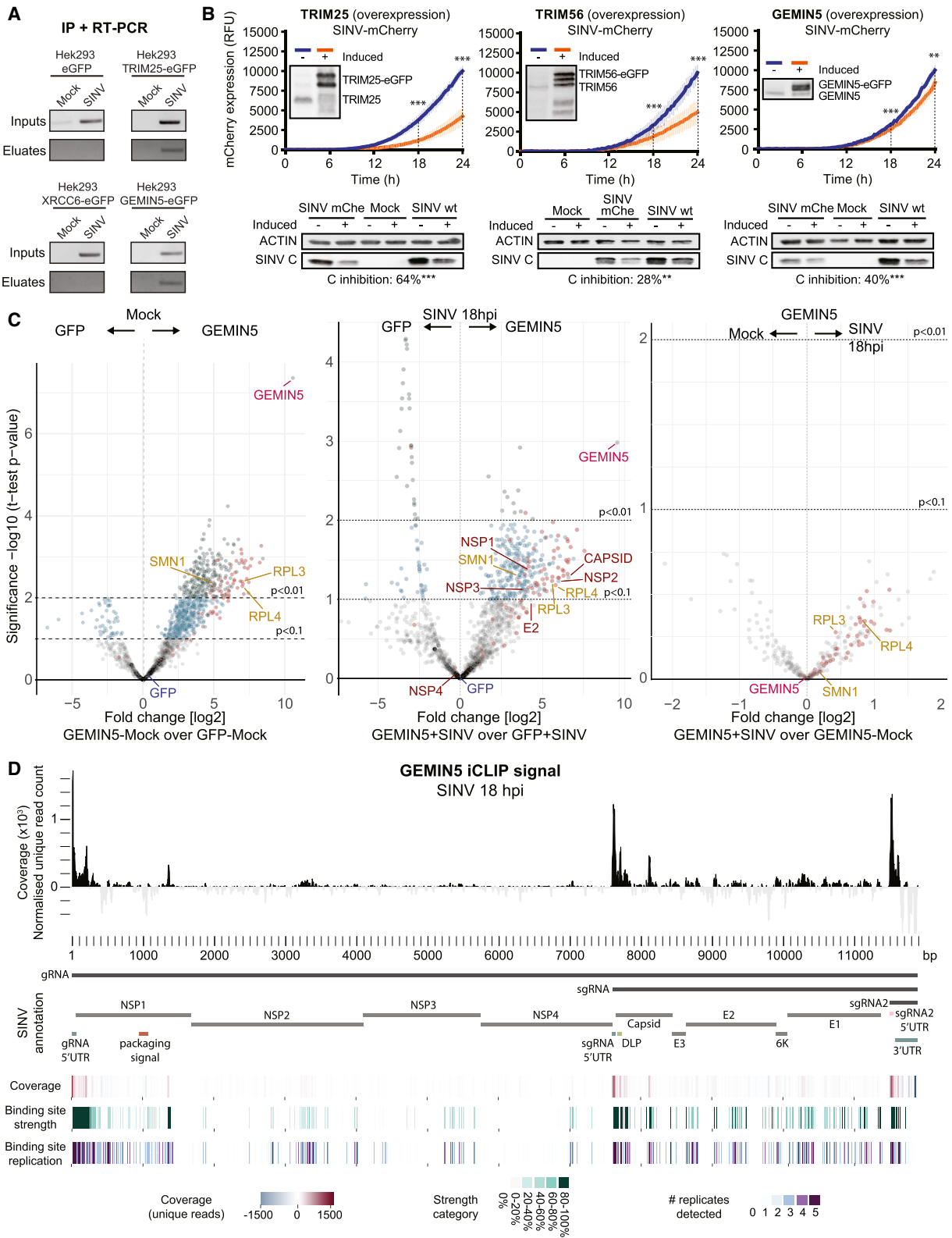
(C) mCherry fluorescence in HSP90AB1 KO cells (top), cells treated with ganetespiib or geldamycin (middle panels), or cells overexpressing HSP90AB1-EGFP (bottom) and infected with SINV-mCherry. KO and overexpression of HSP90AB1 and SINV C accumulation (18 hpi) were assessed by western blotting.

(D) As in (A) but using the PA2G4 inhibitor WS6 (top) and cells overexpressing PA2G4-eGFP (middle). Right: western blots against SINV C at 18 hpi.

(E) As in (A) but with cells overexpressing SRPK1 (top). Overexpression of SRPK1 was assessed by western blotting. Bottom: western blots of SINV C in these cells at 18 hpi.

mCherry fluorescence is shown as the mean ± SD of three independent infections in each of the three biological replicates (n = 9). \*\*\*p < 0.001; \*\*p < 0.01; \*p < 0.05. SINV-mChe, SINV-mCherry; n.s., non-significant.

See also Figure S6.



(legend on next page)



dots, left; [Figures S7C and S7D](#); [Table S5](#)). This interaction is sustained in SINV-infected cells ([Figure 7C](#), pink dots, middle and right). These results are in agreement with previous studies showing that GEMIN5 impacts protein synthesis at the translation elongation step through its direct interaction with the 60S ribosomal subunit and, in particular, with RPL3 and RPL4, which are also enriched in our IPs ([Table S5](#)) ([Francisco-Velilla et al., 2016](#)). We noticed that GEMIN5 is by far the most enriched protein in our IPs and that its Intensity Based Absolute Quantification (iBAQ) score is significantly higher than that of EGFP, suggesting that GEMIN5-EGFP interacts with the endogenous GEMIN5, likely forming oligomers, as previously described ([Xu et al., 2016](#)). Moreover, our data showed that GEMIN5 interacts with various viral proteins, chiefly with NSP1, NSP2, NSP3 and SINV C ([Figure 7C](#), middle). The implications of these interactions in the modulation of GEMIN5 function deserve future considerations.

GEMIN5 is cleaved by the L protease of FMDV, and resulting C-terminal moiety enhances internal ribosome entry site (IRES)-driven translation ([Piñeiro et al., 2013](#)). However, GEMIN5 is not cleaved in SINV-infected cells ([Figure 3E](#)), and SINV RNAs lack an IRES and are capped ([Carrasco et al., 2018](#)). To test whether GEMIN5 binds SINV RNA, we performed an IP and RT-PCR analysis as outlined above. A PCR product was amplified in GEMIN5-EGFP eluates ([Figure 7A](#)), which agrees with the striking co-localization of SINV RNA and GEMIN5 ([Figure S4C](#)). To get insights into how GEMIN5 recognizes SINV RNAs, we employed single-nucleotide-resolution crosslinking and immunoprecipitation followed by sequencing (iCLIP) ([König et al., 2010](#)). Interestingly, the footprints with highest coverage mapped to the 5' ends of the gRNA and sgRNA ([Figures 7D and S7E–S7G](#)). These reads often presented an additional guanosine at the 5' end ([Figure S7H](#)), likely reflecting binding to the cap structure. These results support previous data showing that GEMIN5 is captured in cap-Sepharose beads ([Bradrick and Gromeier, 2009](#)). Additional peaks overlap with the downstream loop (DLP), which is a hairpin structure that stimulates the translation of the sgRNA ([Frolov and Schlesinger, 1996](#)). Interaction with the cap, 5' UTR, and DLP of viral RNAs aligns well with the proposed role as translational regulator and the observed inhibition of capsid expression. Our data support the model in which GEMIN5 recognizes the 5' end of the

gRNA and sgRNA and prevents their translation by interfering with ribosomal function.

### Outlook

We show here that SINV infection induces changes in the active RBPome that affects both well-established and unconventional RBPs. Mechanistically, the RBPome rearrangement can be explained by the loss of cellular RNA and the emergence of the highly abundant viral RNA. Supporting this conclusion, we observed that most of the RBPs with enhanced activity accumulate in the viral factories together with the viral RNA. However, this RNA-driven remodeling of the RBPome is not incompatible with complementary “fine-tuning” regulatory mechanisms affecting RBPs on an individual basis. For example, it is known that virus infection triggers signaling pathways involving kinases ([Figure 1D](#)), E3 ubiquitin ligases, prolyl *cis/trans* isomerases, and chaperones ([Carrasco et al., 2018](#); [Gack et al., 2007](#); [Li et al., 2017](#)). Here, we show that these protein families are represented among the stimulated RBPs, including SRPK1, TRIM25, TRIM56, PPIA, and HSP90AB1. Hence, it is plausible that post-translational control also contributes to RBP regulation in SINV-infected cells. Moreover, interactions with viral proteins can regulate RBP function ([Fros et al., 2012](#)). We show that GEMIN5 interacts with several viral proteins, suggesting that this regulatory mechanism may apply to altered RBPs more broadly ([Figure 7C](#)).

Importantly, changes in the RBPome are biologically important, as perturbation of the altered RBPs strongly affects SINV infection. Therefore, every protein reported here to respond to SINV infection has potential as anti- or pro-viral factor, highlighting cellular RBPs as promising targets for antiviral therapies.

Some of the outstanding questions derived from this work include whether the distinct composition of ribosomes in infected cells affects their translational properties, why the lack of the exonuclease XRN1 makes the cells refractory to SINV, what triggers the degradation of host RNA, and why the transcripts induced by the antiviral response are resistant to degradation. Moreover, GEMIN5 emerges as a highly responsive RBP that impairs SINV infection. The exact mechanisms underpinning GEMIN5 effects in translation require further investigation.

### Figure 7. Effects of RBPs with Antiviral Potential in SINV Infection

(A) UV crosslinking and immunoprecipitation of TRIM25-EGFP, GEMIN5-EGFP, XRCC6-EGFP, or unfused EGFP in cells infected or not with SINV for 18 h. The presence of SINV RNA in eluates and inputs was detected by RT-PCR using specific primers against SINV RNAs.  
(B) Relative mCherry fluorescence produced in cells overexpressing TRIM25-EGFP (top left), TRIM56-eGFP (top middle), GEMIN5-eGFP (top right), and infected with SINV-mCherry (measured as in [Figure 5C](#)). mCherry expression is represented as the mean  $\pm$  SD of three independent infections in each of the three biological replicates ( $n = 9$ ). Overexpression was assessed by western blotting. Bottom: western blots of SINV C at 18 hpi, indicating below the average inhibition of C relative to control cells. \*\*\* $p < 0.001$ ; \*\* $p < 0.01$ .  
(C) Volcano plots comparing the intensity of proteins in GEMIN5-EGFP versus unfused EGFP IPs in uninfected (left) and infected cells (middle); every dot represents a protein. Dark green dots are proteins enriched with  $p < 0.01$ , blue dots are those enriched with  $p < 0.1$ , and gray dots represent nonenriched proteins. Pink dots represent ribosomal proteins. Right: a volcano plot comparing the intensity of proteins in GEMIN5 IPs in infected versus uninfected cells.  
(D) iCLIP analysis of GEMIN5-binding sites on SINV RNA. Top: coverage pileup of 5' first base of unique molecules mapping to the SINV genome, shown as 20-nt sliding mean of five replicates after GFP background subtraction. Each position is given relative to total SINV count (RPM). Middle: key features of SINV annotation. Bottom: the top track shows iCLIP coverage but as a heatmap representation. The middle heatmap shows GEMIN5 binding sites along SINV divided into five groups according to strength of binding. The bottom heatmap shows the number of replicates supporting each binding site when binding sites are called independently for each replicate.  
See also [Figure S7](#) and [Table S5](#).

Finally, cRIC has been applied here to cells infected with SINV. However, it can now be extended to other viruses or physiological cues to improve our understanding of RBP regulation and its biological importance.

## STAR★METHODS

Detailed methods are provided in the online version of this paper and include the following:

- **KEY RESOURCES TABLE**
- **CONTACT FOR REAGENT AND RESOURCE SHARING**
- **EXPERIMENTAL MODEL AND SUBJECT DETAILS**
  - Cell culture
  - Cell culture in SILAC media
  - Viruses
- **METHOD DETAILS**
  - RNA interactome capture
  - Conventional protein analyses
  - Reverse-transcription and quantitative PCR
  - Plasmids and recombinant DNA procedures
  - mCherry-based viral fitness assay
  - Drugs and cell viability assay
  - Protein-protein interactions analysis
  - RBP-RNA interaction analysis: CLIP/RT-PCR
  - Analysis of GEMIN5 binding sites by iCLIP
  - Immunofluorescence and RNA FISH assays
  - Determining the percentage of infected cells
  - Mass spectrometry
  - RNA sequencing
- **QUANTIFICATION AND STATISTICAL ANALYSES**
  - Proteomic quantitative analysis
  - RNA sequencing data analysis
  - Analysis of RNA synthesis, processing, and degradation
  - iCLIP-seq data processing
- **DATA AND SOFTWARE AVAILABILITY**

## SUPPLEMENTAL INFORMATION

Supplemental Information can be found with this article online at <https://doi.org/10.1016/j.molcel.2019.01.017>.

## ACKNOWLEDGMENTS

We dedicate this work to our colleagues and friends Bernd Fischer and Katrin Eichelbaum, who sadly passed away during the development of this work. We thank Matthias W. Hentze, Encarnacion Martinez-Salas, Javier Martinez, Kui Li, Quentin Sattentau, Ilan Davis, Richard Parton, and Jan Rehwinkel for reagents and advice. We thank the Oxford Micron Advanced Bioimaging Unit for support in microscopy experiments. A.C. is funded by MRC Career Development Award MR/L019434/1, MRC grant MR/R021562/1, and John Fell Funds from the University of Oxford. M.G.M. is funded by the European Union's Horizon 2020 research and innovation programme under Marie-Skłodowska-Curie grant agreement 700184. I.D. is funded by Wellcome Trust Investigator Award 209412/Z/17/Z. V.P. is funded by a SciLifeLab Fellowship, the Swedish Research Council (VR 2016-01842), a Wallenberg Academy Fellowship (KAW 2016.0123), and the Ragnar Söderberg Foundation. L.C. is funded by grant DGICYT SAF2015-66170-R (MINECO/FEDER). E.G.A. was awarded with a short-term EMBO fellowship (ASTF 358-2015) and an FPU fellowship FPU15/05709. G.M. was supported by the Wellcome Seed Award

in Science (210144/Z/18/Z) and the Wellcome Trust Centre Core Grant (092076). G.H. was a recipient of a Wellcome Trust PhD studentship (105246/Z/14/Z).

## AUTHOR CONTRIBUTIONS

Conceptualization, M.N., L.C., B.F., S.M., and A.C.; Methodology, M.G.-M., M.N., S.N., A.I.J., E.G.-A., C.E.L., I.D., B.F., S.M., and A.C.; Investigation, M.G.-M., M.N., S.N., A.I.J., E.G.-A., C.E.L., M.B.-P., V.C., R.A., T.D., S.H., T.J.M.S., B.L., M.A.S., E.P.R., V.P., B.F., S.M., and A.C.; Writing – Original Draft, M.G.-M., M.N., A.I.J., and A.C.; Writing – Editing, M.G.-M., M.N., S.N., A.I.J., C.E.L., S.M., and A.C.; Funding Acquisition, M.G.-M. and A.C.; Resources, G.H., G.M., L.C., E.P.R., V.P., I.D., B.F., S.M., and A.C.; Supervision, M.G.-M., M.N., A.I.J., B.F., S.M., and A.C.

## DECLARATION OF INTERESTS

The authors declare no competing interests.

Received: June 18, 2018

Revised: December 18, 2018

Accepted: January 11, 2019

Published: February 21, 2019

## REFERENCES

- Akusjarvi, G. (2008). Temporal regulation of adenovirus major late alternative RNA splicing. *Front. Biosci.* *13*, 5006–5015.
- Au, H.H., and Jan, E. (2014). Novel viral translation strategies. *Wiley Interdiscip. Rev. RNA* *5*, 779–801.
- Balistreri, G., Horvath, P., Schweingruber, C., Zünd, D., McInerney, G., Merits, A., Mühlemann, O., Azzalin, C., and Helenius, A. (2014). The host nonsense-mediated mRNA decay pathway restricts mammalian RNA virus replication. *Cell Host Microbe* *16*, 403–411.
- Baltz, A.G., Munschauer, M., Schwanhäusser, B., Vasile, A., Murakawa, Y., Schueler, M., Youngs, N., Penfold-Brown, D., Drew, K., Milek, M., et al. (2012). The mRNA-bound proteome and its global occupancy profile on protein-coding transcripts. *Mol. Cell* *46*, 674–690.
- Barbalat, R., Ewald, S.E., Mouchess, M.L., and Barton, G.M. (2011). Nucleic acid recognition by the innate immune system. *Annu. Rev. Immunol.* *29*, 185–214.
- Battle, D.J., Kasim, M., Wang, J., and Dreyfuss, G. (2007). SMN-independent subunits of the SMN complex. Identification of a small nuclear ribonucleoprotein assembly intermediate. *J. Biol. Chem.* *282*, 27953–27959.
- Bradrick, S.S., and Gromeier, M. (2009). Identification of gemin5 as a novel 7-methylguanosine cap-binding protein. *PLoS ONE* *4*, e7030.
- Carlson, M., and Pages, H. (2015). Homology information for Homo sapiens from Inparanoid. R package version 3.1.2 (Bioconductor).
- Carrasco, L., Sanz, M.A., and González-Almela, E. (2018). The regulation of translation in alphavirus-infected cells. *Viruses* *10*, E70.
- Castelló, A., Alvarez, E., and Carrasco, L. (2011). The multifaceted poliovirus 2A protease: regulation of gene expression by picornavirus proteases. *J. Biomed. Biotechnol.* *2011*, 369648.
- Castello, A., Fischer, B., Eichelbaum, K., Horos, R., Beckmann, B.M., Strein, C., Davey, N.E., Humphreys, D.T., Preiss, T., Steinmetz, L.M., et al. (2012). Insights into RNA biology from an atlas of mammalian mRNA-binding proteins. *Cell* *149*, 1393–1406.
- Castello, A., Horos, R., Strein, C., Fischer, B., Eichelbaum, K., Steinmetz, L.M., Krijgsveld, J., and Hentze, M.W. (2013). System-wide identification of RNA-binding proteins by interactome capture. *Nat. Protoc.* *8*, 491–500.
- Castello, A., Hentze, M.W., and Preiss, T. (2015). Metabolic enzymes enjoying new partnerships as RNA-binding proteins. *Trends Endocrinol. Metab.* *26*, 746–757.

- Castello, A., Fischer, B., Frese, C.K., Horos, R., Alleaume, A.M., Foehr, S., Curk, T., Krijgsvelde, J., and Hentze, M.W. (2016). Comprehensive identification of RNA-binding domains in human cells. *Mol. Cell* **63**, 696–710.
- Chapman, E.G., Costantino, D.A., Rabe, J.L., Moon, S.L., Wilusz, J., Nix, J.C., and Kieft, J.S. (2014). The structural basis of pathogenic subgenomic flavivirus RNA (sfRNA) production. *Science* **344**, 307–310.
- Chen, C.Y., and Shyu, A.B. (2014). Emerging mechanisms of mRNP remodeling regulation. *Wiley Interdiscip. Rev. RNA* **5**, 713–722.
- Choudhury, N.R., Heikel, G., Trubitsyna, M., Kubik, P., Nowak, J.S., Webb, S., Granneman, S., Spanos, C., Rappsilber, J., Castello, A., and Michlewski, G. (2017). RNA-binding activity of TRIM25 is mediated by its PRY/SPRY domain and is required for ubiquitination. *BMC Biol.* **15**, 105.
- Cox, J., and Mann, M. (2008). MaxQuant enables high peptide identification rates, individualized p.p.b.-range mass accuracies and proteome-wide protein quantification. *Nat. Biotechnol.* **26**, 1367–1372.
- Deutsch, E.W., Csordas, A., Sun, Z., Jarnuczak, A., Perez-Riverol, Y., Ternent, T., Campbell, D.S., Bernal-Llinares, M., Okuda, S., Kawano, S., et al. (2017). The ProteomeXchange consortium in 2017: supporting the cultural change in proteomics public data deposition. *Nucleic Acids Res.* **45** (D1), D1100–D1106.
- Dobin, A., Davis, C.A., Schlesinger, F., Drenkow, J., Zaleski, C., Jha, S., Batut, P., Chaisson, M., and Gingeras, T.R. (2013). STAR: ultrafast universal RNA-seq aligner. *Bioinformatics* **29**, 15–21.
- Durinck, S., Spellman, P.T., Birney, E., and Huber, W. (2009). Mapping identifiers for the integration of genomic datasets with the R/Bioconductor package biomaRt. *Nat. Protoc.* **4**, 1184–1191.
- Francisco-Velilla, R., Fernandez-Chamorro, J., Ramajo, J., and Martinez-Salas, E. (2016). The RNA-binding protein Gemin5 binds directly to the ribosome and regulates global translation. *Nucleic Acids Res.* **44**, 8335–8351.
- Francisco-Velilla, R., Fernandez-Chamorro, J., Dotu, I., and Martinez-Salas, E. (2018). The landscape of the non-canonical RNA-binding site of Gemin5 unveils a feedback loop counteracting the negative effect on translation. *Nucleic Acids Res.* **46**, 7339–7353.
- Frolov, I., and Schlesinger, S. (1996). Translation of sindbis virus mRNA: analysis of sequences downstream of the initiating AUG codon that enhance translation. *J. Virol.* **70**, 1182–1190.
- Fros, J.J., Domeradzka, N.E., Baggen, J., Geertsema, C., Flipse, J., Vlak, J.M., and Pijlman, G.P. (2012). Chikungunya virus nsP3 blocks stress granule assembly by recruitment of G3BP into cytoplasmic foci. *J. Virol.* **86**, 10873–10879.
- Fukuhara, T., Hosoya, T., Shimizu, S., Sumi, K., Oshiro, T., Yoshinaka, Y., Suzuki, M., Yamamoto, N., Herzenberg, L.A., Herzenberg, L.A., and Hagiwara, M. (2006). Utilization of host SR protein kinases and RNA-splicing machinery during viral replication. *Proc. Natl. Acad. Sci. USA* **103**, 11329–11333.
- Gack, M.U., Shin, Y.C., Joo, C.H., Urano, T., Liang, C., Sun, L., Takeuchi, O., Akira, S., Chen, Z., Inoue, S., and Jung, J.U. (2007). TRIM25 RING-finger E3 ubiquitin ligase is essential for RIG-I-mediated antiviral activity. *Nature* **446**, 916–920.
- Garcia-Moreno, M., Järvelin, A.I., and Castello, A. (2018). Unconventional RNA-binding proteins step into the virus-host battlefield. *Wiley Interdiscip. Rev. RNA* **9**, e1498.
- Geller, R., Taguwa, S., and Frydman, J. (2012). Broad action of Hsp90 as a host chaperone required for viral replication. *Biochim. Biophys. Acta* **1823**, 698–706.
- Glisovic, T., Bachorik, J.L., Yong, J., and Dreyfuss, G. (2008). RNA-binding proteins and post-transcriptional gene regulation. *FEBS Lett.* **582**, 1977–1986.
- Gorchakov, R., Frolova, E., and Frolov, I. (2005). Inhibition of transcription and translation in sindbis virus-infected cells. *J. Virol.* **79**, 9397–9409.
- Gubitz, A.K., Mourelatos, Z., Abel, L., Rappsilber, J., Mann, M., and Dreyfuss, G. (2002). Gemin5, a novel WD repeat protein component of the SMN complex that binds Sm proteins. *J. Biol. Chem.* **277**, 5631–5636.
- Hentze, M.W., Castello, A., Schwarzl, T., and Preiss, T. (2018). A brave new world of RNA-binding proteins. *Nat. Rev. Mol. Cell Biol.* **19**, 327–341.
- Howard, J.M., and Sanford, J.R. (2015). The RNAissance family: SR proteins as multifaceted regulators of gene expression. *Wiley Interdiscip. Rev. RNA* **6**, 93–110.
- Huppertz, I., Attig, J., D'Ambrogio, A., Easton, L.E., Sibley, C.R., Sugimoto, Y., Tajnik, M., König, J., and Ule, J. (2014). iCLIP: protein-RNA interactions at nucleotide resolution. *Methods* **65**, 274–287.
- Iwasaki, S., Kobayashi, M., Yoda, M., Sakaguchi, Y., Katsuma, S., Suzuki, T., and Tomari, Y. (2010). Hsc70/Hsp90 chaperone machinery mediates ATP-dependent RISC loading of small RNA duplexes. *Mol. Cell* **39**, 292–299.
- Jurkin, J., Henkel, T., Nielsen, A.F., Minnich, M., Popow, J., Kaufmann, T., Heindl, K., Hoffmann, T., Busslinger, M., and Martinez, J. (2014). The mammalian tRNA ligase complex mediates splicing of XBP1 mRNA and controls antibody secretion in plasma cells. *EMBO J.* **33**, 2922–2936.
- Kolde, R. (2015). pheatmap: Pretty Heatmaps R package version 108.
- König, J., Zarnack, K., Rot, G., Curk, T., Kaykci, M., Zupan, B., Turner, D.J., Luscombe, N.M., and Ule, J. (2010). iCLIP reveals the function of hnRNP particles in splicing at individual nucleotide resolution. *Nat. Struct. Mol. Biol.* **17**, 909–915.
- LaPointe, A.T., Gebhart, N.N., Meller, M.E., Hardy, R.W., and Sokoloski, K.J. (2018). The identification and characterization of Sindbis virus RNA:host protein interactions. *J. Virol.* **92**, e02171-17.
- Lee, A.S., Kranzusch, P.J., Doudna, J.A., and Cate, J.H. (2016). eIF3d is an mRNA cap-binding protein that is required for specialized translation initiation. *Nature* **536**, 96–99.
- Li, J., Tang, S., Hewlett, I., and Yang, M. (2007). HIV-1 capsid protein and cyclophilin A as new targets for anti-AIDS therapeutic agents. *Infect. Disord. Drug Targets* **7**, 238–244.
- Li, H., Handsaker, B., Wysoker, A., Fennell, T., Ruan, J., Homer, N., Marth, G., Abecasis, G., and Durbin, R.; 1000 Genome Project Data Processing Subgroup (2009). The Sequence Alignment/Map format and SAMtools. *Bioinformatics* **25**, 2078–2079.
- Li, M.M., Lau, Z., Cheung, P., Aguilar, E.G., Schneider, W.M., Bozzacco, L., Molina, H., Buehler, E., Takaoka, A., Rice, C.M., et al. (2017). TRIM25 enhances the antiviral action of zinc-finger antiviral protein (ZAP). *PLoS Pathog.* **13**, e1006145.
- Liao, Y., Smyth, G.K., and Shi, W. (2013). The Subread aligner: fast, accurate and scalable read mapping by seed-and-vote. *Nucleic Acids Res.* **41**, e108.
- Lin, J.Y., Shih, S.R., Pan, M., Li, C., Lue, C.F., Stollar, V., and Li, M.L. (2009). hnRNP A1 interacts with the 5' untranslated regions of enterovirus 71 and Sindbis virus RNA and is required for viral replication. *J. Virol.* **83**, 6106–6114.
- Lloyd, R.E. (2015). Nuclear proteins hijacked by mammalian cytoplasmic plus strand RNA viruses. *Virology* **479–480**, 457–474.
- Love, M.I., Huber, W., and Anders, S. (2014). Moderated estimation of fold change and dispersion for RNA-seq data with DESeq2. *Genome Biol.* **15**, 550.
- Lunde, B.M., Moore, C., and Varani, G. (2007). RNA-binding proteins: modular design for efficient function. *Nat. Rev. Mol. Cell Biol.* **8**, 479–490.
- Manokaran, G., Finol, E., Wang, C., Gunaratne, J., Bahl, J., Ong, E.Z., Tan, H.C., Sessions, O.M., Ward, A.M., Gubler, D.J., et al. (2015). Dengue subgenomic RNA binds TRIM25 to inhibit interferon expression for epidemiological fitness. *Science* **350**, 217–221.
- Molleston, J.M., and Cherry, S. (2017). Attacked from all sides: RNA decay in antiviral defense. *Viruses* **9**, 2.
- Monie, T.P., Perrin, A.J., Birtley, J.R., Sweeney, T.R., Karakasiotis, I., Chaudhry, Y., Roberts, L.O., Matthews, S., Goodfellow, I.G., and Curry, S. (2007). Structural insights into the transcriptional and translational roles of Ebp1. *EMBO J.* **26**, 3936–3944.
- Mukherjee, N., Calviello, L., Hirsckorn, A., de Pretis, S., Pelizzola, M., and Olier, U. (2017). Integrative classification of human coding and noncoding genes through RNA metabolism profiles. *Nat. Struct. Mol. Biol.* **24**, 86–96.

- Müller, B., Daecke, J., Fackler, O.T., Dittmar, M.T., Zentgraf, H., and Kräusslich, H.G. (2004). Construction and characterization of a fluorescently labeled infectious human immunodeficiency virus type 1 derivative. *J. Virol.* **78**, 10803–10813.
- Ni, X., Ru, H., Ma, F., Zhao, L., Shaw, N., Feng, Y., Ding, W., Gong, W., Wang, Q., Ouyang, S., et al. (2016). New insights into the structural basis of DNA recognition by HINa and HINb domains of IFI16. *J. Mol. Cell Biol.* **8**, 51–61.
- Perez-Perri, J.I., Rogell, B., Schwarzl, T., Stein, F., Zhou, Y., Rettel, M., Brosig, A., and Hentze, M.W. (2018). Discovery of RNA-binding proteins and characterization of their dynamic responses by enhanced RNA interactome capture. *Nat. Commun.* **9**, 4408.
- Pfaffl, M.W. (2001). A new mathematical model for relative quantification in real-time RT-PCR. *Nucleic Acids Res.* **29**, e45.
- Pijlman, G.P., Funk, A., Kondratieva, N., Leung, J., Torres, S., van der Aa, L., Liu, W.J., Palmenberg, A.C., Shi, P.Y., Hall, R.A., and Khromykh, A.A. (2008). A highly structured, nuclease-resistant, noncoding RNA produced by flaviviruses is required for pathogenicity. *Cell Host Microbe* **4**, 579–591.
- Piñero, D., Fernández, N., Ramajo, J., and Martínez-Salas, E. (2013). Gemin5 promotes IRES interaction and translation control through its C-terminal region. *Nucleic Acids Res.* **41**, 1017–1028.
- Piñero, D., Fernandez-Chamorro, J., Francisco-Velilla, R., and Martinez-Salas, E. (2015). Gemin5: a multitasking RNA-binding protein involved in translation control. *Biomolecules* **5**, 528–544.
- Popow, J., Englert, M., Weitzer, S., Schleiffer, A., Mierzwa, B., Mechtler, K., Trowitzsch, S., Will, C.L., Lüthmann, R., Söll, D., and Martinez, J. (2011). HSPC117 is the essential subunit of a human tRNA splicing ligase complex. *Science* **331**, 760–764.
- Rathore, A.P., Ng, M.L., and Vasudevan, S.G. (2013). Differential unfolded protein response during Chikungunya and Sindbis virus infection: CHIKV nsP4 suppresses eIF2 $\alpha$  phosphorylation. *Viol. J.* **10**, 36.
- Rupp, D., and Bartenschlager, R. (2014). Targets for antiviral therapy of hepatitis C. *Semin. Liver Dis.* **34**, 9–21.
- Sanz, M.A., and Carrasco, L. (2001). Sindbis virus variant with a deletion in the 6K gene shows defects in glycoprotein processing and trafficking: lack of complementation by a wild-type 6K gene in trans. *J. Virol.* **75**, 7778–7784.
- Seo, G.J., Kim, C., Shin, W.J., Sklan, E.H., Eoh, H., and Jung, J.U. (2018). TRIM56-mediated monoubiquitination of cGAS for cytosolic DNA sensing. *Nat. Commun.* **9**, 613.
- Sielaff, M., Kuharev, J., Bohn, T., Hahlbrock, J., Bopp, T., Tenzer, S., and Distler, U. (2017). Evaluation of FASP, SP3, and iST protocols for proteomic sample preparation in the low microgram range. *J. Proteome Res.* **16**, 4060–4072.
- Simsek, D., Tiu, G.C., Flynn, R.A., Byeon, G.W., Leppek, K., Xu, A.F., Chang, H.Y., and Barna, M. (2017). The mammalian ribo-interactome reveals ribosome functional diversity and heterogeneity. *Cell* **169**, 1051–1065.e1018.
- Skabkin, M.A., Skabkina, O.V., Dhote, V., Komar, A.A., Hellen, C.U., and Pestova, T.V. (2010). Activities of Ligatin and MCT-1/DENR in eukaryotic translation initiation and ribosomal recycling. *Genes Dev.* **24**, 1787–1801.
- Smyth, G.K. (2004). Linear models and empirical Bayes methods for assessing differential expression in microarray experiments. *Stat. Appl. Genet. Mol. Biol.* **3**, Article3.
- Sysoev, V.O., Fischer, B., Frese, C.K., Gupta, I., Krijgsveld, J., Hentze, M.W., Castello, A., and Ephrussi, A. (2016). Global changes of the RNA-bound proteome during the maternal-to-zygotic transition in *Drosophila*. *Nat. Commun.* **7**, 12128.
- Szklarczyk, D., Morris, J.H., Cook, H., Kuhn, M., Wyder, S., Simonovic, M., Santos, A., Doncheva, N.T., Roth, A., Bork, P., et al. (2017). The STRING database in 2017: quality-controlled protein-protein association networks, made broadly accessible. *Nucleic Acids Res.* **45** (D1), D362–D368.
- Thompson, M.R., Sharma, S., Atianand, M., Jensen, S.B., Carpenter, S., Knipe, D.M., Fitzgerald, K.A., and Kurt-Jones, E.A. (2014). Interferon  $\gamma$ -inducible protein (IFI) 16 transcriptionally regulates type I interferons and other interferon-stimulated genes and controls the interferon response to both DNA and RNA viruses. *J. Biol. Chem.* **289**, 23568–23581.
- Tsuchida, T., Zou, J., Saitoh, T., Kumar, H., Abe, T., Matsuura, Y., Kawai, T., and Akira, S. (2010). The ubiquitin ligase TRIM56 regulates innate immune responses to intracellular double-stranded DNA. *Immunity* **33**, 765–776.
- Tyanova, S., Temu, T., Sinitcyn, P., Carlson, A., Hein, M.Y., Geiger, T., Mann, M., and Cox, J. (2016). The Perseus computational platform for comprehensive analysis of (prote)omics data. *Nat. Methods* **13**, 731–740.
- Vladimer, G.I., Gónra, M.W., and Superti-Furga, G. (2014). IFITs: emerging roles as key anti-viral proteins. *Front. Immunol.* **5**, 94.
- Wickham, H. (2009). *ggplot2: Elegant Graphics for Data Analysis* (Springer-Verlag).
- Xu, C., Ishikawa, H., Izumikawa, K., Li, L., He, H., Nobe, Y., Yamauchi, Y., Shahjee, H.M., Wu, X.H., Yu, Y.T., et al. (2016). Structural insights into Gemin5-guided selection of pre-snRNAs for snRNP assembly. *Genes Dev.* **30**, 2376–2390.
- Zhang, R., Hryc, C.F., Cong, Y., Liu, X., Jakana, J., Gorchakov, R., Baker, M.L., Weaver, S.C., and Chiu, W. (2011). 4.4 Å cryo-EM structure of an enveloped alphavirus Venezuelan equine encephalitis virus. *EMBO J.* **30**, 3854–3863.

## STAR★METHODS

### KEY RESOURCES TABLE

REAGENT or RESOURCE	SOURCE	IDENTIFIER
<b>Antibodies</b>		
anti-SINV C (304 and 306)	Laboratory of L. Carrasco	N/A
β-ACTIN	Sigma	Cat# A1978; RRID: AB_476692
ALDOA	Cusabio	Cat# PA00015A0Rb
DDX1	Bethyl	Cat# A300-521Q; RRID: AB_451046; Cat# A300-520; RRID: AB_451045
DDX50	Cusabio	Cat# PA861080LA01HU
EIF2α	Santa Cruz Biotechnology	Cat# sc-11386; RRID: AB_640075
Phospho-EIF2α (serine 51)	Cell Signaling Technology	Cat# 9721; RRID: AB_330951
EIF3G	Cusabio	Cat# PA03099A0Rb
EIF4G1 Nt - 981	Laboratory of L. Carrasco	N/A
EIF4G1 Ct - 987	Laboratory of L. Carrasco	N/A
ENO1	Cusabio	Cat# PA02395A0Rb
EPRS	Abcam	Cat# ab31531; RRID: AB_880047
GEMIN5	Abcam	Cat# ab201691
GFP	ChromoTek GmbH	Cat# 3h9-100; RRID: AB_10773374
HNRNP A1	Cusabio	Cat# PA010600HA01HU
HNRNP Q/R	Cell Signaling	Cat# 8588; RRID: AB_10897511
HSP90AB1	Cusabio	Cat# PA00109A0Rb
IFIT5	Cusabio	Cat# PA011023LA01HU
IRE1	Abcam	Cat# ab37073; RRID: AB_775780
MOV10	Cusabio	Cat# PA862068LA01HU
NGDN	Cambridge Bioscience	Cat# 16524-1-AP; RRID: AB_2152270
PA2G4	Cusabio	Cat# PA891987LA01HU
PPIA	Cusabio	Cat# PA07814A0Rb
PTBP1	Sigma	Cat# WH0005725M1; RRID: AB_1843067
RTCB	Cusabio	Cat# PA897546LA01HU
RPS10	Cusabio	Cat# PA02565A0Rb
RPS27	Sigma Aldrich	Cat# SAB4300952
SRPK1	Sino Biological Inc	Cat# 12249-MM03
TRIM25	Abcam	Cat# ab167154; RRID: AB_2721902
TRIM56	Abcam	Cat# ab154862
XRCC5	Cusabio	Cat# PA026233LA01HU
XRCC6	Cusabio	Cat# PA01617A0Rb
XRN1	Santa Cruz	Cat# sc-165985; RRID: AB_2304774
Donkey anti-Mouse IgG (H+L) Highly Cross-Adsorbed Secondary Antibody, Alexa Fluor 488	ThermoFisher Scientific	Cat# A-21202; RRID: AB_141607
Donkey anti-Rabbit IgG (H+L) Highly Cross-Adsorbed Secondary Antibody, Alexa Fluor 488	ThermoFisher Scientific	Cat# A-21206; RRID: AB_141708
Donkey anti-Rabbit IgG (H+L) Highly Cross-Adsorbed Secondary Antibody, Alexa Fluor 594	ThermoFisher Scientific	Cat# A-21207; RRID: AB_141637
<b>Bacterial and Virus Strains</b>		
pT7-SVmCherry	This paper	N/A
pT7-SVwt	Laboratory of L. Carrasco (Sanz and Carrasco, 2001)	N/A

(Continued on next page)



**Continued**

REAGENT or RESOURCE	SOURCE	IDENTIFIER
pNL4-3.R-E- Nef-mCherry	This paper	N/A
pNL4-3.R-E- Gag-mCherry	This paper	N/A
<b>Chemicals, Peptides, and Recombinant Proteins</b>		
L-Arginine HCL 13C, 15N	SILANTES GmbH	Cat# 201604102
L-Arginine HCL 13C	SILANTES GmbH	Cat# 201204102
L-Lysine HCL 13C, 15N	SILANTES GmbH	Cat# 211604102
4.4.5.5-D4-L-Lysine	SILANTES GmbH	Cat# 211104113
Cyclosporin A (CAS N° 59865-13-3)	Insight Biotechnology Ltd	Cat# sc-3503
Ganetespi (CAS N° 888216-25-9)	Cambridge Bioscience Ltd	Cat# 19432
Geldanamycin (CAS N° 30562-34-6)	Cambridge Bioscience Ltd	Cat# SM55-2
IRE1 Inhibitor III, 4 $\mu$ 8C (CAS N° 14003-96-4)	Merck Chemicals Ltd	Cat# 412512
WS6 (CAS N° 1421227-53-3)	Cambridge Bioscience Ltd	Cat# 17672
<b>Critical Commercial Assays</b>		
CellTiter 96 AQ <sub>ueous</sub> One Solution Cell Proliferation Assay (MTS)	Promega	Cat# G3580
<b>Deposited Data</b>		
Proteome Xchange via PRIDE	<a href="#">Deutsch et al., 2017</a>	PXD009789
RNA-seq via GEO		GEO: GSE125182
iCLIP via GEO		GEO: GSE125182
<b>Experimental Models: Cell Lines</b>		
HEK293	ECACC	Cat# 85120602 RRID:CVCL_0045
HeLa Kyoto	ATCC	Cat# CCL-2 RRID:CVCL_1922
Flp-In-T-Rex-293	Thermo Fisher Scientific	Cat#R78007 RRID:CVCL_U427
Flp-In-T-Rex-HeLa	Laboratory of M. Gromeier	N/A
BHK-21	ECACC	Cat# 85011433 RRID:CVCL_1915
<b>Oligonucleotides</b>		
CRISPR guide RNA targeting XRN1: AAUGC <sup>G</sup> AAACA ACACCUCCGUUUUAGAGCUAUGCUGUUUUU	Sigma-Aldrich Co Ltd	HS0000076809
TRIM25 left sgRNA: CCACGTTGCACAGCACCGTGTTTC	This paper	N/A
TRIM25 right sgRNA: CTGCGGTCGCGCCTGGTAGACGG	This paper	N/A
Primers for cloning, see <a href="#">Table S6</a>	This paper	N/A
Primers for RT-PCR, see <a href="#">Table S6</a>	This paper	N/A
<b>Recombinant DNA</b>		
CRISPR/CAS9 plasmid: PX459 HSP90AB1_out_of_frame_67 guide sequence: CTCACACCTTGACTGCCAAG	This paper	N/A
CRISPR/CAS9 plasmid: PX459 PPIA_out_of_frame_57 guide sequence: GCCCGACCTCAAAGGAGACG	This paper	N/A
pOG44	ThermoFisher Scientific	Cat# V600520
pcDNA5/FRT/TO	ThermoFisher Scientific	Cat# V652020
pNL4-3.Luc.R-E-	NIBSC – Centre for AIDS Reagents	Cat# 2128
pNL4-3	NIBSC – Centre for AIDS Reagents	Cat# 2006
pHEF-VSVG	NIH AIDS Reagent Program	Cat# 4693
<b>Software and Algorithms</b>		
REST	<a href="#">Pfaffl, 2001</a>	
STRING	<a href="#">Szklarczyk et al., 2017</a>	<a href="https://string-db.org/">https://string-db.org/</a>

(Continued on next page)

**Continued**

REAGENT or RESOURCE	SOURCE	IDENTIFIER
STAR	Dobin et al., 2013	<a href="https://github.com/alexdobin/STAR">https://github.com/alexdobin/STAR</a>
Subread FeatureCount	Liao et al., 2013	<a href="http://bioinf.wehi.edu.au/subread-package/">http://bioinf.wehi.edu.au/subread-package/</a>
SAMtools	Li et al., 2009	<a href="http://samtools.sourceforge.net/">http://samtools.sourceforge.net/</a>
RBDmap	Castello et al., 2016	<a href="https://www-huber.embl.de/users/befische/RBDmap/">https://www-huber.embl.de/users/befische/RBDmap/</a>
DSseq2	Love et al., 2014	<a href="https://bioconductor.org/packages/release/bioc/html/DESeq2.html">https://bioconductor.org/packages/release/bioc/html/DESeq2.html</a>
Pheatmap	Kolde, 2015	<a href="https://cran.r-project.org/web/packages/pheatmap/index.html">https://cran.r-project.org/web/packages/pheatmap/index.html</a>
iCount		<a href="https://github.com/tomazc/iCount">https://github.com/tomazc/iCount</a>
biomaRt	Durinck et al., 2009	<a href="https://bioconductor.org/packages/release/bioc/html/biomaRt.html">https://bioconductor.org/packages/release/bioc/html/biomaRt.html</a>
ggplot2	Wickham, 2009	<a href="https://cran.r-project.org/web/packages/ggplot2/index.html">https://cran.r-project.org/web/packages/ggplot2/index.html</a>
MaxQuant (version 1.5.0.35)	Cox and Mann, 2008	<a href="https://www.maxquant.org/">https://www.maxquant.org/</a>
Perseus	Tyanova et al., 2016	<a href="http://maxquant.net/perseus/">http://maxquant.net/perseus/</a>
hom.Hs.inp.db	Carlson and Pages, 2015	<a href="http://bioconductor.org/packages/release/data/annotation/html/hom.Hs.inp.db.html">http://bioconductor.org/packages/release/data/annotation/html/hom.Hs.inp.db.html</a>
mRNAinteractomeHeLa	Castello et al., 2012	<a href="http://www.hentze.embl.de/public/RBDmap/">http://www.hentze.embl.de/public/RBDmap/</a>
Semiquantitative test for protein differential analysis	This paper	N/A
limma (for moderated t test)	Smyth, 2004	<a href="https://bioconductor.org/packages/release/bioc/html/limma.html">https://bioconductor.org/packages/release/bioc/html/limma.html</a>
ANOVA		<a href="https://www.itl.nist.gov/div898/handbook/eda/section3/eda355.htm">https://www.itl.nist.gov/div898/handbook/eda/section3/eda355.htm</a>

**CONTACT FOR REAGENT AND RESOURCE SHARING**

Further information and requests for resources and reagents should be directed to and will be fulfilled by the Lead Contact, Alfredo Castello ([alfredo.castellopalomares@bioch.ox.ac.uk](mailto:alfredo.castellopalomares@bioch.ox.ac.uk)).

**EXPERIMENTAL MODEL AND SUBJECT DETAILS**

**Cell culture**

We used here human embryo kidney 293 cells (HEK293, ECACC #85120602), HeLa (ATCC cat. no. CCL-2) and baby hamster kidney cells (BHK-21, clone 13, ECACC #85011433); HEK293 Flp-In TREx are commercially available (Thermo Fisher Scientific, #R78007), while HeLa Flp-In TREx are a generous gift from Dr. Matthias Gromeier (Duke University Medical Center, Durham, NC, USA). All cells were cultured in DMEM with 10% FBS and 1x penicillin/streptomycin (Sigma Aldrich, #P4458) at 37°C with 5% CO<sub>2</sub>. The media of Flp-In TREx (Tet-on) cells was supplemented with 15 µg/ml Blasticidin S and 100 µg/ml Zeocin. To generate RBP-eGFP-expressing cell lines, cells were transfected with pOG44 and the corresponding pcDNA5-FTR-TO plasmid (Table S6) using X-tremeGENE 9 DNA transfection reagent following manufacturer's recommendations (Sigma-Aldrich, #6365787001). For the selection of inducible cell lines, Zeocin was replaced by 150 µg/ml Hygromycin B as indicated in the manufacturer's manual (Thermo Fisher Scientific). Protein induction was achieved by supplementation of the medium with 1 µg/ml doxycycline. To generate KO cells, we transfected HEK293 using TRANSIT-CRISPR (Sigma-Aldrich) with SygRNAs assembled with Cas9 (Sigma-Aldrich, #CAS9PROT-50UG) and tracrRNA (Sigma-Aldrich, #TRACRRNA05N-5NMOL), followed by cell serial dilution and selection of KO cell clones. Alternatively, we generated px459 derived plasmids including sequences targeting the genes of interest (px459 was a gift from Feng Zhang; Addgene plasmid #62988). These plasmids were transiently transfected into HEK293 cells using X-tremeGENE 9. Cells expressing the construct were selected with 1 µg/ml puromycin for 96 h, followed by cell serial dilution to obtain individual clones. To generate TRIM25 KO cells, HEK293 were transfected with 200 ng GeneArt CRISPR nuclease mRNA (Thermo Fisher Scientific, #A29378) along with 50 ng of two distinct, *in vitro* transcribed sgRNAs targeting sequences in exon 1 of the TRIM25 gene. Single cells were seeded, grown and checked for KO by western blotting.

### Cell culture in SILAC media

Cells were grown in SILAC DMEM media (Thermo Scientific, #10107883) containing 10% dialysed FBS (Silantes GmbH, #281000900) and isotopic labeled arginine and lysine (Silantes GmbH amino acids: L-Arginine 13C,15N labeled #201604102; L-Arginine 13C labeled #201204102; L-Lysine 13C,15N labeled #211604102; 4,4.5.5.-D4-L-Lysine #211104113). Prior to experiments, we confirmed by mass spectrometry that the incorporation of isotopic labeled amino acids was superior to 98% using whole cell lysates.

### Viruses

We used the SINV clone pT7-SVwt (Sanz and Carrasco, 2001) to generate the SINV suspension. The plasmid pT7-SVmCherry was generated by inserting mCherry after the duplicated subgenomic promoter in pT7-SVwt. To obtain SINV and SINV-mCherry viruses, pT7-SVwt and pT7-SVmCherry plasmids were first linearized with XhoI and used as a template for *in vitro* RNA transcription with HiScribe T7 ARCA mRNA kit (New England Biolabs, #E2065S). Transcribed genomic RNA was transfected into BHK-21 using Lipofectamine 2000 reagent (Invitrogen, #11668027). Viruses were collected from the supernatant 24 h later and cleared by centrifugation at 2000 rpm for 3 min followed by filtration with 0.45 $\mu$ m PVDF syringe filter units (Merck, #SLHV033RS). Cleared supernatants were titrated by plaque assay using BHK-21 cells.

Pseudotyped HIV-1<sub>Nef-mCherry</sub> and HIV-1<sub>Gag-mCherry</sub> were produced as follows. For HIV-1<sub>Nef-mCherry</sub>, a sequence encoding the end of *env* followed by a linker, mCherry, T2A self-cleaving peptide and the beginning of Nef protein was synthesized using the GeneArt Gene synthesis service (Thermo Fisher Scientific), and cloned between the BamHI and XhoI restriction sites of pNL4-3.Luc.R-E-plasmid (NIBSC – Centre for AIDS Reagents, #2128), which is defective for Vpr and Env. For HIV-1<sub>Gag-mCherry</sub>, a PspXI restriction site flanked by flexible linker was introduced into *gag* of the pNL4-3 plasmid (NIBSC – Centre for AIDS Reagents, #2006) by overlapping PCR (primers in Table S6) as in (Müller et al., 2004). mCherry sequence was amplified by PCR flanked by PspXI restriction sites and cloned into pNL4-3 using the newly generated PspXI site. Finally, the fragment between SpeI and BamHI was replaced by that of pNL4-3.Luc.R-E-. Pseudotyped viral particles were produced by co-transfecting HEK293T cells (kindly provided by Prof. Jan Rehwinkel, University of Oxford, UK) with pNL4-3.R-E<sub>Nef-mCherry</sub> or pNL4-3.R-E<sub>Gag-mCherry</sub> plus pHEF-VSVG (NIH AIDS Reagent Program, #4693), which encodes for the glycoprotein of vesicular stomatitis virus (VSV).

## METHOD DETAILS

### RNA interactome capture

Comparative RNA interactome capture (cRIC) was performed based on the previously described protocol (Castello et al., 2012; Castello et al., 2013) with the following alterations: HEK293 cells, previously grown in media with isotopic labeled amino acids, were seeded in three sets of 3x15 cm dishes at 80% confluence, each set with a different SILAC label. One set of dishes remained uninfected and two sets were infected with SINV at a multiplicity of infection (MOI) of 10. One of these infected cell sets was incubated for 4 h and the other for 18 h. To correct for isotope-dependent effects, we permuted the SILAC labels between the three conditions in the three biological replicates. After incubation, cells were irradiated with 150 mJ/cm<sup>2</sup> of UV light at 254 nm, and lysed with 3 mL of lysis buffer (20 mM Tris-HCl pH 7.5, 500 mM LiCl, 0.5% LiDS wt/vol, 1 mM EDTA, 0.1% IGEPAL (NP-40) and 5 mM DTT). Lysates were homogenized by passing the lysate at high speed through a 5 mL syringe with a 27G needle, repeating this process until the lysate was fully homogeneous. 400  $\mu$ l of lysate were taken for total proteome and transcriptome analysis (Figure 3; Tables S3 and S4). Protein content was measured using a kit compatible with ionic detergents (Thermo Fisher, Pierce 660nm Protein Assay Kit #22662 with IDC reagent #22663) and equal amounts of each of the three lysates were mixed. The final volume was adjusted to 9 mL and 1.5 mL of pre-equilibrated oligo(dT)<sub>25</sub> magnetic beads (New England Biolabs, #S1419S) were added and incubated for 1 h at 4°C with gentle rotation. Beads were collected in the magnet and the lysate was transferred to a new tube and stored at 4°C. Beads were washed once with 10 mL of lysis buffer, incubating for 5 min at 4°C with gentle rotation, followed by two washes with 10 mL of buffer 1 (20 mM Tris-HCl pH 7.5, 500 mM LiCl, 0.1% LiDS wt/vol, 1 mM EDTA, 0.1% IGEPAL and 5 mM DTT) for 5 min at 4°C with gentle rotation and two washes with buffer 2 (20 mM Tris-HCl pH 7.5, 500 mM LiCl, 1 mM EDTA, 0.01% IGEPAL and 5 mM DTT). Beads were then washed twice with 10 mL of buffer 3 (20 mM Tris-HCl pH 7.5, 200 mM LiCl, 1 mM EDTA and 5 mM DTT) at room temperature. Beads were resuspended in 900  $\mu$ l of elution buffer and incubated for 3 min at 55°C with agitation. Eluates were stored at –80°C and beads were recycled as indicated in the manufacturer's manual, and re-used for two additional capture rounds. For RIC experiments followed by western blot analysis, we used the small scale RIC settings described in (Castello et al., 2013).

### Conventional protein analyses

Samples were resolved on SDS-PAGE and analyzed by i) western blotting using specific antibodies, the Li-Cor Odyssey system for visualization and the Image Studio Lite software (Li-Cor) for quantification, ii) Coomassie blue staining with the InstantBlue Protein Stain reagent (Expedeon, #ISB1L) or iii) silver staining using SilverQuest kit (Invitrogen, #LC6070). Data shown in the manuscript are representative gels from at least three independent replicates. Details on antibodies can be found in the key resource table. Radioactive labeling of newly synthesized proteins was performed by replacing the growth media for 1 h with DMEM lacking methionine and cysteine and supplemented with Easytag EXPRESS<sup>35</sup>S Protein Labeling Mix [<sup>35</sup>S]Met-Cys (Perkin Elmer, #NEG772002MC). Samples were then analyzed by SDS-polyacrylamide gels (15%) followed by autoradiography.



### Reverse-transcription and quantitative PCR

Total RNA was isolated using TRIzol (Invitrogen, #15596026). Reverse transcription was performed using Superscript III reverse transcriptase (Invitrogen, #18080044) with random hexamers priming (Invitrogen, #N8080127), following manufacturer's instructions. RT-qPCR analysis was performed with 2x qPCR SyGreen Mix Lo-ROX (PCRBiosystems, #PB20.11-01) and gene specific primers (Table S6) in a BioRad CFX96 Real-Time system, and analyzed with REST software (Pfaffl, 2001).

### Plasmids and recombinant DNA procedures

Plasmids for generation of inducible cell lines were created by conventional cloning methods. Inserts were generally amplified from HEK293 cDNA or template plasmids using specific primers (Table S6). Inserts were cloned into the pcDNA5/FRT/TO with eGFP preceded or followed by a flexible linker encoding for GGSGGGSGG (glycine and serine repeats) to facilitate the folding of the RBP of interest independently from the eGFP. For CRISPR/Cas9 expression plasmids, annealed oligos were inserted into the BbsI site of px459.

### mCherry-based viral fitness assay

$5 \times 10^4$  cells were seeded on each well of a 96-well microplate with flat  $\mu$ Clear bottom (Greiner Bio-One, #655986) in DMEM lacking phenol-red and supplemented with 5% FBS and 1 mM sodium pyruvate. Cells (control, knock-out and Tet-on) were infected with SINV-mCherry at 0.1 MOI in complete DMEM (lacking phenol-red) with 2.5% FBS. Cells were incubated at 37°C and 5% CO<sub>2</sub> in a CLARIOstar fluorescence plate reader (BMG Labtech) for 24 h; eGFP and/or mCherry signal was monitored by measuring fluorescence (eGFP: excitation 470 nm, emission 515 nm; mCherry: excitation 570 nm, emission 620 nm) every 15 min. To monitor the shut off of protein synthesis with this method (Figure S1B), Tet-on HEK293 eGFP-control cells were induced with 1  $\mu$ g/ml doxycycline for 4 h and then infected as indicated above. In experiments with HIV-1 mCherry replicons,  $5 \times 10^4$  cells were seeded on each well of a 96-well plate in clear DMEM supplemented with 2.5% FBS and 1 mM sodium pyruvate, and infected with pseudotyped HIV-1<sub>Nef-mCherry</sub> or HIV-1<sub>Gag-mCherry</sub>. mCherry signal was monitored for 72 h in a fluorescence plate reader as indicated above. In over-expression experiments, Tet-on HEK293 cells expressing RBP-eGFP fusion proteins were either induced with 1  $\mu$ g/ml doxycycline for 16 h or mock-induced and then infected with SINV-mCherry. In inhibitor assays, HEK293 cells were infected with SINV-mCherry as above and inhibitors or vehicle (DMSO) were added at 1 hpi at the concentrations indicated in the figures. Statistical significance of the difference in mCherry expression at 18 and 24 hpi was determined by t test (n = 9).

### Drugs and cell viability assay

The following chemical inhibitors were used in this work: cyclosporin A (Insight Biotechnology Ltd, #sc-3503), Ganetespib (Cambridge Bioscience Ltd, #19432), Geldanamycin (Cambridge Bioscience Ltd, #SM55-2), 4 $\mu$ 8C (Merck Chemicals, #412512) and WS6 (Cambridge Bioscience Ltd, #17672). To test cell viability at the concentrations used,  $5 \times 10^4$  HEK293 cells were seeded on each well of a 96-well microplate with flat, transparent bottom and incubated with DMEM (no phenol red) supplemented with 5% FBS and 1 mM sodium pyruvate. 24 h later cells were treated with the compounds and incubated for another 24 h at 37°C and 5% CO<sub>2</sub>. Cell viability was estimated by adding CellTiter 96 Aqueous One Solution (Promega, #G3580) and measuring 490 nm absorbance following the manufacturer's recommendations. To evaluate cell viability and proliferation in knockout cells,  $2.5 \times 10^4$  cells were seeded per well of a 96-well plate and incubated in DMEM (no phenol red, 5% FBS, 1 mM sodium pyruvate) at 37°C and 5% CO<sub>2</sub>. Cell viability was measured at the indicated times using CellTiter 96 Aqueous One Solution as described above. In parallel, the number of cells was counted using the Countess II FL Automated Cell Counter (Thermo Fisher Scientific).

### Protein-protein interactions analysis

$4.2 \times 10^6$  HEK293 Tet-on cells expressing eGFP or GEMIN5-eGFP proteins were seeded on a 10 cm dish and incubated with DMEM supplemented with 10% FBS and 1  $\mu$ g/ml doxycycline. After 24 h, cells were infected with 10 MOI of SINV in DMEM lacking FBS and incubated for 1 h, followed by media exchange (DMEM with 1% FBS). Cells were harvested at 18 hpi and lysed in 1 mL of Triton-X-lysis buffer (10 mM Tris HCl pH 7.5, 150 mM NaCl, 1% Triton X-100, 5 mM MgCl<sub>2</sub>, 5 mM DTT and 0.1 mM AEBSF serine protease inhibitor). For immunoprecipitation (IP), 40  $\mu$ l GFP-Trap\_A beads slurry (ChromoTek GmbH, #gta-20) were equilibrated in Triton-X-lysis buffer and then added to 500  $\mu$ l of whole-cell lysate. Mixture was diluted with 4.5 mL of Triton-X-lysis buffer, and mixed with gentle rotation for 16 h at 4°C. GFP-Trap beads were washed once with Triton-X-lysis buffer, collecting the beads by gentle centrifugation after each wash (1000 g for 5 min at 4°C). In the second wash, the Triton-X-lysis buffer was supplemented with 1  $\mu$ l/ml RNase A (Sigma Aldrich, #4642) and beads were incubated for 5 min at 37°C with gentle rotation. Beads were washed three additional times with Triton-X-lysis buffer. Proteins were released from the GFP-Trap beads via pH elution by resuspension in 50  $\mu$ l 0.2 M glycine pH 2.5 for 30 s followed by collection of the beads through a quick spin. The supernatant was transferred to a new tube and neutralised with 5  $\mu$ l of 1 M Tris base pH 10.4.

### RBP-RNA interaction analysis: CLIP/RT-PCR

$6.5 \times 10^5$  cells were seeded on each well of a 6-well plate and incubated in DMEM without phenol red and supplemented with 5% FBS and 1  $\mu$ g/ml doxycycline. After 24 h, cells were either mock-infected or infected with SINV at a MOI of 10. At 18 hpi, culture media was removed and cells were irradiated with 150 mJ/cm<sup>2</sup> of UV light at 254 nm. Cells were lysed in 400  $\mu$ l of lysis buffer (100 mM KCl,

5 mM MgCl<sub>2</sub>, 10 mM Tris pH 7.5, 1% IGEPAL, 1 mM DTT, 100 U/ml Ribolock RNase inhibitor [ThermoFisher Scientific, #E00381], 0.1 mM AEBSF, 200 μM ribonucleoside vanydil complex). Lysates were diluted with 5x high-salt buffer (1.25 M NaCl, 100 mM Tris pH 7.5, 0.1% SDS) and H<sub>2</sub>O to reach 500 μl of 1x high-salt buffer. Lysates were then cleared by centrifugation (5000 rpm for 3 min at 4°C). Supernatants were transferred to a new tube and snap frozen in dry ice. An aliquot (50 μl) was taken as 'input'. Lysates were pre-cleared with 15 μl of pre-equilibrated control agarose beads (Pierce Control Agarose resin, Thermo Fisher Scientific, #26150) by incubation under gentle rotation for 30 min at 4°C followed by centrifugation at 1000 g for 2 min at 4°C. Supernatants were transferred to a new tube. 15 μl GFP-Trap\_A bead slurry were equilibrated with 1x dilution buffer (500 mM NaCl, 1 mM MgCl<sub>2</sub>, 0.05% SDS, 0.05% IGEPAL, 50 mM Tris pH 7.5, 100 U/ml Ribolock RNase inhibitor, 0.1 mM AEBSF), incubated with 1 mg/ml *E. coli* tRNA for 15 min and, after two washes with dilution buffer, they were added to the lysates. The mixture was incubated for 2 h at 4°C with gentle rotation and beads were recovered by centrifugation at 1000 g for 2 min at 4°C. Beads were washed twice with 100 μl of ice-cold high-salt buffer (500 mM NaCl, 20 mM Tris pH 7.5, 1 mM MgCl<sub>2</sub>, 0.05% IGEPAL, 0.1% SDS, 100 U/ml Ribolock RNase inhibitor, 0.1 mM AEBSF), three times with 100 μl ice-cold low-salt wash buffer (150 mM NaCl, 20 mM Tris pH 7.5, 1 mM MgCl<sub>2</sub>, 0.01% IGEPAL, 50 U/ml Ribolock RNase inhibitor) and resuspended in 50 μl of proteinase K buffer (100 mM NaCl, 10 mM Tris pH 7.5, 1 mM EDTA, 0.5% SDS). Protein digestion was carried out by incubation with 200 μg/ml of proteinase K (Invitrogen, #AM2546) for 30 min at 37°C with agitation (1100 rpm) and then raising temperature to 50°C for 1 h. After centrifugation at 1000 g and 4°C for 2 min, the supernatant containing the RNA was transferred to a low binding tube. RNA was then purified using RNeasy mini kit (QIAGEN, #74104) in parallel to the total RNA present in inputs. cDNA library was prepared with Superscript III reverse transcriptase and oligo(dT)<sub>20</sub> primer (Thermo Fisher Scientific, #18418020) following the manufacturer's recommendations. Finally, the presence of SINV sequences in cDNA libraries was detected by PCR using Phusion polymerase (New England Biolabs, #M0530S) and SINV C specific primers (Table S6).

#### Analysis of GEMIN5 binding sites by iCLIP

In order to identify GEMIN5 binding sites on SINV RNA at a high resolution, we employed iCLIP-seq (König et al., 2010). 10x10<sup>6</sup> HEK293 Tet-on GEMIN5-eGFP cells were seeded in 5 sets of 3x15 cm dishes and induced for 24 h with doxycycline. Each cell set was then infected with 10 MOI of SINV. Similar procedure was carried out for 1 set 3x15 cm dishes of control HEK293 Tet-on eGFP cells with 8 h doxycycline induction. At 18 hpi, cells were washed with PBS 1x and UV irradiated with 150 mJ/cm<sup>2</sup> at 254 nm. Cells were then lysed with 1 mL of lysis buffer (NaCl 100 mM, MgCl<sub>2</sub> 5 mM, Tris pH 7.5 10 mM, IGEPAL 0.5%, SDS 0.1%, Na deoxycholate 0.5%, DTT 1 mM, 0.1 mM AEBSF) and the three plates of each condition set were pooled (3 mL of final volume). Lysates were then passed through a 27G needle three times and sonicated with three cycles of 10 s, with 15 s pause between pulses, using a Digenonde bioruptor at level M at 4°C. The homogenate was centrifuged 17900 g at 4°C for 10 min, and topped up to 3 mL with lysis buffer. To obtain RNA fragments of suitable length and to degrade DNA, 3 mL (replicates 1-2, control) or 1 mL (replicates 3-5) of thawed lysate was incubated with 20 U RNase I (Life Technologies, #AM2295) and 4 U Turbo DNase (Life Technologies, #AM2238) per ml of lysate for 3 min at 37°C, with 1100 rpm agitation. Subsequently, lysates were placed on ice and supplemented with 440 U RiboLock RNase Inhibitor. 40 μL of control agarose bead slurry per ml of lysate was pre-equilibrated in lysis buffer and resuspended in 50 μl of lysis buffer. Beads were added to the lysate and incubated for 30 min at 4°C with gentle rotation. The supernatants were then collected by centrifugation for 2 min at 4°C and 2500 g, and then incubated with 40 μL of pre-equilibrated GFP\_trap\_A beads per ml of lysate for 2 h at 4°C with gentle rotation. Next, the beads were collected by centrifugation (2 min, 4°C, 2500 g) and washed twice with 1 mL of high salt buffer (NaCl 500 mM, Tris HCl pH 7.5 20 mM, MgCl<sub>2</sub> 1 mM, IGEPAL 0.05%, SDS 0.1%, 0.1 mM AEBSF, 1 mM DTT), twice with 1 mL of medium salt buffer (NaCl 250 mM, Tris HCl pH 7.5 20 mM, MgCl<sub>2</sub> 1 mM, IGEPAL 0.05%, 0.1 mM AEBSF, 1 mM DTT), and twice with 1 mL of PNK wash buffer (20 mM Tris-HCl pH 7.4, 10 mM MgCl<sub>2</sub>, 0.2% Tween-20) (replicates 1-2, GFP control) or low salt buffer (NaCl 150 mM, Tris HCl pH 7.5 20 mM, MgCl<sub>2</sub> 1 mM, IGEPAL 0.01%, 0.1 mM AEBSF, 1 mM DTT) (replicates 3-5). Beads were resuspended in 20 μL PNK mix [15 μL H<sub>2</sub>O, 4 μL 5x PNK buffer pH6.5 (350 mM Tris-HCl pH 6.5, 50 mM MgCl<sub>2</sub>, 25 mM DTT), 5 U of PNK enzyme (NEB, #M0201S), 20 U of Ribolock] and incubated for 20 min, at 37°C at 1100 rpm. Beads were then washed once with low salt buffer, once with high salt buffer, and twice with low salt or PNK wash buffer. Beads were then resuspended in 20 μL ligation mix [ligation buffer (50 mM Tris-HCl, 10 mM MgCl<sub>2</sub>, 10 mM DTT), 10 U of RNA ligase (NEB, M0204S), 20 U of Ribolock, 1.5 μM pre-adenylated linker L3 (TriLink Biotechnologies, # T1-BGV01A), 4 μL PEG400 (Sigma-Aldrich, #202398-250G)] and incubated O/N at 16°C shaking at 1100 rpm. Subsequently, beads were washed with 500 μL of cold low salt or PNK wash buffer and three times with 1 mL of high salt buffer. Beads were transferred to a low binding tube during the third wash. The beads were further washed twice with 1 mL ice-cold low salt or PNK wash buffer and resuspended in 20 μL low salt or PNK wash buffer, 1x NuPAGE loading buffer (Invitrogen, #NP0007) and 100 mM DTT and denatured at 70°C (1200 rpm, 10 min). The supernatant was collected by centrifugation (1 min at 4°C and 2500 g), loaded on a 4%–12% Bis-Tris NuPage gel (Invitrogen, #NP0321) and run 90 min at 150 V in 1x MOPS running buffer (Life Technologies, #NP0001). Protein-RNA complexes were transferred to a membrane of nitrocellulose (30 V for 1 h). Region matching 190-280 kDa was then cut out, transferred to a fresh microfuge tube, topped up with 200 μL of proteinase K mix (80 mM Tris-Cl pH 7.4; 40 mM NaCl; 8 mM EDTA and 800 μg of proteinase K), and incubated for 20 min at 37°C and 1100 rpm. Subsequently, 200 μL of PKurea buffer (100 mM Tris-Cl pH 7.4; 50 mM NaCl; 10 mM EDTA; 7 M urea) was added and the sample then incubated for 20 min at 37°C at 1100 rpm. RNA was then phenol/chloroform extracted as in (Huppertz et al., 2014; König et al., 2010). Pellets were resuspended in 5 μL of nuclease free H<sub>2</sub>O and stored at –20°C. Reverse transcription was carried out using Superscript III

(Life Technologies, #18080-044) and unique Rclip primers as in (Huppertz et al., 2014; König et al., 2010). The reaction was then transferred to a low DNA binding tube and precipitated with ethanol as in (König et al., 2010). The pellets were resuspended in 12  $\mu$ L of 1x TBE-urea loading buffer, heated for 3 min at 80°C and separated on a 6% TBE-urea precast gel (Life Technologies, #EC6865BOX) for 40 min at 180 V. For replicates 1-2 and the control, the region of the gel corresponding to 85-200 nucleotides was cut off the gel and placed in a 0.5 mL microtube pierced with a needle inside a 1.5 mL microtube. Samples were spun at 16000 g for 1 min, and the flow-through topped up with 400  $\mu$ L of diffusion buffer (0.5 M ammonium acetate, 10 mM magnesium acetate, 1 mM EDTA, 0.1% SDS) and incubated at 50°C for 30 min. For replicates 3-5, two regions of the gel containing cDNA fragments of 120-200 nucleotides and 85-120 nucleotides were cut off from the gel and crushed into small pieces using a pestle in 400  $\mu$ L TE buffer. The samples were then incubated for 1 h at 37°C and 1100 rpm, placed on dry ice for 2 min, and incubated again for 1 h at 37°C and 1100 rpm. In all cases, the disrupted gel was then filtered by spinning through a Costar SpinX column (Sigma, #CLS8160-96EA) by centrifugation at 16000 g. The cDNA was then extracted using phenol/chloroform as in (König et al., 2010). Pellets were resuspended in 8  $\mu$ L ligation mix [1x CircLigase Buffer II; 2.5 mM MnCl<sub>2</sub>; 30 U of CircLigase II (Epicenter, #CL9025K)] and incubated for 1 h at 60°C. We next added 30  $\mu$ L of oligo annealing mix [25  $\mu$ L H<sub>2</sub>O; 4  $\mu$ L NEBuffer 4 (NEB, #B7004S); 0.3  $\mu$ M cut\_oligo (Sigma-Aldrich)] and the sample was heated for 1 min at 95°C followed by a temperature decrease of 1°C every 40 s until reaching 25°C. The samples were then digested with 2  $\mu$ L of BamHI (Thermo Fisher, #FD0054) and incubated for 30 min at 37°C. After incubation at 80°C for 5 min, cDNA was ethanol precipitated (König et al., 2010). Pellets were resuspended in 20  $\mu$ L H<sub>2</sub>O and mixed with 1  $\mu$ L of 10  $\mu$ M primer mix P5/P3 Solexa and 20  $\mu$ L Accuprime Supermix 1 (Life Technologies, #12342-010). The libraries were then amplified for 18 cycles (replicate 1), 23 cycles (replicate 2), 25 cycles (replicates 3-5) or 30 cycles (control GFP) and the products were then analyzed on a 6% TBE precast gel (Life Technologies, #EC6265BOX) in TBE buffer for 60 min at 140 V. The gel was stained with 1x TBE plus 1x SybrGold for 20 min (Life Technologies, #S11494) and bands of appropriate size cut out under blue light trans-illuminator. The gel slices were dissolved with a pestle in 100  $\mu$ L diffusion buffer (0.5 M ammonium acetate; 10 mM magnesium acetate; 1 mM EDTA pH 8.0; 0.1% SDS), incubated for 30 min at 50°C at 1100 rpm and filtered in a Costar SpinX column as above. The library was purified using QIAquick Gel Extraction Kit (QIAGEN, #28704) and quantified on a Bioanalyser using a DNA high-sensitivity chip. Libraries were pooled for sequencing and processed using single-end sequencing mode with a NextSeq 500/550 High Output v2 kit (75 cycles, Illumina, #FC-404-2005).

### Immunofluorescence and RNA FISH assays

High Precision Coverslips (Marienfeld, #0107052) were washed once in 1 M HCl for 30 min on a rocking machine, twice in double distilled water for 10 min and once in ethanol 70% for 10 min. 150,000 cells were seeded on the dried coverslips and incubated in DMEM with 10% FBS. In the case of the Tet-on cells, protein induction was performed with 1  $\mu$ g/ml doxycycline. 16 h later cells were either mock-infected or infected for 1 h at 37°C with 10 MOI of SINV in DMEM without FBS, followed by the replacement of the medium with DMEM supplemented with 1% FBS. At the corresponding times post-infection, cells were rinsed once in PBS and fixed in 4% methanol-free formaldehyde for 10 min. After three 5 min washes in PBS, cells were permeabilised for 5 min with 1x PBS supplemented with 0.1% Triton X-100 (PBST). Next, cells were rinsed twice in PBST and once in PBST supplemented with 2% BSA, and blocked for 1 h with PBST supplemented with 2% BSA. Cells were later incubated for 1 h with primary antibodies ( $\alpha$ -SINV C at 1:200 dilution or  $\alpha$ -XRN1 at 1:50 dilution) in PBST + 2% BSA. Cells were subsequently rinsed in PBST + 2% BSA and washed three times with PBST + 2% BSA for 10 min. Cells were then incubated for 1 h in darkness with the secondary antibodies ( $\alpha$ -rabbit Alexa488,  $\alpha$ -rabbit Alexa594 or/and  $\alpha$ -mouse Alexa488; Thermo Fisher Scientific, #A-21206, #A-21207, #A-21202 respectively) and/or GFP-Booster\_Atto488 (ChromoTek GmbH, #gba488-100) at 1:500 dilution in PBST supplemented with 2% BSA. Cells were washed once with PBST supplemented with 2% BSA and three additional times with PBST supplemented with 2% BSA for 10 min. Cells were incubated with 2  $\mu$ g/ml of DAPI in PBS for 5 min. Finally, cells were washed twice in PBST, once in PBS for 5 min, once in milliQ H<sub>2</sub>O and mounted on glass slides using Vectashield Antifade mounting medium (Vector Laboratories, #H-1000).

For combined immunofluorescence and RNA FISH, cells were seeded in coverslips and fixed and permeabilised as described above. Then, cells were rinsed three times in PBST and incubated for 1 h with primary antibody ( $\alpha$ -SINV C at 1:200 dilution) in PBST + 0.5 U/ $\mu$ L RiboLock RNase inhibitor. Next, cells were washed once in PBST and three additional times with PBST for 10 min. Cells were then incubated with secondary antibody ( $\alpha$ -rabbit Alexa488 at 1:500 dilution) in PBST supplemented with 0.5 U/ $\mu$ L RiboLock RNase inhibitor for 1 h in darkness. Cells were washed once with PBST, and two additional times with PBST for 10 min, once in PBS for 10 min and fixed again in 4% methanol-free formaldehyde for 10 min. Cells were washed twice in PBS for 5 min, once in 1x PBS / 1x SSC for 5 min, once with 2x SSC for 5 min and twice with pre-hybridization buffer (2x SSC and 10% deionized formamide in DEPC water) at 37°C for 10 min. Next, cells were incubated with RNA probes [2 pmol/ $\mu$ L oligo(dT)<sub>25</sub> or oligo(dA)<sub>25</sub> coupled to Alexa 594 (Life technologies Ltd), or 125 nM SINV RNAs-specific Stellaris probes (LGC Biosearch Technologies)] in hybridization buffer (2x SSC, 10% deionized formamide and 10% dextran sulfate in DEPC water) for 16 h at 37°C in a wet chamber. In the case of Tet-on cells expressing GEMIN5-eGFP or MOV10-YFP proteins, GFP-Booster\_Atto488 (1:500 dilution) was included at this step. Cells were subsequently washed twice with pre-hybridization buffer for 10 min at 37°C and incubated for 5 min at 37°C with 2  $\mu$ g/ml DAPI in pre-hybridization buffer. Finally, cells were washed twice with 2x SSC for 5 min, twice with 1x PBS, once for 5 min with 1x PBS and once in milliQ H<sub>2</sub>O. The coverslip was mounted immediately after on glass slides using Vectashield.

In both cases, images were acquired on an API DeltaVision Elite widefield fluorescence microscope using a 100X oil UPlanSApo objective (1.4 NA) and deconvolved with SoftWoRx v6.5.2 (GE Healthcare). Fluorescence intensity profiles were obtained using the

script “Multichannel Plot Profile” in the BAR collection for ImageJ (<https://imagej.net/BAR>). In Figures 4 and S4, RBPs were classified as ‘enriched’ when accumulating in viral factories co-localizing with SINV C; ‘absent’ when undetectable in viral factories; and ‘diffused’ RBPs when distributed across the cytoplasm and thus present but not enriched in viral factories.

### Determining the percentage of infected cells

$9 \times 10^5$  HEK293 cells were seeded on washed coverslips and incubated in DMEM minus phenol red + 5% FBS + 1 mM sodium pyruvate for 24 h. Cells were infected with different MOI of SINV-mCherry in complete DMEM (lacking phenol-red) with 2.5% FBS. At 18 hpi, cells were fixed and processed for immunofluorescence as indicated above using  $\alpha$ -SINV C antibody and DAPI. Images were acquired on an API DeltaVision Elite widefield fluorescence microscope using a 60X oil PlanApo objective (1.42 NA). The percentage of infected cells was calculated by counting C-expressing cells and the total number of DAPI-stained cells using the “Cell Counter” plugin in ImageJ. To define the MOI of SINV used in cRIC experiments and fitness assays, different concentration of viruses were tested. We selected 10 MOI for cRIC experiments because it is the minimal dose promoting high percentage of infected cells in a reproducible manner. We selected 0.1 MOI for fitness experiments as it allows optimal measurement of the mCherry fluorescence in the CLARIOstar plate reader.

### Mass spectrometry

cRIC inputs (whole cell lysates) and eluates were processed following the filter aided sample preparation (FASP) as in (Castello et al., 2013). GEMIN5-eGFP and eGFP IPs were processed with a single-pot solid-phase-enhanced sample preparation (SP3) protocol using 70% acetonitrile for protein binding (Sielaff et al., 2017). All samples were acidified with 5% formic acid prior to mass spectrometric analysis.

Peptides from the cRIC inputs, and GEMIN5-eGFP and eGFP IPs were analyzed on an Ultimate 3000 ultra-HPLC system (Thermo Fisher Scientific) and electrosprayed directly into a QExactive mass spectrometer (Thermo Fisher Scientific). They were initially trapped on a C18 PepMap100 pre-column (300  $\mu$ m inner diameter x 5 mm, 100Å, Thermo Fisher Scientific) in solvent A (0.1% [vol/vol] formic acid in water). The peptides were then separated on an in-house packed analytical column (75  $\mu$ m inner diameter x 50cm packed with ReproSil-Pur 120 C18-AQ, 1.9  $\mu$ m, 120 Å, Dr. Maisch GmbH) using a linear 15%–35% [vol/vol] acetonitrile gradient (2 h for whole cell lysates and 1 h for protein-protein interaction samples) and a flow rate of 200 nl/min. Full-scan mass spectra were acquired in the Orbitrap (scan range 350–1500 m/z, resolution 70000, AGC target  $3 \times 10^5$ , maximum injection time 50 ms) in a data-dependent mode. After the mass spectrum scans, the 20 (for whole cell lysates) or 10 (GEMIN5 IPs) most intense peaks were selected for higher-energy collisional dissociation fragmentation at 30% of normalized collision energy. Higher-energy collisional dissociation fragmentation spectra were also acquired in the Orbitrap (resolution 17500, AGC target  $5 \times 10^4$ , maximum injection time 120 ms) with first fixed mass at 180 m/z.

For cRIC eluates, liquid chromatography (LC) was performed using an EASY-nano-LC 1000 system (Thermo Fisher Scientific) in which peptides were initially trapped on a 75  $\mu$ m internal diameter guard column packed with Reprosil-Gold 120 C18, 3  $\mu$ m, 120 Å pores (Dr. Maisch GmbH, #13.9g) in solvent A using a constant pressure of 500 bar. Peptides were then separated on a 45°C heated EASY-Spray column (50 cm x 75  $\mu$ m ID, PepMap RSLC C18, 2  $\mu$ m, Thermo Fisher Scientific #164540) using a 3 h linear 8%–30% [vol/vol] acetonitrile gradient and constant 200 nl/min flow rate. Peptides were introduced via an EASY-Spray nano-electrospray ion source into an Orbitrap Elite mass spectrometer (Thermo Fisher Scientific). Spectra were acquired with resolution 30000, m/z range 350–1500, AGC target  $1 \times 10^6$ , maximum injection time 250 ms. The 20 most abundant peaks were fragmented using CID (AGC target  $5 \times 10^3$ , maximum injection time 100 ms, normalized collision energy 35%) in a data dependent decision tree method.

Peptide identification and quantitation of all proteomics experiments was then performed using MaxQuant (v1.5.0.35) (Cox and Mann, 2008). Data were searched against the Human Uniprot database (version, January 2016) alongside a custom database including all the known SINV polypeptides and a list of common contaminants provided by the software. eGFP protein sequence was included in the analysis of GEMIN5-eGFP and eGFP IPs (Uniprot ID C5MKY7). The search parameters for the Andromeda search engine were: full tryptic specificity, allowing two missed cleavage sites, fixed modification was set to carbamidomethyl (C) and the variable modification to acetylation (protein N terminus), oxidation (M). Match between runs was applied. All other settings were set to default, leading to a 1% FDR for protein identification. Raw and processed proteomic data have been deposited to the ProteomeXchange Consortium (Deutsch et al., 2017) via the PRIDE partner repository with the dataset identifier PXD009789.

### RNA sequencing

RNA from the ‘inputs’ (whole cell lysate) of cRIC experiments was extracted using TRIzol. Strand-specific RNA-seq was performed with 100 ng of total RNA. Libraries were prepared using NEBNext Ultra Directional RNA library Prep Kit for Illumina (New England Biolabs, #E7420S) according to manufacturer instructions. In brief, RNA was fragmented for 15 min at 94°C and then reverse transcribed. cDNA and double-stranded cDNA was purified with AMPure XP beads (Beckman Coulter, #A63881). After end repair, NEBNext Adaptors for Illumina (New England Biolabs, #E7335S) were ligated onto the cDNA according to the kit manual. Libraries were amplified by 15 cycles of PCR. We used the following combination of barcodes for sample multiplexing: S1\_Mock ATCACG, S1\_SV4h CGATGT, S1\_SV18h TTAGGC, S2\_Mock ACAGTG, S2\_SV4h CAGATC, S2\_SV18h ACTTGA, S3\_Mock GATCAG, S3\_SV4h TAGCTT and S3\_SV18h GGCTAC. Libraries with an average length of 320 nt were pooled and sequenced with an Illumina



NextSeq instrument, using 78 nt paired-end sequencing mode with a NextSeq 500/550 High Output v2 kit (150 cycles, Illumina #FC-404-2002). Raw and processed RNA-seq are available at GEO: GSE125182.

## QUANTIFICATION AND STATISTICAL ANALYSES

### Proteomic quantitative analysis

To compare the cRIC inputs and eluates under different conditions, peptide intensity ratios between two samples were computed and summarized. The log<sub>2</sub>-intensity ratio of each protein was tested to be different from zero in the three biological replicates using moderated t test, which is implemented in the R/Bioconductor package *limma* (Smyth, 2004). p values were corrected for multiple testing by controlling the false discovery rate with the method of Benjamini-Hochberg. For proteins for which the protein intensity was 'zero' in one of the two conditions, we applied a semiquantitative approach that assumes that proteins without quantitative information are below the detection limit (Sysoev et al., 2016). The approach compiles the number of replicates in each condition in which a given protein has an intensity value. When comparing 2 conditions and three biological replicates, this leads to a matrix with 16 different groups (detected 0, 1, 2 or 3 times in condition 1 versus detected 0, 1, 2 or 3 times in condition 2). A protein is classified as 'altered RBP' by the semiquantitative method if an intensity value is assigned to it in 3 or 2 of the replicates in one of the two conditions, while only 1 or 0 intensity values are detected in the other condition.

The fraction of RNA-bound RBPs was determined by computing the ratio between the protein intensity of each individual RBP in the cRIC eluates and that in the whole cell lysate (Figure S3D). Hence, this calculation reflects amount of protein crosslinked to RNA (cRIC eluates) divided by the total amount of protein (cRIC inputs).

Results were visualized using the R package *ggplot2* (Wickham, 2009). To assess the scope of previously known RBPs within the RBPome of uninfected and SINV-infected HEK293 cells, proteins identified by cRIC here were compared to those comprising the superset of human RBPs reported in (Hentze et al., 2018). GO annotations were obtained from the R package *mRNAinteractomeHeLa* (<http://www.hentze.embl.de/public/RBDmap/>) (Castello et al., 2012) (Key Resources Table), and gene set enrichment analysis was performed by applying Fisher's exact test to categories of GO annotations with at least three annotated proteins.

We compared the repertoire of RBPs with differential RNA-binding activity at 18 hpi (Table S1) with the mouse ribo-interactome (Table S2) (Simsek et al., 2017). Specifically, we considered proteins in the Table S3 of (Simsek et al., 2017) with negative predictive values (NPV)  $\geq 0.99$  in puromycin and RNase samples as 'ribosome-associated proteins', as described in that study. To find mouse orthologs for RBPs responding to SINV infection, we used the R package *biomaRt* to identify ENSEMBL peptide IDs for our RBPome dataset and *hom.Hs.inp.db* (Carlson and Pages, 2015) to provide mapping between human and mouse proteins using these IDs (Key Resources Table). If a mouse ortholog of an altered RBP identified at 18 hpi was found in the 'ribo-interactome' (Simsek et al., 2017) or if the gene symbols between human and mouse matched directly, the human RBP was considered as 'ribosome-associated'. Results of this analysis are provided in Table S2.

For GEMIN5 protein-protein interaction analysis, protein quantification was performed by label free quantification using MaxQuant. Ratios were compiled and normalized to eGFP protein intensity in each sample, which is expected to be the same across samples. Significance of the fold changes was estimated by t test using the software *Perseus* (Tyanova et al., 2016). We performed three main comparisons with the data from the IPs: i) GEMIN5-eGFP versus eGFP both in uninfected cells; ii) GEMIN5-eGFP versus eGFP both in SINV-infected cells; and iii) GEMIN5-eGFP in uninfected cells versus GEMIN5-eGFP in SINV-infected cells (Figure 7C, left, middle and right, respectively). Resulting data are summarized in Table S5. Raw and processed proteomic data from GEMIN5-eGFP IPs have been deposited to the ProteomeXchange Consortium via the PRIDE partner repository with the dataset identifier PXD009789.

The R package *ggplot2* was utilized to visualize GEMIN5-eGFP proteomics data in volcano plots (Figures 7C). Only proteins that were identified as high-confidence interactors of GEMIN5-eGFP (i.e., p value < 0.01 and positive log<sub>2</sub> fold change) in the left panel of Figure 7C were displayed in the comparison between infected and uninfected cells in the right panel. Proteins with names starting with 'RPS' or 'RPL', were classified as 'ribosomal' and displayed in the volcano plots as pink dots.

STRING (Szklarczyk et al., 2017) was used to display the connectivity between altered RBPs in SINV-infected cells (Figures S2C and S2D) and between the proteins comprising the GEMIN5 interactome (Figure S7D). Protein networks were generated using the following parameters: display – confidence; Interaction sources – experiments and databases; interaction score – high-confidence (0.700). Disconnected nodes were hidden from display and nodes colored based on functional enrichment within the network as determined by STRING. GEMIN5 protein interactome (Figure S7D) was defined as proteins enriched in GEMIN5-eGFP IPs over eGFP IPs with p value < 0.01. STRING-based GO enrichment for GEMIN5 protein interactome is provided in Table S5.

### RNA sequencing data analysis

We combined the human genome (version hg38) with SINV sequence as our reference genome. RNA-seq reads were then mapped to this reference genome using STAR (Dobin et al., 2013). Reads mapping to each transcript were counted with *featureCounts* in Sub-read software package (Liao et al., 2013). Only uniquely mapped reads are considered for counting. SINV infection is known to shut off transcription globally (Gorchakov et al., 2005), which may bias (underestimate) differential expression results if normalization is carried out assuming that overall RNA abundance remains unchanged. Therefore, we decided to normalize read counts in each condition to the corresponding rRNA expression by dividing a factor proportional to the total rRNA read counts in 3 conditions

(0.899, 1 and 0.473 for Mock, 4 hpi and 18 hpi respectively). We confirmed by RT-qPCR that rRNA does not change in abundance in course of infection. The R package DESeq2 (Love et al., 2014) was used for differential gene expression analysis based on rRNA normalized read counts. As DESeq2 requires the reads counts to be un-normalized and in the form of integer values, rRNA normalized read counts were rounded to the closest integer to make the “DESeqDataSet” to start the differential analysis. We estimated the size factor of each sample separately in DESeq2, instead of pooling all the samples prior to estimating this parameter.

Differential RNA expression between infected (4 and 18 hpi) and uninfected cells was visualized in MA plots (Figures 3F and 3G) using DESeq2. To visualize the overall effect of experimental covariates and potential batch effects, a principal component plot of the samples was generated using the plotPCA function in DESeq2, based on the principal component analysis (PCA) of the variance stabilized expression of the top 500 genes with the highest expression variance among samples. As shown in Figure S3F, the variance explained by the first and second PC (on X and Y-axes) combined accounts for a high percentage (96%) of the total variance, and samples within the same condition clustered better between them than with the other two conditions. It is interesting to note that the first PC along accounts for 94% of the total variance, and it distinctly separates 18 hpi to the other samples (i.e., uninfected and 4 hpi), indicating that the cellular transcriptome is dramatically altered at 18 hpi.

Genes related to GO terms ‘Response to virus’ (GO:0009615) and ‘Defense response to virus’ (GO:0051607) were extracted from “hsapiens\_gene\_ensembl” dataset (GRCh37) from Bioconductor package biomaRt (Durinck et al., 2009) and plotted as a heatmap using the R package pheatmap (Kolde, 2015) (Figure S1E). This package was also used to make a heatmap for differentially expressed cellular RNAs, including those transcripts passing the following thresholds: i) log2 fold change > 3 or < -3 and ii) adjusted p value < 0.01 (Figure S3E).

Reads mapping to positive and negative strands of viral RNAs were separated using SAMtools view utility (Li et al., 2009). In Illumina reverse paired end sequencing, paired reads came from opposite strands. Therefore, reads with the second pair mapping to the positive strand, or with the first pair mapping to the negative strand, were both counted as mapping to the positive strand and vice versa. The total read counts mapping to each strand were compiled and counted using SAMtools merge and SAMtools depth, respectively.

### Analysis of RNA synthesis, processing, and degradation

We used analysis of variance (ANOVA) to evaluate in what extent the changes in transcript levels are explained by the rate of RNA synthesis, processing and degradation. The measurement of the rate of these RNA processes for each individual RNA were obtained from (Mukherjee et al., 2017). We built a multiple linear regression using the rate of the above-mentioned RNA processes as ‘predictors’ or ‘factors’, and the transcriptome changes in SINV infected cells as the ‘response variable’.

$$T_i = A_0i + A_1iD_i + A_2iP_i + A_3iS_i + E_i$$

$i$  indicates all the individual RNA molecules;  $T_i$  is the expression change for the molecule between the two conditions compared;  $A_0i$  is the regression intercept;  $D_i$ ,  $P_i$  and  $S_i$  are the rate of degradation, processing and synthesis, respectively;  $E_i$  is the ‘error term’ in the multiple linear regression.

After fitting the model, the total variance explained, or R-squared, is defined as the sum of squares (SS) contributed to the total SS by different factors, i.e., the three predictor variables and the error term, as indicated in the equation below:

$$SS_{total} = SS_{Degradation} + SS_{Processing} + SS_{Synthesis} + SS_{Error}$$

Therefore, the contribution of the three predictors to the alterations in the transcriptome can be measured by their proportion of SS. The partial SS for each predictor is obtained using the “sequential sum of squares” method implemented in ANOVA function in R (Key Resources Table). These data (mock compare to 4 hpi and mock compare to 18 hpi) are shown in Figure 5A. A more detailed description of ANOVA can be found in NIST/SEMATECH e-Handbook of Statistical Methods (<https://www.itl.nist.gov/div898/handbook/eda/section3/eda355.htm>).

### iCLIP-seq data processing

To identify GEMIN5 binding sites on SINV RNAs, reads in the fastq files from sequencing were demultiplexed to separate the samples according to the sample barcodes. Molecular and sample barcodes as well as trailing adaptor sequences were trimmed off. Molecular barcode information was stored in the read name. Reads were then mapped to a combined human (GRCh38) and SINV genome (pT7-SVwt) sequence using STAR. Uniquely aligned reads were then extracted using SAMtools. Binding sites were determined as the 5’-most base of each uniquely mapped read. PCR duplicates were identified as reads with the same mapping position and molecular barcode and each unique fragment counted just once. The 5’-most base in sequenced reads corresponds to the base directly 3’ of the crosslinked base. The number of unique fragment counts per position gives a measure of GEMIN5 interaction strength with that position along the RNA.

Due to the sheer abundance of SINV RNA at 18 hpi, some background signal could be observed in GFP control. To account for this background, GFP signal was subtracted from GEMIN5 signal after correction to total SINV reads. Signal along SINV was then visualized individually per replicate (Figure S7) and as an average of all five replicates (Figure 7) as a coverage track and heatmap.

Because the binding sites are narrow (sharp) and hence difficult to see when plotting the full SINV region, the plot shows an average over a sliding window of 20 nt. Note that the negative signal from y axis (higher signal in GFP) is cut off to better highlight GEMIN5 enriched regions.

Significantly crosslinked sites were determined using iCount peaks ([Key Resources Table](#)). iCount peaks was run to generate a background distribution by randomly distributing the crosslinked sites a hundred times along the SINV genome and compare the actual observed distribution to this background to generate a false discovery rate. Since regions corresponding to genomic, subgenomic and 3' end region have different overall abundance, they were indicated as individual gene segments in the calculation to account for potentially higher background. Sites meeting FDR cutoff of 0.01 within 5 nt of each other were then merged using iCount clusters to form binding sites. Binding sites were then given a 'strength score' calculated as counts within the binding site divided by its width, and visualized in a heatmap in five bins to differently highlight the strengths of binding at different sites ([Figures 7 and S7](#)). This process was done for the GEMIN5 replicates separately as well as for the library size normalized average of the five replicates. [Figure 7D](#) additionally shows a heatmap that indicates how many replicates support a genomic position as binding site when determined individually per replicate. ggplot2 was used to facilitate plotting the heatmaps.

To look at base composition around the start of the SINV sgRNA, the 5'-most base of unique fragments was extracted from aligned reads taking softclipping into account. Count per base relative to total count in the sgRNA region is show in [Figure S7H](#) to indicate relative binding site frequency and whether the sequenced base matches the genome.

Raw and processed iCLIP-seq data are available at GEO: GSE125182.

#### **DATA AND SOFTWARE AVAILABILITY**

The accession number for the mass spectrometry data reported in this paper is ProteomeXchange: PXD009789. The accession number for the RNA-seq and iCLIP data reported in this paper is GEO: GSE125182.